Universidad del País Vasco

Facultad de Medicina y Enfermería

Departamento de Fisiología

Antitumoral actions of *Vismia baccifera* on human hepatocellular carcinoma HepG2

Tesis doctoral para optar al grado de Doctor, presentada por:

Jenifer Trepiana Arín

Leioa, Julio 2016

Directores de tesis:

Mª Begoña Ruiz Larrea

José Ignacio Ruiz Sanz

In order to conduct this Doctoral Thesis I have been awarded a Predoctoral Research Training grant by the University of the Basque Country, UPV/EHU during the period 2012-2016.

In addition, I have also been awarded a mobility grant for researchers from the University of the Basque Country, UPV/EHU for a three months stay in the INSERM VINCO U916, Institute Bergonié, Bordeaux, France, under the supervision of Dr. Mojgan Djavaheri-Mergny.

This work was supported by research grants from the Basque Country Government (Department of Education, Universities and Research, ref. IT687-13, and DCIT, ref. S-PE12UN056), and University of the Basque Country, UPV/EHU (CLUMBER UFI11/20). Technical and human support provided by SGIKer (UPV/EHU, MICINN, GV/EJ, ESF) is gratefully acknowledged.

AGRADECIMIENTOS

Ante todo me gustaría agradecer a mis directores de tesis, Mª Bego y José Ignacio, por permitirme formar parte del grupo de investigación y por enseñarme a lo largo de estos años. Gracias por vuestra disponibilidad, por vuestra ayuda y por vuestros consejos durante todo el doctorado.

También me gustaría agradecer a Mojgan Djavaheri-Mergny, por darme la oportunidad de pasar tres meses en el laboratorio del Instituto Bergonié de Burdeos. Muchas gracias por todo lo que me has enseñado y el buen trato recibido durante toda la estancia, tanto por tu parte como por la de los compañeros del laboratorio.

Agradecer a toda la gente del "labo", tanto a los que ya estaban cuando llegué como a los que acaban de empezar. En especial, a todo el grupo de "Radicales libres" por el buen ambiente, que ha sido mucho mejor de lo que me podría haber imaginado.

En primer lugar a Oihana, porque fuiste la primera persona que conocí en el laboratorio y por enseñarme tan bien durante mis primeros meses. A Susana, por todo lo que me has ayudado, por tu alegría y por todas las horas que hemos compartido. A Irantzu, por todas esas charlas en el despacho y por el ánimo que me has dado. En definitiva, a todos los "Radicales", porque ya podría trabajar siempre con gente como vosotros.

A Josean, por todo lo que me has ayudado con los cultivos celulares durante estos años, y por estar siempre dispuesto a echar una mano.

A todos los del grupo de "Colesterol", del primero al último, porque después de pasar tanto tiempo juntos os habéis convertido en algo más que compañeros de trabajo. Siempre voy a recordar esas celebraciones y despedidas con todos los de "Radicales" y "Colesterol", algunas con "gincana" y regalo de embutidos incluidos.

A todos los que ya han terminado su etapa en el laboratorio. En especial a Juan, porque sigues siendo el alma positiva incluso cuando estás a miles de kilómetros; así da gusto.

A mis amigos, por su interés en mis investigaciones. En especial a los de Miranda, que siempre han creído que voy a llegar lejos.

A mis padres y hermanas, por apoyarme y mostrar tanto interés en mis experimentos. A mi hermana Juncal y mi cuñado Víctor, por preguntarme cada día "¿Qué tal tus células?", y por escuchar mis "batallitas" en el laboratorio. Gracias a todos por vuestro apoyo y ánimo, porque sin vosotros no hubiese llegado hasta aquí.

Y por último, me gustaría agradecer de forma especial a Iñaki. Gracias por escucharme siempre y haberme ayudado en los días más duros. Porque has conseguido que sobretodo estos últimos meses hayan sido más llevaderos con todas esas "risotadas" y "chanzas" juntos, que me hacen desconectar del trabajo cuando estás a mi lado.

A todos vosotros, gracias.

Jenifer.

TABLE OF CONTENTS

TABLE OF CONTENTS

ABBREVIATIONS

ABBREVIATIONS

APC	Anaphase promoting complex
ASK1	Apoptosis signal-regulated kinase 1
ATF4	Activating transcription factor 4
ATF6	Activating transcription factor 6
ATM	Ataxia-telangiectasia mutated kinase
ATR	ATM and Rad 3-related kinase
Bid	BH3 interacting-domain death agonist
Cdh1	APC activator
CDKs	Cyclin-dependent kinases
CHOP	CAAT/enhancer-binding protein (C/EBP) homologous protein
CKI	CDK inhibitor
DbF4	Protein DbF4 homolog A
DFCP1	Double FYVE-containing protein 1
DP	DP protein
DR5	Death receptor 5
E2F	E2F transcription factor
eIF2	Eukaryotic translation initiation factor 2
ERK1/2	Extracellular signal-related kinases 1/2
ERO1	Endoplasmic reticulum oxidoreductin
ETC	Electron transport chain
FIP200	FAK family kinase-interacting protein of 200 kDa
FOXO	Forkhead family transcription factor
GADD34	Growth arrest and DNA damage 34-inducible protein
GADD45	Growth arrest and DNA damage 45-inducible protein
GSK-3	Glycogen synthase kinase 3
HIF1α	Hypoxia-inducible factor-1 α
HMGB1	High mobility group box 1 protein
IKK	IκB kinase
IRE1	Inositol-requiring kinase 1
JNK1/2/3	c-Jun amino-terminal kinases 1/2/3
Keap1	Kelch-like ECH-associated protein 1
MAM	Mitochondria associated membrane
MAPK	Mitogen-activated protein kinase
Mdm2	Murine double minute 2 protein
MK2	MAPK-activated protein kinase 2
mTORC1/2	Mammalian target of rapamycin complex 1/ 2

NES	Nuclear export signal
NFκB	Nuclear factor κB
NLS	Nuclear localization signal
Nrf2	Nuclear factor erythroid 2-related factor 2
$p21^{CIP1/WAF1}$	Cyclin-dependent kinase inhibitor 1
$p27^{KIP1}$	Cyclin-dependent kinase inhibitor 1B
PARP	Poly ADP-ribose polymerase
PDI	Protein disulfide isomerase
PDK1	Phosphoinositide-dependent kinase 1
PE	Phosphatidylethanolamine
PERK	Pancreatic ER eukaryotic translation initiation factor 2 eIF2α kinase
PH	Pleckstrin homology domain
PI3K	Phosphatidylinositol-3 kinase
PI3P	Phosphatidylinositol 3 phosphate
PIKKs	Phosphoinositide 3-kinase related kinases
PIP_2	Phosphatidylinositol-4,5-bisphosphate
PIP_3	Phosphatidylinositol-3,4,5-trisphosphate
PKC	Protein kinase C
PP2A	Protein phosphatase 2A
pRB	Retinoblastom protein
PTEN	PIP_3 phosphatase
Ras	Rat sarcoma GTPases
Rheb	Ras homology enriched in brain
RIDD	Regulated IRE1-dependent decay of mRNA
RTK	Receptor tyrosine kinase
S1P	Serine protease site-1 protease
S2P	Metalloprotease site-2 protease
TK	Thymidine kinase
TMPK	Thymidylate kinase
TNF-α	Tumor necrosis factor α
TRAF2	Tumor necrosis factor alpha TNFα receptor associated factor 2
TRB3	Telomere repeat binding factor 3
TSC1/2	Tuberous sclerosis complex protein 1/2
ULK1	UNC-51-like kinase 1
WIPI	WDrepeat protein interacting with phosphoinositide
XBP1	X-box-binding protein 1

RESUMEN

RESUMEN

1. Introducción

Colombia presenta una gran variedad de especies vegetales que son fuente de compuestos bioactivos naturales, que pueden ser utilizados para el tratamiento de enfermedades. Una planta típica de la Amazonía es *Vismia baccifera*, perteneciente a la familia Clusiaceae. La corteza, hojas, tallos y raíces de *V. baccifera* se utilizan comúnmente en la medicina tradicional por las poblaciones indígenas con diferentes propiedades curativas. Así, se utiliza como purgante, en el tratamiento de desórdenes del tracto urinario, frente a picaduras de serpiente, desórdenes de la piel (tratamiento de heridas, herpes e infecciones fúngicas), como antirreumático y antipirético. Las hojas de *V. baccifera* se recomiendan también en diversas condiciones inflamatorias, incluyendo hemorragias uterinas, y asimismo presentan actividad leishmanicida (Gallego y cols., 2006). Un estudio reciente revela las propiedades anti-*Plasmodium*, antioxidante, antimicrobiana y antifúngica del género *Vismia* (Vizcaya y cols., 2012). El extracto de las hojas de esta planta también presentó actividades anti-trasncriptasa inversa del VIH y micobactericida (Gomez-Cansino y cols., 2015).

Hasta la fecha no ha sido identificada *in vivo* actividad antitumoral de *V. baccifera. Hussein y cols.* aislaron constituyentes de extractos metanólicos de *V. baccifera,* que contenían: ferrugininas A, B y C, vismina, harunganina, vismiona B, diacetilo de vismiona H y diacetilo de vismiona A (Hussein et al., 2003). Estos compuestos presentaron efectos citotóxicos frente a líneas celulares humanas de cáncer de mama, pulmón y del sistema nervioso central.

2. Hipótesis y objetivos

Actualmente hay un creciente interés en identificar agentes quimioterapéuticos que puedan prevenir la iniciación, disminuir o incluso parar el crecimiento de los tumores, y por tanto la consiguiente metástasis. Los productos naturales derivados de plantas han recibido recientemente una considerable atención debido a su actividad antioxidante, antiinflamatoria y antitumoral. En estudios previos realizados por nuestro grupo de investigación se determinó

el contenido total de fenoles y flavonoides y la actividad antioxidante de extractos acuosos provenientes de plantas Amazónicas que comúnmente se utilizan en la medicina tradicional (Lizcano y cols, 2010; Lizcano y cols, 2012). De entre ellos se seleccionaron por su alto potencial antioxidante, varios extractos de hojas de plantas del género *Vismia* y *Piper* para analizar su actividad antitumoral en células de carcinoma hepatocelular humanas y de rata (Lizcano y cols, 2014). De los resultados obtenidos destacamos los efectos producidos por la planta *Vismia baccifera;* en líneas celulares de hepatoma indujeron toxicidad celular, mientras que en hepatocitos no trasnformados de rata el extracto fue inocuo o incluso aumentó la viabilidad celular. Estos resultados nos han llevado a analizar en profundidad las acciones de esta planta para ampliar el conocimiento que permita establecer las bases de su utilización como coadjuvante o en la terapia anticancerígena.

La HIPÓTESIS de este trabajo plantea que *V. baccifera* promueve una desregulación *redox* que conlleva la inhibición del crecimiento tumoral. El OBJETIVO principal de éste proyecto de Tesis Doctoral es elucidar las rutas citotoxicas inducidas por el extracto vegetal en las células de carcinoma hepatocelular humano HepG2.

Para ello, se llevaron a cabo los siguientes OBJETIVOS OPERATIVOS:

1. Determinar la toxicidad, evaluando el IC_{50}, la acumulación intracelular de ROS y mitocondrial de $O_2^{\cdot-}$, el potencial de membrana mitocondrial, el ciclo celular y la migración, el sistema antioxidante diana de *V. baccifera*, la autofagia y la implicación de la apoptosis en la muerte celular.
2. Determinar la implicación de ROS y del peróxido de hidrógeno en la toxicidad inducida por *V. baccifera*.
3. Establecer las rutas de señalización inducidas por *V. baccifera*.
4. Estudiar la influencia de pO_2 en la toxicidad inducida por *V. baccifera*.

3. Materiales y métodos

Para llevar a cabo estos objetivos se ha utilizado como sistema biológico células de carcinoma hepatocelular humano HepG2, que fueron expuestas al extracto de *V. baccifera*. El extracto se preparó a partir de infusiones acuosas de las hojas de la planta, según se utiliza en la medicina

tradicional. Se caracterizó la actividad antioxidante total de los extractos mediante los ensayos de decoloración del radical $ABTS^+$ y el método ORAC (capacidad de absorbancia del radical oxígeno). Durante la realización de la tesis se han utilizado técnicas de biología celular, molecular y bioquímicas. En relación a las técnicas de biología celular, en particular hemos utilizado cultivos celulares, que requieren condiciones de esterilidad, microscopía óptica para el contaje celular, microscopía electrónica de transmisión para el estudio ultraestructural de las células, técnicas de fraccionamiento por centrifugación diferencial para la obtención de extractos celulares, y citometría de flujo para determinar los niveles intracelulares de ROS y mitocondriales de anión superóxido, el ciclo celular y el potencial de membrana mitocondrial; la migración celular y la localización de proteínas se determinó por microscopía confocal e inmunofluorescencia. En relación a las técnicas bioquímicas se han utilizado ensayos enzimáticos para la determinación de actividades de enzimas antioxidantes y de caspasas, técnicas espectrofotométricas para la determinación de glutatión, y para el análisis proteico técnicas de separación por electroforesis y su cuantificación por densitometría. En relación a técnicas de biología molecular, analizamos mediante RT-PCR el splicing alternativo de XBP1. Finalmente, el análisis estadístico de los datos se llevó a cabo mediante los programas estadísticos SPSS 19.0 (SPSS Inc., Chicago, IL, USA) y GraphPad Prism 4 (San Diego, CA, USA). Los datos se expresaron como la media ± el error estándar de al menos tres experimentos independientes. La significación estadística de las diferencias de las medias se estimó por el test de la t de Student para distribuciones paramétricas o el test de Wilcoxon para distribuciones no paramétricas. Las diferencias entre las medias se consideraron estadísticamente significativas para $P<0,05$. El IC_{50} (concentración que inhibe un 50% el crecimiento celular) se derivó de la curva semilogarítmica dosis-respuesta. Los datos se ajustaron mediante regresión no lineal ($R_2 \geq 0.99$), utilizando el programa GraphPad Prism 4 para Windows (San Diego, CA, USA).

4. Resultados y discusión

El extracto de hojas de *V. baccifera* provocó efectos citotóxicos en las células HepG2 de carcinoma hepatocelular, disminuyendo el crecimiento de HepG2 en función de la dosis y el tiempo de exposición al tratamiento. El IC_{50}, concentración del extracto que inhibe un 50% el crecimiento celular, fue 48,75 µg/ml. Cabe destacar que en la línea celular HH4, derivada de

hepatocitos no transformados, el extracto de la planta no ocasionó efectos citotóxicos, lo que indica que el efecto de *V. baccifera* es exclusivo de células tumorales. A continuación, utilizamos un modelo experimental con tres líneas celulares que presentan diferente expresión del gen p53. HepG2 cuenta con una expresión de p53 normal, Hep3B presenta una deleción en p53, y Huh7 contiene una mutación en el gen p53 que disminuye su actividad transactivadora. La línea celular Hep3B fue la más resistente a *V. baccifera*, mientras que HepG2 fue la línea celular más sensible al extracto. Estos resultados sugieren que la proteína p53 podría estar implicada en la toxicidad que induce *V. baccifera*.

Como ya se ha descrito anteriormente en nuestro grupo, *V. baccifera* contiene un alto contenido en polifenoles. Por ello, quisimos determinar si el efecto citotóxico de *V. baccifera* estaba mediado por uno de los polifenoles que la constituyen: la epicatequina. El monómero de (-)-epicatequina comercial, aislado de té verde, no inhibió la proliferación celular ni indujo toxicidad en las células HepG2, incluso cuando se ensayó a la concentración tan alta de 200 µM, lo que indica que el monómero de (-)-epicatequina no es responsable de la actividad antitumoral inducida por *V. baccifera* en HepG2.

V. baccifera provocó un aumento de los niveles intracelulares de ROS y mitocondriales de anión superóxido desde 1 h de incubación en las células HepG2. Además, el extracto incrementó el potencial de membrana mitocondrial. Asimismo, *V. baccifera* bloqueó el ciclo celular en la fase G_2/M a las 24 h, y aumentó el número de células en la fase subG_0, lo cual indicaba muerte celular por apoptosis. Efectivamente, el extracto indujo un aumento de las actividades caspasa-2 (iniciadora) y caspasa-3 (efectora).

Para determinar la fuente generadora de ROS en la respuesta tóxica a la *V. baccifera*, se utilizaron compuestos eliminadores de ROS e inhibidores de enzimas pro-oxidantes. Los resultados mostraron que los enzimas NADPH oxidasa y xantina oxidasa no estaban implicados en la generación de ROS. La catalasa (eliminador del peróxido de hidrógeno) y en menor medida el Tirón (que elimina O_2^-) evitaron la acumulación de ROS a tiempos cortos y la toxicidad por *V. baccifera*. Mediante el uso de la sonda fluorescente no permeable Amplex, determinamos que *V. baccifera* aumentó significativamente la producción de H_2O_2 a 3 y 24 h de tratamiento.

Respecto al efecto de *V. baccifera* sobre el sistema antioxidante, comprobamos que el extracto produjo un aumento de la actividad enzimática SOD y una disminución de GPx a 24 h, lo que indicaría un aumento de la cantidad de peróxido de hidrógeno intracelular a este tiempo. Sin embargo, no detectamos ningún cambio en las actividades antioxidantes a tiempos cortos. Esto sugiere que el estrés oxidativo temprano inducido por el extracto puede ser responsable de los subsiguientes cambios de las actividades antioxidantes, provocando una respuesta tóxica a largo plazo. Además, *V. baccifera* provocó una disminución drástica de los niveles de GSH a 24 h de incubación. Este efecto fue revertido por N-acetilcisteína, precursor de GSH, que, sin embargo, no evitó la muerte celular. Estos datos indican que el vaciado de GSH no es la causa, sino la consecuencia de la toxicidad por *V. baccifera*.

Datos obtenidos a partir de ensayos con catalasa indicaron que ésta revertía la hiperpolarización de la membrana mitocondrial, evitaba el bloqueo del ciclo celular y la apoptosis. Asimismo, observamos que el extracto de *V. baccifera* inducía un aumento de la expresión de la isoforma mitocondrial Mn-SOD, pero no de la citosólica Cu,Zn-SOD. La catalasa prevenía el aumento de Mn-SOD, sin alterar la actividad SOD.

Estos resultados indicaron que el aumento intracelular de peróxido de hidrogeno es clave para inducir toxicidad tras la exposición de las células HepG2 al extracto de la planta, y cómo juega un papel muy importante en el desencadenamiento de la apoptosis.

A continuación, caracterizamos las principales rutas de señalización celular implicadas en la citotoxicidad inducida por *V. baccifera* y la implicación del H_2O_2 en dichas rutas. *V. baccifera* indujo la activación (fosforilación) de las proteínas JNK y p38, implicadas en estrés oxidativo, e inhibió la ruta de supervivencia de Akt, y ERK. En relación con ERK, observamos una disminución de la migración de las células HepG2 incubadas con el extracto, lo que se puede deber a que el extracto disminuye la migración mediante la inactivación de ERK a 24 h.

V. baccifera provocó un aumento de la chaperona GRP78 a 3 y 6 h, que se evitó en presencia de catalasa; estos resultados indican que el peróxido de hidrógeno estaría implicado en el estrés reticular que induce el extracto vegetal. Además, los ROS regularon la expresión de las proteínas apoptóticas y el procesamiento de PARP, lo que concuerda con el aumento de

las actividades de las caspasas -2 y -3. El aumento de la fosforilación de la histona γH2AX sugiere que *V. baccifera* indujo daño genotóxico en las células HepG2.

V. baccifera indujo la acumulación de las proteínas biomarcadoras de autofagia LC3 y p62. Las células HepG2 activarían el proceso de autofagia en respuesta a la citotoxicidad, tal vez como un mecanismo de adaptación y supervivencia.

A la vista de estos resultados comprobamos si el efecto de *V. baccifera* en las células HepG2 se veía modificado por la presión parcial de oxigeno (pO_2). Disminuyendo la concentración de oxígeno al 8%, presión normal a la que se pueden encontrar los tejidos, determinamos que la respuesta a *V. baccifera* era similar a la detectada a concentraciones atmosféricas de oxígeno (21%), en lo que se refiere a la generación intracelular de ROS y mitocondrial de anión superóxido.

5. Conclusiones

1. El extracto acuoso de hojas de *V. baccifera* provoca una respuesta citotoxica en células de carcinoma hepatocelular humano HepG2, aumentando los niveles intracelulares de ROS (en particular, peróxido de hidrógeno), mitocondriales de anión superóxido, e induciendo vaciado intracelular de GSH, detención del ciclo celular en la fase G_2/M, estrés en el retículo endoplásmico, autofagia y apoptosis.

2. La acción citotoxica ejercida por *V. baccifera* es exclusiva de células cancerosas, ya que el extracto no afectó a hepatocitos humanos no transformados HH4.

3. El peróxido de hidrógeno, cuya acumulación intracelular es inducida por el extracto de forma temprana, media la respuesta citotoxica.

4. *V. baccifera* induce la desregulación de enzimas antioxidantes, este efecto siendo secundario a la acumulación de peróxido de hidrógeno.

5. El agotamiento de GSH intracelular no es la causa, sino la consecuencia de la toxicidad inducida por *V. baccifera*.

6. *V. baccifera* afecta a la señalización de HepG2 mediante la activación de JNK y p38 MAPK, e inhibiendo las vías de supervivencia Akt y ERK. Las alteraciones de los estados de activación de Akt, JNK y ERK dependen de peróxido de hidrógeno, mientras que p38 se activa por mecanismos independientes del H_2O_2.

7. Se observa una respuesta similar en términos de producción temprana de ROS tanto a la pO_2 atmosférica del 21% como a la pO_2 normal de los tejidos del 8%. Estos resultados sugieren que se están llevando a cabo mecanismos similares de señalización y toxicidad, validando, así, el enfoque experimental en el que se ha utilizado 21% de pO_2 para estudiar la respuesta a la toxicidad de *V. baccifera*, y descartando cualquier posible estrés oxidativo superpuesto derivado de las condiciones de cultivo.

6. Referencias

Gallego, A., Torres, F., Robledo, S., Vélez, ID., Carrillo, L., Muñoz, DL., Quiñones, W., Fonnegra, R., Roldán, J., Valencia, L., Triana, O., Echeverri, F. (2006). Actividad leishmanicida y tripanocida de acacia farnesiana, piper arierianum, P. subpedale y Vismia baccifera subsp. Ferruginea.28: 39-49.

Gomez-Cansino, R., Espitia-Pinzon, C.I., Campos-Lara, M.G., Guzman-Gutierrez, S.L., Segura-Salinas, E., Echeverria-Valencia, G., Torras-Claveria, L., Cuevas-Figueroa, X.M., and Reyes-Chilpa, R. (2015). Antimycobacterial and HIV-1 Reverse Transcriptase Activity of Julianaceae and Clusiaceae Plant Species from Mexico. Evid Based. Complement. Alternat Med. 183036.

Hussein, A.A., Bozzi, B., Correa, M., Capson, T.L., Kursar, T.A., Coley, P.D., Solis, P.N., and Gupta, M.P. (2003). Bioactive constituents from three Vismia species. J. Nat. Prod. 6, 858-860.

Lizcano, L.J., Siles, M., Trepiana, J., Hernandez, M.L., Navarro, R., Ruiz-Larrea, M.B., and Ruiz-Sanz, J.I. (2014). Piper and Vismia species from Colombian Amazonia differentially affect cell proliferation of hepatocarcinoma cells. Nutrients 1, 179-195.

Lizcano, L.J., Viloria-Bernal, M., Vicente, F., Berrueta, L.A., Gallo, B., Martinez-Canamero, M., Ruiz-Larrea, M.B., and Ruiz-Sanz, J.I. (2012). Lipid oxidation inhibitory effects and phenolic composition of aqueous extracts from medicinal plants of Colombian Amazonia. Int. J. Mol. Sci. 5, 5454-5467.

Lizcano, L.J., Bakkali, F., Begoña Ruiz-Larrea, M., and Ignacio Ruiz-Sanz, J. (2010). Antioxidant activity and polyphenol content of aqueous extracts from Colombian Amazonian plants with medicinal use. Food Chem. 4,1566-1570.

Vizcaya M, Morales A, Rojas J, Nuñez R. (2012). Revisión bibliográfica sobre la composición química y actividades farmacológicas del género Vismia (Guttiferae).

1. INTRODUCTION

1. INTRODUCTION

1.1. Traditional medicine and *Vismia baccifera*

Plants have formed the basis of traditional medicine systems that have been in existence for thousands of years and continue to provide mankind with new remedies. Natural products and their derivatives represent more than 50% of all the drugs in clinical use in the world. Approximately half of the world flowering plant species live in the tropical forests. Tropical rain forests continue to provide natural product chemists with invaluable compounds of starting points for the development of new drugs. To date about 50 drugs have come from tropical plants. Medicinal plants typically contain mixtures of different chemical compounds that may act individually, additively or in synergy to improve health. Traditional medicine often aims to restore balance by using chemically complex plants, or by mixing together several different plants in order to maximize a synergistic effect or to improve the likelihood of an interaction with a relevant molecular target (Gurib-Fakim, 2006).

Colombia has a great diversity of plant species that are a source of natural products that can be used in treating diseases. One typical plant from the Amazonian rainforest is *Vismia baccifera,* a plant species of the Clusiaceae (Hypericaceae) family, described by Triana and Planchon in 1862. It is commonly used in the traditional healing in indigenous populations. The folk medicine employs the preparation of macerations and decoctions of barks, leaves, stem, and roots of the plants with different curative purposes. *Vismia* was reported as an important purgative or treating disorder of the urinary tract, and as an effective treatment for protecting against snake bites (Ewan, 1962).

Figure 1.1. Image of *Vismia baccifera* species.

It is also used against skin diseases (treatment of wounds, herpes and fungal infections of the skin), and its bark and leaves are used as an antirheumatic and antipyretic (Peres, 1978). Interestingly, the leaves of *V. baccifera* are recommended for a variety of inflammatory conditions, including uterine haemorrhage, and also present leishmanicidal activity (Gallego et al., 2006). A more recent study revealed the anti-plasmodium, antioxidant, antimicrobial and antifungal properties of *Vismia* genus extracts (Vizcaya et al., 2012). In addition to its pharmacological actions, the yellow-orange fruit juice of *Vismia* species can be used as a dye of wool and in food preparations (Peres and Nagin, 1997). In an ethnobotanical study, *Vismia* sp. and three other species were the plants with the highest Use Value among more than 170 species habitually used in a Coreguaje indigenous community located in the upper Caquetá in the Colombian Amazon (Trujillo-C and Correa-Múnera, 2010).

Taxonomy	
Kingdom	Plantae
Phylum	Magnoliophyta
Class	Magnoliopsida
Order	Malpighiales
Family	Hypericaceae
Genus	Vismia
Species	*Vismia baccifera*
Common name	Carate/Punta de lanza

Figure 1.2. Taxonomy of *Vismia baccifera* specie.

An important tool for cancer treatment is the induction of apoptosis in cancer cells (Kornblau, 1998). *In vitro* the cytotoxic effects of various methanolic extracts of leaves from plants belonging to the genus *Vismia* on the human cancer cell lines from breast, lung and central nervous system was reported (Hussein et al., 2003). The authors also isolated from the plants leaves various bioactive anthraquinone constituents (vismione B, deacetylvismione H, deacetylvismione A and bivismiaquinone).

Accordingly, dietary natural products could provide novel preventive or therapeutic options for liver cancer, such as inhibiting tumor cell growth and metastasis, protecting against liver carcinogens, immunomodulating and enhancing effects of chemotherapeutic drugs. For example, black currant bioactive anthocyanins had chemopreventive actions against hepatocarcinogenesis by attenuating oxidative stress through activation of Nrf2 signaling pathway (Thoppil et al., 2012).

1.2. Polyphenols as chemotherapeutic agents

Polyphenols are common constituents of foods of plant origin, and secondary metabolites widely dispersed throughout the plant kingdom. Polyphenols comprise a wide variety of molecules that have a polyphenol structure, several hydroxyl groups on one or more aromatic rings. Polyphenols are divided into several classes according to the number of phenol rings that they contain and to the structural elements that bind these rings to one another. The main groups of polyphenols are: flavonoids, phenolic acids, phenolic alcohols, stilbenes and lignans (D'Archivio et al., 2007).

Flavonoids share a common carbon skeleton of diphenyl propanes, two benzene rings (ring A and B) joined by a linear three-carbon chain. The central three-carbon chain may form a closed pyran ring (ring C) with one of the benzene rings (Fig. 1.3).

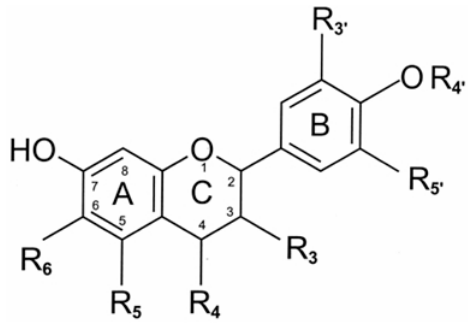

Figure 1.3. General structure and numbering pattern for common food flavonoids.

Flavonoids are themselves classified into 6 subclasses, depending on the oxidation state of the central pyran ring: flavonols, flavones, flavanones, isoflavones, anthocyanidins and flavanols. Flavonols (5%) and flavanols (95%) were characterized by HPLC as the major flavonoids contained in *V. baccifera* leaf extract that has been used in this study (Lizcano et al., 2012).

Flavonols have a double bond between C_2 and C_3, with a hydroxyl group in the C_3-position (Fig. 1.4). They represent the most ubiquitous flavonoids in foods, with quercetin as the more representative compound. The main sources of flavonols are onions (up to 1.2 g/kg fresh wt), curly kale, leeks, broccoli, and blueberries. It is important to note that flavonols biosynthesis is stimulated by light, so they accumulate in the outer and aerial tissue of fruits.

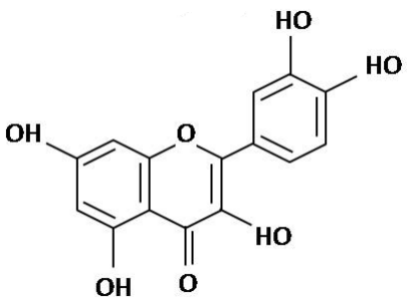

Figure 1.4. Chemical structure of quercetin (flavonol).

Flavanols contain a saturated three-carbon chain with a hydroxyl group in the C_3 (Fig. 1.5). They exist in both the monomer and the polymer form (catechins and proanthocyanidins respectively). Unlike other classes of flavonoids, flavanols are not glycosylated in foods. The main representative flavanols in fruit are catechin and epicatechin, whereas gallocatechin, epigallocatechin, and epigallocatechin gallate are found especially in tea. Green tea (up to 800 mg/L) and chocolate (up to 600 mg/L) are by far the richest sources of catechins, which are also present in red wine (up to 300 mg/L).

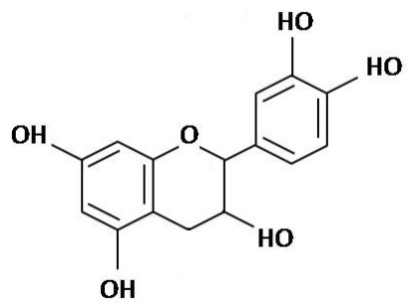

Figure 1.5. Chemical structure of catechin (flavanol).

Generally, food contains complex mixtures of polyphenols. For instance, the polyphenol profiles of all varieties of apples are practically identical, but concentrations may significantly differ among different varieties. Furthermore, numerous factors, such as ripeness at the time of harvest, environmental factors, and storage, may affect the polyphenol content of plants. Regarding the degree of ripeness, phenolic acid concentrations decrease during ripening, whereas anthocyanin concentrations increase.

Polyphenols are the most abundant antioxidants in our diet and are widespread constituents of fruits, vegetables, cereals, olive, dry legumes, chocolate and beverages, such as tea, coffee and wine. Emerging findings suggest a variety of potential mechanisms of action of polyphenols in preventing disease, which may be independent of their conventional antioxidant activities. Furthermore, prooxidant effects of polyphenols have been described (Elbling et al., 2005), having opposite effects on basic cell physiological processes: as antioxidants they improve cell survival, as prooxidant they may induce apoptosis and block cell proliferation. It is worth of note that bioavailability appears to differ greatly among the various polyphenols, and the most abundant ones in our diet are not necessarily those that have the best bioavailability profile.

Diets rich in vegetables and fruits which contain high levels of polyphenols are associated with lower incidence of cancer. Polyphenols has been suggested to be the bioactive compound responsible for this protection. The polyphenols anticancer effect relies on their chemical structure, concentration and on the type of cancer. In solid tumors and hematological malignancies polyphenols exert an important role in apoptosis induction, cell growth inhibition, cell cycle arrest, oxidative stress, and in cell migration and differentiation (Kwee, 2015). In other studies it was provided that an important anticancer mechanism of plant polyphenols is mediated through intracellular copper mobilization and reactive oxygen species (ROS) generation leading to cancer cell death (Khan et al., 2014). In the bibliography, some authors agree that the prooxidative action of polyphenols is responsible of triggering the proapoptotic effect in tumor cells, via ROS increase (Lecci et al., 2014). Furthermore, the prooxidative activity of some polyphenols may also provide a basis for their use as chemotherapeutic adjuvants, reducing Nrf2 expression, and increasing the chemosensitivity of cancer cells to cytostatic drugs, due to the fact that activation of the Nrf2-mediated signaling pathways in cancer cells results in chemoresistance (Stepanic et al., 2015). These results showed that combination of polyphenols and chemotherapy seems to be an interesting approach for cancer treatment.

1.3. ROS sources in hepatocarcinoma cell lines

Liver tumors are an important cause of morbidity and mortality worldwide. Among the most common injuries is hepatocellular carcinoma (HCC). It is a highly chemoresistant tumor that usually develops on a cirrhotic liver with poor tolerance to cytotoxic agents. Currently there is still no standard procedure for treating this disease and the treatments options are palliative.

Reactive Oxygen Species (ROS) consist of radical and non-radical oxygen species formed by the partial reduction of oxygen. They include oxygen radicals such us superoxide ($O_2^{\bullet -}$), hydroxyl ($HO^{\bullet}$), peroxyl ($RO_2^{\bullet}$), and alkoxyl (RO·); and certain non-radicals that are either oxidizing agents and easily converted into radicals, such as hypochlorous acid (HOCl), ozone (O_3), singlet oxygen ($^1O_2$), and hydrogen peroxide (H_2O_2). Nitrogen-containing oxidants, such as nitric oxide, are called reactive nitrogen species (RNS).

Oxidative stress is increased through the generation of ROS and defects in antioxidant defence. Mitochondria include the most important and abundant source of intracellular ROS. Mitochondrial dysfunction therefore plays a central role in the pathological mechanisms of chronic hepatic inflammation and subsequent hepatocarcinogenesis (Wang et al., 2013). An imbalance in the mitochondrial respiratory chain is the main source of reactive oxygen species (ROS).

The transport of high-energy electrons through the mitochondrial electron transport chain is an important step for ATP production. This energy-producing pathway also generates ROS, which accounts for up to 4%-5% of the consumed O_2. The amount of resulting O_2^- increases in damaged mitochondria.

Under physiological conditions, reactive and incompletely reduced forms of oxygen such as O_2^- are detoxified into water by anti-oxidant defences and repair enzymes to maintain a low steady state of toxic oxidants. The main cell antioxidant defenses are superoxide dismutase (SOD), catalase, glutathione (GSH) and its related enzymes: glutathione peroxidase (GPx) and glutathione reductase.

In the bibliography, several researchers aimed to reveal the principal sources of ROS in hepatocarcinoma. For instance, hepatitis virus C (HCV) has been shown to activate several

different pathways that lead to ROS production (reviewed in Ivanov et al., 2013). To date, two different concepts were approved in the field, which assign ROS production either to NADPH oxidases (NOX) or mitochondria (Fig. 1.6). It has been observed that HCV leads to mitochondrial deregulation, often resulting in apoptosis (Okuda et al., 2002). These mitochondrial alterations are accompanied by massive ROS production due to inhibition of electron transport complex I activity. Induction of ROS by HCV has also been shown to be activated through calcium redistribution between ER, cytoplasm and mitochondria (Fig. 1.6) (Presser et al., 2011). A family of NADPH oxidases represents an additional source of ROS in HCV-infected cells (Bedard and Krause, 2007). This family is comprised of seven transmembrane enzymes (NOX 1-5, DUOX 1,2), involved in electron transport through the membranes and thus producing superoxide anion or H_2O_2. In HCV-infected hepatocytes NOX 1 and 4 may act as a primary source of superoxide anion and contribute to production of hydrogen peroxide.

ROS production in HCC might also arise from other sources than mitochondria or NADPH oxidases. One of such potential sources is the ER-residing cytochrome P450 2E1 which is involved in xenobiotic metabolism. Increased production of ROS can also arise from ER stress and the unfolded protein response (UPR), which can be induced by a number of chemicals and various viral infections, which alter protein folding or cause ER overload (Cao and Kaufman, 2012). To tackle ER stress, eukaryotic cells possess a number of defence mechanisms involving expression of various chaperones and other components of the folding machinery, activation of the degradation machinery that targets misfolded polypeptides and suppression of translation.

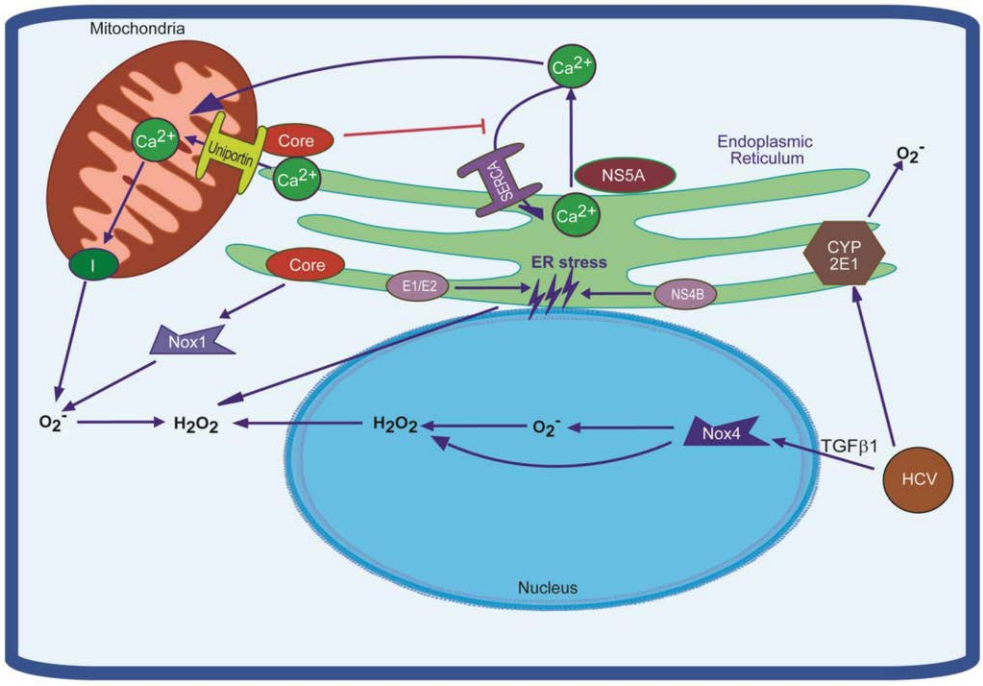

Figure 1.6. Schematic representation of mechanisms of oxidative stress induction in the HCV-infected cells. They include alteration of functioning of the respiratory chain complex I in response to accumulation of calcium ions in mitochondria. This accumulation is achieved via activation of mitochondrial Ca^{2+} uniporter and enhanced passive leakage of the ions from the ER and suppressed SERCA pump, responsible for Ca^{2+} import into the ER. In addition, Hepatitis C virus (HCV) proteins induce NADPH oxidases (NOX) 1 and 4 which contribute to production of H_2O_2 and O_2^-. Finally, the ROS can be generated through ER CYP and induced ER stress (Ivanov et al., 2013).

1.4. ROS influence in the main transduction pathways implicated in HCC

To understand signal pathway regulation by ROS, it is important to know how ROS alters protein function. The oxidative process consists mainly on the oxidation of redox sensitive cysteine residues of proteins by ROS.

Oxidation of these residues forms: reactive sulfenic acid (-SOH), that can form disulfide bonds (-S-S-) with nearby cysteines or undergo further oxidation to sulfinic ($-SO_2H$) or sulfonic ($-SO_3H$) acids; sulfenic acid may also form a sulfenamide if nearby nitrogen is available (Ray et al., 2012) (Fig. 1.7).

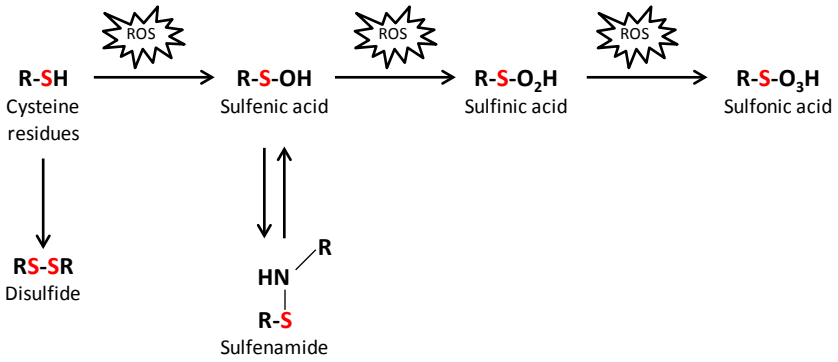

Figure 1.7. Cysteine oxidation states.

These oxidative modifications result in changes in structure and/or function of the protein. With the exception of sulfonic acid, and to a lesser degree sulfinic acid, these redox modifications are reversible by reducing systems such as thioredoxin and peroxiredoxin, which play important roles in signaling (Roos and Messens, 2011).

1.4.1. PI3K/Akt pathway

The first step in the signaling cascade involves the activation of PI3K. Via cell-surface receptor, class I PI3K is recruited to the plasma membrane and associated with the receptor RTK. This leads to transform the substrate PIP_2 in the second messenger PIP_3 (Vara et al., 2004). Afterwards, PIP_3 binds to the pleckstrin homology (PH) domain, present in a large number of downstream effectors, among which Akt (also called PKB) is the main downstream mediator of PI3K signaling cascade.

Akt interacts with PIP_3, causing its translocation to the inner membrane (Fig. 1.8). The interaction of Akt PH domain with phosphoinositides is thought to provoke conformational changes in Akt, resulting in exposure of its two main phosphorylation sites, Thr308 and Ser473 (located at the catalytic domain and the C-terminal hydrophobic motif, respectively). Phosphorylation at both sites is required for Akt activation, and it occurs at the cell membrane (Bellacosa et al., 1998). In fact, phosphorylation at Ser473 is essential for the phosphorylation at Thr308 residue. PDK1 phosphorylates Akt at Thr308; and many kinases have been postulated as responsible for Ser473 phosphorylation (Sarbassov et al., 2005).

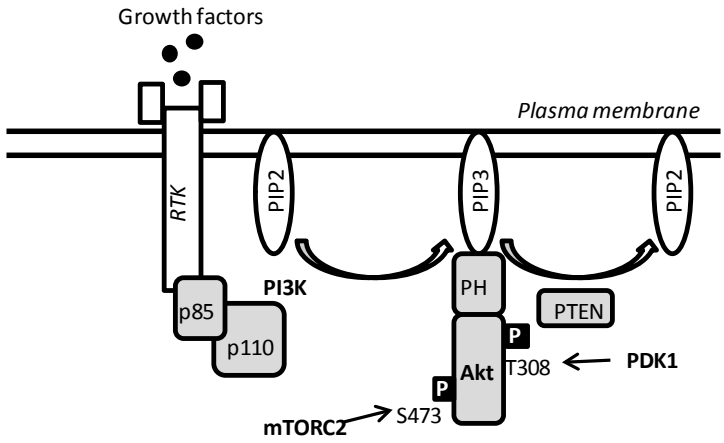

Figure 1.8. PI3K/Akt signaling pathway. PI3K (formed by p85 and p110 subunits) is recruited to the membrane by directly binding to phosphotyrosine consensus residues of growth factor receptors or adaptors through one or both SH2 domains in the adaptor subunit. This leads to allosteric activation of the catalytic subunit. Activation results in production of the second messenger PIP_3. The lipid product of PI3K, PIP_3, recruits a subset of signaling proteins with PH domains to the membrane, including PDK1 and Akt. Phosphorylation at Thr308 and Ser473 sites is required for Akt activation. PTEN is a PIP_3 phosphatase that negatively regulates the PI3K/Akt pathway.

Regarding PI3K/Akt pathway, the synthesis of PIP_3 is negatively regulated primarily by the PTEN phosphatase, which dephosphorylates PIP_3 to PIP_2 (Fig.1.8). Through PTEN, the PI3K pathway is the subject to reversible redox regulation by ROS. H_2O_2 was shown to oxidize and inactivate human PTEN through disulfide bond formation between the catalytic domain Cys124 and Cys71 residues (Lee et al., 2002). PTEN oxidation is reversed by peroxiredoxin II, a cytoplasmic peroxiredoxin isoform that eliminates H_2O_2 generated in response to growth factors (Kwon et al., 2004).

The most important target substrates of Akt promote (Fig. 1.9):

1) Cell survival. Akt enhances the survival of cells by blocking the function of proapoptotic proteins and processes. Akt negatively regulates the function or expression of several Bcl-2 homology domain 3 (BH3)-only proteins, which exert their proapoptotic effects by binding to and inactivating prosurvival Bcl-2 family members. For instance, Akt directly phosphorylates and inhibits the BH3-only protein BAD on Ser136 (Shimamura et al., 2003). Non-phosphorylated BAD promotes apoptosis by binding to and neutralising anti-apoptotic Bcl-2 proteins.

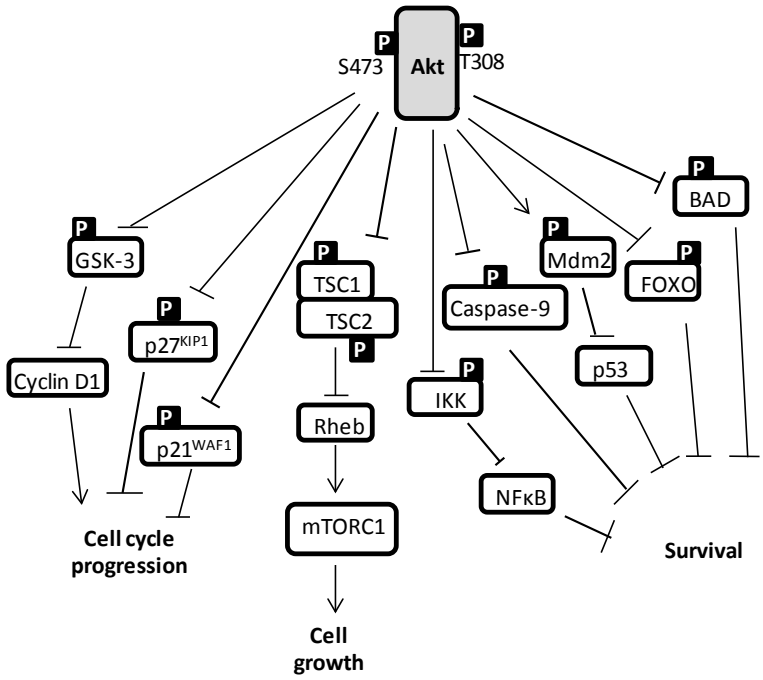

Figure 1.9. Target substrates and main biological functions of Akt signaling. Akt participates in some of the most representative biological processes, such as survival, cell growth and cell cycle progression, by direct phosphorylation of target substrates. (→) activation; (⊣) inhibition; (P) phosphorylation.

Akt also inhibits the expression of BH3- only proteins through effects on transcription factors, such as FOXO and p53. The FOXO transcription factor induces the transcription of genes involved in apoptosis promotion. It is phosphorylated by Akt and retained in the cytoplasm inactivating its transcriptional activity (Brunet et al., 1999). Another target of Akt that promotes survival by inhibiting BH3-only proteins is Mdm2, an E3 ubiquitin ligase that triggers p53 degradation. Akt phosphorylates Mdm2, promoting its translocation into the nucleus, where it diminishes cellular levels of p53, and decreases proapoptotic p53 transcriptional activity (Mayo and Donner, 2001). Akt activation also prevents the processing of procaspase-9 by phosphorylation at Ser196 (Cardone et al., 1998). Akt can also induce NFκB-mediated transcription of pro-survival genes via phosphorylation and proteasomal degradation of IκBα, a negative regulator of NFκB (Ozes et al., 1999).

2) Cell growth. One of the best-conserved functions of Akt is its role in promoting cell growth. The predominant mechanism appears to be through activation of mTOR complex 1,

which is regulated by both nutrients and growth factor signaling (Manning and Cantley, 2007). mTORC1 is a critical regulator of translation initiation and ribosome biogenesis and plays an evolutionarily conserved role in cell growth control. Therefore, Akt activates mTORC1 indirectly by inhibiting the TSC2 tumor suppressor, a critical negative regulator of mTORC1 signaling, thereby allowing Rheb-GTP to activate mTORC1 signaling (Gao and Pan, 2001).

3) Cell proliferation. Akt activation can also stimulate proliferation through multiple downstream targets impinging on cell-cycle regulation. Akt regulates cytoplasmic retention of the $p21^{CIP1/WAF1}$ and $p27^{KIP1}$ cyclin-dependent kinase inhibitors, by direct phosphorylation at Thr145 and Thr157, respectively (Zhou, B.P. et al., 2001; Liang et al., 2002). Furthermore, Akt might also inhibit p21 expression through the phosphorylation and activation of Mdm2 and subsequent down-regulation of p53-mediated transcription of p21 (Mayo and Donner, 2001).

On the other hand, GSK-3 was the first physiological target of Akt to be identified. Akt phosphorylates a serine residue within the N-terminal domain (Woodgett, 2005). Moreover, Akt promotes cell proliferation by preventing cyclin D1 degradation. GSK-3-mediated phosphorylation of the G_1 cyclins cyclin D and cyclin E and the transcription factors c-jun and c-myc, which all play a central role in the G_1-to-S phase cell-cycle transition, promotes its nuclear export and targets them for proteasomal degradation (Ryves and Harwood, 2003). Therefore, phosphorylation and inhibition of GSK-3 by Akt should enhance the stability of these proteins.

1.4.2. The MAPK pathway

Mitogen-activated protein kinase (MAPK) cascades are key signaling pathways involved in the regulation of normal cell proliferation, survival and differentiation. Mammalian cells possess four well characterized and widely studied MAPKs (Fig. 1.10). These cascades are comprised of three Ser/Thr protein kinases that act as a signaling relay controlled, in part, by protein phosphorylation: a MAPK kinase kinase (MAPKKK), a MAPK kinase (MAPKK) and a MAPK (Johnson and Lapadat, 2002). The MAPKs are classified in the extracellular signal-related kinases (ERK1/2), the c-Jun amino-terminal kinases (JNK1/2/3), p38 MAPK (p38 α/β/γ/δ) and ERK5. Generally, the ERK pathway is activated by growth factor-stimulated cell surface

receptors and function in the control of cell division, whereas the JNK, p38 and ERK5 pathways are activated by stress and growth factors.

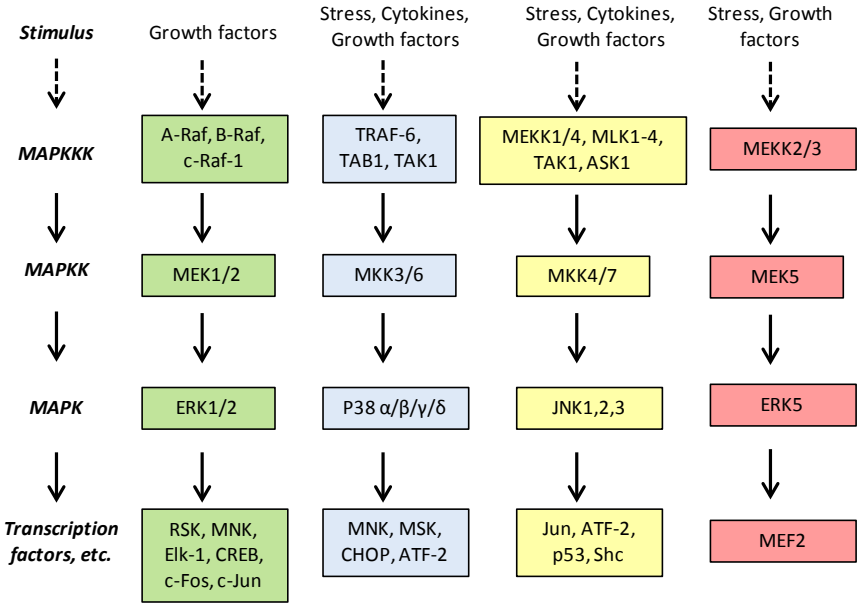

Figure 1.10. Mammalian MAPK cascades.

ERK1/2 are widely expressed and are involved in the regulation of meiosis, mitosis, and postmitotic functions in differentiated cells. Many different stimuli, such as growth factors and cytokines, ligands for heterotrimeric-G protein–coupled receptors, activated the ERK1/2 pathways. ERK1/2 are both components of a three-kinase level that includes the MAPKKK c-Raf1, B-Raf, or A-Raf, which can be activated by the proto-oncogene Ras. Oncogenic Ras persistently activates the ERK1/2 pathways, which contributes to the increased proliferative rate of tumor cells.

The enzymes p38 kinases are classified in four families: p38 α, β, γ, and δ. They regulate the expression of many cytokines. p38 is activated in immune cells by inflammatory cytokines and has an important role in activation of the immune response. p38 MAPKs are also activated by many other stimuli, including hormones, ligands for G protein–coupled receptors, and stresses.

JNK represents a group of enzymes that are activated by exposure of cells to cytokines and environmental stress. JNK is activated by dual phosphorylation of Thr and Tyr residues within a Thr-Pro-Tyr motif located in the kinase domain (Ip and Davis, 1998). The JNKs were discovered to bind and phosphorylate the DNA binding protein c-Jun and increase its transcriptional activity. c-Jun is a component of the AP-1 transcription complex, which is an important regulator of gene expression. AP-1 contributes to the control of many cytokine genes and is activated in response to environmental stress. There are 13 MAPKKKs that regulate the JNKs, and this diversity allows a wide range of stimuli to activate this MAPK pathway. JNKs are important in controlling programmed cell death or apoptosis.

1.4.3. MAPK pathway regulated by ROS

Apoptosis signal-regulated kinase 1 (ASK1) is a conserved mitogen-activated protein 3-kinase which is upstream MAPKKK that regulates the JNK and p38 MAPK cascades, which are essential for inducing apoptosis. p38 and JNK activation via ASK1 may be triggered by ROS (Tobiume et al., 2001) (Fig. 1.12). The molecular mechanism throughout ASK1 is activated consists on the homo-oligomerized by both C- and N-terminal coiled-coil domain interaction and through phosphorylation of a Thr838 residue in the activation loop of the human ASK1 kinase domain (Fig. 1.11). Only the reduced form of thioredoxin interacts with ASK1. Thioredoxin inhibits complete ASK1 oligomerization and subsequent activation. ASK1 is activated when oxidants or ROS oxidize two cysteine residues in the redox centre of thioredoxin; this promotes the dissociation of thioredoxin from ASK1, allowing the oligomerization of ASK1 (Fig. 1.11).

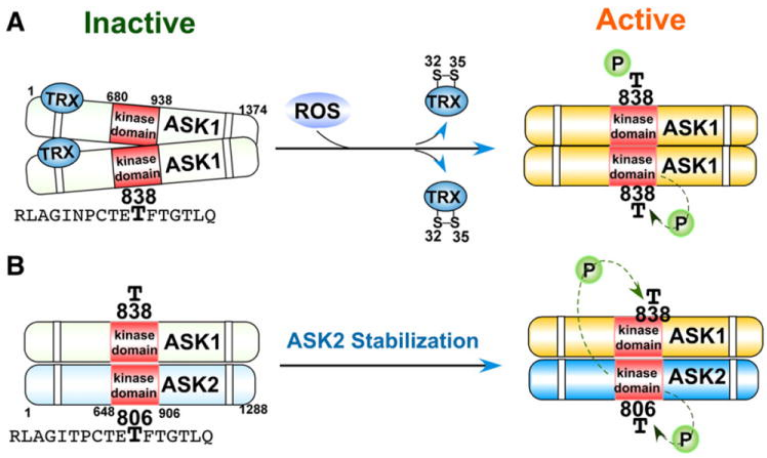

Figure 1.11. Activation of ASK kinases in response to oxidative stress. A) Oxidation of thioredoxin (TRX) results in disulfide bond formation between Cys32 and Cys35 and subsequent dissociation from ASK1. ASK1 undergoes complete homo-oligomerization and subsequent autophosphorylation at Thr838 located in the kinase domain. B) Hetero-oligomerization of ASK1 and ASK2 stabilizes ASK2, resulting in 1) the autophosphorylation of ASK2 at Thr 806, and 2) the subsequent phosphorylation of ASK1 at Thr 838 by ASK2 (Ray et al., 2012).

Another interaction of ROS with the MAPK pathway is the involvement of p38 in apoptosis. ASK1-activation is crucial for p38 ROS-dependent activation and for triggering apoptosis (Pan et al., 2009). A positive feedback may be formed in the ASK1-p38 pathway, which enhances ROS-mediated apoptosis. ASK1 activates both JNK and p38 MAPK; then the activated p38 translocates into the nucleus and stimulates the expression of MK2. After moving out of the nucleus, MK2 increases the TNF-α production. On the other hand, enhanced TNF-α and ROS activate ASK1 (Kuo et al., 2007), which leads to the activation of JNK. JNK inhibits the mitochondria-related anti-apoptotic Bcl-2 (Fig. 1.12). The initial ROS-independent activations of JNK, Bax, and caspase-3 are not sufficient for cell death, and thus, should be re-activated by ROS in order to kill the cells. This role of ROS appears to allow Bcl-2 to block the signaling events, which are initially, induced upstream (Kim et al., 2008). p38α MAPK contributes to the further activation of p53 through a positive feedback loop that strongly enhances the initial p53 activation; at the same time p53 enhances ROS production (Bragado et al., 2007). On the other hand, via MAPKs regulation, the PKCδ mediates apoptosis involving ROS. The localization of PKCδ in response to apoptotic stimuli differentially affects the activation of MAPKs. PKCδ in the cytosol increases the phosphorylation of p38, whereas PKCδ in the nucleus increases JNK phosphorylation (Yacoub et al., 2006).

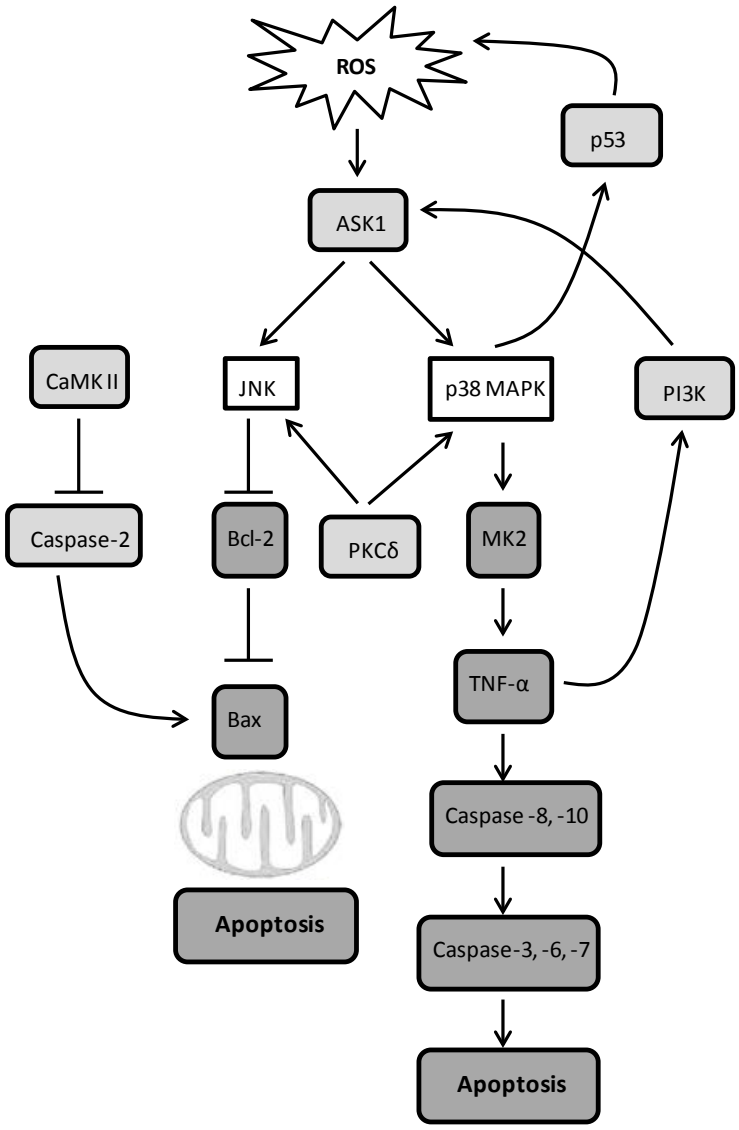

Figure 1.12. ROS-mediated apoptosis. *(→) activation; (┤) inhibition.*

MAPK pathways are also activated by ROS through the direct inhibition of MAPK phosphatases. ROS inhibit JNK-inactivating phosphatases through reversible oxidation of a catalytic cysteine to sulfenic acid, thus sustaining JNK activation (Kamata et al., 2004). ROS, particularly H_2O_2, are used as second messenger that activate p38 in part via the transient inactivation of regulatory protein phosphatases (Robinson et al., 1999). Thus, the MAPK pathway is regulated by ROS in a similar manner as the PI3K pathway.

1.5. Cell cycle control and ROS

Cell division is divided into two stages: 1) mitosis (M), the process of nuclear division, including prophase, metaphase, anaphase and telophase phases; and 2) interphase, the interlude between two M phases, counting with G_1, S and G_2 phases (Vermeulen et al., 2003) (Fig. 1.13). Replication of DNA occurs in the interphase or S phase. Before that, in the G_1 phase, the cell is preparing for DNA synthesis. After S phase, during G_2, the cell prepares for mitosis. Cells in G_1, before DNA replication, can enter in a resting state G_0 where cells neither grow nor proliferate.

Two types of mechanisms exist for cell cycle control: 1) the cyclin-dependent kinases (CDK) system, a cascade of Ser/Thr protein kinases that relay a cell from one stage to the next one, and 2) a set of checkpoints that delay progression to the next stage if necessary.

1.5.1. Cyclin-CDK complexes

The cyclin-CDKs constitute active complexes with unique substrate specificity, ensuring well-delineated transitions between cell cycle stages. CDK protein levels remain stable during the cell cycle, in contrast to their activating proteins, the cyclins. Cyclin protein levels rise and fall during the cell cycle and in this way they periodically activate CDK. Different cyclins are required at different phases of the cell cycle, forming cyclin-CDK complexes (Fig. 1.13). During G_1 several complexes can be formed: cyclins D (D1, D2 and D3)/CDK4, cyclins D/CDK6, and the cyclin E/CDK2, which regulates progression from G_1 into S phase and directs entry into S-phase (Nurse et al., 1998). S-phase progression is directed by the cyclin A/CDK2 complex (Girard et al., 1991). In late G_2 and early M, cyclin A/CDK1 complex promotes entry into M phase. Mitosis is further regulated by cyclin B/CDK1 complex (Sánchez and Dynlacht, 2005). These cyclins require specific protein sequences for efficient ubiquitin-mediated cyclin proteolysis at the end of a cell cycle phase (Glotzer et al., 1991). Cyclins A and B contain a destruction box, and cyclins D and E contain a PEST sequence. On the other hand, CDK activity can be regulated by cell cycle inhibitory proteins, called CDK inhibitors (CKI) which bind to CDK alone or to the CDK-cyclin complex and regulate CDK activity. Two families of CKI have been defined based on their structure and CDK targets: 1) the Ink4 (Inhibitors of CDK4) family ($p15^{Ink4b}$, $p16^{Ink4a}$, $p18^{Ink4c}$ and $p19^{Ink4d}$), which bind to monomeric CDK4 and CDK6 but not to CDK2, thereby precluding the

association of these CDKs to cyclins D (Ortega et al., 2002), and 2) the Cip/Kip family ($p21^{Cip1/Waf-1}$, $p27^{Kip1}$ and $p57^{Kip2}$) all of them containing characteristic motifs at their N-terminal moieties that able them to bind both CDK and cyclins, inactivating CDK-cyclin complexes (Lee et al., 1995).

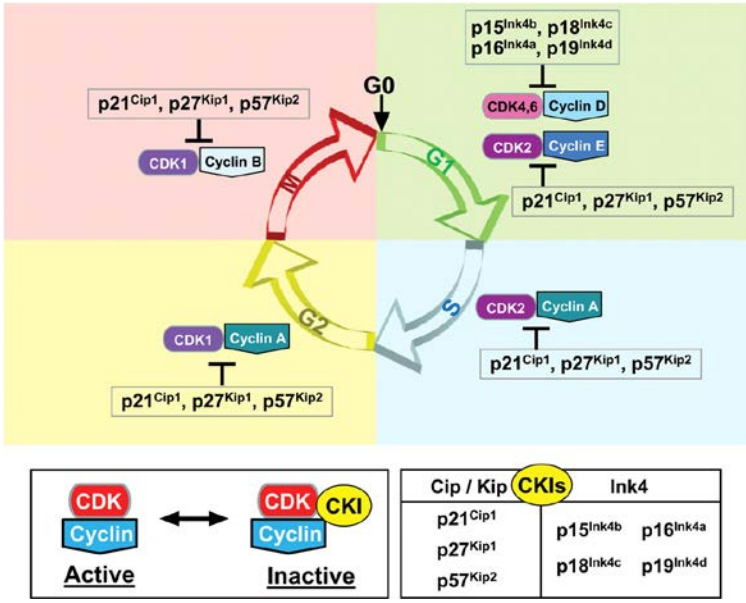

Figure 1.13. Mammalian cell cycle regulation by CDK/cyclin holoenzymes and CKIs. (Fuster et al., 2010).

1.5.2. The G_1 checkpoint

The decision to continue through the cell cycle after mitosis in growing cells is made in G_1 and requires signaling through Ras and expression of cyclin D1 (Hitomi and Stacey, 1999). All the cells continuing through G_1 pass across the central regulatory decision at the restriction point. The restriction point (or R point) is defined as a point of no return in G_1, following which the cell is committed to entry into S phase. The R point functionally corresponds to phosphorylation of retinoblastom protein (pRB) by cyclin D/CDK complexes (Fuster et al., 2010).

pRB is a negative regulator of cell proliferation that regulates transcription (Dick, 2007). Although pRB is transiently inactivated as cells progress through the cell cycle in normal cells, this control mechanism is disrupted in most tumor cells (Weinberg, 1995). The best known targets of pRB are the E2F transcription factors (Chellappan et al., 1991; Girling et al., 1993).

E2Fs form heterodimeric complexes that bind to DNA in a sequence- specific manner, and regulate the expression of many S-phase genes.

pRb binding to E2F transcription factors blocks their ability to induce transcription of genes that are needed to advance the cell cycle (Fig. 1.14). In turn, once pRB is brought to a promoter by an E2F it can recruit chromatin remodelling proteins such as histone methyltransferases, DNA methyltransferases, histone deacetylases, and helicases among others to further repress transcription (Magnaghi-Jaulin et al., 1998). Stimulation of cell cycle entry results in phosphorylation of pRB by cyclin/CDK complexes which causes the release from E2Fs and chromatin regulators at the G_1 to S-phase transition, thereby activating the S-phase gene expression program (Fig. 1.14).

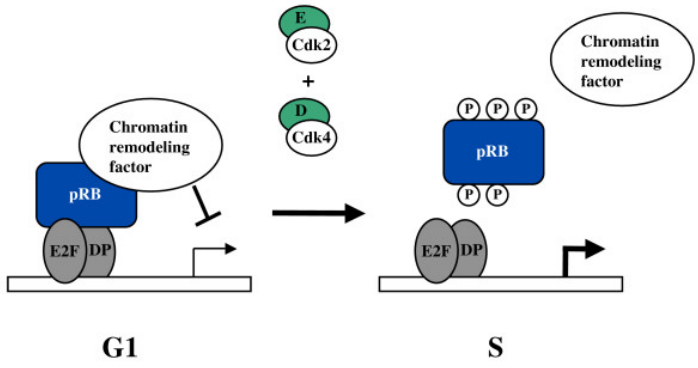

Figure 1.14. Transcriptional control of the cell cycle by pRB (Dick, 2007).

The ability of pRB family members to repress E2F dependent transcription is controlled by CDKs (Lees et al., 1991). Cyclin D/CDK4/6 complexes promote early G_1 progression, but cyclin E/CDK2 activity (Aleem et al., 2005) is required to inactive pRb by hyperphosphorylation to transit the restriction point into late G_1 phase (Fig. 1.14). The pRb inactivation, realising the E2F transcription factors, induces late-G_1-specific genes: such as cyclin A (Hsu et al., 2002). Although the cyclin A required to initiate DNA synthesis is transcriptionally induced by E2F at the restriction point, it does not accumulate until the late G_1/S phase transition due to ubiquitination by the anaphase promoting complex (APC) and subsequent proteolysis by the 26S proteasome (Hsu et al., 2002). APC is active throughout G_1 phase by association with Cdh1 (APC^{Cdh1}), an activator that confers substrate specificity (Fang et al., 1998) (Fig. 1.15). However,

before initiating of S phase, APC^{Cdh1} is inactivated by the binding of Emi1 to Cdh1, resulting in stabilization of cyclin A, activation of cyclin A-associated kinase activity, and subsequent inactivation of Cdh1 by phosphorylation (Reimann et al., 2001). In addition to cyclin A, other proteins necessary for DNA replication have been identified as APC substrates (Ferreira et al., 2000).

Regarding the possibility that ROS regulate the transition from G_1 to S phase, it has been asserted that an increase in the steady-state levels of endogenous ROS is required to inactivate APC^{Cdh1}, allowing cyclin A accumulation, and transition into S phase (Fig. 1.15) (Havens et al., 2006).

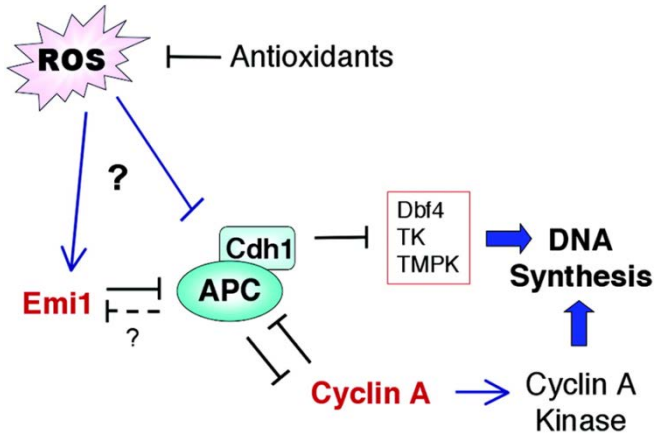

Figure 1.15. Model of APC^{Cdh1} activity inhibition by ROS. Increase in ROS levels results in inactivation of a late G_1 phase checkpoint, characterized by active cyclin E-CDK2 complexes, inactive hyperphosphorylated pRb, and induction of E2F target genes, including cyclin A and Emi1 (Havens et al., 2006).

Another ROS regulatory mechanism consists on redox-dependent effects on the phosphorylation of pRB that emerges from studies with antioxidants (Menon et al., 2003). When mouse embryonic fibroblasts were treated with *N*-acetyl-l-cysteine (NAC), a GSH precursor, the intracellular redox state became more reducing, and cells arrested in G_1 with a 70% decrease in cyclin D1 levels, increased levels of p27 and pRB hypophosphorylated. When NAC was removed, p27 levels dropped, cyclin D1 levels and phosphorylation of pRB increased, entering cells in the S phase (Menon et al., 2003).

Moreover, the G_1 checkpoint also depends on increased expression and activation of the TP53 gen product (Kastan et al., 1991). p53 tumor suppressor is mutated in more than 50% of human tumors, and is activated through post-translational mechanism in response to DNA damage or oxidative stress (Nelson and Kastan, 1994).

p53 structure reveals many potential levels at which the activity of the tumor suppressor could be regulated. Human p53 contains 393 amino acids distributed in 6 well differentiated domains (Olsson et al., 2007) (Fig. 1.16):

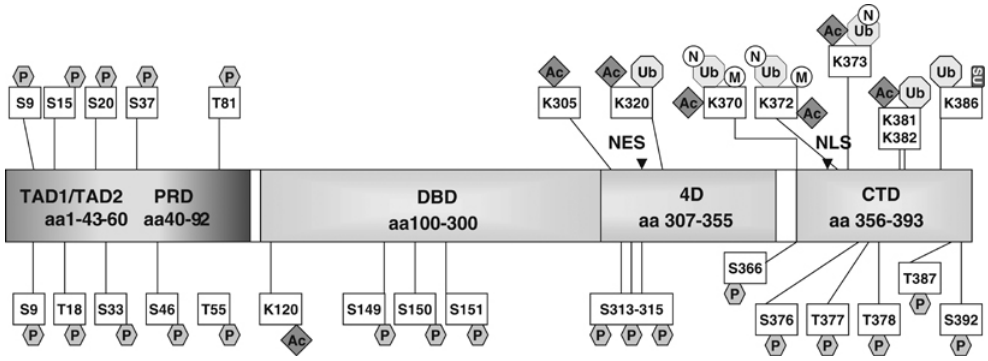

Figure 1.16. Domain-structure of human p53. The p53 protein consists of six major domains: TAD1 and 2 (transactivation domains), PRD (proline-rich domain), (DBD) DNA binding domain, (4D) tetramerization domain, and (CTD) the carboxy-terminal regulatory domain. Post-translational modifications are depicted in the individual domains of p53: P (phosphorylation), Ac (acetylation), Ub (ubiquitination), M (methylation), N (neddylation) and SU (sumoylation). *NLS, nuclear localization signal; NES, nuclear export signal.* (Olsson et al., 2007)

Regarding post-translational modifications of p53, different stimuli such as irradiation, genotoxic stress or DNA damage stabilize and activate p53. This involves a series of post-translational modifications all along its structure leading to a more stable protein (Fig. 1.16). Phosphorylation at the N-terminus region of the molecule is one of the most common modifications, while the C-terminus domain can also be subjected to ubiquitination, neddylation, methylation, sumoylation and acetylation (Olsson et al., 2007).

p53 is constitutively polyubiquitinated by Mdm2 and targeted for proteasomal degradation (Haupt, 1997). After stress stimulus, p53 acts as a transcription factor accumulating in the nucleus, where it enhances the transcription of several target genes, including Mdm2 (Michieli et al., 1994) (Toledo and Wahl, 2006).

Under stress, p53 promotes cell cycle arrest, preventing the replication of damaged DNA, or apoptosis, eliminating defective cells. The choice between both events depends on the type, duration and intensity of the stress, the p53 machinery present in the cell, the cell Rb/E2F balance, and the efficiency of DNA repair process (Sionov and Haupt, 1999). p53 regulates the expression of proteins implicated in cell cycle arrest (Fig. 1.17), such as $p21^{WAF1}$ (Sionov and Haupt, 1999). Interestingly, oxidants can induce p21 expression in a p53-independent manner (Esposito et al., 2001).

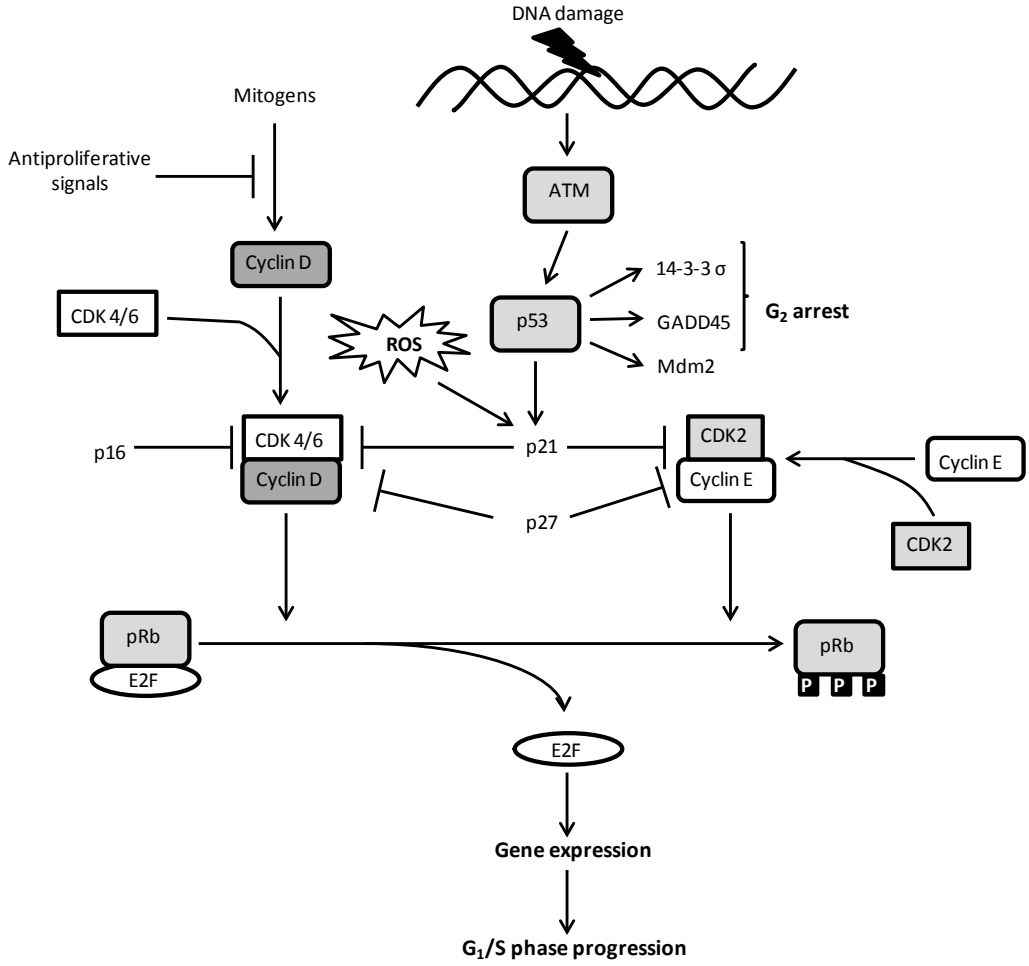

Figure 1.17. Schematic representation of cyclin/CDK protein kinase regulation in the G1 transition into S phase.

On the other hand, p53 also regulates the programmed cell death or apoptosis to eliminate severely injured cells, avoiding perpetuation damaged DNA. p53 plays an essential

role in both intrinsic and extrinsic apoptotic pathways (Fig.1.18) (Sionov and Haupt, 1999). In both cases, p53 plays an essential role (Haupt et al., 2003). Furthermore, ROS are downstream mediators of p53-dependent apoptosis (Johnson et al., 1996) (Cardaci et al., 2008).

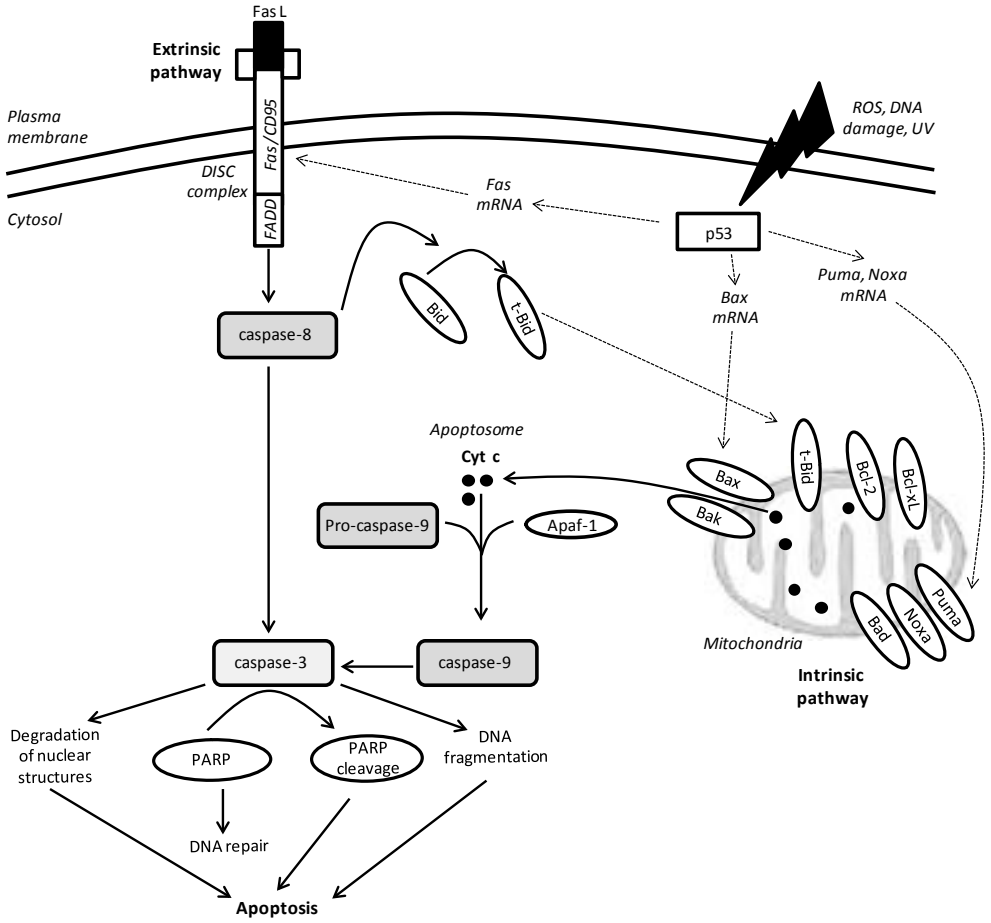

Figure 1.18. Role of p53 in apoptosis. p53 induces the expression of FAS receptor mRNA. Through binding to FAS ligand (Fas L), the sequential induction of caspase-8 and -3 promotes DNA fragmentation and cell death. At the same time, p53 induces the expression of Puma, Noxa and Bax genes triggering programmed cell death via mitochondrial pathway. The released of cytochrome c from the mitochondrial compartment to the cytosol induces a sequential activation of caspase-9 and -3, leading to cell death.

At the molecular level, the control of S phase entry may be due to the regulation of cyclin A and cyclin D levels, as well as the regulation of pRb and p53 phosphorylation.

1.5.3. Control of S phase

Similar to the G_1 and G_2 checkpoint responses, the S checkpoint response can be induced by a wide variety of DNA damages. Furthermore, experiments with human fibroblasts exposed to ionizing radiation proved that p53 is not involved in the immediate S-phase response to DNA damage (Cistulli and Kaufmann, 1998). However, cyclin A/CDK2 activity is thought to be required for S phase progression and DNA synthesis (Fuster et al., 2010). In addition, the gene mutated in ataxia-telangiectasia product (pATM) may be an upstream regulator of cyclin A/CDK2 activity (Beamish et al., 1996).

ROS can also induce cell cycle arrest in S phase through mechanisms in addition to the classical ATM-dependent DNA-damage response. As in G_1, pRB is an important target of oxidative stress in S phase. When cycling endothelial cells were treated with H_2O_2, pRB became rapidly dephosphorylated and DNA synthesis was inhibited; but this dephosphorylation was not dependent on p21 or p53, otherwise because of the activity of PP2A (Cicchillitti et al., 2003). PP2A binding and dephosphorylation of pRb in S phase in response to oxidants suggests cells may anticipate oxidative DNA damage (Magenta et al., 2008). For this reason, it could be possible that pRB serves as a redox-dependent sensor and may become dephosphorylated, inducing S-phase arrest in response to modest levels of oxidants well before replicating DNA is subjected to excessive oxidative damage (Burhans and Heintz, 2009).

1.5.4. The G_2 checkpoint

Movement of cells from G_2 to M phase is regulated by cyclin A, and by cyclin B/CDK1. ROS production can trigger a G_2 checkpoint response that results in a delay in the activation of cyclin B/CDK1 at the G_2/M transition. Treatment of cells with ionizing radiation results in an accumulation of CDK1 phosphorylated in Thr14 and Tyr15, resulting in inhibition of cyclin B/CDK1 (Fig. 1.19) (Herzinger et al., 1995). Activation of cyclin B/CDK1 occurs through the action of the CDC25C phosphatase, which removes the Thr14 and Tyr15 phosphates (Gautier et al., 1991). Hyperphosphorylation of CDC25C, correlated with increased phosphatase activity, does not occur in cells arrested in G_2 by DNA damage (O'Connor et al., 1994). In addition, the association between the cyclin B/CDK1 complex and CDC25C may be blocked

through Chk1 and Chk2 kinases. Throughout interphase, but not in mitosis, Chk1 and Chk2 phosphorylate CDC25C on Ser216, inhibiting its activity by binding to 14-3-3σ proteins and sequestering it in the cytoplasm (Peng et al., 1997). p53 is implicated in blocking the transition through G_2/M cell-cycle checkpoint by inducing the expression of 14-3-3σ and GADD45. Both proteins inhibit the activity of cyclin B/CDK1 complex which is essential during G_2-to-M phase transition (Peng et al., 1997; Wang et al., 1999). It appears that Chk2 is activated through phosphorylation by pATM (Fig. 1.19) (Matsuoka et al., 1998).

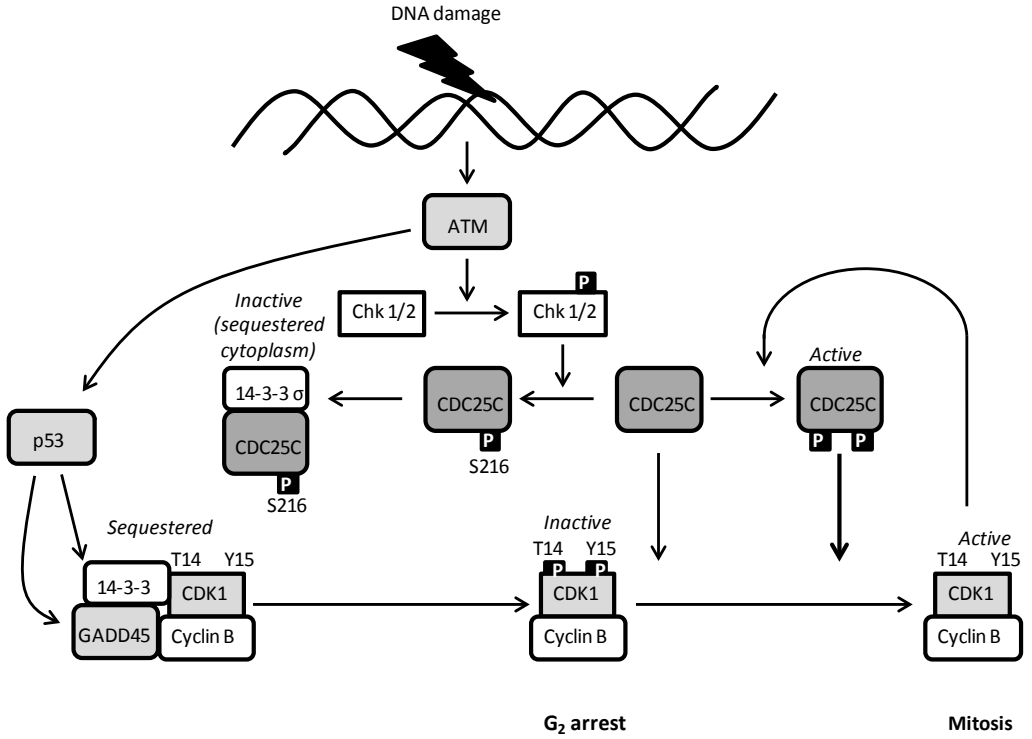

Figure 1.19. A schematic representation of the suggested interactions of proteins in the G_2 checkpoint signal transduction response to double-stranded DNA breaks.

Other levels of G_2 checkpoint regulation exist. Cyclin B/CDK1 complexes are cytoplasmic in S/G_2, and enter into the nucleus in late G_2 for controlling mitotic entry (Gallant and Nigg, 1992). Cyclin B/CDK1 complexes are retained in the cytoplasm after ionizing radiation treatment, suggesting that differential localization for the complex may account for some aspects of the G_2 checkpoint function (Jin et al., 1998).

1.5.5. DNA damage response

During the very earliest stages of checkpoint activation, DNA damage sensors send information to members of a family of phosphoinositide 3-kinase related kinases (PIKKs) (Baretic and Williams, 2014). The PIKKs family is formed by mTOR, ATM, ATR, SMG-1, TRRAP and DNA-PK proteins. In mammalian cells, the two PIKK family members, ATM (ataxia-telangiectasia mutated) and ATR (ATM and Rad 3-related), play critical roles in early signal transmission through cell cycle checkpoints (Marechal and Zou, 2013).

ATM exists as dimers or oligomers in undamaged cells, and under DNA damage is converted into monomers and is autophosphorylated (Fig. 1.20) (Bakkenist and Kastan, 2003).

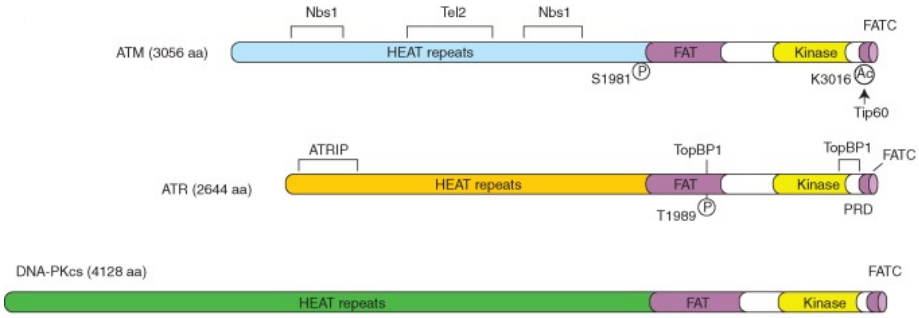

Figure 1.20. Schematic of the functional domains and selected post-translational modifications of ATM, ATR, and DNA-PKcs. The bulk of ATM and ATR are composed of a large number (40–50) of α-helical HEAT repeats. The kinase domains of ATM and ATR are located near their carboxyl termini, and are flanked by FAT and FATC domains. ATM and ATR are autophosphorylated in or near their FAT domains after DNA damage, which regulates their activation (Marechal and Zou, 2013).

The two main signaling pathways activated by DNA damage consist on the ATM–Chk2 and ATR–Chk1 protein kinases (Sancar et al., 2004). Among ATM and ATR substrates, are the Ser/Thr checkpoint effector kinases Chk1 and Chk2, which are selectively phosphorylated and activated by ATR and ATM, respectively (Bartek and Lukas, 2003). Both ATM and ATR proteins respond to different damage; whereas ATM is primarily activated by double-stranded DNA breaks (DSBs), ATR responds to a broad spectrum of DNA damage, like single-stranded DNA (ssDNA) (Zou and Elledge, 2003).

Following the initial activation of ATM by DNA ends (Lee and Paull 2005), ATM phosphorylates the histone H2AX (known as γH2AX), within minutes after DNA damage, and it rapidly spreads over large chromatin domains flanking the DNA breaks (Fig. 1.21) (Savic et al., 2009). For recognizing specifically the chromatin flanking DSBs, ATM needs the key mediator Mdc1. Through its BRCT domains, Mdc1 directly binds to phosphorylated γH2AX (Stucki et al., 2005). Autophosphorylation of ATM has been implicated in Mdc1 binding. Interestingly, ROS may directly trigger ATM autophosphorylation and promote its localization to DSBs (Guo et al. 2010).

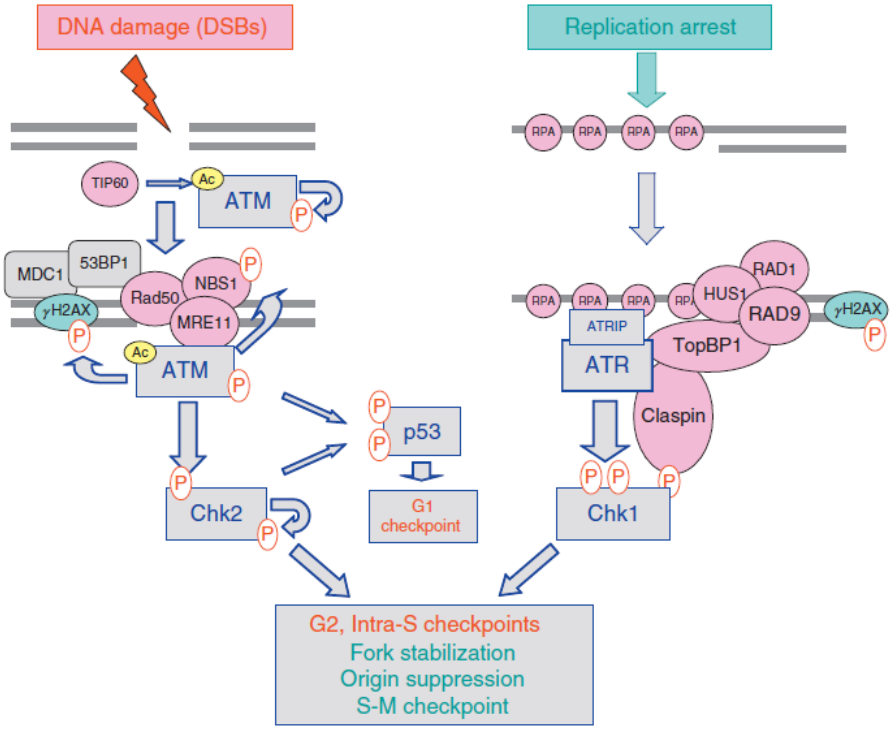

Figure 1.21. Activation of the ATM–Chk2 and ATR–Chk1 pathways in response to DNA damage. The ATM–Chk2 and ATR–Chk1 pathways are activated selectively by DSBs and tracts of ssDNA complexed with RPA respectively. DSBs in chromatin stimulate ATM autophosphorylation and acetylation but full activation also requires recruitment to sites of damage in conjunction with the MRN complex where ATM modifies multiple substrates including the downstream effector kinase, Chk2. ATR is recruited to tracts of ssDNA-RPA through its interacting partner, ATRIP, where it phosphorylates and activates Chk1 in conjunction with the TopBP1 and Claspin mediator proteins. *Phosphorylation events are indicated by (P) in orange, acetylation by (Ac) in yellow.* (Smith et al., 2010)

The localization of ATR kinase and its regulatory partner ATR-interacting protein (ATRIP) to sites of DNA damage is dependent on the direct interaction between ATRIP and replication protein A (RPA)-coated ssDNA (single-stranded DNA), suggesting that ssDNA may be the key structure that elicits the ATR response at sites of DNA damage (Zou and Elledge, 2003) (Fig. 1.21).

The binding of ATR-ATRIP to RPA-ssDNA not only provides a mechanism to recruit the kinase to sites of DNA damage, but also a mean to promote ATR autophosphorylation at Thr1989 and activation (Liu et al., 2011; Mordes and Cortez, 2008).

Although ATM is activated by DSBs and ATR primary by ssDNA, they are known to cross talk with each at multiple levels: 1) ATM and ATR can influence the localization of each other to sites of DNA damage. ATM promotes the activation of ATR by enhancing DNA end resection (Shiotani and Zou, 2009). On the other hand, ATR was shown to phosphorylate γH2AX in response to DNA replication stress, which may recruit ATM to the chromatin (Ward and Chen, 2001). 2) ATM and ATR may directly phosphorylate each other. ATM is phosphorylated by ATR at Ser1981 in response to DNA replication stress (Stiff et al., 2006). 3) ATM and ATR may affect the function and localization of each other's regulators. Many proteins are phosphorylated in an ATM/ATR-dependent manner during the DNA damage response (Matsuoka et al., 2007). There is evidence that ATM and ATR function redundantly in the phosphorylation of some of these proteins, due to the fact that both ATM and ATR may phosphorylate the same sites or different sites in these substrates.

1.6. Endoplasmic reticulum stress

The endoplasmic reticulum (ER) contains chaperones and enzymes, which are involved in protein folding. Only properly folded proteins are modified at the Golgi apparatus and translocated to their destined sites. On the other hand, misfolded or immature proteins aggregate in the ER lumen and are degraded by the ER-associated degradation (ERAD) machinery or by autophagy (Smith, 2011). This is due to the fact that misfolded proteins are able to expose their hydrophobic residues that enhance protein aggregation, triggering ER stress (Fazi et al., 2009). Cells activate the *unfolded protein response* (UPR) in response to this

situation. This ER stress response has four main purposes: 1) attenuation of protein synthesis to prevent any further protein aggregation, 2) transcriptional induction of ER chaperone genes, 3) transcriptional induction of ERAD genes to increase ERAD capacity, and 4) induction of apoptosis to remove stressed cells and to ensure the survival of the organism (Yoshida, 2007).

Three different protein sensors exist in the ER membrane to initiate the UPR: inositol-requiring kinase 1 (IRE1), pancreatic ER eukaryotic translation initiation factor 2 eIF2α kinase (PERK), and activating transcription factor 6 (ATF6). Binding of the ER luminal protein chaperone BiP/GRP78 to the UPR sensors prevents their signaling.

1.6.1. IRE1-XBP1 pathway

The most conserved ER stress sensor is IRE1, a type I ER transmembrane protein with both a Ser/Thr kinase domain and an endoribonuclease (RNase) domain in the cytosolic portion (Maly and Papa, 2014) (Fig.1.22). There are two homologues in mammals: IREα, expressed in most cells and tissues, and IREβ, whose expression is mostly restricted to the intestinal epithelium (Wang et al., 1998). IRE1 is maintained in an inactive monomeric form through interactions with the GRP78 chaperone in not non-stressed cells. However, under conditions of ER stress the luminal domain of IRE1 is released from GRP78 and undergoes homodimerization and trans-autophosphorylation to activate its RNase activity (Welihinda and Kaufman, 1996). The activated IRE1 initiates the cleavage and removal of a 26-base intron from the mRNA encoding X-box-binding protein 1 (XBP1) (Yoshida et al., 2001). This splicing reaction creates a translational frameshift to produce the active CREB/ATF transcription factor, a larger form of XBP1, which contains a transcriptional activation domain in the C-terminus. A variety of UPR target genes are activated by the spliced XBP1 such as those genes that encode functions involved in ERAD, in ER protein folding, intracellular trafficking, phospholipid biosynthesis, and ER membrane expansion (Yoshida et al., 2003). In addition, the RNase domain of IRE1 also degrades a subset of mRNAs localized in the ER during ER stress, a process called regulated IRE1-dependent decay of mRNA (RIDD), thus reducing protein synthesis to alleviate ER stress. Furthermore, IREα kinase domain integrates ER stress with pro-inflammatory responses through direct binding with the TRAF2 adaptor protein, in the TNFα signaling pathway. The IREα-TRAF2 complex activates NFκB through phosphorylation and degradation of IκB.

Moreover, the IREα-TRAF2 complex also recruits ASK1, which activates JNK pathway to induce pro-apoptotic pathway in response to ER stress (Urano et al., 2000). In addition, IRE1α degrades specific miRNAs that target the mRNA encoding casapase-2, thereby boosting caspase-2-dependent apoptosis during ER stress (Upton et al., 2012).

1.6.2. PERK-eIF2α-ATF4-CHOP

PERK is a type I ER-associated transmembrane protein with a cytosolic Ser/Thr kinase domain (Fig.1.22). During ER stress the chaperone GRP78 is released from PERK, which then undergoes dimerization and trans-autophosphorylation (Harding et al., 2000). Activated PERK phosphorylates Ser51 on the α subunit of eIF2α, which attenuates translation initiation to reduce the ER protein-folding load. In addition, phosphorylated eIF2α is required for selective translation of a subset of mRNAs, including ATF4, a potent bZIP transcription factor that activates genes for amino acid biosynthesis, trafficking machinery and ER chaperones, antioxidative stress responses, and autophagy (Harding et al., 2003). One of the downstream targets of ATF4 is CHOP, a bZIP transcription factor whose promoter contains the binding sites for transactivators of the UPR, including ATF4 and ATF6. Furthermore, CHOP plays a crucial role in ER stress-induced apoptosis, inducing pro-apoptotic factors such as Bid, Puma, DR5 and TRB3, and inhibiting the Bcl-2 anti-apoptotic protein (Ghosh et al., 2012) (Tabas and Ron, 2011). In addition, CHOP causes oxidative stress by inducing ERO1α *(reviewed in section 1.6.4.)*, which transfers electrons from protein disulfide isomerase to O_2 to produce H_2O_2. When protein folding is defective, the increase in protein synthesis produces more misfolding inducing cell death through oxidative stress.

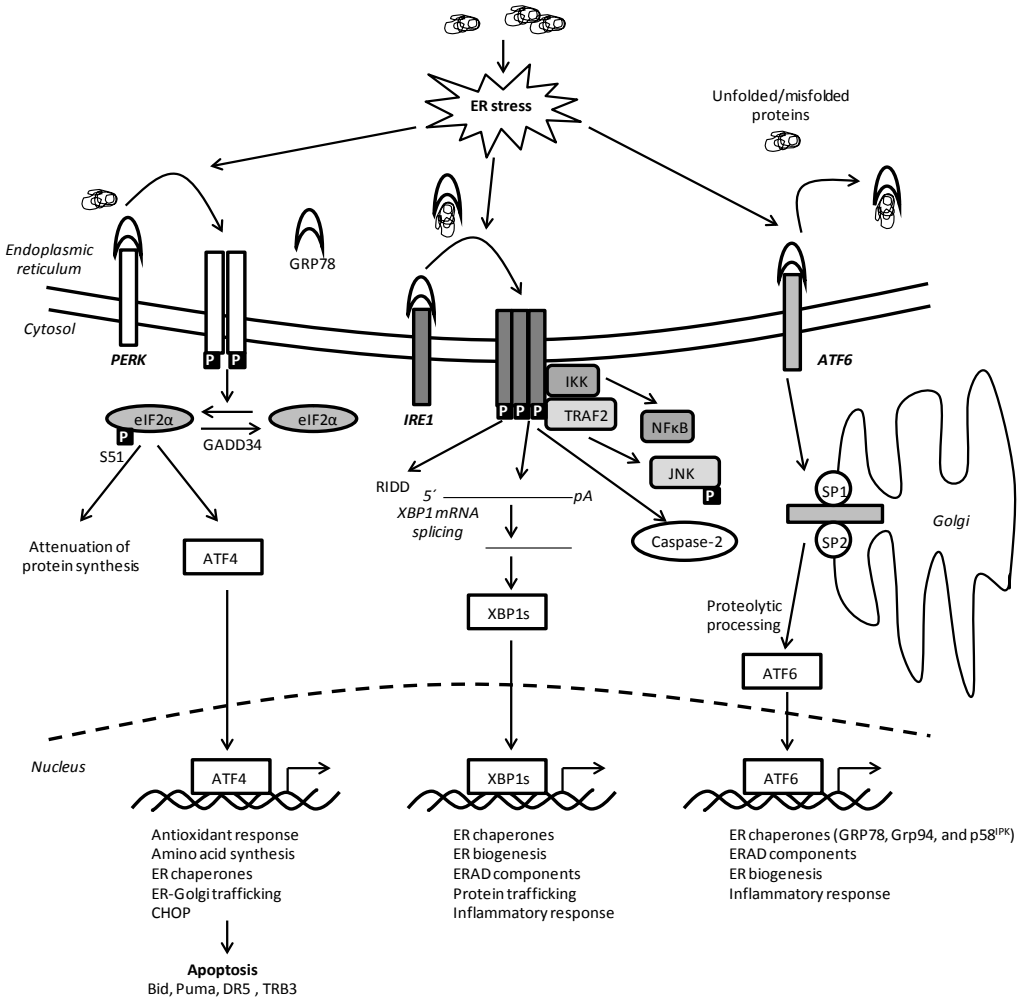

Figure 1.22. Endoplasmatic reticulum (ER) stress and unfolded protein response (UPR) induction. In most mammalian cells, three UPR branches were identified: the PERK-eIF2α-ATF4-CHOP pathway, the IRE1α-XBP1 pathway, and the ATF6 pathway. *(→) activation; (P) phosphorylation.*

1.6.3. ATF6

The ATF6 is a type II ER transmembrane protein with a CREB/ATF bZIP domain at its N-terminal domain (Fig.1.22). In response to ER stress, release of the GRP78 chaperone from the luminal domain permits trafficking of ATF6 to the Golgi apparatus, where ATF6 is sequentially cleaved by two proteases: the S1P cleaves ATF6 in the luminal domain, and the S2P cleaves the N-terminal domain (Ye et al., 2000). After that, the released ATF6 cytosolic fragment migrates to the nucleus to activate gene transcription binding to the ER stress response element (Yoshida

and Mori, 2001). ER chaperone genes such as GRP78 and some ERAD components are regulated by ATF6. In addition, PERK/eIF2α/ATF4 pathway also induces ATF6 activation and its target genes (Teske et al., 2011). It is known that the regulatory networks of the UPR are fully integrated, because ATF6α can heterodimerize with XBP1 in response to ER stress, inducing the expression of ERAD components (Lee et al., 2002).

1.6.4. The role of ROS in ER stress

ROS and oxidative stress are integral UPR components, being triggered by distinct types of ER stressors. Thus, ROS generation can be upstream or downstream of UPR targets. The major enzymatic mechanisms of ROS production during UPR activation are: 1) multiple thiol-disulfide exchanges involving ER oxidoreductases including the ERO1 and PDI, 2) mitochondrial electron transport, and 3) Nox4 oxidase complex (Santos et al., 2009).

The redox status in the lumen of the ER affects protein folding and disulfide formation. The lumen of the ER has a highly oxidizing environment, with a high GSSG/GSH ratio, which facilitates disulfide bond formation and prevents the aggregation or accumulation of misfolded proteins in the ER (van der Vlies et al., 2003). Before secreting the properly folded proteins from the ER lumen, the thiol groups of cysteines of proteins are oxidized and form disulfide bonds for protein stability and maturation. The formation of disulfide bonds is driven by PDI and ERO1. ERO1 uses a FAD-dependent reaction to transfer electrons from PDI to molecular oxygen (Gross et al., 2004). When incorrect disulfide bonds are formed, GSH assists in reducing them, and this increases the GSSG/GSH ratio. This condition alters the redox environment in the ER. Indeed, two mechanisms have been proposed for ROS generation during disulfide bonds formation: 1) ROS are formed as a by-product during the transfer of electrons from protein thiol to molecular oxygen by ERO1 and PDI, or 2) ROS are generated during protein misfolding due to the depletion of GSH; thus ROS may be generated by unfolded proteins independently of the disulfide bonds formation (Tu and Weissman, 2002).

ER and mitochondria seem to be tuned during ER stress through (Fig. 1.23): 1) close proximity between mitochondria and ER supporting physical interaction, and 2) alternation in Ca^{2+} regulation, which affect to membrane potential, ATP depletion and ROS formation. Indeed, protein folding in the ER lumen is a highly energy-dependent process, and ATP

depletion may stimulate mitochondrial oxidative phosphorylation to increase ATP and ROS production. Moreover, accumulation of misfolded proteins in the ER induces Ca^{2+} leakage from the ER into the cytosol through inositol trisphosphate receptor, increasing mitochondrial ROS production (Malhotra and Kaufman, 2007). Ca^{2+} ions passed from the ER to the mitochondria increase metabolism and the Kreb´s cycle to further induces of oxidative phosphorylation. ROS generation during electron transport chain increases cytochrome c release, thus altering mitochondrial membrane potential. Furthermore, ROS can also send a feedback signal to sensitize the Ca^{2+} release channel at the ER membrane.

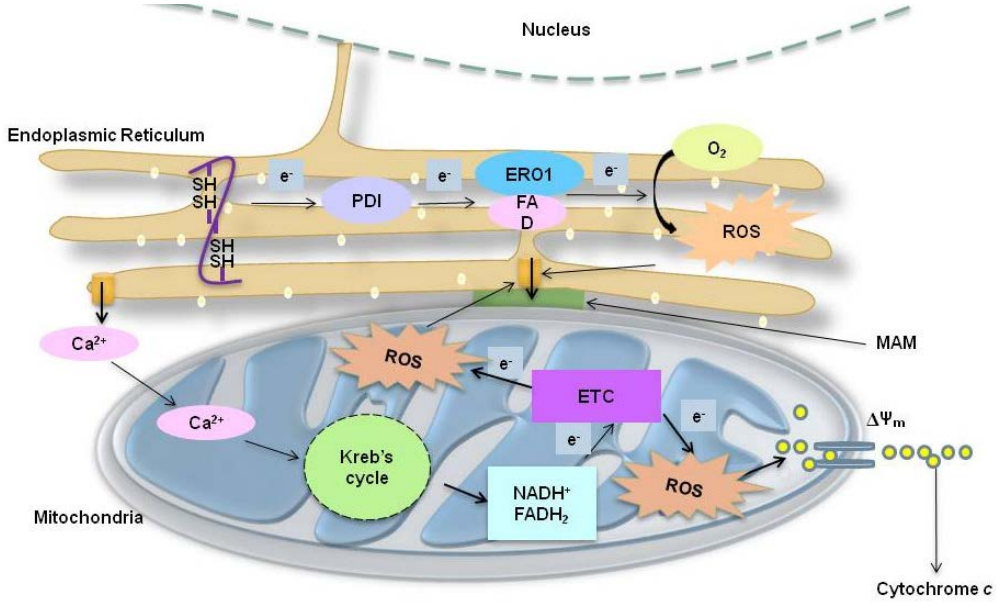

Figure 1.23. ER stress-induced ROS production in the cell. ROS are usually generated by cell process, including oxidative protein folding and mitochondrial respiration, which is augmented during ER stress. (Bhandary et al., 2012).

1.7. Autophagy

Autophagy is a catabolic process focused on recycling cellular components and damaged organelles in response to diverse conditions of stress, such as nutrient deprivation, genotoxic stress or misfolded proteins during ER stress (*reviewed in section 1.6.*). There are three types

of autophagy mediated by lysosome-mediated degradation: 1) macroautophagy, that involves the sequestration of damaged portions of cytoplasm within double-membrane vesicles (called autophagosomes); 2) microautophagy, by which the cytosolic material is directly engulfed by the lysosome; and 3) chaperone-mediated autophagy (Filomeni et al., 2015). Macroautophagy (hereafter referred as autophagy) is an adaptative cellular process, which fuse autophagosomes with lysosomes to form autolysosomes where autophagic cargo is degraded. However, the role of autophagy is not the simple elimination of materials indeed through autophagy cells obtain new building blocks for cellular renovation and homeostasis (Mizushima and Komatsu, 2011).

1.7.1. Mechanism of autophagy

Autophagy pathway starts with the formation of an isolation membrane (called phagophoro) in the ER-mitochondria contact sites, with membranes derived from the ER, the mitochondria, and the plasma membrane (Hailey et al., 2010; Hamasaki et al., 2013). These membranes are the sources for the generation of the autophagosome, coordinated by the ULK1 (Atg1 homolog) complex, including ULK1, Atg13, FIP200, and Atg101 proteins (Fig. 1.24). This complex is functionally coupled to the negative autophagy regulator mTORC1 (Jung et al., 2009). The ULK1 complex is activated and translocates to a domain of the ER, where it regulates the class III PI3K complex (including Beclin 1, Atg14, Vps15, Vps34, and Ambra1), and this regulation is promoted by RalB and an Exo84-containing exocyst complex. However, recruitment of Beclin 1 to the PI3K complex is sensitive to starvation, and it is usually inactivated by Bcl-2 under nutrient-rich conditions, and is released upon phosphorylation by JNK1. The active PI3K complex drives the early stage of autophagosome formation through Atg9L, a multimembrane-spanning protein. Formation of PI_3P recruits DFCP1 and promotes the formation of the isolation membrane (also called the omegasome) from which autophagosomes appear to be generated. Moreover, WIPI binds to PI_3P for further omegasome maturation. The complex Atg12–Atg5–Atg16L1 acts as an E3 ligase and catalyzes the formation of covalent bonds between LC3 with phosphatidylethanolamine (PE) for elongating and closing of the isolation membrane (He and Klionsky, 2009). In addition to that, several SNARE-like proteins mediate the fusion of autophagosomes with lysosomes for the formation of autolysosomes, where the substrates are degraded (Kroemer et al., 2010).

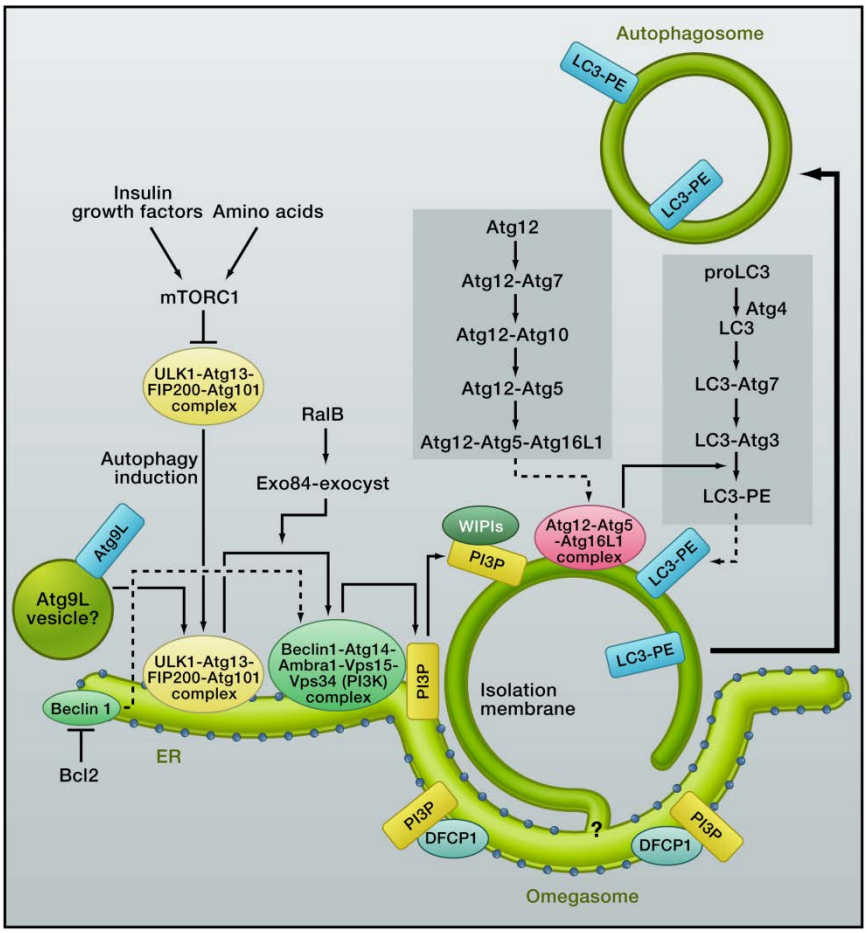

Figure 1.24. Autophagosome formation in mammalian cells. (Mizushima and Komatsu, 2011).

1.7.2. The role of ROS in autophagy

Several evidences indicate that mechanism that sense ROS can control autophagy under a variety of cellular contexts (Dewaele et al., 2010). Indeed, the direct addition of exogenous H_2O_2, promotes up-regulation of autophagy in a range of cancer cell lines. In addition, NFκB is able to regulate autophagy by a redox-sensitive mechanism in cells exposed to TNFα (Djavaheri-Mergny et al., 2007). The very fast induction of autophagy upon ROS production is mediated by redox-sensitive proteins, among them AMPK, the major mediator of indirect activation of autophagy by ROS (Fig. 1.25). Indeed, the energy-dependent activity of mTOR is regulated by AMPK, which is in turn activated by phosphorylation in response to high intracellular AMP/ATP ratios. Under starvation conditions, AMPK phosphorylates the TSC2

tumor suppressor, and the mTORC1 subunit Raptor, required for the inhibition of mTORC1, and therefore inducing autophagy (Gwinn et al., 2008). Moreover, a direct role of AMPK in the induction of autophagy has been shown. Under glucose deprivation, AMPK induces autophagy by directly activating ULK1 through phosphorylation of Ser317 and Ser777 (Kim et al., 2011). Another redox sensitive protein that can promote autophagy through AMPK pathway in cells under oxidative stress is ATM, the kinase that coordinates the cellular response to DNA damage *(reviewed in section 1.5.5.)*. In response to elevated ROS, ATM increases TSC2 in the cytoplasm via the LKB1/AMPK metabolic pathway, thus resulting in mTORC1 inactivation and autophagy induction (Alexander et al., 2010). On the other hand, mitochondrial ROS generated in response to hypoxia prevent degradation of the HIF1α and induce the transcription of target genes, including BNIP3 and BNIP3L, which induce autophagy (Bellot et al., 2009). HMGB1 is a chromatin-associated protein that is released from the nucleus to the cytoplasm in response to autophagy-inducing stimuli in a ROS-dependent manner. HMGB1 is highly redox sensitive and disrupts the Beclin1-Bcl-2 interaction through oxidation of cysteine residues at position 23 and 45, enhancing ERK1/2 activity (Tang et al., 2010). Regarding Atg proteins, they contain cysteine residues which can be redox regulated. Indeed, a cysteine residue located near the Atg4 catalytic site is required for inactivating its delipidating activity on LC3, which is critical for correct autophagosome formation (Scherz-Shouval et al., 2007). In addition, Atg7-Atg3 and Atg7-Atg10, and the phosphatase PTEN also contain reactive cysteines which are reversible redox regulated (Filomeni et al., 2010). Other mediators of autophagy induction in response to ROS include the forkhead transcriptional regulator FOXO1 and FOXO3 (Sengupta et al., 2011), the p38 (McClung et al., 2010), ERK and JNK MAPKs (Wong et al., 2010), and the ER kinase PERK *(reviewed in section 1.6.2.)* (Avivar-Valderas et al., 2011).

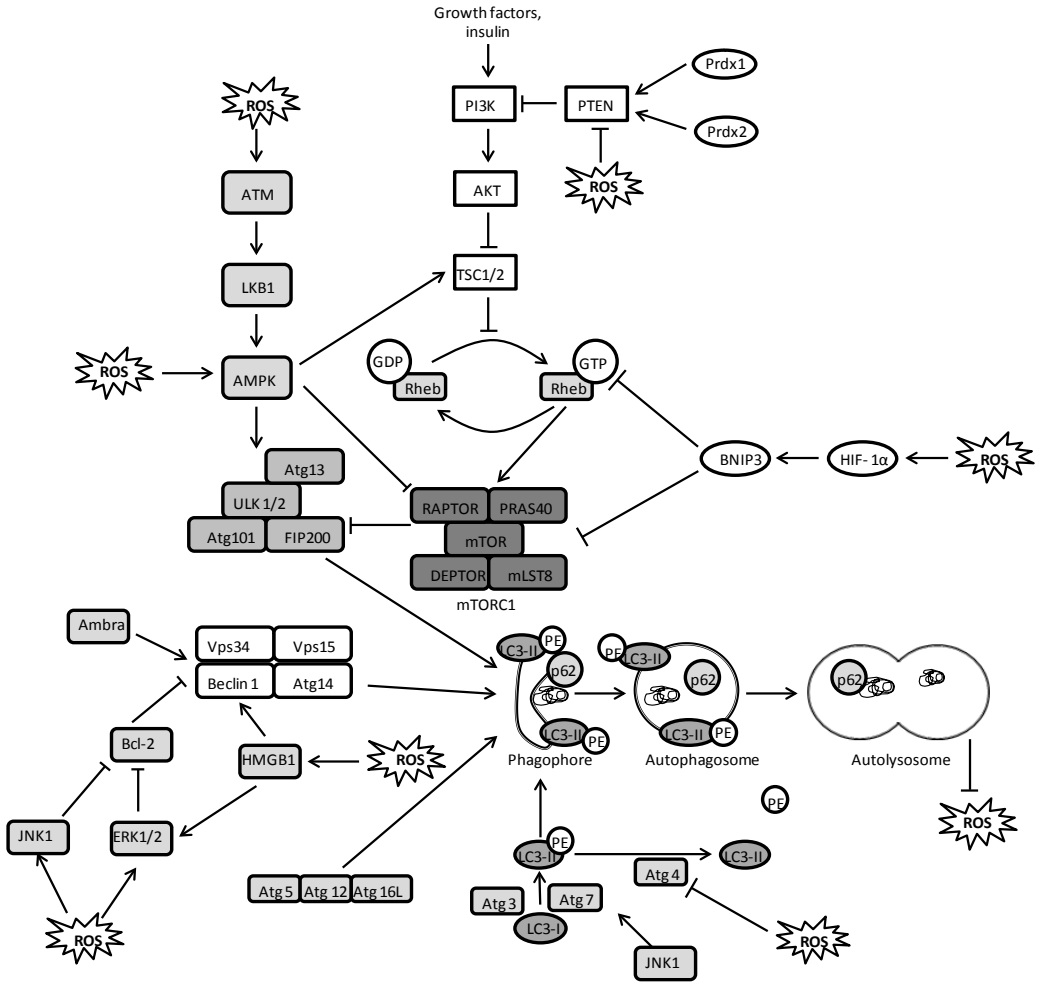

Figure 1.25. Reactive oxygen species-mediated autophagy regulation. The PI3K-Akt-mTORC1 pathway suppresses autophagy by inhibiting the ULK1/2-FIP200-Atg13 complex. PI3K suppresses TSC1/2 activity, thus resulting in mTORC1 inactivation and suppressing autophagy. The phosphatase PTEN antagonizes PI3K, while the peroxiredoxins Prdx 1 and 2 maintain PTEN function by preventing its oxidation. mTORC1 is also negatively regulated by HIF1α via BNIP3 induction and by ATM via LKB1/AMPK. The Beclin1-Vps34-Vps15 complex is positively regulated by AMBRA, and HMGB1, and negatively regulated by Bcl-2. Autophagy results in ROS suppression upon its induction. *(→) activation; (┤) inhibition.*

In summary, regarding ROS positive regulation of autophagy at least three main mechanisms exist: 1) S-glutathionylation of cysteines located in the α and β subunits of AMPK; 2) oxidation of cysteine 81 of Atg4 that inactivates its delipidating activity on LC3 and induces accumulation of pro-autophagic LC3-II isoform; and 3) alteration of thiol redox state, through increasing of the GSSG/GSH ratio and oxidized thiols.

In the same way, autophagy can modulate both ROS production and oxidative damages through at least two major mechanisms. These include the selective degradation of damaged cellular components including damaged mitochondria and oxidized cellular substrates, and the activation of antioxidant responses driven by the autophagy receptor p62/SQSTM1.

Nrf2 regulates autophagy upon induction of oxidative stress through the activation of transcription of genes encoding cellular defence enzymes (Itoh et al., 1997). Under normal conditions, Nrf2 is repressed through sequestration within the cytosol by the Nrf2 suppressor Keap1 that functions as an adapter protein of Cul3-ubiquitin ligase complex responsible for Nrf2 ubiquitination and its subsequent degradation through proteasome pathway (Komatsu et al., 2010). However, under oxidative stress conditions, the interaction between Nrf2 and Keap1 is disrupted, allowing the translocation of Nrf2 to the nucleus where it binds to the antioxidant response elements (AREs) located in the promoter regions of genes encoding several antioxidant enzymes, as well as genes involved in DNA damage response (Kobayashi et al., 2004) (Valavanidis et al., 2009). Nrf2 under oxidant conditions mediates the induction of p62 gene transcription (Jain et al., 2010). Thus, Nrf2 has a dual role in the regulation of autophagy under oxidative stress. On the one hand, Nrf2-mediates induction of transcription of antioxidant enzyme genes, thus Nrf2 inhibits the initial activation of autophagy induced by ROS. On the other hand, Nrf2 facilitates termination of autophagy by enhancing the expression of p62/SQSTM1, which actively participates in the degradation of oxidized proteins by delivering them to the autophagosomes. Furthermore, Nrf2 and p62/SQSTM1 form a positive feedback regulatory loop that controls autophagy in the presence of ROS. Indeed, p62/SQSTM1 has been shown to induce Nrf2-activation through inactivation of Keap1 (Komatsu et al., 2010). Activation of Nrf2 is sustained by sestrins through Keap1 degradation (Bae et al., 2013). Sestrins are a highly conserved family of small antioxidant-like proteins transcriptionally induced by p53 upon stressful conditions. Moreover, sestrins are implicated in defense against ROS due to their sulfinic acid reductase activity, whose activity is necessary to maintain peroxiredoxins in an active state.

2. HYPOTHESIS AND OBJECTIVES

2. HYPOTHESIS AND OBJECTIVES

There is growing interest in identifying chemotherapeutic agents that can prevent tumor initiation, slow or stop tumor growth or reduce metastasis and mortality. Natural products derived from plants have recently received considerable attention because of their antioxidant, anti-inflammatory and antitumor activities. In previous studies by our research group, the content of total phenols and flavonoids of aqueous extracts from various Amazonian plants commonly used in traditional medicine, and their antioxidant activities in various cell-free systems were described (Lizcano et al., 2010; Lizcano et al., 2012). Several leaf extracts of plants of the *Vismia* and *Piper* genera were selected for their high antioxidant potential to analyze their antitumor activities on human and rat hepatocellular carcinoma cells (Lizcano et al., 2014). From the results we highlight the effects exerted by *V. baccifera*; in hepatoma cell lines they had a toxic effect, whereas in primary nontransformed rat hepatocytes they were innocuous or even improved cell viability. These results have led us to analyze in depth the actions of this plant to generate knowledge that can lay the bases for coadjuvant or anti-cancer therapy.

The HYPOTHESIS of this work is that *V. baccifera* triggers a *redox* disbalance that drives the inhibition of the tumor cell growth. The main OBJECTIVE of this project of Doctoral Thesis is to unravel the cytotoxic pathways induced by the extract in human hepatocellular carcinoma HepG2 cells. To achieve this aim, the following OPERATIVE OBJECTIVES were raised:

1. To determine toxicity by measuring the IC_{50}, the intracellular ROS and mitochondrial $O_2^{\cdot}$ accumulation, the mitochondrial membrane potential, cell cycle and migration, the antioxidant system targeted by *V. baccifera*, autophagy, and the involvement of apoptosis in cell death.
2. To determine ROS and hydrogen peroxide implication in *V. baccifera*-induced toxicity.
3. To establish the signal transduction pathways induced by *V. baccifera.*
4. To study the influence of pO_2 on *V. baccifera*-induced toxicity.

3. MATERIALS AND METHODS

3. MATERIALS AND METHODS

3.1. Materials

Apocynin, N-acetyl-L-cysteine (NAC), 2,2'-azino-bis (3-ethylbenzothiazoline-6-sulfonic acid) diammonium salt (ABTS), bis-(3-carboxy-4-nitrophenyl)-disulfide (DTNB), catalase from bovine liver, carbonyl cyanide-4-(trifluoromethoxy) phenylhydrazone (FCCP), cumen hydroperoxide, 4,5-dihydroxybenzene-1,3-disulfonic acid disodium salt monohydrate (Tiron), (−)-epicatechin**,** ethylenediaminetetraacetic acid (EDTA), glutathione, glutathione oxidized (GSSG), glutathione reductase, horseradish peroxidase (HRP), hydrogen peroxide, 4-hydroxypyrazolo[3,4-d]pyrimidine (allopurinol), (±)-6-hydroxy-2,5,7,8-tetramethylchromane-2-carboxylic acid (Trolox), 1-methyl-2-vinylpyridinium triflate (M2VP), NADPH, nitroblue tetrazolium (NBT), sulfosalicylic acid, triethanolamine, Triton X-100, trypsin, xanthine and xanthine oxidase (XOD), were all obtained from Sigma-Aldrich (St Louis, MO, USA). Fluorescein was purchased from Merck (Darmstadt, Germany), 2,2'-azobis(2-amidinopropane) dihydrochloride (AAPH) from Polysciences (Warrington, PA, USA), and doramapimod from Santa Cruz Biotechnology (Dallas, Texas, USA), and SB 203580 from Tocris (Bristol, UK).

3.2. Methods

3.2.1. Preparation of *Vismia baccifera* extract

Vismia baccifera species of native Amazonia was collected from the Macagual Research Centre forest in Florencia, Caquetá (Colombia), and taxonomically identified by botanical experts and deposited at the Herbarium of the Botanical Garden of Amazonia University—HUAZ (Florencia, Colombia). The plant was processed in the laboratory within a maximum of 24 h after harvesting. Otherwise, the material was stored under refrigeration at 4 ºC. The plant extract was obtained from infusion prepared as generally used in folk medicine. For this purpose, the leaves of the fresh plant were rinsed in water, cut into tiny pieces and boiled in 500 ml of water with constant shaking for 15 min. The mixture was allowed to settle for 10 min and

stored at −20 ºC. The sample was carried to the Physiology Department at the Medicine and Nursing School of the University of the Basque Country (UPV/EHU).

Once defrosted the extract was centrifuged at 1,200xg for 5 min at 4 ºC, and the supernatant was sterilized by filtration (0.22 µm pore size). Aliquots were stored at −80 ºC until use. Aliquots of the extract were dried in a Savant A290 SpeedVac concentrator (Thermo Fisher Scientific, Waltham, MA, USA) to estimate the dry weight.

3.2.2. Characterization of the total antioxidant activity

The total antioxidant activity was determined by the $ABTS^+$ radical cation decolorization assay (Re et al., 1999), and oxygen radical absorbance capacity (ORAC) using fluorescein as a fluorescence probe (Ou et al., 2001). The ORAC assay was carried out using the adapted method on 96-well microplates (Huang et al., 2002).

3.2.2.1. $ABTS^+$ radical cation decolorization assay

The ABTS radical cation was prepared the day before the experiment by mixing at room temperature 4.35 mM ABTS and 0.7 mM $K_2S_2O_2$ in milli-Q water. The mixture was incubated overnight in the dark. The reaction was started with the addition of 250 µl of the $ABTS^+$ solution (0.70 ± 0.01 at λ = 734 nm) to 10 µl of the appropriate diluted plant extract per well maintained at 30 ºC. The absorbance readings were taken 30 s after initial mixing and every min up to 12.5 min at 734 nm, using a SynergyTM HT spectrophotometer microplate reader (BioTek, Winooski, VT, USA). A standard curve was built using different Trolox concentrations (0.0625-1.25 mM) in milli-Q water. The antioxidant activity of *V. baccifera* was calculated comparing the area under the curve derived from plotting the percentage inhibition of the absorbance as a function of time with the area under the curve for Trolox standard. All the determinations were carried out using different dilutions of the plant extracts in duplicate. The antioxidant activity was expressed as µmol of Trolox equivalents per gram of dry weight. The method precision and exactitude was determined using ascorbic acid, whose known antioxidant activity is 1 Trolox equivalent.

3.2.2.2. Oxygen radical absorbance capacity (ORAC)

The ORAC assay was carried out using fluorescein as a fluorescence probe and in 96-well microplates. 25 µl of the appropriate diluted *V. baccifera* extract was added in each well with 100 µl of fluorescein (61.2 nm final concentration), and the mixture was incubated during 15 min at 37 ºC in the microplate. Then, 75 µl of 51 mM AAPH were added and the microplate was shaken for 30 s. The fluorescence was reordered (λ_{exc} = 485 nm, λ_{em} = 520 nm) every 75 s for 50 min in a SynergyTM HT fluorimeter microplate reader (BioTek, Winooski, VT, USA). All the samples were analyzed at four dilutions and in triplicates. Freshly prepared Trolox solutions (1.25-50 µM) in phosphate buffer were used for building the calibration curve. Results were calculated based upon differences in areas under the fluorescence decay curve between blank, samples and standards. Final ORAC values were expressed as µmol Trolox equivalents per gram of dry weight.

3.2.3. Culture and maintenance of cell lines

The human hepatoma cell lines HepG2, Huh7 and Hep3B were purchased from ATTC (American Type Culture Collection) (Manassas, USA). These cells were maintained in Eagle's Minimum Essential Medium (EMEM) (ATCC) supplemented with 10% heat inactivated fetal bovine serum (FBS) (ATCC), 2 mM L-glutamine, 0.1 mg/ml streptomycin and 100 U/ml penicillin (all from Sigma-Aldrich, St Louis, MO, USA). The human fetal hepatocyte-derived HH4 cell line was maintained in Nutrient Mixture F-12 Coon´s modification (HAM F-12) (Sigma) containing 15% heat inactivated FBS, 0.1 mg/ml streptomycin and 100 U/ml penicillin and 32 mM sodium bicarbonate.

All cell lines were grown in 75 cm^2 flasks at 37 ºC in humidified atmosphere with 5% CO_2 under atmospheric oxygen pressure (21%) or under 8% pO_2 depending on the kind of experiment. Medium was replaced every 2 to 3 days. When the cell monolayer reached around 75% of confluence, cells were detached with a solution of 0.1% trypsin-0.04% EDTA and then harvested to perform subsequent experiments.

3.2.4. Cytotoxicity assay

The live cell number was evaluated with the crystal violet assay based on the cell staining with crystal violet (Gillies, 1986). Briefly, cells were seeded onto 96-well tissue culture plates at $5x10^3$ cells per well, and 24 h after plating the cells were treated without (control) or with *V. baccifera* for 24 and 48 h. When the effects of different antioxidants or protein modulators were studied, the compounds were added one hour before the addition of the plant extract. After treatments cells were washed, fixed in 3.7% formaldehyde and stained with 0.25% crystal violet (Merck, Darmstadt, Germany) for 20 min in the dark. Finally, the resultant crystals were solubilised with 33% acetic acid and the absorbance was registered at 590 nm in a Synergy HT microplate reader (BioTek, Winooski, VT, USA). Cells number was expressed as the percentage of the control cells at the corresponding time.

3.2.5. Intracellular ROS detection

Intracellular ROS levels were measured using the cell-permeant 2',7'-dichlorodihydrofluorescein diacetate (H_2DCF-DA) probe (Molecular Probes, Eugene, OR, USA). This compound is deacetylated by endogenous esterases rendering non-fluorescent 2',7'-dichlorodihydrofluorescein (H_2DCF) and causing it to be trapped inside the cell. H_2DCF is oxidized by ROS to the highly fluorescent 2',7'-dichlorofluorescein (DCF) compound, with different fluorescence spectrum.

The cells were seeded at a density of $2.5x10^5$ cell per well onto 6-well plates 48 h before starting the corresponding treatments. The medium was renewed and cells were incubated with *V. baccifera* for the indicated times. After treatments, cells were washed and incubated with 20 µM H_2DCF-DA for 30 min at 37 ºC in the dark. Then the probe solution was removed and, after being washed with PBS, the cells were trypsinized and harvested to analyze. The fluorescence intensity from live cells was analyzed by flow cytometry in a Beckman Coulter Gallios Flow cytometer (λ_{exc} = 485/20 and λ_{em} = 528/20) in the General Research Services SGIker of the UPV/EHU (http://www.ikerkuntza.ehu.es/p273-sgikerhm/en/). At least 10,000 cells (events) were detected for each group. Data obtained from flow cytometry were analyzed using Summit 4.3 software (Dako, Hovedstaden, Denmark).

Intracellular ROS levels were expressed as the percentage fluorescence of control cells at the same time of incubation.

3.2.6. Mitochondrial O_2^- detection

The mitochondrial superoxide anion levels were measured using MitoSOX™ Red reagent (Molecular Probes, Eugene, OR, USA), which permeates live cells where it selectively targets mitochondria and is oxidized by superoxide.

After treatments, cells were incubated with 4 µM MitoSOX for 30 min at 37 ºC in the dark. Then the probe solution was removed and after being washed with PBS, the cells were trypsinized and harvested. The fluorescence intensity from live cells was analyzed by flow cytometry in a Beckman Coulter Gallios cytometer (λ_{exc} = 485/20 and λ_{em} = 620/20) in the General Research Services SGIker of the UPV/EHU. At least 10,000 cells (events) were detected for each group. Data obtained from flow cytometry were analyzed using Summit 4.3 software (Dako, Hovedstaden, Denmark). Results were expressed as the percentage fluorescence of control cells at the same time of incubation.

3.2.7. Mitochondrial membrane potential (Δψm)

To analyze the mitochondrial membrane potential (Ψm) the fluorescent TMRE (tetramethylrhodamine ethyl ester) probe was used. TMRE is a cationic lipophilic dye that is accumulated in the negatively charged mitochondrial matrix in active respiring mitochondria (Ehrenberg et al., 1988).

The cells were seeded at a density of $2.5x10^5$ cell per well onto 6-well plates 48 h before starting the corresponding treatments. The medium was renewed and cells were incubated without (control) or with *V. baccifera* for 24 h. After treatments, cells were washed and incubated with 0.4 µM TMRE (Calbiochem) in serum-free EMEM cell solution for 30 min at 37 ºC in the dark. Then the probe solution was then removed and, after being washed with PBS, the cells were trypsinized and harvested for the analysis. FCCP (carbonyl cyanide-4-(trifluoromethoxy) phenylhydrazone), a potent uncoupler of oxidative phosphorylation, was added at 120 µM as reference of total mitochondrial membrane uncoupling. The TMRE-fluorescence was determined by flow cytometry utilizing a Beckman Coulter Gallios cytometer

(λ_{exc} = 488/20 and λ_{em} = 575/20) in the General Research Services SGIker of the UPV/EHU, with a total acquisition of 10,000 events. The fluorescence in the presence of FCCP was subtracted to all samples for assuring that mitochondrial membrane potential indeed was measured in the assay.

3.2.8. Cell cycle analysis

Cell cycle assay was performed using propidium iodide (PI). The staining is based on the property of the PI to bind to DNA by intercalating between double stranded nucleic acids (both DNA and RNA) and its ability to fluoresce. RNase is required in the assay for the study of the amount of DNA in each cell and, therefore, its stage in the cell cycle.

Cells were seeded at a density of $2.5x10^5$ cells per well onto 6-well plates 48 h before incubating without (control) or with *V. baccifera*. After 24 h of treatment, no-adherent cells were harvested by centrifugation (1,200 rpm 5 min 4 ºC). Then the cells of the plate were washed with PBS 37 ºC, trypsinized and collected with no-adherent cells for fixing overnight at 4 ºC in 70% ice-cold ethanol. After washing with ice-cold PBS, cells were stained with a 25 µg/ml propidium iodide solution in the presence of 200 µg/ml RNase A for 45 min at 37 ºC in the dark. The cell cycle distribution of the cells was determined by flow cytometry in a Beckman Coulter Gallios Flow cytometer in the General Research Services SGIker of the UPV/EHU, with a total acquisition of 10,000 events. The percentage of cells in different phases of the cell cycle was analyzed by Summit 4.3 software (Dako, Hovedstaden, Denmark).

3.2.9. Caspase activities

HepG2 were seeded at a density of $1x10^6$ cells onto Petri dishes for 72 h before starting the corresponding treatments. The medium was renewed, and cells were incubated without (control) or with *V. baccifera* for the indicated times. Cells were washed with ice-cold PBS and resuspended in ice-cold lysis buffer (1 mM NaF, 10 mM EGTA, 40 mM β-glycerol phosphate, 1% NP-40, 2.5 mM $MgCl_2$, 2 mM orthovanadate, 1 mM dithiothreitol (DTT), 10 µg/ml protease inhibitor cocktail, 20 mM Hepes, pH 7.5) and incubated for 30 min on ice. Cell extracts were centrifuged at 16,000xg for 10 min at 4 ºC. The supernatant protein was quantified

spectrophotometrically at 595 nm by Coomassie Blue dying (Bradford, 1976), using bovine serum albumin as standard.

The caspase-2 activity was carried out using the specific fluorogenic substrate Ac-Val-Asp-Val-Ala-Asp-AFC (Ac-VDVAD-AFC) (BioVision, Milpitas, California, USA). 50 µg protein was used in an assay medium (200 mM NaCl, 0.2 % CHAPS, 2 mM EDTA, 20 % glycerol, 5 mM DTT, 100 mM Hepes, pH 7.4) with 50 µM Ac-VDVAD-AFC as substrate. In the presence of caspase-2 the substrate Ac-VDVAD-AFC was hydrolyzed releasing the fluorogenic AFC. The activity was determined by continuous recording of the fluorescence (λ_{exc} = 400 nm, λ_{em} = 505 nm) at 37 ºC for 2 h at 5 min intervals in a Synergy HT fluorometer microplate reader (BioTek, Winooski, VT, USA). Results were expressed as the percentage fluorescence of control cells.

The caspase-3 activity was carried out using the specific fluorogenic substrate Ac-(N-acetyl)-DEVD-AMC (7-amino-4-methylcoumarin) (Ac-DEVD-AMC) (BD Pharmigen Biosciences, San Diego, CA, USA). 50 µg protein was used in an assay medium (200 mM NaCl, 0.2 % CHAPS, 2 mM EDTA, 20 % glycerol, 5 mM DTT, 100 mM Hepes, pH 7.4) with 37 µM Ac-DEVD-AMC as substrate. In the presence of caspase-3 the substrate Ac-DEVD-AMC was hydrolyzed releasing the fluorogenic AMC. The activity was determined by continuous recording of the fluorescence (λ_{exc} = 360 nm, λ_{em} = 460 nm) at 37 ºC for 2 h at 5 min intervals in a Synergy HT fluorometer microplate reader. Results were expressed as the percentage fluorescence of control cells.

3.2.10. Sample preparation for transmission electron microscopy

Samples for transmission electron microscopy were processed at the Analytical Microscopy Service in the General Research Services SGIker of the UPV/EHU. Briefly, HepG2 cells were fixed with 2% glutaraldehyde in 0.1 M PBS (pH 7.4) for 90 min at room temperature, and post-fixed in 1% osmium tetraoxide for 120 min at 4 ºC. After washing with PBS, the cells were progressively dehydrated in a 20% graded series of 30%-100% acetone for 30 min each change at room temperature in the dark and embedded in Epon 812 resin. The blocks were cut into ultrathin sections with a microtome, which were then stained with saturated uranyl acetate and lead citrate. The ultrastructure of the cells was then observed under a Philips CM120 Biofilter transmission electron microscope (Eindhoven, The Nederlands).

3.2.11. Scratch wound assay

The migration of the HepG2 cells was detected using the scratch wound assay. Briefly, the hepatoma cells were seeded at a density of $4x10^5$ cells per well onto 6-well plates, and incubated at 37 ºC for 24 h. Then, a vertical scratch wound was made through the middle of each well using a 10-µl pipette tip. The cells were then washed three times with potassium phosphate buffered saline, PBS (10 mM Na_2HPO_4, 1.8 mM KH_2PO_4, 2.7 KCl, 150 mM NaCl, pH 7.4) to remove the scratched cells, and it was replaced with EMEM supplemented with 2.5% inactivated FBS (control) and containing the *V. baccifera* extract (treatment). After 24, 48 and 72 h of incubation, the cells were examined and photographed under an Olympus CH optical microscope (Olympus, Tokyo, Japan) to determine the resealing of the cell monolayer by measuring the width of the remaining wound.

3.2.12. Transwell migration and invasion assay

The migration ability of cells was carried out using 24-well transwell migration chambers (Greiner bio-one, Switzerland) with 8 µm pore size polyethylene membranes. For cell invasion assay, transwell inserts were precoated with 68 µl of 5 µg/ml fibronectin (Sigma-Aldrich, St Louis, MO, USA) at 37 ºC for 1 h for gelling. The upper chambers were inoculated with $6x10^4$ cells/well, in 0.2 ml serum-free EMEM cell solution. Lower chambers were filled with 0.6 ml of the corresponding medium containing the chemoattractant (10% FBS or medium plus *V. baccifera*) and cells were allowed to migrate for 24 h under atmospheric oxygen pressure or under two pO_2 conditions (21% and 8% pO_2), at 37 ºC in humidified atmosphere with 5 $\%CO_2$. After the incubation, cells located upon the upper membranes were wiped with cotton swabs. The cells that migrated to the lower surface of the polyethylene membranes were fixed in 70% ethanol overnight. Subsequently, cells were stained overnight with 25 µg/ml propidium iodide (Sigma-Aldrich, St Louis, MO, USA) and 200 µg/ml RNasa A (Roche Biochemicals, Indianapolis, IN, USA). The inserts were photographed under an Olympus Fluoview FV500 confocal microscope in the General Research Services SGIker of the UPV/EHU (http://www.ikerkuntza.ehu.es/p273-sgikerhm/en/). The number and area of migrated cells were calculated using the ImageJ software (NIH, Bethesda, Maryland, USA).

3.2.13. Antioxidant enzyme activities

Antioxidant enzyme activity determinations were carried out with the extracts of cells lysed by freeze-thawing in liquid N_2 and centrifuged at 16,000xg for 10 min at 4 ºC. Protein concentration of the supernatant was determined spectrophotometrically at 595 nm by the Coomassie Blue dying (Bradford, 1976), using bovine serum albumin as standard.

3.2.13.1. Superoxide dismutase (SOD)

SOD activity was determined indirectly by the method of nitroblue tetrazolium (NBT) (Zhou et al., 2006). This method uses the xanthine-xanthine oxidase (XOD) system to generate superoxide anions (Fig.3.1). The superoxide anion reduces NBT, which is converted into NBT-diformazan. This reduced form is blue, and the absorbance is recorded at 570 nm in a spectrophotometer. In presence of SOD, O_2^- undergoes a dismutation into O_2 and H_2O_2, decreasing the NBT-diformazan formation. Hence, this competing assay yields to the indirect measurement of SOD activity.

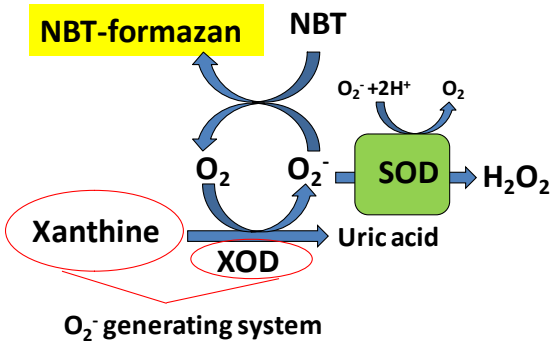

Figure 3.1. Scheme for the method to detect superoxide dismutase activity. The compound detected is represented in yellow.

The method was adapted to 96 well plates. Increasing amounts of cellular protein were assayed for each independent experiment and the absorbance was determined *versus* the incubation time. The reaction was started by the addition of 60 µM NBT in a final volume of 250 µl. The increase of absorbance was determined every 60 seconds for 12 minutes at a temperature of 37 ºC. The slope of the curve for each protein concentration was calculated, and the percentage inhibition relative to a control without protein was calculated. To calculate

the IC_{50} (amount of protein required to inhibit the formation of NBT-diformazan by 50%) the % inhibition was plotted *versus* the log of protein concentration, and the graphs were adjusted to semilogarithmic curves, using GraphPad Prism 4 for Windows (San Diego, CA, USA).

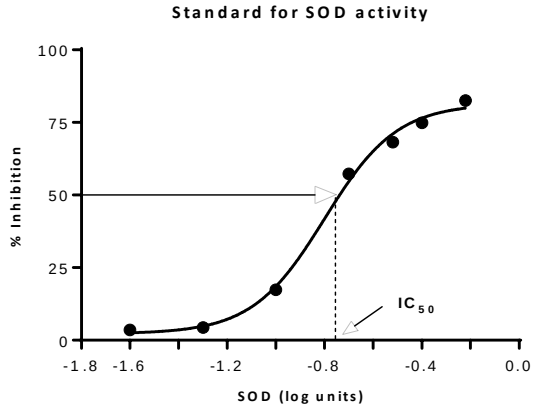

Figure 3.2. Example of the inhibition curve built with commercial SOD to express the results as SOD units/mg protein.

An inhibition curve was prepared using commercially available SOD (Sigma-Aldrich, St. Louis, MO, USA) to transform the IC_{50} value into SOD units. Results are expressed as SOD U/mg of protein. One unit of SOD activity was defined as the amount of the enzyme in a sample solution causing 50% inhibition (IC_{50}) of the rate of reduction of tetrazolium salt (McCord and Fridovich, 1969).

3.2.13.2. Glutathione peroxidase (GPx)

Total GPx activity was assayed by the indirect method of Güntzler and Flohé, (1985). GPx activitiey was measured in a coupled enzyme system where NADPH is consumed by glutahione reductase (GR) to convert the formed glutathione disulfide (GSSG) to its reduced form (GSH) (Fig.3.3). The decrease in absorbance of NADPH was monitored at 340 nm every 60 seconds for 15 min in a 96-well plate reader at 30 ºC. The final volume was 225 µl containing 50 mM potassium phosphate buffer (pH 7.0), 1 mM EDTA-Na_2, 0.5 mM sodium azide, 0.45 mM GSH, 0.2 mM NADPH and 0.45 U of GR. The reaction started by the addition of cumene hydroperoxide (0.72 mM final concentration) for total-GPx. The results are expressed as nmol/min/mg protein, using the NADPH experimental coefficient $\varepsilon = 3.065\ mM^{-1}$.

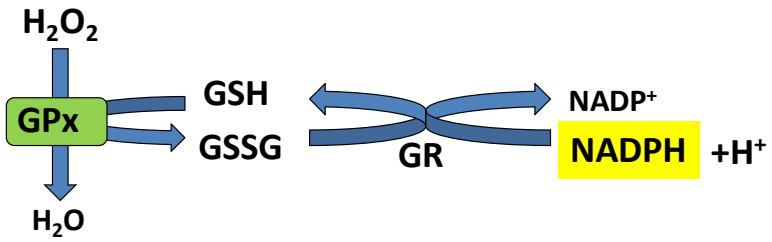

Figure 3.3. Scheme for the method to detect glutathione peroxidase activity. The compound detected is represented in yellow.

3.2.14. Determination of GSH and GSSG levels

HepG2 were seeded at a density of $1x10^6$ cells onto Petri dishes for 72 h before starting the corresponding treatments. The medium was renewed, and cells were incubated without (control) or with the corresponding treatment for 24 h. Cells were washed with ice-cold PBS and resuspended in ice-cold lysis buffer (0.1% Triton X-100 and 0.6% sulfosalicylic acid) and lysed by a freezing and thawing process. After that, cells were centrifuged at 4,000xg for 5 min at 4 ºC and the supernatant was collected and separated into two aliquots (in order to measure GSH and GSSG, respectively). The supernatant protein was quantified spectrophotometrically at 595 nm by Coomassie Blue dying (Bradford, 1976), using bovine serum albumin as standard.

The measurement of glutathione (GSH) and glutathione disulfide (GSSG) was evaluated with the glutathione reductase-DTNB recycling method, as reported previously (Rahman et al., 2006) (Fig.3.4).

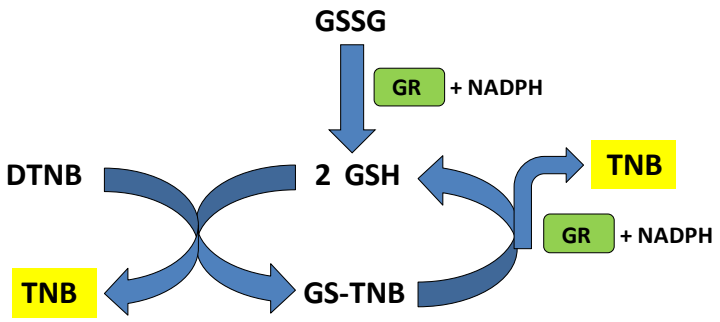

Figure 3.4. Scheme for the glutathione reductase-DTNB recycling method for the measurement of GSH and GSSG. The compound detected is represented in yellow.

GSSG was determined after blocking the thiol group in GSH by the addition of 6 mM 1-methyl-2-vinylpyridinium triflate (M2VP) to 100 µl of deproteinized sample. This mixture was kept for 1 h in ice and neutralized by the adding 634 mM triethanolamine. Reactions were run in 96-well microplates; 5 µl of each sample were distributed per well for quantification of total GSH, and 40 µl for GSSG. Glutathione reductase (1.82 Units/well), DTNB (458 µM) and NADPH (0.3 mM for GSH and 0.22 mM for GSSG) were then added to a final volume of 220 µl/well. Absorbance was monitored at 412 nm. GSH and GSSG concentrations were estimated from standard curves. Results were expressed as nmol of GSH or GSSG per mg of protein.

3.2.15. H_2O_2 measurement

H_2O_2 concentrations in the culture medium were determined using Amplex Red reagent (Sigma-Aldrich, St Louis, MO, USA). In the presence of horseradish peroxidase (HRP), the Amplex Red reagent reacts with H_2O_2 to produce highly fluorescent resorufin (Fig.3.5).

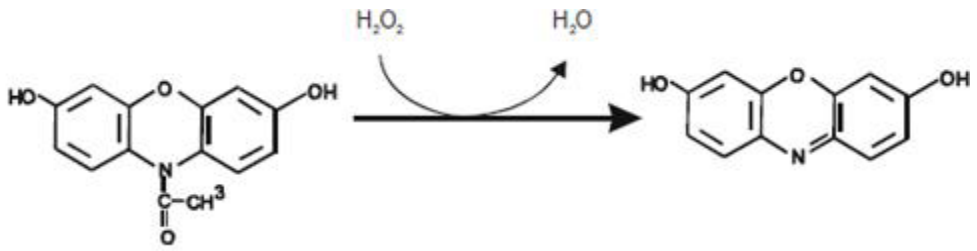

Amplex Red **Resorufin**

Figure 3.5. Amplex Red reagent reaction with H_2O_2.

All the H_2O_2 measurements were done in 96-well tissue culture plates, where $5x10^3$ cells per well were seeded. After treatment, the cells were washed with PBS at 37 ºC and the reaction was started by the addition of 0.1 U/ml of HRP and 50 µM Amplex Red in Krebs-Ringer phosphate buffered, KRPG (145 mM NaCl, 5.7 mM Na_2HPO_4, 4.86 mM KCl, 0.54 mM $CaCl_2$, 1.22 mM $MgSO_4$, 5.5 mM glucose, pH 7.35). For the H_2O_2 standard curve, 20 µl/well of different dilutions of hydrogen peroxide (2.5-10 µM) in reaction buffer (50 µM Na_2HPO_4 pH=7.4) were added to 100 µl of reaction mixture in 96-well plates. Fluorescent variations in the well solution were determined by continuous recording of the fluorescence (λ_{exc} = 538 nm,

λ_{em} = 604 nm) at 37 ºC for 2 h at 5 min intervals in a Synergy HT fluorometer microplate reader (BioTek, Winooski, VT, USA). The concentration of H_2O_2 was determined by subtracting the fluorescence remaining in sample wells after the addition of catalase (10 U/well). Fluorescent changes from the H_2O_2 release from cells were converted to nmol H_2O_2/mg protein using the hydrogen peroxide standard curve.

3.2.16. Protein immunodetection by western blot

The expression of proteins was analyzed by western blot. Cellular proteins were denatured by boiling at 95 ºC for 5 minutes in Laemmli sample buffer 5X (300 mM Tris-HCl, pH 6.8, 50% glycerol, 10% SDS, 250 mM DTT, 0.01% bromophenol blue) (Laemmli, 1970). Equal amounts of proteins (30-50 µg) were separated by SDS-PAGE electrophoresis in 10-15% polyacrylamide gels, depending on the protein molecular weight. Gels were transferred onto PVDF membranes by electroblotting with constant amperage (1 mA/cm^2). After blocking for 1 h at room temperature, membranes were incubated overnight at 4 ºC with the corresponding primary antibody. After washing, membranes were probed with the secondary antibody conjugated to horseradish peroxidase for 1 h at room temperature. The immunoreactive proteins were incubated with the Clarity Western ECL Substrate (Bio-Rad, Hercules, California, USA), and the blots were imaged by scanning with the C-DiGit LI-COR blot scanner (Bonsai Advanced technologies S.L., Madrid, Spain). Results were expressed as the percentage of the integrated optic density from control cells.

Protein	Blocking dilution	Primary ab. dilution	Primary ab. supplier	Species secondary ab.	Secondary ab. dilution	Secondary ab. supplier
Bax	5% BSA + TTBS	1:500 (5% BSA* + TTBS*)	SCB* (493)	Rabbit	1:2000 (5% BSA + TTBS)	CST* (7074)
Bcl-2	5% BSA + TTBS	1:500 (5% BSA + TTBS)	SCB (492)	Rabbit	1:2000 (5% BSA + TTBS)	CST (7074)
BID	5% BSA + TTBS	1:500 (5% BSA + TTBS)	SCB (11423)	Rabbit	1:2000 (5% BSA + TTBS)	CST (7074)
Bcl-$X_{L/S}$	5% BSA + TTBS	1:500 (5% BSA + TTBS)	SCB (634)	Rabbit	1:2000 (5% BSA + TTBS)	CST (7074)
p-p38 (Thr180/ Tyr182)	5% BSA + TTBS	1:2000 (5% BSA + TTBS)	CST (9211)	Rabbit	1:2000 (5% BSA + TTBS)	CST (7074)
p38	5% BSA + TTBS	1:1000 (5% BSA + TTBS)	CST (9212S)	Rabbit	1:2000 (5% BSA + TTBS)	CST (7074)
p-JNK 1/2	5% BSA + TTBS	1:5000 (5% BSA + TTBS)	Promega (V7931)	Rabbit	1:2000 (5% BSA + TTBS)	CST (7074)

JNK 1/2	5% BSA + TTBS	1:2000 (5% BSA + TTBS)	CST (9252)	Rabbit	1:2000 (5% BSA + TTBS)	CST (7074)
p-ERK 1/2 (Thr202/ Tyr204)	5% BSA + TTBS	1:2000 (5% BSA + TTBS)	CST (9106)	Rabbit	1:2000 (5% BSA + TTBS)	CST (7076)
ERK 1/2	5% BSA + TTBS	1:1000 (5% BSA + TTBS)	CST (9102S)	Rabbit	1:2000 (5% BSA + TTBS)	CST (7074)
p-Akt (Thr308)	5% BSA + TTBS	1:1000 (5% BSA + TTBS)	SCB (16646-R)	Rabbit	1:2000 (5% BSA + TTBS)	CST (7074)
Akt	5% BSA + TTBS	1:1000 (5% BSA + TTBS)	SCB (sc-8312)	Rabbit	1:2000 (5% BSA + TTBS)	CST (7074)
GRP78	5% BSA + TTBS	1:1000 (5% BSA + TTBS)	Enzo Life (ADI-SPA-827)	Mouse	1:2000 (5% BSA + TTBS)	CST (7076)
p-p53 (Ser15)	5% BSA + TTBS	1:1000 (5% BSA + TTBS)	CST (9286)	Mouse	1:2000 (5% BSA + TTBS)	CST (7076)
γH2AX (Ser140)	5% BSA + TTBS	1:1000 (5% BSA + TTBS)	Abcam (ab22551)	Mouse	1:2000 (5% BSA + TTBS)	CST (7076)
p-ATM (Ser1981)	5% milk + TTBS	1:7000 (5% milk* + TTBS)	Abcam (81292)	Rabbit	1:2000 (5% BSA + TTBS)	CST (7074)
ATM	5% milk + TTBS	1:5000 (5% milk + TTBS)	Abcam (ab32420)	Rabbit	1:2000 (5% BSA + TTBS)	CST (7074)
PARP	5% milk + TTBS	1:1000 (5% milk + TTBS)	CST (9542)	Rabbit	1:2000 (5% BSA + TTBS)	CST (7074)
p62	5% milk + TTBS	1:1000 (5% BSA + TTBS)	BD (610833)	Mouse	1:2000 (5% BSA + TTBS)	CST (7076)
LC3B	5% milk + TTBS	1:2000 (5% BSA + TTBS)	Sigma (L8918)	Rabbit	1:2000 (5% BSA + TTBS)	CST (7074)
IκBα	10 % milk + TTBS	1:1000 (5% milk + TTBS)	CST (371)	Mouse	1:2000 (5% BSA + TTBS)	CST (7076)
p65	10 % milk + TTBS	1:500 (5% milk + TTBS)	SCB (372)	Rabbit	1:2000 (5% BSA + TTBS)	CST (7074)
Cu,Zn-SOD	5% BSA + PBS	1:7000 (3% milk + PBS)	Calbiochem (574597)	Sheep	1:2000 (3% milk + PBS)	SCB (2770)
Mn-SOD	3 % milk + PBS	1:2000 (3% milk + PBS)	Millipore (06-984)	Rabbit	1:2000 (3% milk + PBS)	CST (7074)
GAPDH	2,5% BSA + TTBS	1:10000 (1% BSA + TTBS)	Abcam (ab 8245)	Mouse	1:2000 (5% BSA + TTBS)	CST (7076)

Table 3.1. Incubation conditions for each antibody used in western blot immunodetection. *Abbreviations: *CST, Cell Signaling Technology; SCB, Santa Cruz Biotechnology, in brackets the reference number; BSA, bovine serum albumin; milk, skim milk; TTBS, (0.05% tween 20, 15mM NaCl, 1mM Tris-HCl, pH 7.5).*

3.2.17. Samples preparation for immunofluorescence confocal microscopy

The subcellular localization of proteins was analyzed by immunocytochemistry. HepG2 cells were plated on coverslips and incubated under the corresponding treatment. Afterwards, the cells were fixed in 4% formaldehyde, washed with PBS and permeabilized with 0.05% Triton X-100 in TBS 10 mM (pH 7.4) and blocked with 1% preimmune goat serum/1% BSA for 1 h at

room temperature. Then, the cells were incubated overnight with the corresponding primary antibody, washed and incubated for 1 h with secondary antibodies Alexa Fluor 488 conjugated goat anti-rabbit or anti-mouse (ThermoFisher scientific, Walthan, Massachusetts, USA). Nuclei were counterstained using 5 µg/ml DAPI. Images were obtained with an Olympus Fluoview FV500 confocal microscope (Olympus, Tokyo, Japan) at the Analytical Microscopy Service in the General Research Services SGIker of the UPV/EHU. The nuclear and cytoplasm fluorescence was analyzed by ImageJ software (NIH, Bethesda, Maryland, USA) determining the protein fluorescence inside and outside the nuclei region.

Primary antibody	Primary antibody dilution	Primary ab. supplier	Species secondary ab.	Secondary ab. dilution
p-p38 (Thr180/Tyr182)	1:100 (1% BSA, 1% PGS* + TTBS*)	CST* (9211)	Rabbit	1:200 (1% BSA, 1% PGS + TTBS)
p-JNK 1/2	1:100 (1% BSA, 1% PGS + TTBS)	Promega (V7931)	Rabbit	1:200 (1% BSA, 1% PGS + TTBS)
p-p53 (Ser15)	1:100 (1% BSA, 1% PGS + TTBS)	CST (9286)	Mouse	1:200 (1% BSA, 1% PGS + TTBS)
p-ATM (Ser1981)	1:200 (1% BSA, 1% PGS + TTBS)	Abcam (81292)	Rabbit	1:200 (1% BSA, 1% PGS + TTBS)
p62	1:100 (1% BSA, 1% PGS + TTBS)	BD (610833)	Mouse	1:200 (1% BSA, 1% PGS + TTBS)
LC3B	1:100 (1% BSA, 1% PGS + TTBS)	Sigma (L8918)	Rabbit	1:200 (1% BSA, 1% PGS + TTBS)
AIF	1:100 (1% BSA, 1% PGS + TTBS)	SCB (493)	Rabbit	1:200 (1% BSA, 1% PGS + TTBS)

Table 3.2. Incubation conditions for each antibody used in immunocytochemistry. *Abbreviations: *CST, Cell Signaling Technology; SCB, Santa Cruz Biotechnology, in brackets the reference number; PGS, preimmune goat serum; TTBS, (0.05% tween 20, 15mM NaCl, 1mM Tris-HCl, pH 7.5).*

3.2.18. XBP1 alternative splicing determination by RT-PCR

The RNA extraction was carried out with TRIzol® reagent (ThermoFisher scientific, Waltham, Massachusetts, USA) as described by the manufacturer (Chomezynski, 1993). Briefly, after homogenizing the cells with TRIzol® reagent, chloroform is added for extracting the RNA.

Isopropanol was used to precipitate the RNA. Following, DNA precipitation was performed with the addition of ethanol.

RNA concentration of the samples was determined spectrophotometrically at 260 nm in a NanoDrop ND-1000 (ThermoFisher scientific, Walthan, Massachusetts, USA). Purity of the RNA was assessed by the absorbance ratio A_{260}/A_{280}, and this was always greater than 1.8.

RNA integrity was analyzed by horizontal electrophoresis in 1% agarose gel with 0.6 μg/ml ethidium bromide solution in TAE (40 mM Tris-acetate, pH 8, 1 mM EDTA). The electrophoresis was carried out at constant voltage (130 V) and gel was imaged by scanning with the Molecular Imager FX scanner (Bio-Rad, Hercules, California, USA).

Before the RNA retrotranscription, the DNA contamination was removed by treatment with DNase I (Invitrogen, Carlsbad, California, USA), which digest single strand as well as double strand DNA. 1.5 μg RNA was treated during 15 min at room temperature with 1 μl DNase buffer (200 mM Tris-Cl, pH 8.4, 20 mM $MgCl_2$, 500 mM KCl), 1 μl DNase I (1U/μl) and DEPC-water was added to a final volume of 10 μl. Reaction was stopped by the addition of 1 μl of 25 mM EDTA and incubation at 65 ºC for 10 min.

The reverse transcription-polymerase chain reaction (RT-PCR) assay was performed with the *Superscript III first strand synthesise system for RT-PCR* Kit (Invitrogen, Carlsbad, California, USA), as described by the manufacturer. A reaction mix was prepared containing 1 μg of RNA previously treated with DNase I, 1 μl of 50 μM oligo-$(dT)_{20}$, 1 μl of 10 mM dNTP and DEPC-water up to a final volume of 10 μl. The mix was incubated during 5 min at 65 ºC for RNA denaturalization. Following, 10 μl of the cDNA synthesis mix was added to each sample, containing 2 μl 10X RT buffer, 4 μl 25 mM $MgCl_2$, 2 μl 0.1 M DTT, 1 μl RNase recombinant inhibitor (40 U/μl) and 1 μl Superscript TM III RT enzyme (200 U/μl). The reaction was carried out at 50 ºC for 75 min, and finalized with a step of 5 min at 85 ºC. Remaining RNA was removed by incubation at 37 ºC for 20 min with 1 μl of *E. coli* RNase H (2 U/μl).

The cDNA of the RT was PCR amplificated. For this purpose, 2 μl of the RT product previously diluted (1/100) was mixed with 5% DMSO, immolase buffer 10X, 1.8 μl of 50 mM $MgCl_2$, 0.32 μl of 25 mM dNTP, 1 μl of each XBP1 primer (10 μM) (XBP1_for: 5'-GAATGAAGTGAGGCCAGTGG-3'; XBP1_rev: 5´-ACTGGGTCCTTCTGGGTAGA-3'), 0.5 μl of

BIOTAQ™ DNA polymerase (5U/µl) (Bioline, Luckenwalde, Germany), and milliQ-water to a final volume of 28 µl. Thermocycler PCR conditions were as follow:

95 ºC	7 min	Enzyme activation	
95 ºC	30 s	Denaturation	30 cycles
55 ºC	30 s	Annealing	
72 ºC	30 s	Extension	
72 ºC	5 min	Final extension	

Products of the PCR were analyzed by horizontal electrophoresis in 2% agarose gel in TBE at constant voltage (120 V) for 1 h. The bands were stained with Syber green (ThermoFisher scientific, Walthan, Massachusetts, USA). The conventional 235 pb fragment and the unconventional processed 261 pb fragment from XBP1 mRNA was analyzed by densitometry after scanning the gel with the Molecular Imager FX scanner (Bio-Rad, Hercules, California, USA).

3.2.19. Adhesion assay

Adhesion capability of cells was studied under two pO_2 conditions (21% and 8% pO_2). Cells were seeded onto 96-well plates in both different oxygen conditions at 20,000 cells per well. The cell adhesion was determined at 1 h after incubation by the crystal violet stain method. The number of adherent cells was determined interpolating the obtained absorbance at 590 nm in a standard curve formed by different cell concentrations.

3.2.20. Statistical analysis

The statistical package SPSS 19.0 (SPSS Inc., Chicago, IL, USA) was used for data analysis. Data were expressed as mean ± standard error (SE) from at least three independent experiments. Statistical significance for the differences of the means was estimated by parametric Student's t-test or non-parametric Wilcoxon test, depending on the sample distributions for paired data. Differences between means were considered significant if $P < 0.05$. The IC_{50} (concentration that inhibits cell growth by 50%) was derived from the semilog dose-response curve. The data were adjusted by nonlinear regression ($R^2 = 0.99$) using GraphPad Prism 4 for Windows (San Diego,CA,USA).

4. RESULTS

4. RESULTS

4.1. Cytotoxic actions of *V. baccifera* on human hepatocarcinoma HepG2 cell line

In this thesis we have used leaf extracts of the *V. baccifera* plant collected from the Macagual Research Centre forest in Florencia, Caquetá (Colombia). The extract was characterized in terms of the content of total phenols and flavonoids (by colorimetric assays), and the total antioxidant activity, measured as the Trolox equivalent antioxidant capacity (TEAC) and the oxygen radical absorbance capacity (ORAC). The leaf extracts that we have used in this work contained per gram of dry weight: a) 43.2 ± 0.3 mg gallic acid (total phenols) and 23.4 ± 0.2 mg catechin (total flavonoids), and the total antioxidant activities were: a) 355.3 ± 5.2 µmol Trolox/g (TEAC) and 922.3 ± 19.5 µmol Trolox/g (ORAC).

4.1.1. Cell toxicity

Human hepatoma HepG2 cells were exposed to a range of concentrations of the *V. baccifera* leaf extract and cytotoxicity was assayed by the crystal violet method.

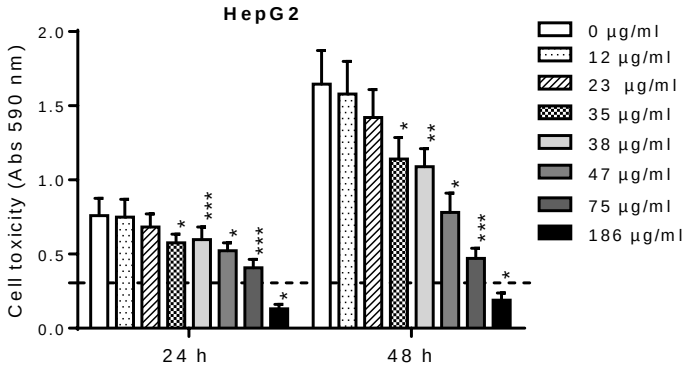

Figure 4.1. Effect of *V. baccifera* on HepG2 toxicity. Cells were treated with increasing concentrations of the extract for the indicated times. Results are the mean + SE from 4-7 experiments. The value of the control at zero time was 0.306 absorbance units at 590 nm, and is represented as a dashed line in the figure. *P < 0.05, **P < 0.01, ***P < 0.001.

The extract significantly reduced cell growth in a dose- and time-dependent manner (Fig. 4.1). At the concentration of 75 µg/ml, *V. baccifera* decreased the number of viable cells to 54% at 24 h and to 29% at 48 h. The highest concentration of the extract caused cell death. The IC_{50} value derived from the dose-response curve was 48.75 µg/ml at 48 h (Fig. 4.2).

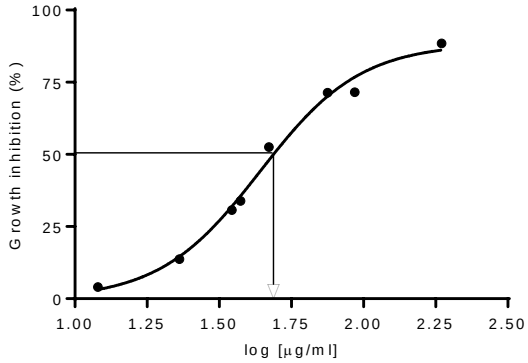

Figure 4.2. Dose-response curve to *V. baccifera* and calculation of the concentration that inhibits 50% of HepG2 cell growth (IC_{50}) at 48 h. The data were fit to a sigmoid dose-response curve by nonlinear regression ($R^2 = 0.99$).

HH4 cells, a nontransformed hepatocyte line derived from immortalized human fetal hepatocytes, was also used as the biological system to study the effect of *V. baccifera*.

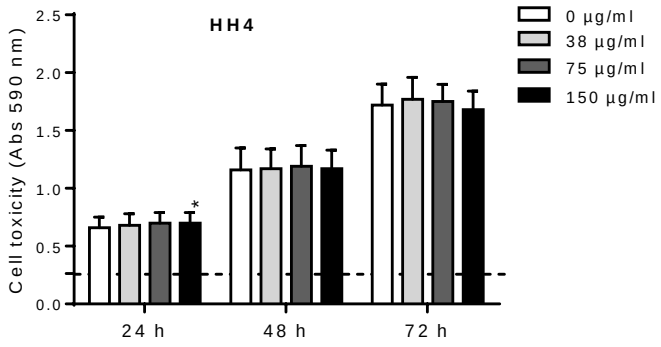

Figure 4.3. Effect of *V. baccifera* on toxicity to HH4. Cells were treated with increasing concentrations of the leaf plant extract for the indicated times. Results are the mean + SE from 3 experiments. The value of the control at time zero was 0.264 absorbance units at 590 nm, and is represented as a dashed line in the figure. *P < 0.05.

In this model, the extract did not affect HH4 viability; indeed, the highest concentration of the extract even caused a marginal cell growth increase at 24 h (Fig. 4.3).

V. baccifera *decreased HepG2 growth as a function of the dose and length of exposure. In contrast, the nontransformed human HH4 hepatocytes were not sensitive to* V. baccifera*.*

To further evaluate the possible role of the tumor suppressor p53 protein on *V. baccifera*-induced toxicity on hepatocarcinoma cells, two human hepatoma cell lines with different expression of p53 were used, Hep3B and Huh7. HepG2 carry wild-type p53; in Hep3B the p53 gene is deleted (Lin et al., 1996); and Huh7 expressed p53 conserves around 4% wild type transactivating activity (Hsu et al., 1993).

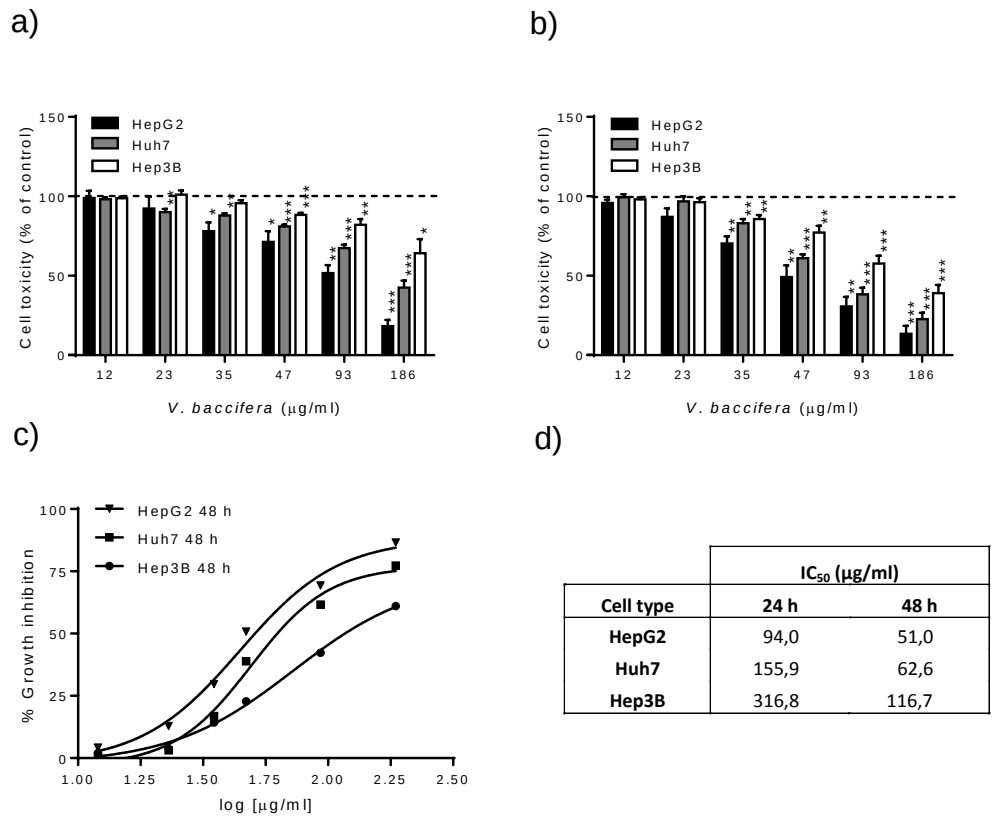

	IC_{50} (µg/ml)	
Cell type	**24 h**	**48 h**
HepG2	94,0	51,0
Huh7	155,9	62,6
Hep3B	316,8	116,7

Figure 4.4. Role of p53 on *V. baccifera*-induced toxicity. HepG2, Huh7 and Hep3B cells were incubated without (control) and with *V. baccifera* at the indicated concentrations. Graphical representation of the cell toxicity at (a) 24 h and (b) 48 h represented as the percentage of the control values, and are the mean + SE from 4-6 experiments. (c) Dose-response curve to *V. baccifera* at 48 h for HepG2, Huh7 and Hep3B cells. The data were fit to a sigmoid dose-response curve by nonlinear regression (R_2 = 0.99). (d) Calculated values for the *V. baccifera* concentration that inhibits 50% of cell growth (IC_{50}). *P < 0.05, **P < 0.01, ***P < 0.001 compared with control (without *V. baccifera*).

As can be seen in Fig. 4.4, the p53-null Hep3B cell line was the most resistant to *V. baccifera* toxicity, while the wt-p53 HepG2 was the most sensitive to the extract. The concentration of *V. baccifera* that inhibited 50% of cell growth (IC_{50}) in Hep3B at 24 h was 2-fold higher than the value in Huh7 and 3.3-fold higher than in HepG2.

These data suggest that p53 could play a role in V. baccifera*-induced toxicity of hepatocarcinoma cells.*

We have previously reported that the *V. baccifera* leaf extract contained high levels of epicatechin flavanols (monomers, dimers and trimers) (Lizcano et al., 2012). These compounds could be responsible of the cytotoxic effects exerted by *V. baccifera* in HepG2. Because of its commercial abailability, we analyzed the effect of purified (−)-epicatechin monomer on toxicity to HepG2 cells.

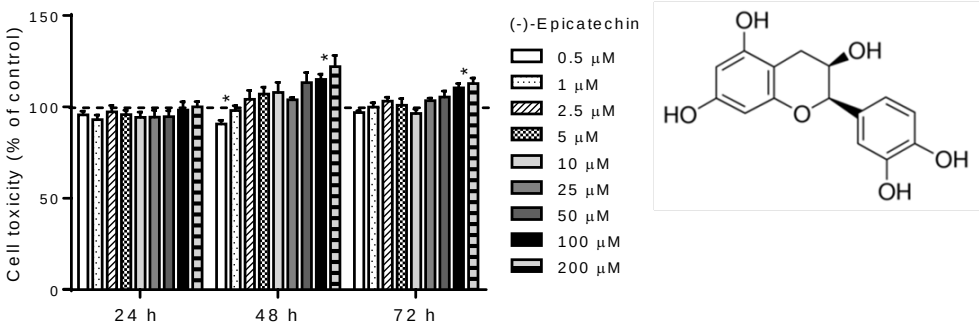

Figure 4.5. Effect of (−)-epicatechin on HepG2 toxicity. Cells were treated without (control) and with increasing (−)-epicatechin concentrations for the indicated times. Results are expressed as the percentage of the control values and are the mean + SE from 3 experiments. *P < 0.05.

The assayed (−)-epicatechin concentrations (0.5 to 200 μM) did not reduce HepG2 cell growth. Indeed, 100 μM of (−)-epicatechin induced a significant increase in HepG2 proliferation at 48 h and 72 h (Fig. 4.5).

(−)-Epicatechin monomers are not the bioactive component responsible of V. baccifera*-induced toxicity.*

4.1.2. Intracellular ROS and mitochondrial O_2^-

To determine whether *V. baccifera* induced ROS in HepG2, the cells were exposed to two concentrations of *V. baccifera* at periods up to 24 h and changes in DCF and MitoSOX fluorescence were measured by flow cytometry.

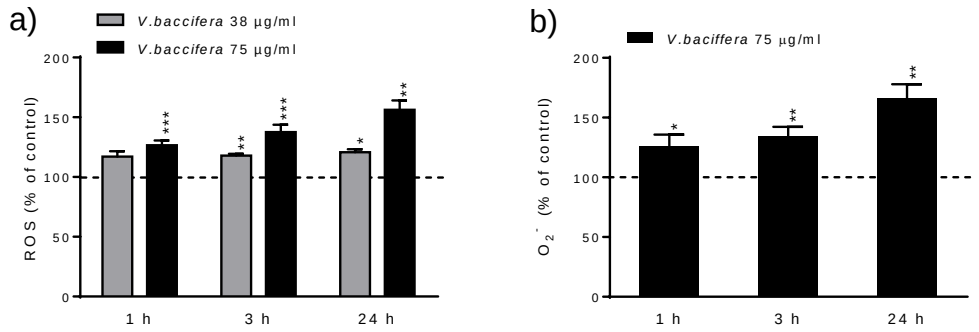

Figure 4.6. Effect of *V. baccifera* on (a) intracellular ROS and (b) mitochondrial O_2^- in HepG2. Cells were incubated without (control) and with *V. baccifera* at the indicated times. Results are the mean + SE from 4-13 experiments. *P < 0.05, **P < 0.01, ***P < 0.001.

The intracellular ROS levels increased as early as 1 h in a dose- and time- dependent manner, and were maintained elevated over control at 24 h (Fig. 4.6.a). Similarly, the plant extract increased time-dependently mitochondrial O_2^- (Fig. 4.6.b).

Intracellular ROS were also determined in human nontransformed HH4 hepatocytes. Changes in DCF fluorescence were measured in HH4 exposed to the plant extract at periods up to 24 h.

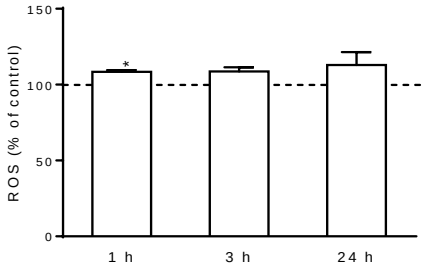

Figure 4.7. Effect of *V. baccifera* on the intracellular ROS in HH4 cell line. Cells were incubated without (control) and with *V. baccifera* (75 mg/ml) at the indicated times. Results are the mean + SE from 3 experiments. *P < 0.05.

Only an occasional ROS increase (8%) was detected at 1 h of *V. baccifera* exposure (Fig. 4.7).

V. baccifera increased intracellular ROS and mitochondrial O_2^- levels as early as 1 h in HepG2.

4.1.3. Mitochondrial membrane potential

Since numerous death signals converge on mitochondria through the activation of pro-apoptotic signals, mitochondria play an important role in apoptotic cell death (Kroemer et al., 1998). *V. baccifera* could induce cell death through mitochondrial damage leading to apoptosis.

To study this possibility, the mitochondrial membrane potential was determined using TMRE, a cell permeant positively-charged dye that readily accumulates into the matrix of actively respiring mitochondria due to its relative negative charge. Depolarized or inactive mitochondria have decreased membrane potential and fail to sequester TMRE. The FCCP uncoupler was used as positive control.

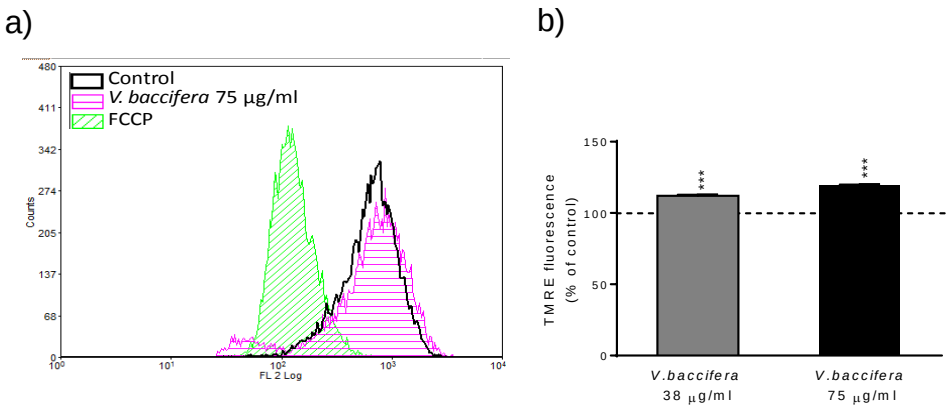

Figure 4.8. Effect of *V. baccifera* on the mitochondrial membrane potential (ψm) in HepG2. (a) Flow cytometry profiles and (b) flow cytometry analysis of the TMRE fluorescence. Cells were incubated without (control) and with *V. baccifera* (38 and 75 µg/ml) for 24 h. The fluorescence sensitive to the membrane potential was determined substracting the fluorescence of cells in presence of the FCCP uncoupler. Results are expressed as the percentage of the control values and are the mean + SE from 5 experiments. ***P < 0.001, compared with controls (without *V. baccifera*).

TMRE fluorescence increased by 12% in HepG2 exposed to 38 µg/ml *V. baccifera*, and by 20% in cells exposed to 75 µg/ml of the plant extract (Fig. 4.8).

V. baccifera *induced an increased of the mitochondrial membrane potential in HepG2.*

4.1.4. Cell cycle

In order to gain knowledge from the cytotoxic effects triggered by *V. baccifera* on HepG2, the cell cycle progression was studied in cells exposed to the plant extract by flow cytometry.

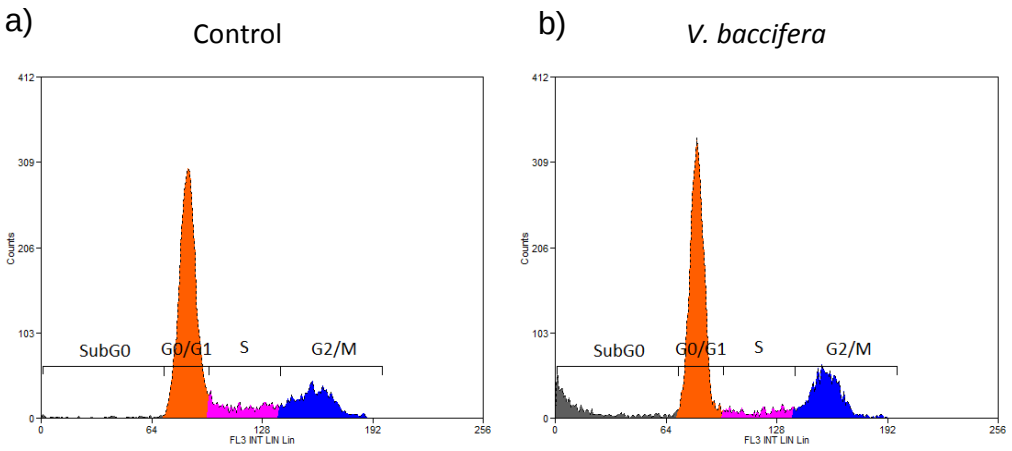

	Cell cycle			
	SubG$_0$ (%)	**G$_0$/G$_1$ (%)**	**S (%)**	**G$_2$/M (%)**
Control	1.6 ± 0.2	67.9 ± 1	13.2 ± 0.7	18.8 ± 0.4
V. baccifera	11.7 ± 0.7***	68.9 ± 0.6	7.9 ± 0.4**	23.4 ± 0.8**

Figure 4.9. Flow cytometry profiles (above) and flow cytometry analysis (below) of the effects of *V. baccifera* on HepG2. Cells were incubated for 24 h (a) without (control) and (b) with *V. baccifera* (75 µg/ml). Cells in subG$_0$-phase were expressed as the percentage of the total cells (SubG$_0$ + G$_0$/G$_1$ + S+ G$_2$/M). Results are the mean ± SE from 6-8 experiments. **P < 0.01, ***P < 0.001 compared with control (without *V. baccifera*).

V. baccifera markedly increased the number of cells in subG$_0$ (P < 0.001) (Fig. 4.9). The extract also increased by 24% the number of cells in G$_2$/M and reduced by 40% the number of cells undergoing DNA replication (S-phase; P < 0.01).

V. baccifera *blocked cell cycle at G$_2$/M in HepG2 cells.*

4.1.5. Caspase-2 and caspase-3 activities

Caspase-2 is an initiator caspase, which has been implicated in the regulation of the G_2/M checkpoint (Puccini et at., 2013). It is known that caspases play an essential role during the execution phase in apoptosis, and caspase-3 is one of the effectors (executioner) caspases. Here we determined caspase-2 and caspase-3 activities in HepG2 cells exposed to *V. baccifera*.

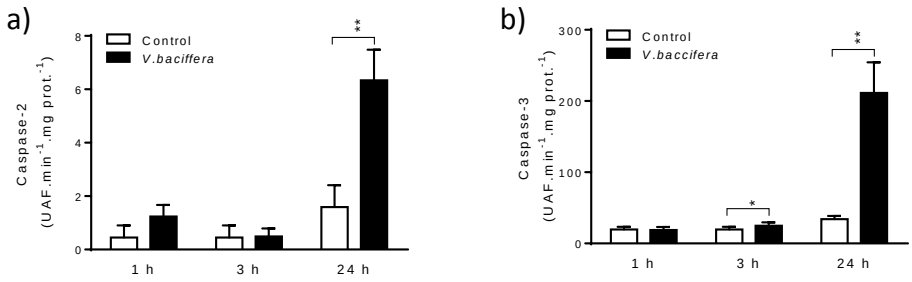

Figure 4.10. Effect of *V. baccifera* on the (a) caspase-2, and (b) caspase-3 activities in HepG2. *V. baccifera* (75 µg/ml) was added at the indicated times. Caspase-2 and caspase-3 activities were measured using fluorogenic substrates. Results are expressed as UAF/min/mg protein and are the mean + SE from 4-8 experiments. *P<0.05, **P < 0.01 compared with controls (without *V. baccifera*) at the same times.

V. baccifera markedly increased the caspase-2 activity (**P < 0.01) in HepG2 at 24 h of treatment (Fig. 4.10.a). The plant extract also significantly activated caspase-3 as early as 3 h, the activity being 3.5-fold higher than the control value at 24 h (**P < 0.01) (Fig. 4.9.b).

These data indicate that V. baccifera *induces HepG2 death through a caspase-dependent mechanism, in which the initiator caspase-2 and the executioner caspase-3 are implicated.*

4.1.6. Cell ultrastructure

In the next step, the morphological changes of HepG2 cells exposed to *V. baccifera* were studied by electron microscopy.

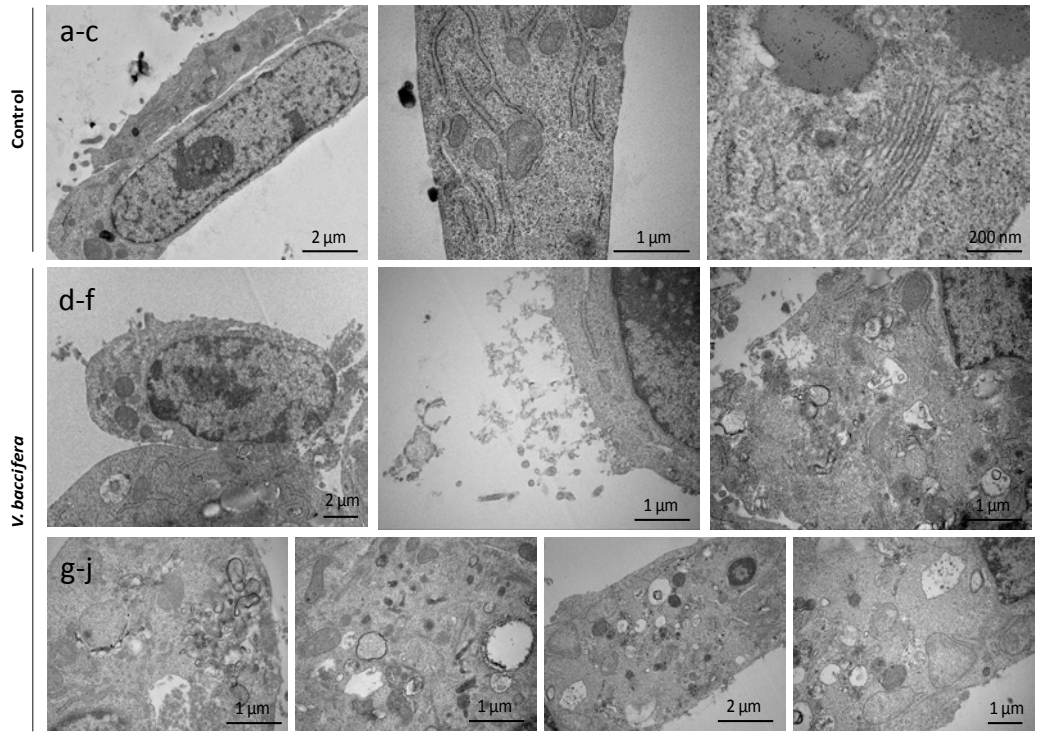

Figure 4.11. Electron microscopy images showing ultrastructural features of control HepG2 cells (a-c) and HepG2 cells exposed to *V. baccifera* (75 µg/ml) for 24 h (d-j).

As can be seen in Fig. 4.11, HepG2 cells revealed typical morphological characteristics of apoptosis, such as cell shrinkage, plasma membrane blebbing, condensation of cytoplasm and chromatin, fragmentation of the rough endoplasmic reticulum (RER), loss of ribosomes, and changes in mitochondrial ultrastructure (Fig. 4.11). A heavily vacuolized cytoplasm containing disintegrated cellular structures was also observed in HepG2 cells incubated with *V. baccifera*.

4.1.7. Cell migration

The effect of *V. baccifera* on HepG2 migration was estimated using two different methods, the scratch wound assay and the transwell assay. The former was carried out measuring the migration distance after 24, 48 and 72 h of the plant extract treatment (Fig. 4.12.a).

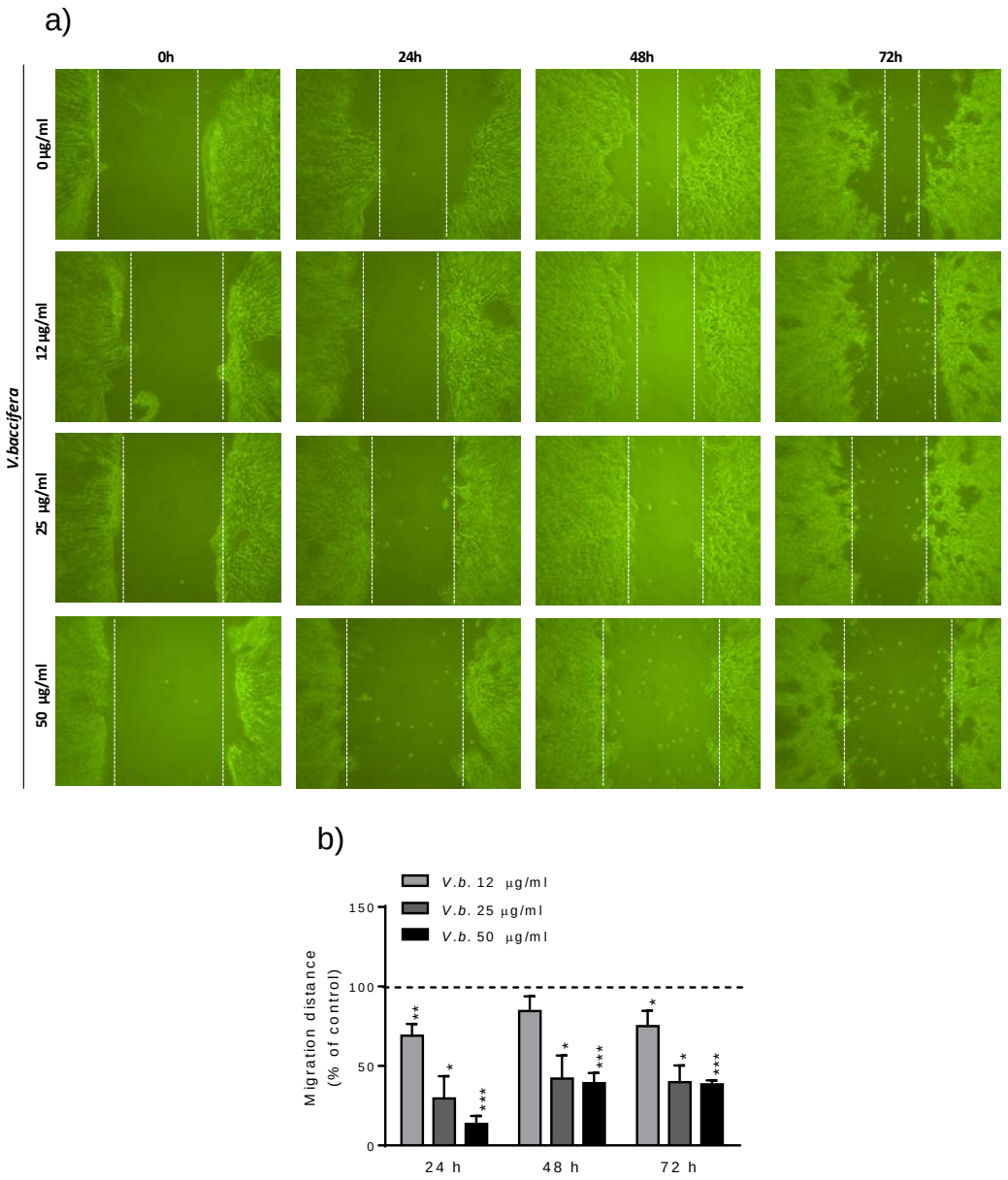

Figure 4.12. Effect of *V. baccifera* on HepG2 migration determined by the scratch wound assay. Cells were cultured as confluent monolayers in complete medium with 2.5% inactivated FBS, and a scratch wound was carried out by removing cells across the well with a pipette tip. After incubation for 24, 48 and 72 h without (control) and with *V. baccifera* (12, 25 and 50 µg/ml), the wound closure was photographed under an inverted phase contrast microscope. (a) Representative photomicrographs of HepG2 migration. (b) Graphical representation of the cell migration expressed as the percentage of the control values. Results are the mean + SE from 3 experiments. *P<0.05, **P < 0.01, ***P < 0.001 compared with controls.

The distance migrated by HepG2 at 24 h of treatment with *V. baccifera* decreased dose-dependently (30%, 70% and 86% lower with 12, 25 and 50 µg/ml of *V. baccifera,* respectively) (Fig. 4.12.b).

The influence of *V. baccifera* on HepG2 migration was also studied by transwell assay inoculating the cells into the upper chamber in complete medium with 2.5% FBS. The extract was added into either the upper or the bottom chamber (Fig. 4.13.a). As shown in the figure, the presence of the extract in the bottom chamber influenced HepG2 migration (2.5-fold higher migration than control). The extract in the upper chamber inhibited the migration but the effect was not statistically significant.

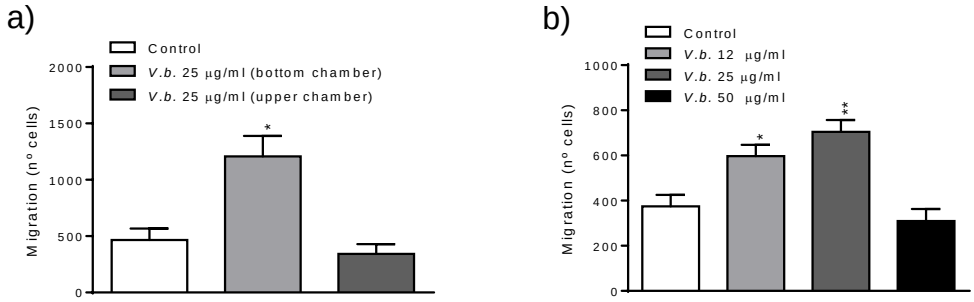

Figure 4.13. Effect of *V. baccifera* on HepG2 migration determined by transwell assay. Cells were inoculated in the upper chamber and incubated for 24 h without (control) and with *V. baccifera*. (a) *V. baccifera* was added in diluted medium with 2.5% FBS into either the bottom or the upper chamber. (b) Increasing concentrations of *V. baccifera* diluted in serum-free medium were added in the bottom chamber. Results are expressed as the number of migrated cells and are the mean + SE from 3-6 experiments. *P<0.05, **P < 0.01 compared with controls.

Taking into account these results increasing concentrations of *V. baccifera* diluted in serum-free EMEM solution were assayed in the bottom chamber for 24h (Fig. 4.13.b). The sub-toxic doses of *V. baccifera* (12-25 µg/ml) triggered an increasing migration of the cells (60% and 88% higher than control respectively). There was no difference in migration at 50 µg/ml dose, a toxic concentration.

V. baccifera *inhibits HepG2 migration, although it exhibits chemotactic properties for HepG2 transmigration.*

4.2. ROS implication in *V.baccifera*-induced toxicity

To evaluate whether the generation of ROS was a significant factor in the cytotoxicity of *V. baccifera*, different free radical scavengers (NAC, Trolox, Tiron and catalase) and inhibitors of ROS-generating enzymes (apocynin and allopurinol) were examined on cell toxicity and the intracellular ROS levels.

NAC

N-Acetyl cysteine (NAC) is a potent antioxidant due to its ability to stimulate glutathione synthesis therefore maintaining the GSH intracellular levels. NAC is a thiol compound, which crosses cell membranes, and is deacetylated in the hepatocyte to cysteine, the source for GSH synthesis. Previous cytotoxic studies with different concentrations of NAC (1-10 mM) established that NAC doses higher than 1 mM inhibited cell growth. Therefore, 1 mM NAC was selected for further assays.

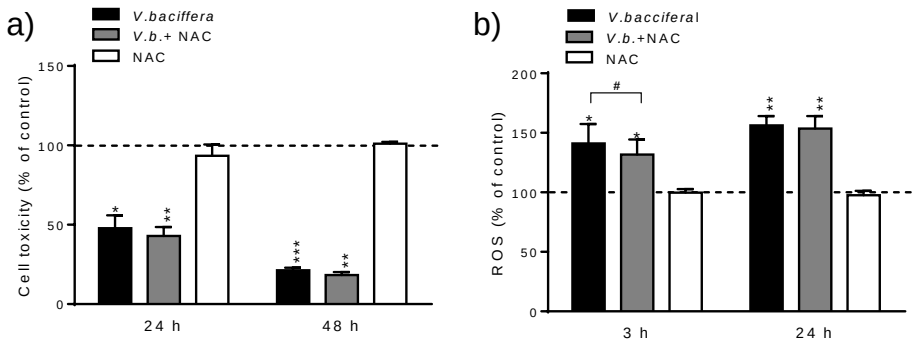

Figure 4.14. Effect of NAC on *V. baccifera*-induced (a) toxicity and (b) ROS in HepG2. Cells were exposed to 1 mM NAC 1 h before the addition of *V. baccifera* (75 µg/ml). Results are expressed as the percentage of the control values (without *V. baccifera*) and are the mean + SE from 3-4 experiments. *P < 0.05, **P < 0.01, ***P < 0.001 compared with controls. #P < 0.05 compared with *V. baccifera*.

Results revealed that *V. baccifera* toxicity to HepG2 was unaffected by co-exposure with NAC (Fig. 4.14.a). NAC marginally reverted *V. baccifera*-induced intracellular ROS levels at 3 h (Fig. 4.14.b).

Trolox

Trolox is a lipoperoxyl radical scavenger and a water-soluble analogous of vitamin E. In preliminary assays we found that concentrations of Trolox higher than 100 µM reduced the cell growth rate. Therefore we selected 100 µM Trolox for further experiments.

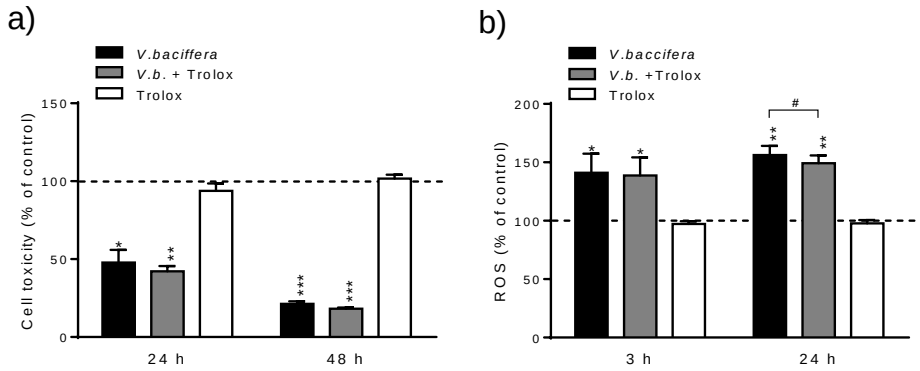

Figure 4.15. Effect of Trolox on *V. baccifera*-induced (a) toxicity and (b) ROS production in HepG2. Cells were exposed to 100 µM Trolox 1 h before the addition of *V. baccifera* (75 µg/ml). Results are expressed as the percentage of the control values and are the mean + SE from 3-4 experiments. *P < 0.05, **P < 0.01, ***P < 0.001 compared with controls (without *V. baccifera*). #P < 0.05 compared with *V. baccifera*.

The co-incubation of HepG2 with 100 µM Trolox and the plant extract for 24 h and 48 h did not prevent toxicity (Fig. 4.15.a). This peroxyl radical scavenger partially reduced ROS accumulation at 24 h of co-treatment (Fig. 4.15.b).

Trolox was unable to prevent V. baccifera-*induced cytotoxicity and ROS accumulation in HepG2.*

Tiron

Tiron has been reported to be an O_2^- scavenger (Fang et al., 2012); we have used this compound in this work to study the involvement of O_2^- in *V. baccifera*-induced toxicity. In preliminary studies we found that Tiron exerted a dose-dependent (0.5-5 mM) inhibition of HepG2 cell growth up to 48 h.

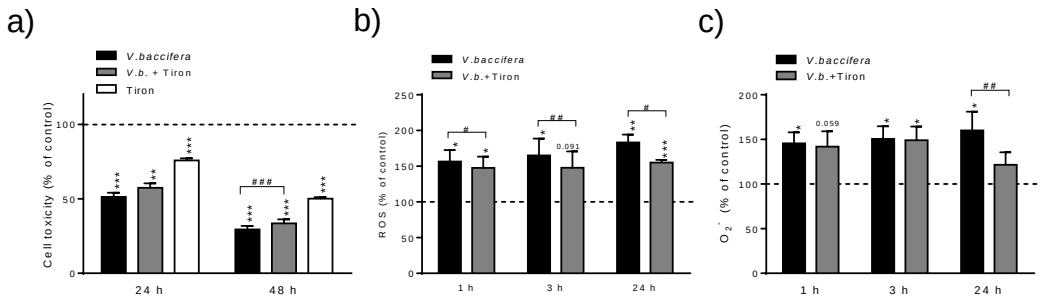

Figure 4.16. Effect of Tiron on *V. baccifera*-induced (a) toxicity, (b) ROS levels and (c) mitochondrial O_2^- in HepG2. Cells were exposed to 1 mM Tiron 1 h before the addition of *V. baccifera* (75 mg/ml). Results are expressed as the percentage of the control values (without *V. baccifera*) and are the mean + SE from 3-6 experiments. *P < 0.05, **P < 0.01, ***P < 0.001 compared with controls. #P < 0.05, ##P < 0.01 compared with *V. baccifera*.

At 1 mM Tiron induced toxicity (Fig. 4.16.a). Paradoxically, it reduced cell toxicity 14% at 48 h ($p<0.001$) when it was co-incubated with *V. baccifera*. Moreover, Tiron partially prevented ROS accumulation as early as 1 h after co-treatment with the extract (Fig. 4.16.b). Regarding mitochondrial O_2^-, Tiron reverted its levels to control values at 24 h (Fig. 4.16.c).

Apocynin and allopurinol

Apocynin is an inhibitor of NADPH oxidase and is thus effective in preventing the enzymatic production of superoxide anion. Allopurinol is a hypoxanthine analogue and xanthine oxidase inhibitor, avoiding the generation of free radicals from the xanthine/xanthine oxidase system.

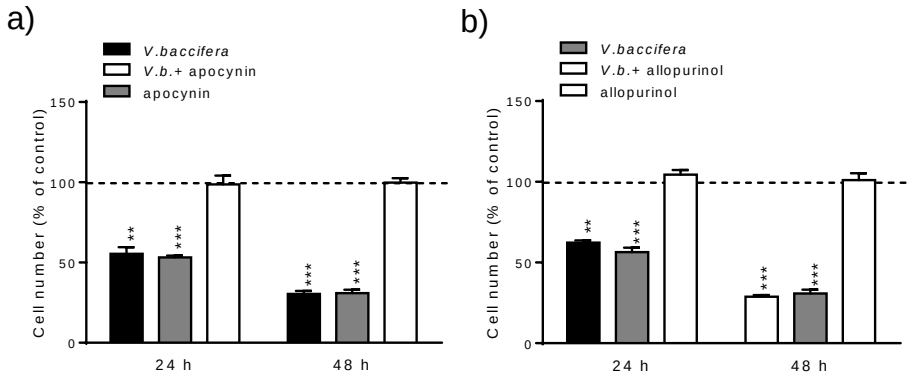

Figure 4.17. Effect of (a) apocynin and (b) allopurinol on *V. baccifera*-induced toxicity in HepG2. Cells were exposed to 300 µM apocynin or 100 µM alopurinol 1 h before the addition of *V. baccifera* (75 µg/ml). Results are expressed as the percentage of the control values and are the mean + SE from 4 experiments. **P < 0.01, ***P < 0.001 compared with controls (without *V. baccifera*).

Neither apocynin nor allopurinol prevented the decrease in the cell number after incubation with the *V. baccifera* extract (Fig. 4.17).

Catalase

Catalase decomposes hydrogen peroxide in oxygen and water. Consequently, catalase was used in this work to elucidate whether H_2O_2 was involved in *V. baccifera*-induced toxicity in HepG2.

Different concentrations of catalase (2.5-10 kU/ml) were assayed for 24 h and 48 h.

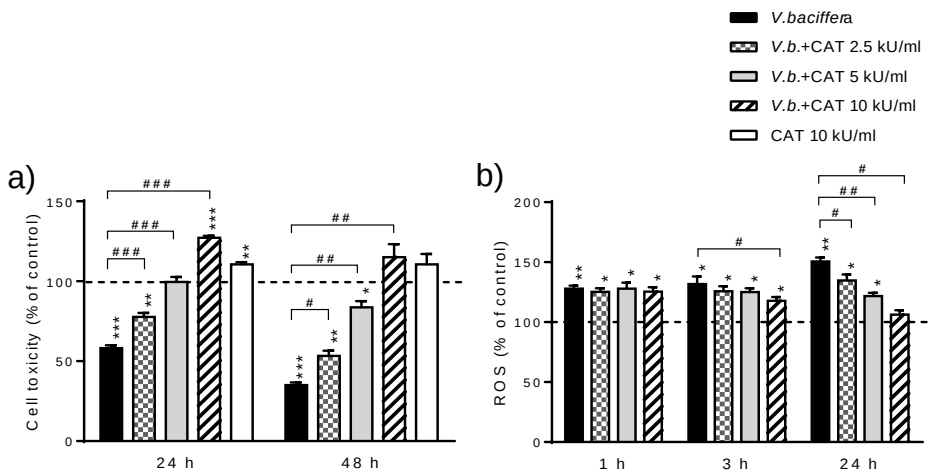

Figure 4.18. Effect of catalase on *V. baccifera*-induced (a) toxicity and (b) ROS production in HepG2. Cells were exposed to catalase at the indicated concentrations 1 h before the addition of *V. baccifera* (75 µg/ml). Results are expressed as the percentage of the control values (without *V. baccifera*) and are the mean + SE from 3-5 experiments. *P < 0.05, **P < 0.01, ***P < 0.001 compared with controls. #P < 0.05, ##P < 0.01, ###P < 0.001 compared with *V. baccifera*. CAT, catalase.

The exposure to the enzyme protected the cells dose- and time-dependently against *V. baccifera*-induced toxicity (Fig. 4.18.a). Catalase (10 kU/ml) completely prevented toxicity at 24 and 48 h, and even increased cell growth at 24 h. The enzyme alone also induced cell proliferation by 10% at 24 h, compared with the control (no additions).

Concerning ROS levels, the enzyme dose-dependently decreased their accumulation at 24 h (Fig. 4.18.b). This effect on the intracellular ROS reduction was observed as early as 3 h

for the highest concentration of catalase (10 kU/ml); at this dose, ROS levels reverted to control values at 24 h. According to these data, the catalase concentration of 10 kU/ml was used for further studies.

All these data point to the involvement of hydrogen peroxide as the main mediator of the cytotoxic effect exerted by V. baccifera *not excluding some role for superoxide anion.*

4.3. Antioxidant system targeted by *V. baccifera*

The cellular antioxidant responses are mediated by enzymatic and nonenzymatic antioxidant systems. There are several antioxidant enzymes that catalyze reactions to neutralize free radicals and reactive oxygen species, such as superoxide dismutase (SOD), glutathione peroxidase (GPx), glutathione reductase, and catalase (CAT) (Pisoschi et al., 2015, review).

On the other hand, the major constituent of the nonenzymatic antioxidant defence is glutathione, an important water-soluble antioxidant, which can neutralize ROS either directly or by an enzyme catalyzed reaction.

4.3.1. SOD and GPx activities

The antioxidant activities of SOD and GPx were measured in the presence of *V. baccifera* at periods up to 24 h in HepG2.

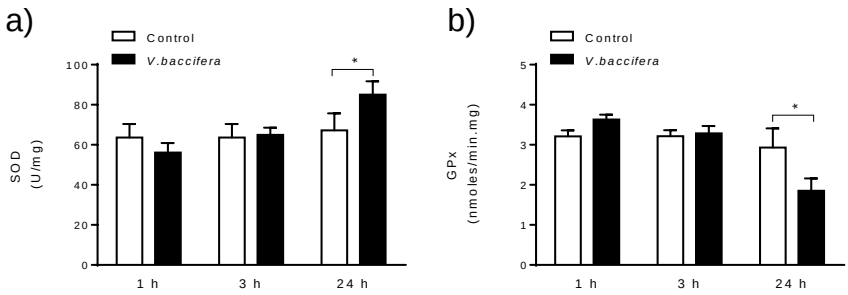

Figure 4.19. SOD and GPx activities in HepG2 exposed to *V. baccifera*. Cells were incubated without (control) and with *V. baccifera* (75 µg/ml) for the indicated times. Results are expressed as the percentage of the control values (without *V. baccifera*) and are the mean + SE from 4-10 experiments. *P < 0.05, **P < 0.01 compared with controls.

Under basal conditions, the measured enzymatic activities remained constant along the incubation time (Fig. 4.19.a). The *V. baccifera* extract significantly increased SOD activity at 24 h (29% increment, $p < 0.05$). By contrast, GPx activity decreased a 36% in the presence of the plant extract at 24 h ($p< 0.05$) (Fig. 4.19.b).

These data suggest an increase in the intracellular steady-state levels of hydrogen peroxide at 24 h.

4.3.2. Glutathione

GSH has a key role in the intracellular redox homeostasis. We investigated the effects of *V. baccifera* on the intracellular glutathione levels in HepG2 cells.

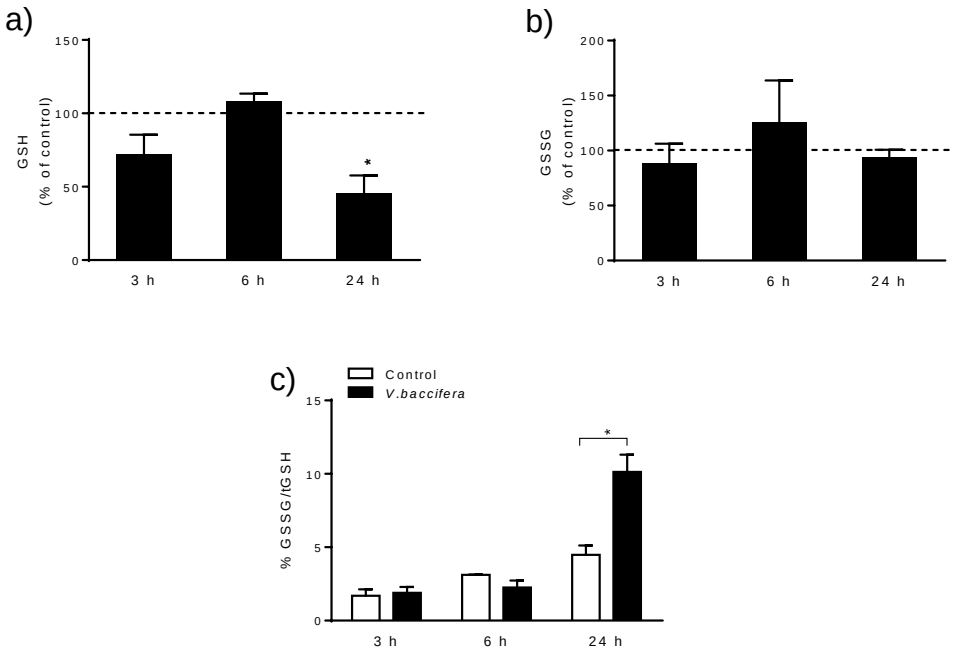

Figure 4.20. Effects of *V. baccifera* on (a) GSH, (b) GSSG and (c) the GSSG/total GSH ratio in HepG2. Cells were incubated for the indicated times without (control) and with *V. baccifera* (75 µg/ml). Results are the mean + SE from 3-7 experiments. *P < 0.05 compared with controls at the same times.

The plant extract significantly reduced by 50% the intracellular levels of GSH at 24 h (Fig 4.20.a), not modifying the concentration of GSSG at any time (Fig 4.20.b); this resulted in a

dramatically increase of the ratio of GSSG to total glutathione at 24 h (125%, $p<0.05$) (Fig 4.20.c).

4.4. Involvement of hydrogen peroxide in the *V. baccifera*-induced toxicity

4.4.1. H_2O_2 production

The H_2O_2 production into the cells can be estimated by measuring the H_2O_2 released to the medium, since this molecule freely crosses the plasma membrane. For this purpose, the non-permeant Amplex probe (specific for H_2O_2 detection) was used.

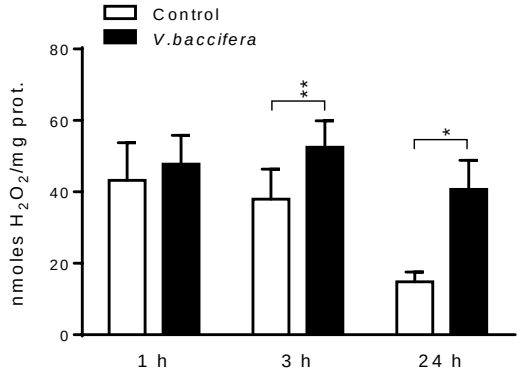

Figure 4.21. Effect of *V. baccifera* on the extracellular H_2O_2 levels in HepG2. Cells were incubated for the indicated times without (control) and with *V. baccifera* (75 µg/ml). After incubation, the cells were washed and the corresponding medium was added to determine H_2O_2 using Amplex Red reagent for 2 h. Results are the mean + SE from 5 experiments. *P < 0.05, **P < 0.01 compared with *V. baccifera*.

Under basal conditions, the rate of H_2O_2 production decreased progressively from 1 h to 24 h of incubation. *V. baccifera* significantly increased the rate of hydrogen peroxide production at 3 h and 24 h of treatment (Fig. 4.21).

4.4.2. Effect of catalase on SOD and GPx

We have described previously that *V. baccifera* increased SOD and decreased GPx activities. To study the involvement of H_2O_2 on these effects, these enzyme activities were assayed in the presence of catalase and the plant extract.

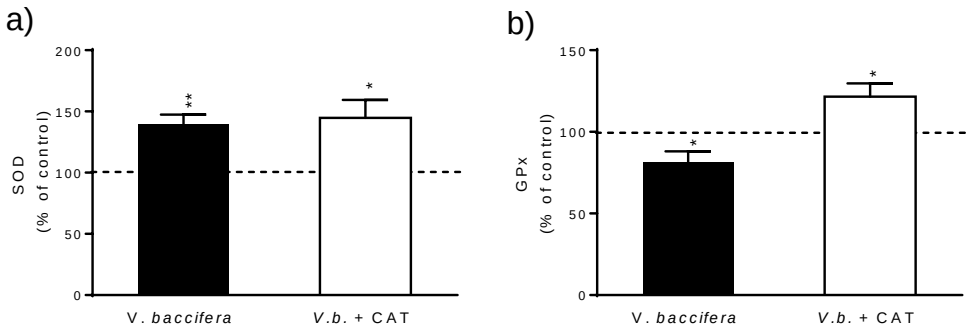

Figure 4.22. Effect of catalase on (a) SOD and (b) GPx activities in HepG2 exposed to *V. baccifera*. Cells were incubated with *V. baccifera* (75 µg/ml) either alone (control) or with catalase (10 kU/ml) for 24 h. Results are expressed as the percentage of the control values (without *V. baccifera*) and are the mean + SE from 5-10 experiments. *P < 0.05, **P < 0.01 compared with controls. CAT, catalase.

The increment in SOD activity was unaffected by catalase (Fig. 4.22.a). However, in the case of GPx, catalase not only reverted its inhibition, but also increased its activity over control cells (22% increase, P < 0.05) (Fig. 4.22.b).

Superoxide anion is enzymatically dismutated in mammalian cells by Cu,Zn-SOD (cytosolic) and Mn-SOD (mitochondrial). To determinate whether the expression of any of these isoforms were modulated by *V. baccifera*-induced hydrogen peroxide, HepG2 cells were co-incubated with catalase and *V. baccifera*, and the protein extracts were analyzed by immunoblot (Fig. 4.23.a). Recombinant SOD protein was used to derive a standard curve and get absolute amounts of both isoforms present in the cell extracts.

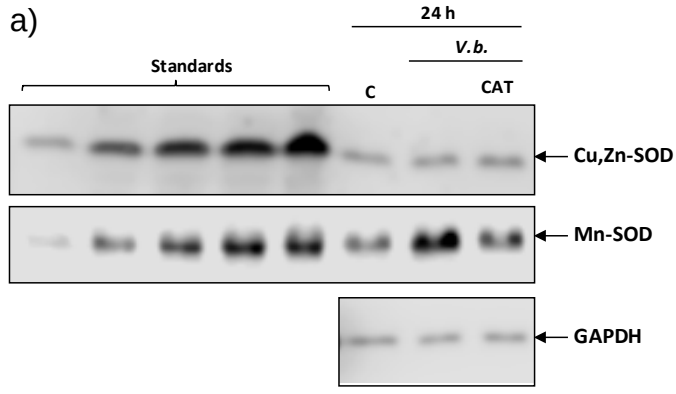

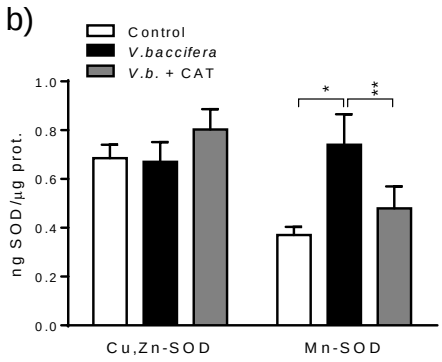

Figure 4.23. Cu,Zn-SOD and Mn-SOD expression in HepG2 exposed to V. *baccifera*. Cells were incubated for 24 h without (control, C) and with *V. baccifera* (75 µg/ml) either alone or with catalase (10 kU/ml). (a) Protein extracts analyzed by western blotting (representative experiment). GAPDH was used as the loading control. (b) Representation of the densitometry changes from the western blot experiments represented in (a). Recombinant proteins were used to derive a curve from each sample and determine the absolute amounts of Cu,Zn-SOD and Mn-SOD. Results are the mean + SE from 4-5 experiments. *P < 0.05, **P < 0.01. CAT, catalase.

Under basal conditions, the Cu,Zn-SOD protein was near two-fold higher expressed than Mn-SOD (Fig. 4.23). *V. baccifera* did not affect Cu,Zn-SOD expression. However, the plant extract dramatically increased Mn-SOD protein levels. The addition of exogenous catalase reduced the quantity of Mn-SOD to control values.

Results suggest that H_2O_2 is involved in the regulation of GPx activity and the expression of Mn-SOD induced by V. baccifera*. SOD activity is independent of H_2O_2 levels.*

4.4.3. Effect of catalase on GSH depletion

To further examine the involvement of hydrogen peroxide on GSH depletion induced by *V. baccifera*, cells were co-incubated with catalase.

Catalase markedly prevented GSH depletion, and reverted to control values the ratio of GSSG to total GSH (Fig. 4.24).

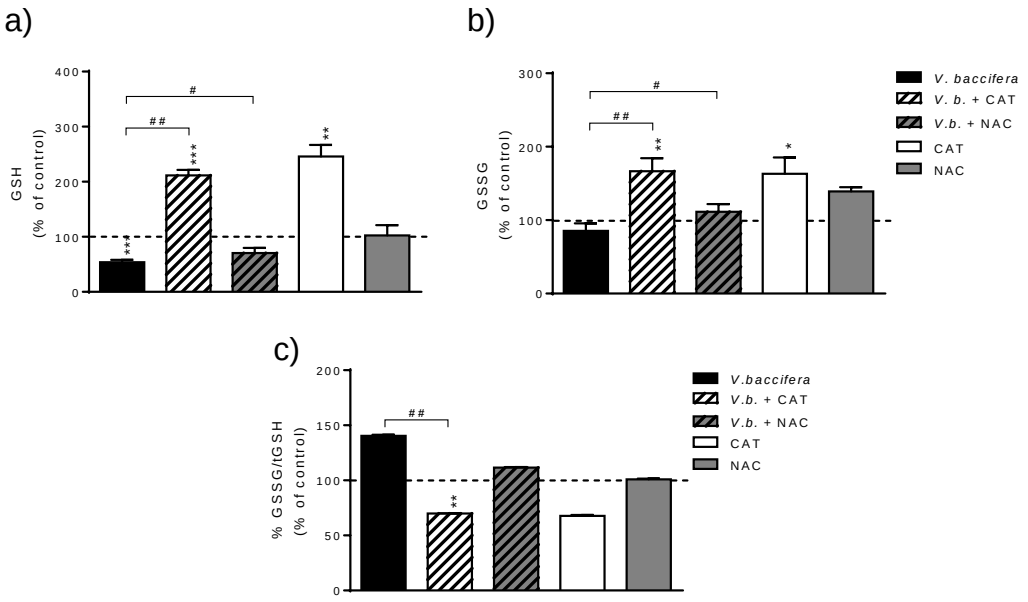

Figure 4.24. Effect of catalase and NAC on (a) GSH, (b) GSSG, and (c) the GSSG/total GSH ratio, in the presence of *V. baccifera* in HepG2. Cells were incubated for 24 h without (control) and with *V. baccifera* (75 µg/ml) alone or plus catalase (10 kU/ml) or NAC (1 mM). Results are the mean + SE from 4-10 experiments. The absolute amounts of total glutathione and GSSG in control cells were 40 nmol/mg protein and 1.3 nmol/mg protein, respectively. *P < 0.05, **P < 0.01; ***P < 0.001, compared with control (without *V. baccifera*). #P < 0.05 and ##P < 0.01 compared with *V. baccifera*. CAT, catalase.

We have previously described that NAC did not prevent either ROS accumulation or cell toxicity. The co-incubation of cells with NAC significantly reverted GSH to control levels (Fig. 4.24.a).

These results suggest that hydrogen peroxide is mediating GSH depletion; however, GSH depletion is not the cause of V. baccifera*-induced cytotoxicity.*

4.4.4. Effect of catalase on mitochondrial membrane potential

To investigate whether alteration of the mitochondrial membrane potential was attributed to intracellular ROS, HepG2 cells were exposed to *V. baccifera* in the presence of catalase.

The *V. baccifera*-induced mitochondrial hyperpolarization was prevented by catalase, rendering a 28% depolarization (P < 0.01) respecting control (Fig. 4.25).

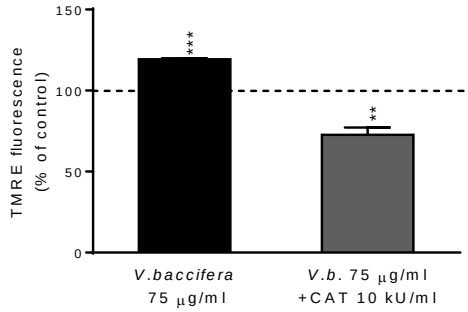

Figure 4.25. Effect of catalase on mitochondrial membrane potential in HepG2 exposed to V. *baccifera* for 24 h. Cells were incubated without (control) and with *V. baccifera* (75 µg/ml) either alone or with catalase (10 kU/ml) for 24 h. The absolute fluorescence was determined subtracting the FCCP uncoupler fluorescence from the cells exposed to the plant extract. Results are expressed as the percentage of the control values and are the mean + SE from 5 experiments. **P < 0.01, ***P < 0.001, compared with controls. CAT, catalase.

4.4.5. Effect of catalase on cell cycle arrest

To determine the involvement of H_2O_2 in cell cycle arrest at G_2/M induced by *V. baccifera*, we studied the effect of commercial catalase co-incubated with the plant extract.

		Cells in cell cycle		
	SubG$_0$ (%)	**G$_0$/G$_1$ (%)**	**S (%)**	**G$_2$/M (%)**
Control	1.6 ± 0.2	67.9 ± 1.0	13.2 ± 0.7	18.8 ± 0.4
V. baccifera	11.7 ± 0.7 ***	68.9 ± 0.6	7.9 ± 0.4 **	23.4 ± 0.8 **
***V. baccifera* + CAT**	2.9 ± 0.3 **, ###	67.8 ± 0.7	12.7 ± 0.5 #	19.5 ± 0.4 #

Table 4.1. Flow cytometry analysis of the effects of catalase on cell cycle in HepG2 exposed to *V. baccifera*. Cells were incubated for 24 h without (control) and with *V. baccifera* (75 µg/ml) either alone or with catalase (10 kU/ml). Cells in subG$_0$-phase were expressed as the percentage of the total cells (SubG$_0$ + G$_0$/G$_1$ + S+ G$_2$/M). Results are the mean ± SE from 6-9 experiments. **P < 0.01, ***P < 0.001 compared with control. #P < 0.05, ###P < 0.001 compared with *V. baccifera*. CAT, catalase.

Catalase significantly decreased the number of cells in subG$_0$ and completely prevented cell cycle arrest (Table 4.1).

4.4.6. Effect of catalase on caspase-3 activation

To determinate whether H_2O_2 was involved in *V. baccifera*-induced apoptosis, exogenous catalase was co-treated with the plant extract and caspase-3 activity was determined.

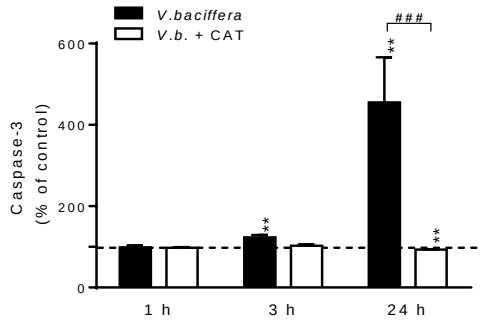

Figure 4.26. Effect of catalase on caspase-3 activity in HepG2 exposed to *V. baccifera*. Cells were incubated with *V. baccifera* (75 µg/ml) either alone or with catalase (10 kU/ml). Results are the mean + SE from 6-14 experiments and are expressed as the percentage of the control values. **p < 0.01 compared with controls (without *V. baccifera*). ###p < 0.001 compared with *V. baccifera* alone. CAT, catalase.

Catalase completely prevented the activation of caspase-3 at 24 h (p< 0.001) (Fig. 4.26).

Moreover, it was also studied the poly ADP ribose polymerase (PARP) cleavage, which is a caspase-3 substrate. *V. baccifera* significantly increased the induction of PARP processing by caspase-3 (Fig. 4.27). The presence of catalase completely inhibited PARP cleavage.

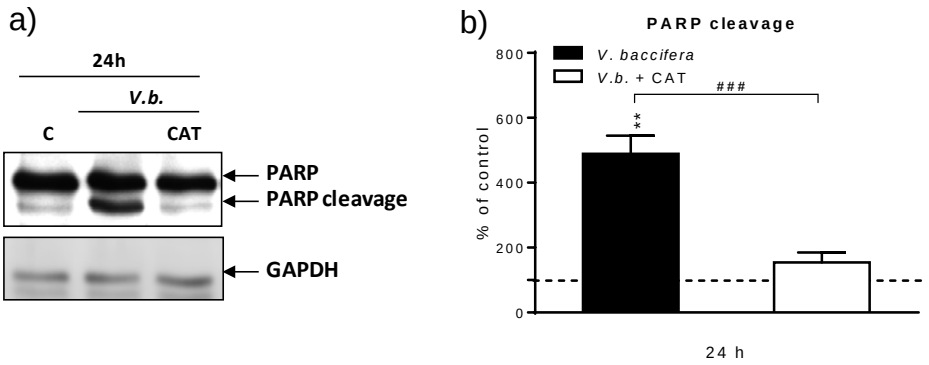

Figure 4.27. Effect of *V. baccifera* on PARP cleavage in HepG2. Cells were incubated without (control, C) and with *V. baccifera* (75 µg/ml) alone or plus catalase (10 kU/ml) at 24 h. (a) Proteins from the cell extracts were analyzed by

western blot using the indicated antibodies. GAPDH was used as the loading control. The bands shown are representative of at least 3 independent experiments. (b) Representation of the densitometry changes from the western blot experiments represented in (a). Results are the mean + SE from 3 experiments. **P < 0.01, compared with control. ###P < 0.001 compared with *V. baccifera*. CAT, catalase.

All these data suggest that ROS, particularly hydrogen peroxide, triggers the mitochondrial membrane potential hyperpolarization, the cell cycle arrest at G_2/M and the caspase-3 activation.

4.5. Effect of *V. baccifera* on signal transduction pathways

In this section we studied several ROS sensitive signal transduction pathways in HepG2 exposed to *V. baccifera* by western blot and immunocytochemistry, examining the phosphorylated forms at specific amino acidic residues of the kinases (activated forms).

The role of hydrogen peroxide in these pathways was challenged by the addition of catalase.

4.5.1. Akt pathway

The Akt pathway promotes survival and growth in response to extracellular signals.

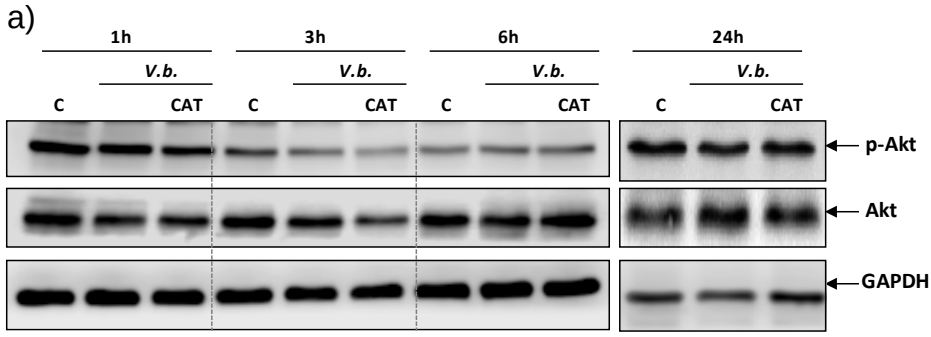

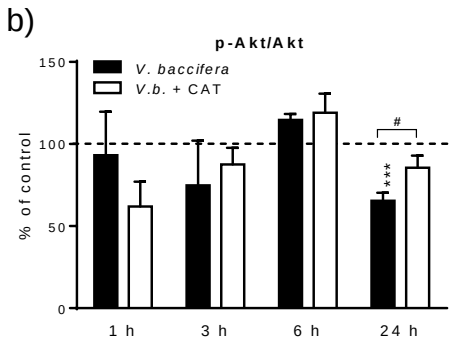

Figure 4.28. Effect of *V. baccifera* on Akt phosphorylation in HepG2. Cells were incubated without (control, C) and with *V. baccifera* (75 µg/ml) alone or plus catalase (10 kU/ml) at the indicated times. (a) Proteins from the cell extracts were analyzed by western blot using the indicated antibodies. GAPDH was used as the loading control**.** The bands shown are representative of at least 3 independent experiments. (b) Representation of the densitometry changes from the western blot experiments represented in (a). Results are the mean + SE from 3-9 experiments. ***P < 0.001, compared with control. #P < 0.05 compared with *V. baccifera*. CAT, catalase.

V. baccifera inhibited significantly Akt phosphorylation at 24 h (Fig. 4.28), without modifying total Akt expression. The treatment of cells with catalase reverted Akt phosphorylation.

These results suggest that V. baccifera*-induced hydrogen peroxide inhibits Akt prosurvival pathway.*

4.5.2. MAPKs pathways

MAPKs, such as ERK, JNK and p38 MAPK, are important mediators of signal transduction that can be activated via oxidative stress (McCubrey et al., 2006). Here we examined the time-course of these MAPKs pathways in the presence of *V. baccifera*.

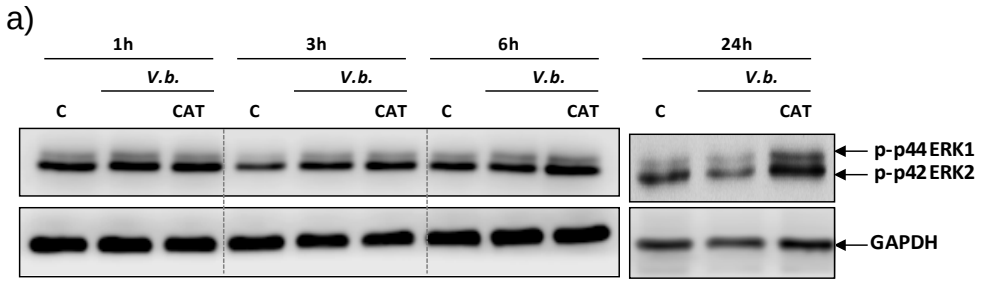

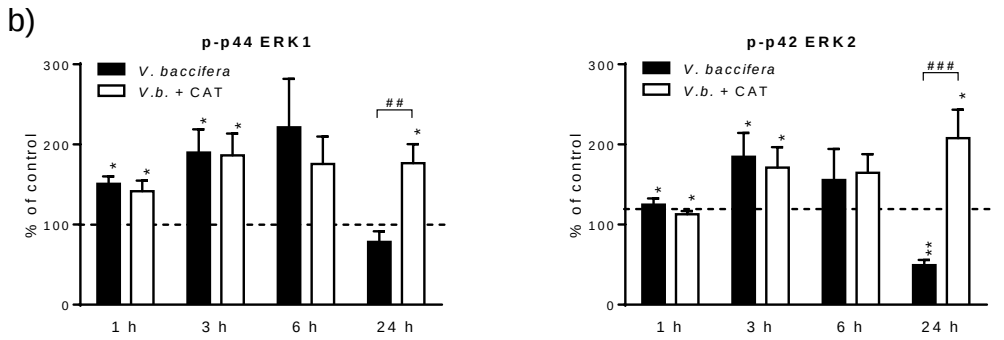

Figure 4.29. Effect of *V. baccifera* on ERK phosphorylation in HepG2. Cells were incubated without (control, C) and with *V. baccifera* (75 µg/ml) alone or plus catalase (10 kU/ml) at the indicated times. (a) Proteins from the cell extracts were analyzed by western blot using the indicated antibodies. GAPDH was used as the loading control. The bands shown are representative of at least 3 independent experiments. (b) Representation of the densitometry changes from the western blot experiments represented in (a). Results are the mean + SE from 4-6 experiments. *P < 0.05, **P < 0.01, compared with control (without *V. baccifera*). ##P < 0.01 and ###P < 0.001 compared with *V. baccifera*. CAT, catalase.

V. baccifera triggered a biphasic effect on ERK modification. A fast increase in ERK1/2 phosphorylation (1 h and 3 h) was followed by a reversion to control levels at 24 h (ERK1) and even a lower phosphorylation of ERK2 ($p<0.01$) (Fig. 4.29). Catalase modified the effects of the plant extract only at 24 h, rendering ERK1/2 in a higher phosphorylation state.

These results suggest that hydrogen peroxide has not a role in the early ERK1/2 phosphorylation, but perhaps is involved in ERK inactivation.

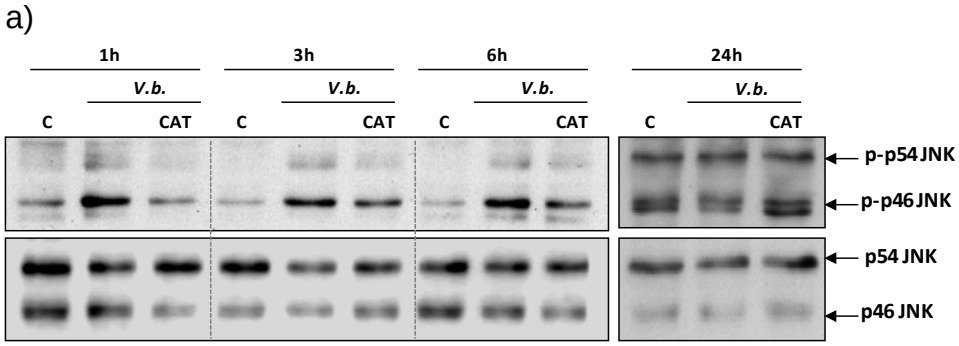

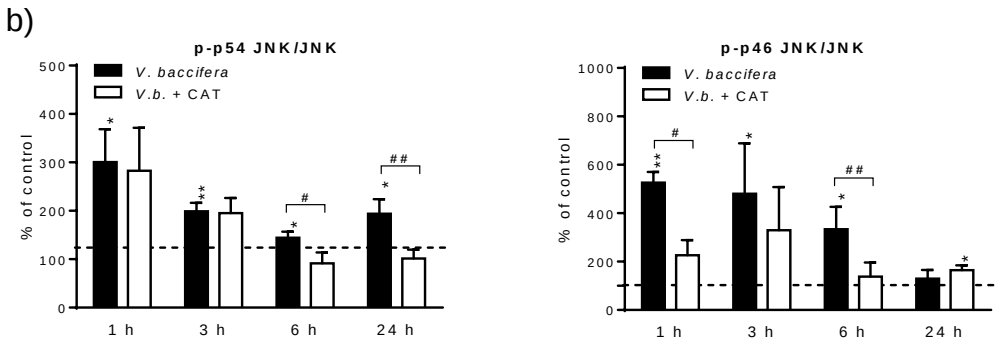

Figure 4.30. Effect of *V. baccifera* on JNK phosphorylation in HepG2. Cells were incubated without (control, C) and with *V. baccifera* (75 µg/ml) alone or plus catalase (10 kU/ml) at the indicated times. (a) Proteins from the cell extracts were analyzed by western blot using the indicated antibodies. The bands shown are representative of at least 3 independent experiments. (b) Representation of the densitometry changes from the western blot experiments represented in (a). Results are the mean + SE from 3-5 experiments. *P < 0.05, **P < 0.01, compared with control (without *V. baccifera*). #P < 0.05 and ##P < 0.01 compared with *V. baccifera*. CAT, catalase.

V. baccifera promoted sharply JNK phosphorylation from the first time assayed, which was sustained in the time (Fig. 4.30). Only the phosphorylation state of the p46 isoform was similar to control at 24 h. Catalase reverted JNK phosphorylation to control values.

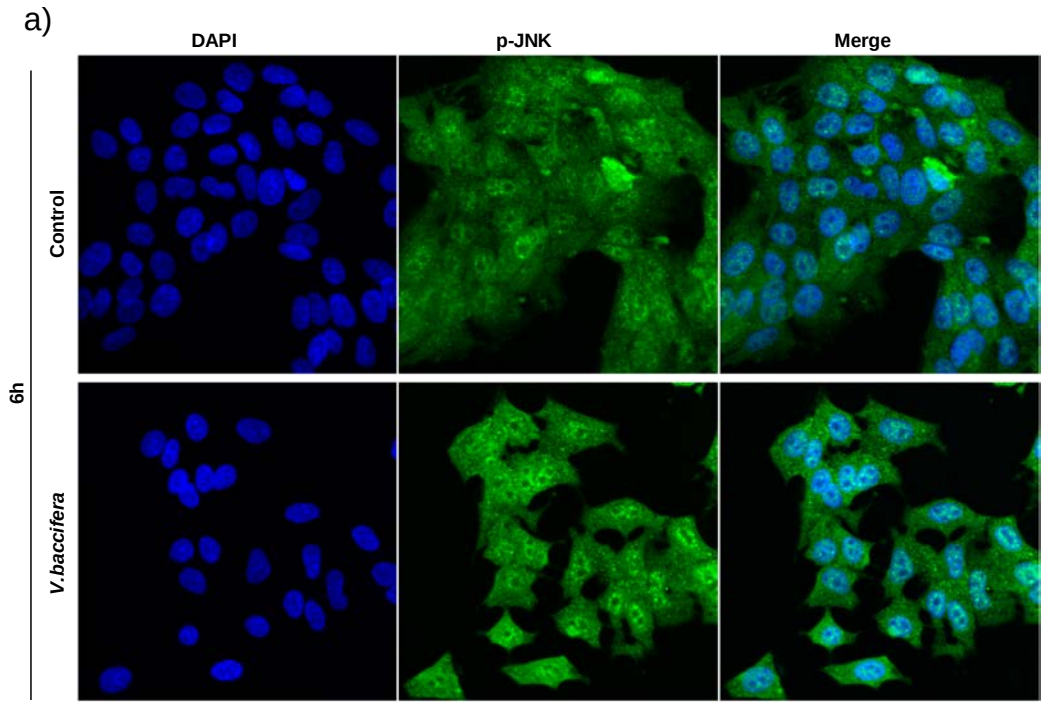

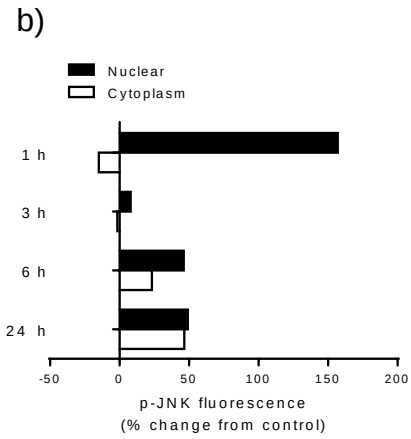

Figure 4.31. Effect of *V. baccifera* on p-JNK localization in HepG2. (a) Cells were incubated without (control) and with *V. baccifera* (75 μg/ml) at the indicated times and phosphoprotein was detected by immunocytochemistry. (b) Representation of the subcellular fluorescence distribution in the micrography analyzed using the ImageJ software.

Inmunofluorescence confocal microscopy revealed the cellular distribution of pJNK, showing higher intensity in the nuclear compartment (Fig. 4.31.a). According to the analysis of the digital images, a clear enrichment of the phosphoprotien in the nucleus was stimulated by *V. baccifera* (150% increase over control at 1 h) (Fig. 4.31.b). A significant increase in the cytoplasmic compartment was also observed from 6 h.

These data suggest a ROS-dependent mechanism for V. baccifera-*induced JNK activation that is sensitive to catalase inhibition.*

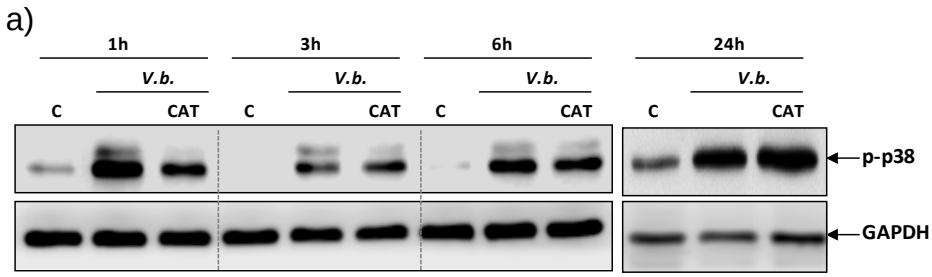

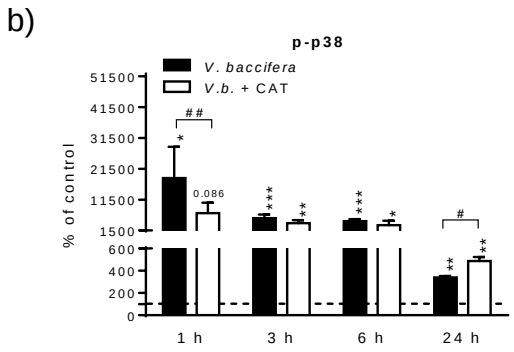

Figure 4.32. Effect of *V. baccifera* on p38 phosphorylation in HepG2. Cells were incubated without (control, C) and with *V. baccifera* (75 µg/ml) alone or plus catalase (10 kU/ml) at the indicated times. (a) Proteins from the cell extracts were analyzed by western blot using the indicated antibodies. GAPDH was used as the loading control**.** The bands shown are representative of at least 3 independent experiments. (b) Representation of the densitometry changes from the western blot experiments represented in (a). Results are the mean + SE from 3-5 experiments. *P < 0.05, **P < 0.01, ***P < 0.001 compared with control (without *V. baccifera*). #P < 0.05 and ##P < 0.01 compared with *V. baccifera*. CAT, catalase.

We observed a very sharp increase in p38 phosphorylation very early after the treatment with *V. baccifera* (Fig. 4.32). This p38 activation was maintained elevated all the time, but with a progressively decrease. The co-incubation with catalase significantly decreased the p38 activation at 1 h.

The phosphorylated p38 protein has mainly a nuclear localization (Fig. 4.33.a). The addition of the plant extract triggered an increase in phosphorylation and subsequent translocation from the cytoplasm into the nucleus (Fig. 4.33.b).

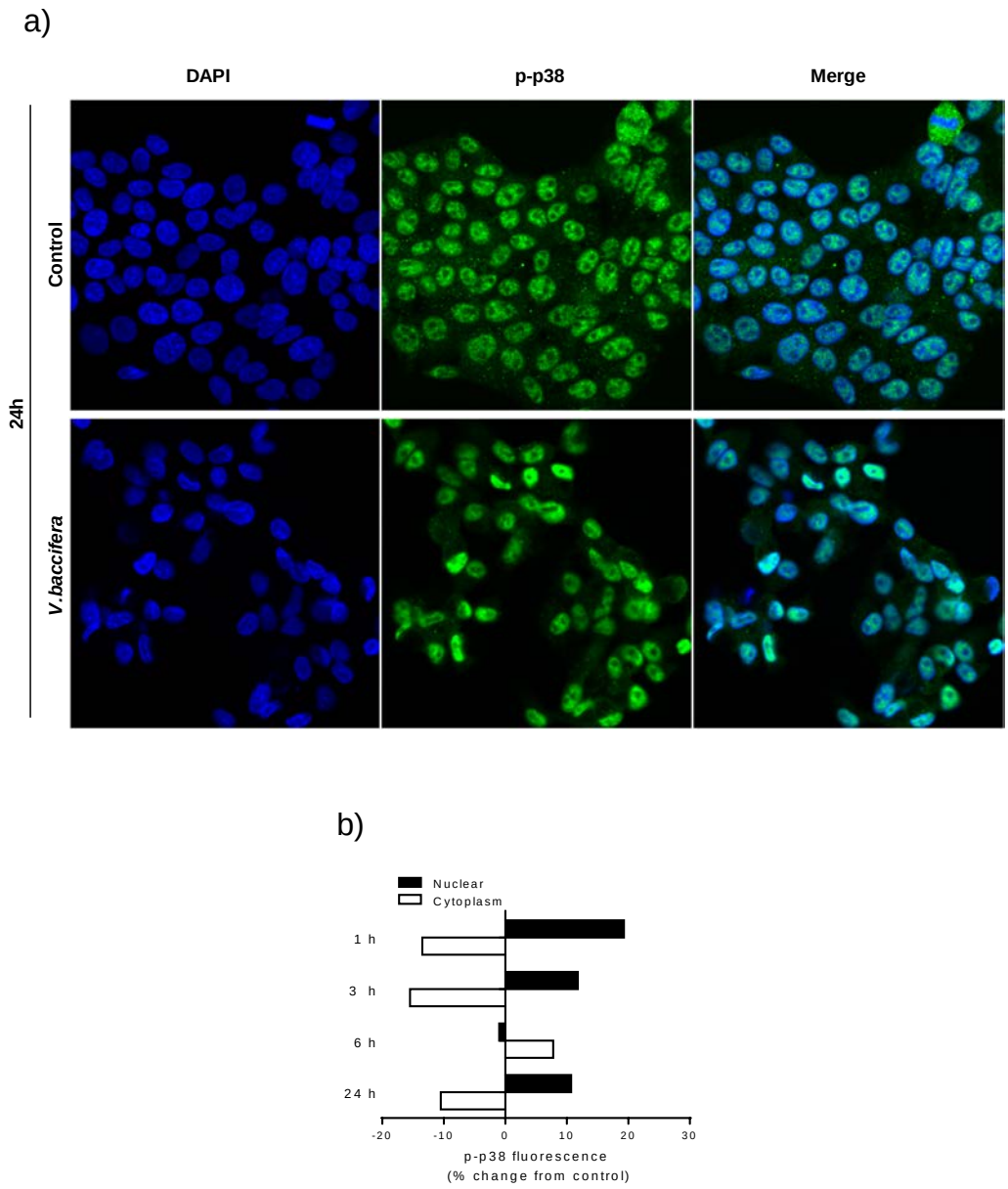

Figure 4.33. Effect of *V. baccifera* on p-p38 localization in HepG2. (a) Cells were incubated without (control) and with *V. baccifera* (75 µg/ml) at the indicated times and phosphoprotein was detected by immunocytochemistry. (b) Representation of the subcellular fluorescence distribution in the micrography analyzed using the ImageJ software.

We have described that *V. baccifera* induced apoptosis and the activation of p38. To explore the role of this kinase in the apoptotic response, cells were exposed to *V. baccifera* in the presence of two different p38 inhibitors. SB203580 inhibits p38 catalytic activity, but does not inhibit phosphorylation of p38 by upstream kinases. Doramapimod is a selective p38α MAPK, which inhibits Raf-1.

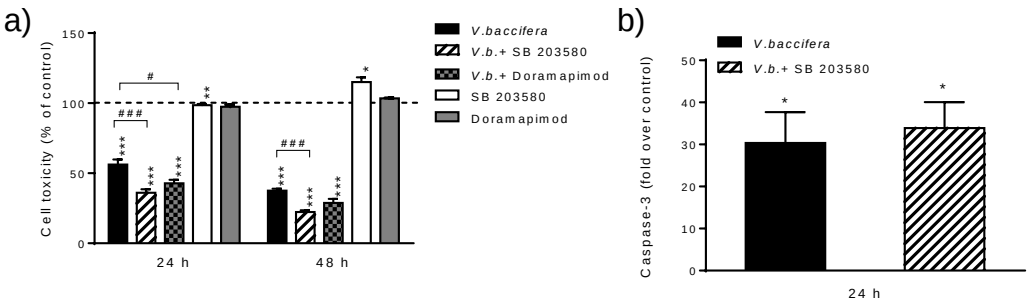

Figure 4.34. Effect of p38 inhibition on *V. baccifera*-induced cell death in HepG2. Cells were incubated without (control) and with *V. baccifera* (75 μg/ml), either alone or with SB203580 (50 μM) or Doramapimod (5 μM) p38 inhibitors for the indicated times. (a) Representation of cell toxicity; results are expressed as the percentage of the control and are the mean + SE from 5 experiments. (b) Caspase-3 activity represented as fold over control and are the mean + SE from 4 experiments. *P < 0.05, **P < 0.01, ***P < 0.001 compared with controls (without *V. baccifera*). ###P < 0.001 compared with *V. baccifera*.

Data showed that both SB203580 and doramapimod p38 inhibitors emphasized *V. baccifera*-caused cell death in a time-dependent manner (Fig. 4.34.a). Caspase-3 activity was also evaluated in HepG2 co-incubated with SB203580. The p38 inhibitor was unable to prevent *V. baccifera*-activation of caspase-3 (Fig. 4.34.b).

4.5.3. NFκB pathway

It is described that ROS interacts with NFκB pathway at different levels. The transcription of NFκB-dependent genes influences the levels of ROS in the cell, and in turn, the levels of NFκB activity are also regulated by the ROS levels (Morgan et al., 2011). The effect of *V. baccifera* on NFκB pathway was determined analyzing IκBα and p65 by western blot.

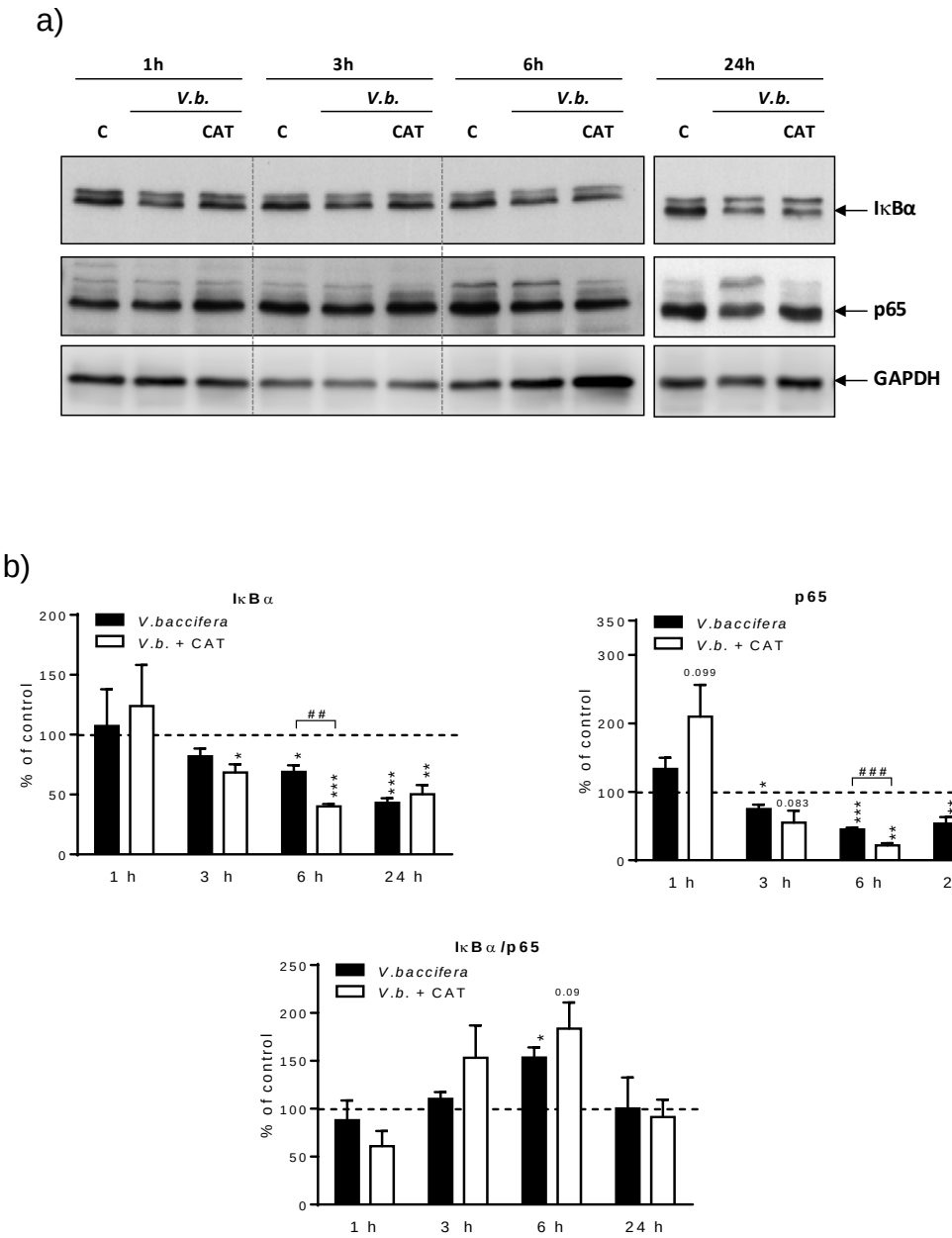

Figure 4.35. Effect of *V. baccifera* on IκBα and p65 expression in HepG2. Cells were incubated without (control, C) and with *V. baccifera* (75 µg/ml) alone or plus catalase (10 kU/ml) at the indicated times. (a) Proteins from the cell extracts were analyzed by western blot using the indicated antibodies. GAPDH was used as the loading control. The bands shown are representative of at least 3 independent experiments. (b) Representation of the densitometry changes from the western blot experiments represented in (a). Results are the mean + SE from 3-5 experiments. *P < 0.05, **P < 0.01, ***P < 0.001 compared with control (without *V. baccifera*). ##P < 0.01 and ###P < 0.001 compared with *V. baccifer*a. CAT, catalase.

V. baccifera induced reduction of both p65 and IκBα; this effect was not reverted by the presence of catalase. The decrease in IκBα content was lower than the p65 decrease, suggesting an inhibition of the p65 translocation into the nucleus (Fig. 4.35).

4.5.4. The p53/ATM/γH2AX pathway

The critical tumor suppressor p53 plays important roles in cell-cycle arrest, apoptosis, senescence, and differentiation in response to various genotoxic and cellular stresses, including oxidative stress (Vurusaner et al., 2012). In our scenario, it was postulated that p53 had a role in *V. baccifera*-induced toxicity since the HepG2, Huh7, and Hep3B cell lines, with different status of p53, demonstrated a differentiated sensitivity to the plant extract (Fig. 4.4).

Activation of p53 by oxidative stress involves ATM kinase, a protein which functions in response to DNA damage (Chen et al., 2003). We studied whether ATM was activated in the presence of *V. baccifera* by immunoblotting and confocal microscopy.

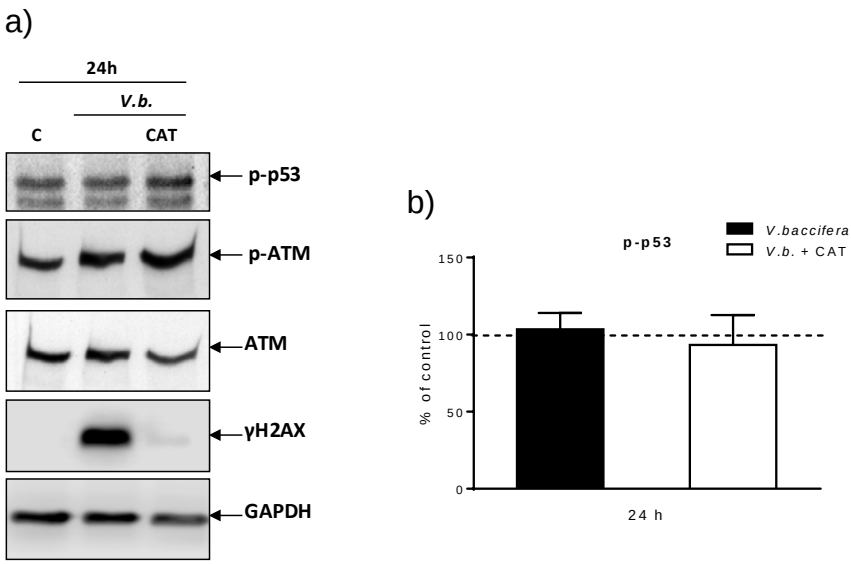

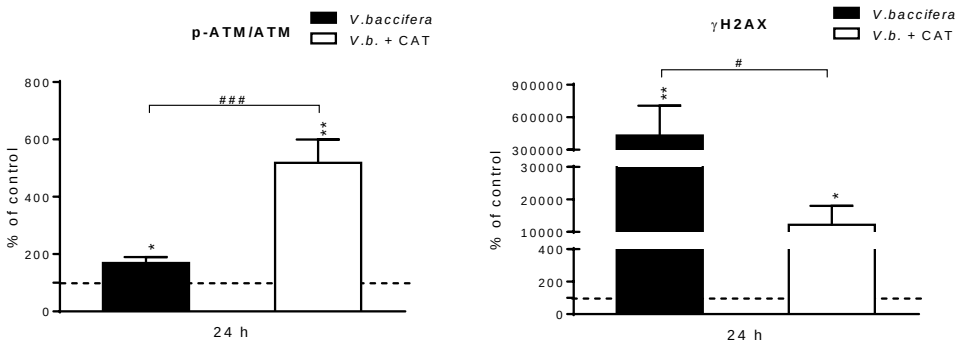

Figure 4.36. . Effect of *V. baccifera* on p53, ATM and γH2AX expression in HepG2. Cells were incubated without (control, C) and with *V. baccifera* (75 μg/ml) alone or plus catalase (10 kU/ml) at the indicated times. (a) Proteins from the cell extracts were analyzed by western blot using the indicated antibodies. GAPDH was used as the loading control. The bands shown are representative of at least 3 independent experiments. (b) Representation of the densitometry changes from the western blot experiments represented in (a). Results are the mean + SE from 3-5 experiments. *P < 0.05, **P < 0.01 compared with control (without *V. baccifera*). #P < 0.05 and ###P < 0.001 compared with *V. baccifer*a. CAT, catalase.

The data from the immunoblotting study of this pathway did not reveal any effect of the extract on p53 phosphorylation from 1 h until 24 h of treatment (Fig. 4.36). The co-incubation with catalase did not alter p-p53 status. However, analysis of confocal micrographies rendered enrichment of this phosphoprotein in the nucleus (Fig. 4.37).

The phospho-ATM protein increased at 24 h of treatment (Fig. 4.36). This increase was observed both in the nucleus and in the cytoplasm (Fig. 4.38). The levels of p-ATM were even higher in the presence of catalase. There was a sharp increase of γH2AX phosphorylation at 24 h of treatment that was completely prevented by catalase (Fig. 4.36).

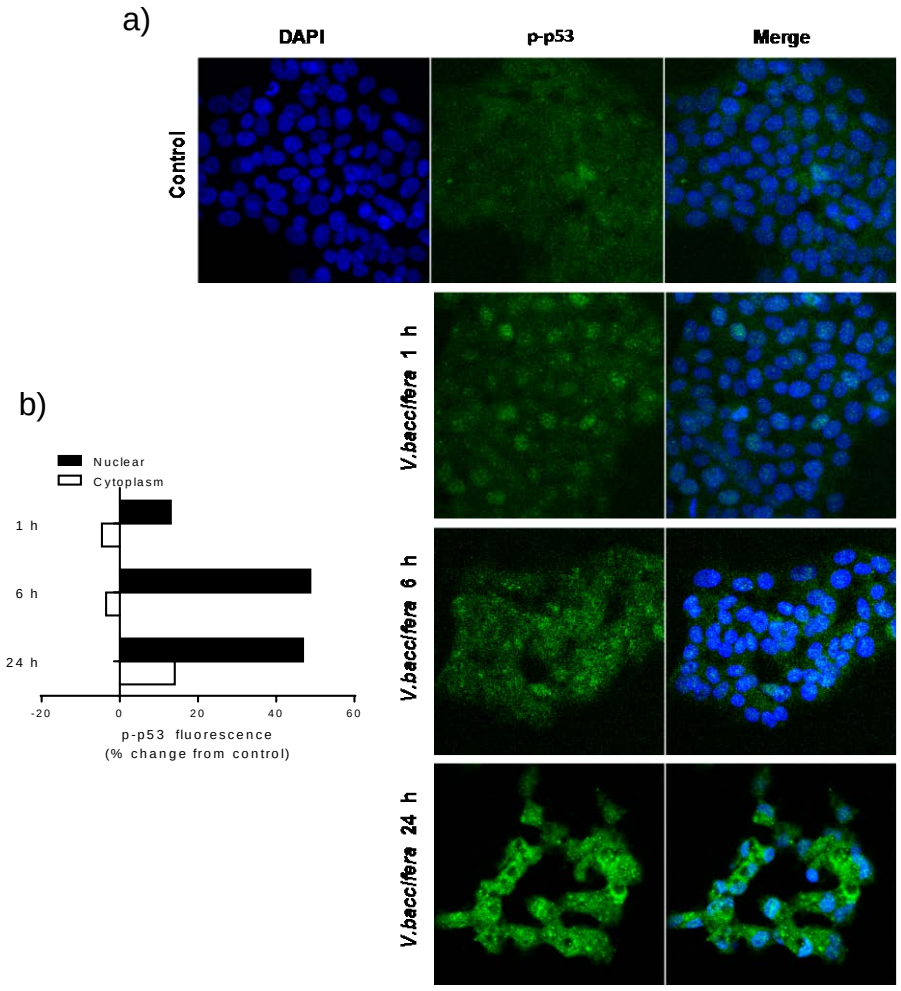

Figure 4.37. Effect of *V. baccifera* on p-p53 localization in HepG2. (a) Cells were incubated without (control) and with *V. baccifera* (75 µg/ml) at the indicated times and the phosphoprotein was detected by immunocytochemistry. (b) Representation of the subcellular fluorescence distribution in the micrography analyzed using the ImageJ software.

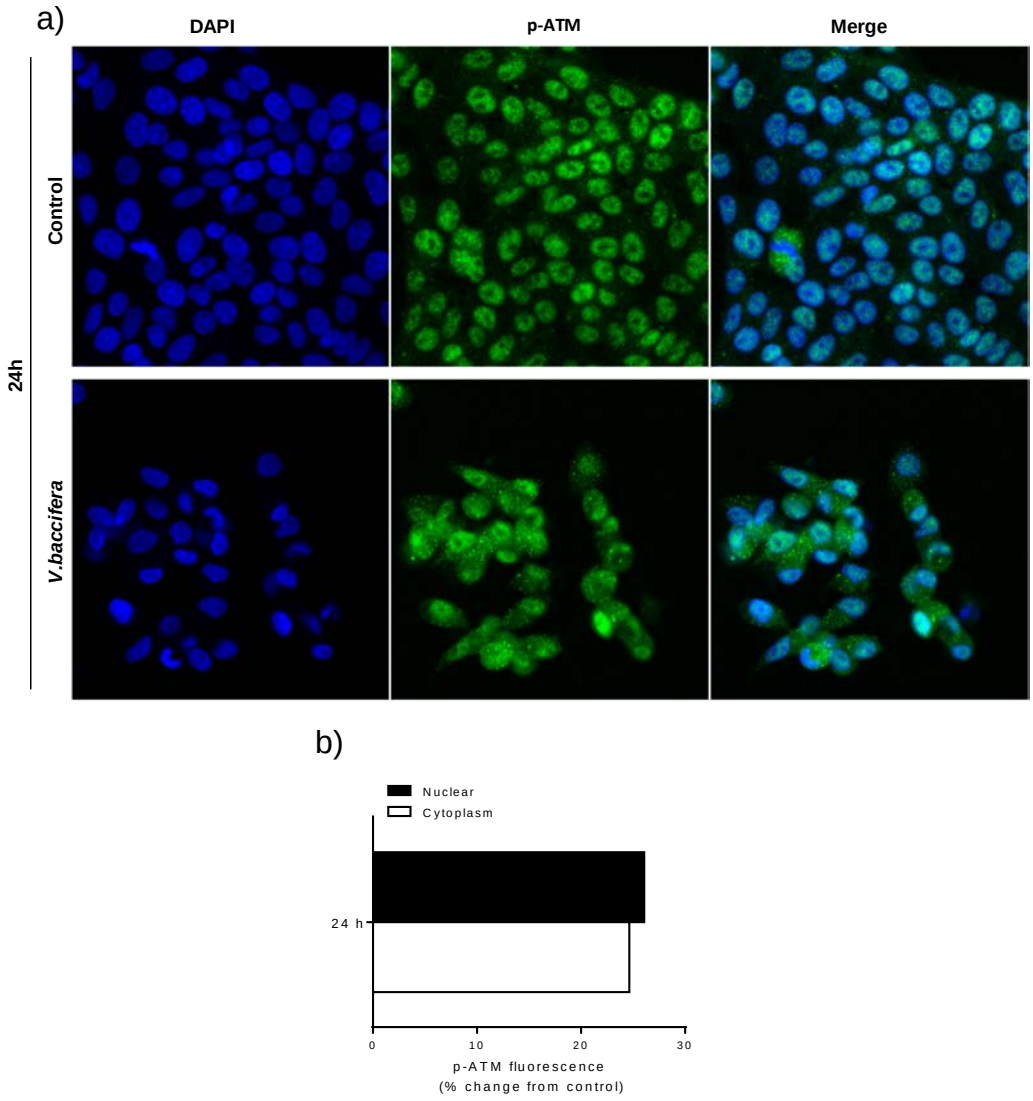

Figure 4.38. Effect of *V. baccifera* on p-ATM localization in HepG2. (a) Cells were incubated without (control) and with *V. baccifera* (75 µg/ml) at the indicated times and the phosphoprotein was detected by immunocytochemistry. (b) Representation of the subcellular fluorescence distribution in the micrography analyzed using the ImageJ software.

These data suggest that hydrogen peroxide is involved in γH2AX phosphorylation independently of ATM.

4.5.5. Endoplasmic reticulum stress

GRP78, also known as BiP, is a molecular chaperone that in unstressed conditions interacts with the luminal domains of PERK, IRE1 and ATF6, blocking homodimerization of PERK and IRE1, and preventing translocation of ATF6. Apart from the translocation of GRP78 from PERK, IRE1 and ATF6 to unfolded proteins during ER stress, this stress induces *de novo* synthesis of GRP78 to assist in protein folding in the ER. Therefore, the induction of GRP78 expression is a well-stabilized hallmark of ER stress and UPR-activation.

GRP78 expression was analyzed in HepG2 exposed to *V. baccifera* at periods up to 24 h.

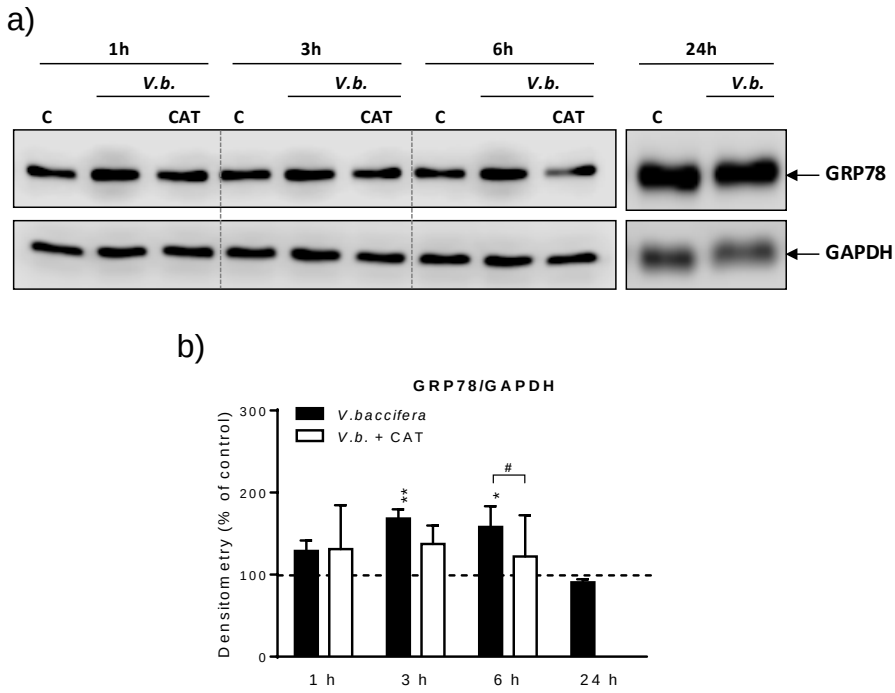

Figure 4.39. . Effect of *V. baccifera* on GRP78 expression in HepG2. Cells were incubated without (control, C) and with *V. baccifera* (75 µg/ml) alone or plus catalase (10 kU/ml) at the indicated times. (a) Proteins from the cell extracts were analyzed by western blot using the indicated antibodies. GAPDH was used as the loading control**.** The bands shown are representative of at least 3 independent experiments. (b) Representation of the densitometry changes from the western blot experiments represented in (a). Results are the mean + SE from 3-6 experiments. *P < 0.05, **P < 0.01 compared with control (without *V. baccifera*). #P < 0.05 compared with *V. baccife*ra. CAT, catalase.

The plant extract induced GRP78 accumulation as early as 3 h, and was maintained elevated at 6 h after *V. baccifera* addition (Fig. 4.39). Moreover, GRP78 induction was prevented by catalase.

Taking these results into account, V. baccifera-*induced hydrogen peroxide provokes ER stress, involving GRP78 chaperone to support protein folding.*

To further understand the IREα pathway (Jiang et al., 2015), XBP1 splicing under *V. baccifera* exposure was studied. Activated IRE1α catalyzes the excision of an intron from ubiquitously expressed XBP1 mRNA. The spliced XBP1 acts as a transcription factor for genes involved in ER protein maturation an ER-associated degradation. Thus, the XBP1-spliced/XBP1-unspliced ratio is related to the level of expressed proteins in order to adapt the folding capacity of the ER to the respective requirements.

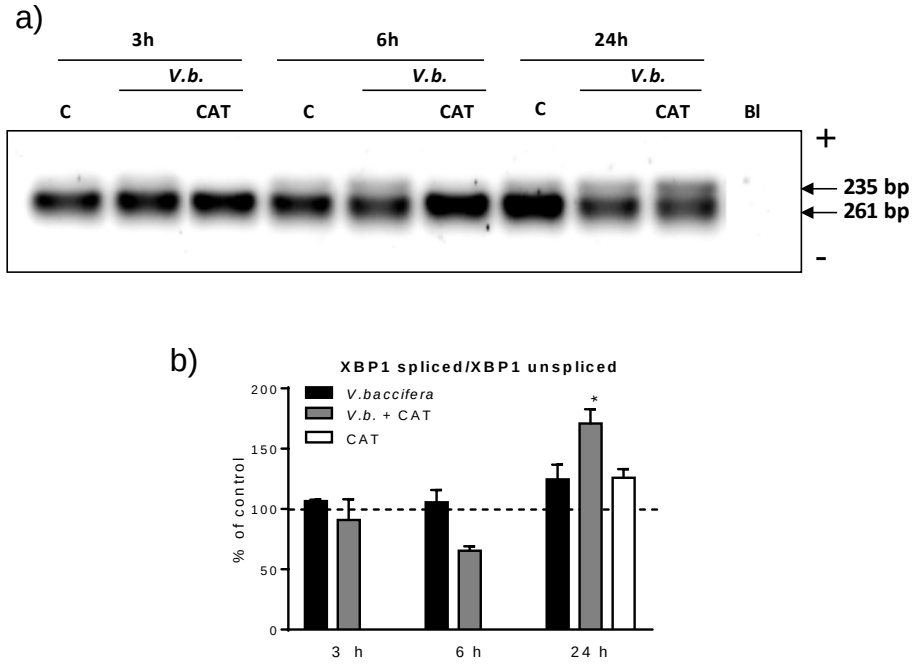

Figure 4.40. Effect of *V. baccifera* on XBP1 splicing in HepG2. Cells were incubated without (control, C) and with *V. baccifera* (75 µg/ml) alone or plus catalase (10 kU/ml) at the indicated times. (a) Expression of 235 bp spliced and 261 bp unspliced XBP1 transcripts in HepG2. (b) Representation of the densitometry changes of the experiment represent in (a). Results at 24 h are the mean + SE from 3 experiments. *P < 0.05 compared with control (without *V. baccifera*). CAT, catalase.

We could not detect any significant increase in the splicing in the XBP1 mRNA induced by the plant extract. However, co-incubation with catalase induced XBP1 splicing at 24 h ($p<0.0.5$) (Fig. 4.40).

These results suggest that the catalase protective effect includes the contribution to repair the unfolded proteins caused by V. baccifera*-generated ER stress.*

4.5.6. Apoptotic response to *V. baccifera*

Apoptosis inducing factor (AIF) was originally described as a mitochondrial intermembrane protein that, after apoptosis translocates into the nucleus triggering chromatin condensation and DNA fragmentation (Joza et al., 2009). To study AIF mobilization in HepG2 incubated with the plant extract live cells were stained for mitochondria detection.

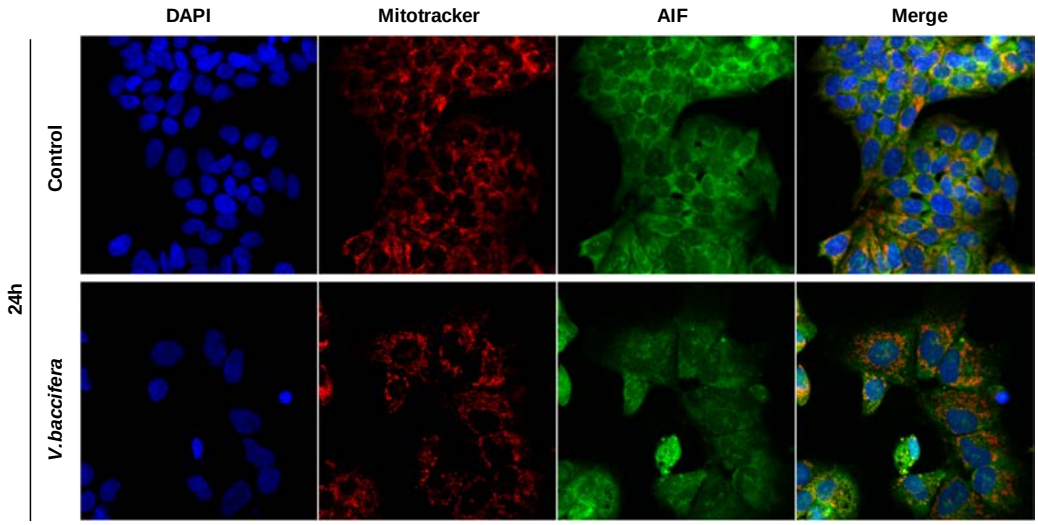

Figure 4.41. Effect of *V. baccifera* on AIF localization in HepG2. (a) Cells were incubated without (control) and with *V. baccifera* (75 μg/ml) for 24 h, and after treatment HepG2 cells were stained with Mitotracker Red to detect the mitochondria (red color). AIF subcellular localization was detected in green color.

According to the micrograph, AIF is mainly located in mitochondria and virtually absent in the nucleus in control cells. *V. baccifera* induces the nuclear translocation of AIF at 24 h, not affecting the protein location at early times (Fig. 4.41).

The mitochondria play a role in triggering pro-apoptotic signals, thus inducing apoptosis cell death. In this sense, the pro- and anti-apoptotic Bcl-2 family proteins regulate the mitochondrial membrane permeabilization (Green et al., 2015).

Then, the expression of the Bax, Bcl-2, Bcl-x and Bid apoptosis regulator proteins was analyzed by western blot. The Bax/Bcl-2 ratio is an important index to evaluate the apoptotic process (Colitti, 2012). An increased amount of Bax and reduction of Bcl-2 is associated with a greater permeability of the outer mitochondrial membrane due to the formation of pores by the Bax family protein, which allows the release of factors involved in cell death (Tian et al, 2012).

a)

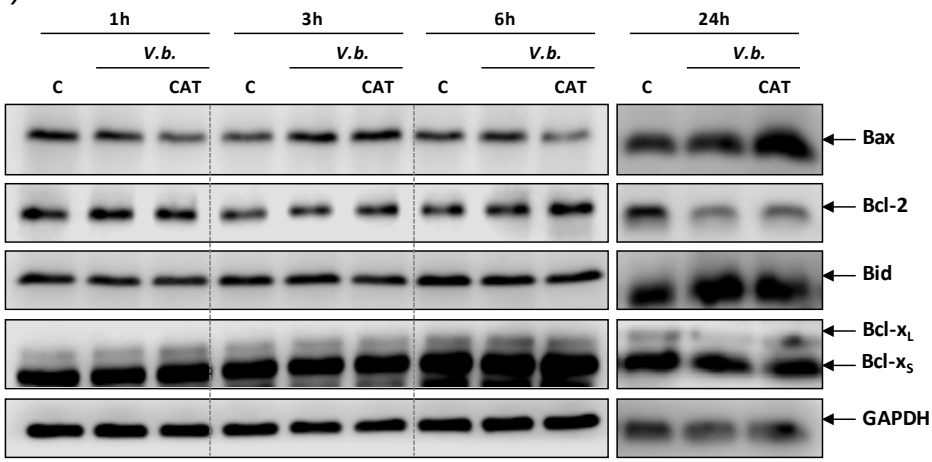

b)

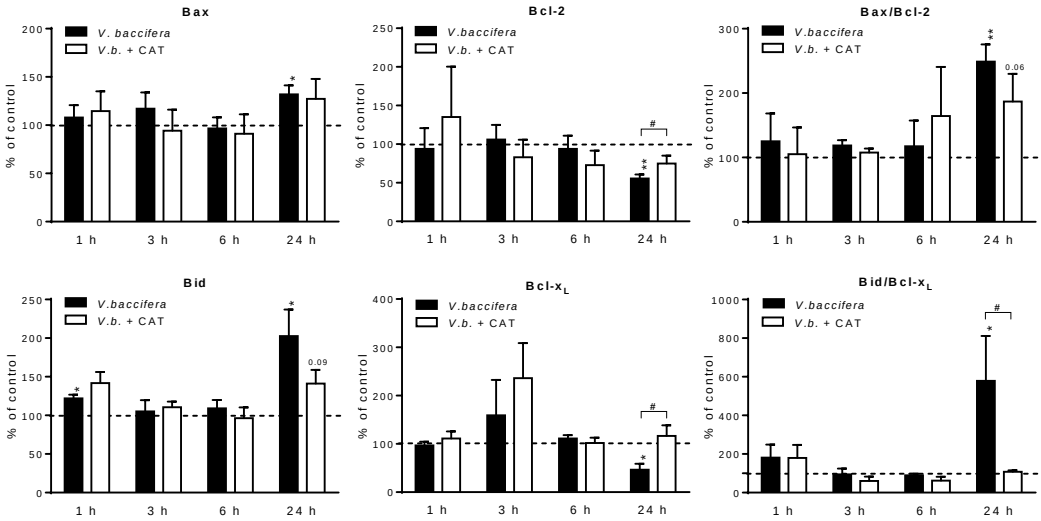

Figure 4.42. Effect of *V. baccifera* on Bcl-2 family proteins in HepG2. Cells were incubated without (control, C) and with *V. baccifera* (75 μg/ml) alone or plus catalase (10 kU/ml) at the indicated times. (a) Proteins from the cell extracts were analyzed by western blot using the indicated antibodies. GAPDH was used as the loading control. The bands shown are representative of at least 3 independent experiments. (b) Representation of the densitometry changes from the western blot experiments represented in (a). Results are the mean + SE from 3-6 experiments. *P < 0.05, **P < 0.01 compared with control (without *V. baccifera*). #P < 0.05 compared with *V. baccife*ra. CAT, catalase.

V. baccifera triggered a significantly increase of the proapoptotic Bax and reduced the antiapoptotic Bcl-2 expression at 24 h, thus increasing the ratio of Bax to Bcl-2 ($p<0.01$) (Fig. 4.42). Co-incubation with catalase prevented the Bcl-2 decrease, thus resulting in a lower Bax/Bcl-2 ratio.

Regarding the expression of the apoptotic Bid protein, the extract increased significantly the amount of the protein and concomitantly reduced markedly the expression of the Bcl-x_L anti-apoptotic protein at 24 h (Fig. 4.42). The interaction of Bcl-x_L with Bid has been reported to avoid its pro-apoptotic activity (Garcia-Saez et al., 2009). The almost 6-fold increase of the Bid to Bcl-x_L ratio induced by *V. baccifera* was completely prevented by catalase.

These data point to a relevant role of hydrogen peroxide as a regulator of this family of proteins leading to a pro-apoptotic signal.

4.5.7. Autophagy response to *V. baccifera*

Autophagy is considered an adaptive response for cells under stressful conditions, and hepatic apoptosis has been described to be regulated by autophagic activity (Wang, 2015). Autophagy starts with the formation of a doubled-membrane surrounded vacuole (autophagosome) that engulfs fractions of the cytoplasm in an either unselective or selective manner. The p62/SQSTM1 protein establishes a bridge between the target and the growing autophagosome membrane. This protein binds both LC3 and ubiquitinated proteins, driving them to selective autophagic degradation (Lorin et al., 2013).

According to this, we studied the effect of *V. baccifera* on the p62/LC3 pathway in HepG2 by immunodetection.

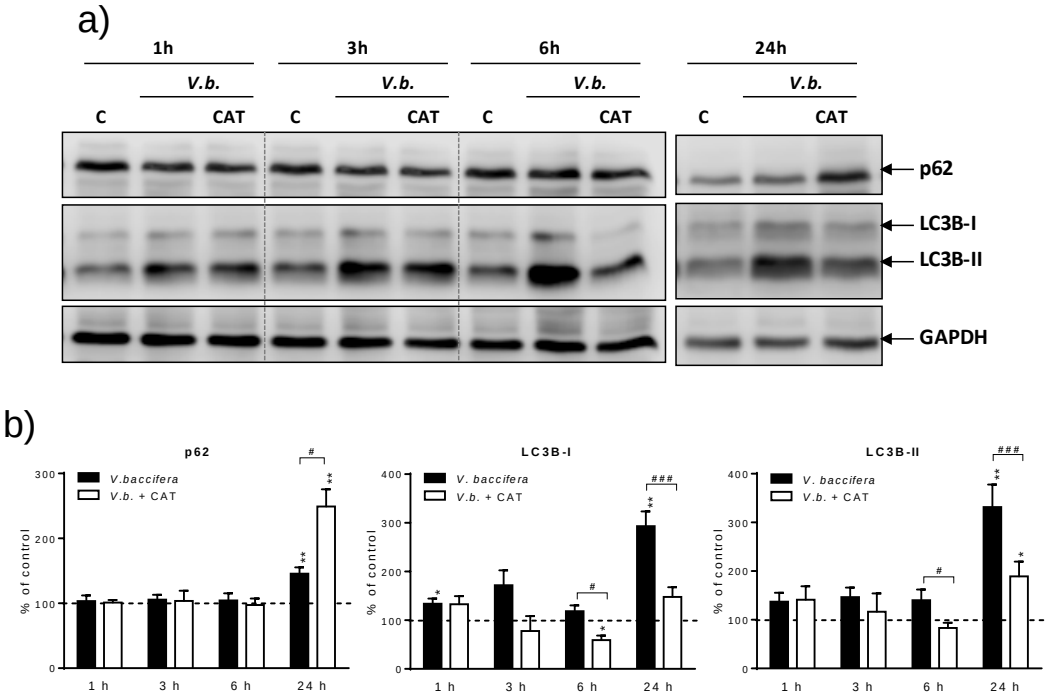

Figure 4.43. .Effect of *V. baccifera* on p62 and LC3B proteins in HepG2. Cells were incubated without (control, C) and with *V. baccifera* (75 µg/ml) alone or plus catalase (10 kU/ml) at the indicated times. (a) Proteins from the cell extracts were analyzed by western blot using the indicated antibodies. GAPDH was used as the loading control**.** The bands shown are representative of at least 3 independent experiments. (b) Representation of the densitometry changes from the western blot experiments represented in (a). Results are the mean + SE from 4-6 experiments. *P < 0.05, **P < 0.01 compared with control (without *V. baccifera*). #P < 0.05, ###P < 0.001 compared with *V. baccifer*a. CAT, catalase.

The plant extract induced a p62 accumulation at 24 h of treatment, and this increase was higher in the presence of catalase ($p<0.05$) (Fig. 4.43). By confocal microscopy, we could detect a shuttling of p62 from the nuclear compartment to the cytoplasm for the incubation time (Fig. 4.44).

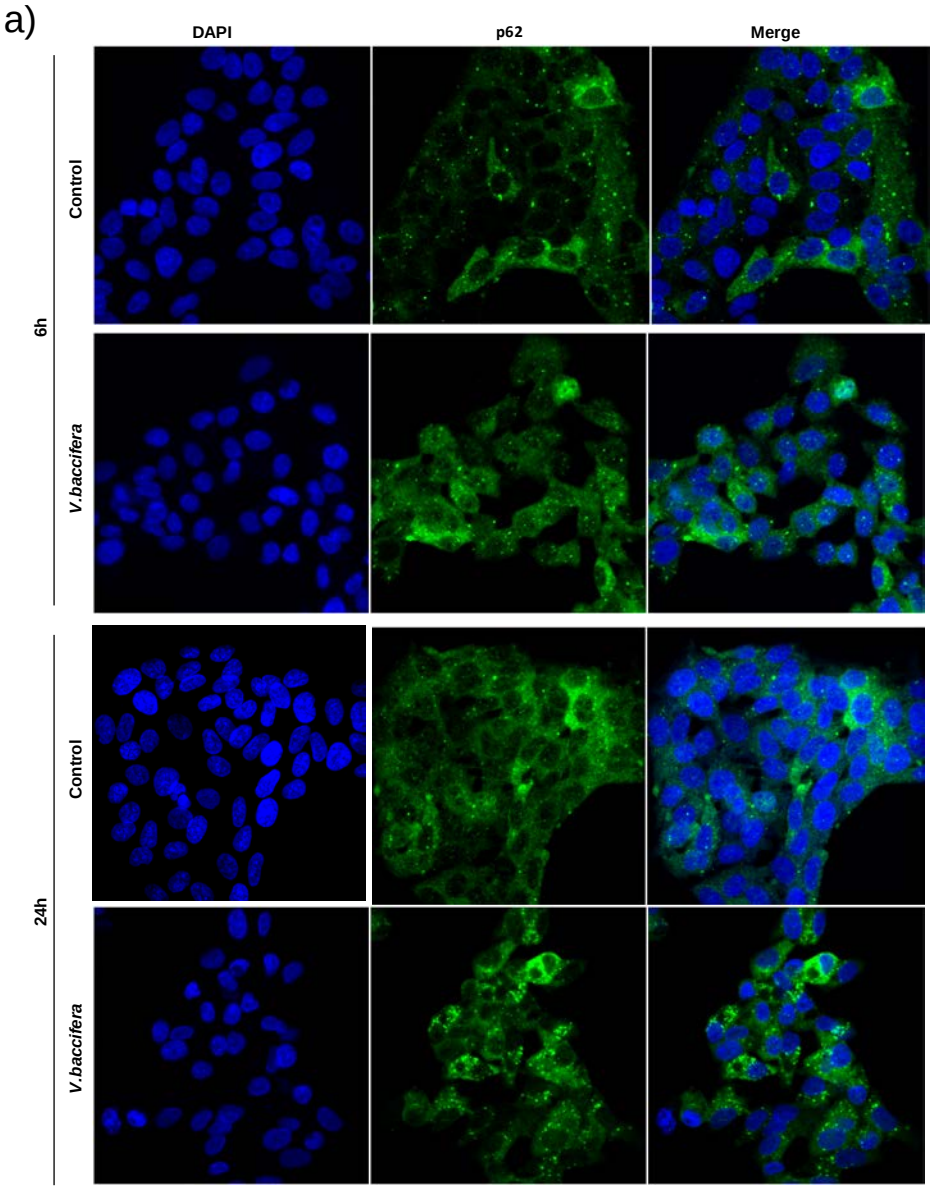

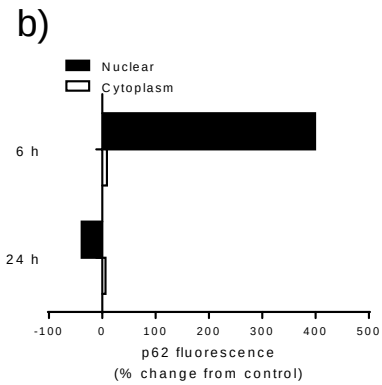

Figure 4.44. Effect of *V. baccifera* on p62 localization in HepG2. (a) Cells were incubated without (control) and with *V. baccifera* (75 µg/ml) at the indicated times and the protein was detected by immunocytochemistry. (b) Representation of the subcellular fluorescence distribution in the micrography analyzed using the ImageJ software.

The autophagy biomarker LC3B-II protein increased with the *V. baccifera* treatment, that reached statistical significance at 24 h (Fig. 4.43.a). Catalase partially prevented the accumulation of LC3B-II at longer times. Higher LC3B fluorescence was detected by confocal microscopy both in the nucleus and the cytoplasm as a result of the treatment with *V. baccifera* (Fig. 4.45).

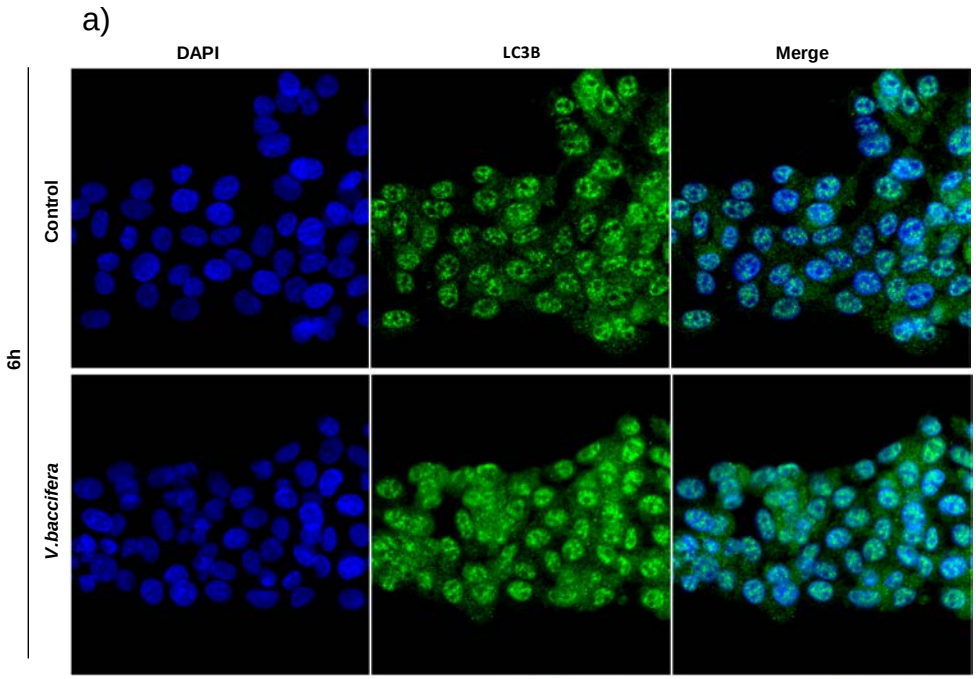

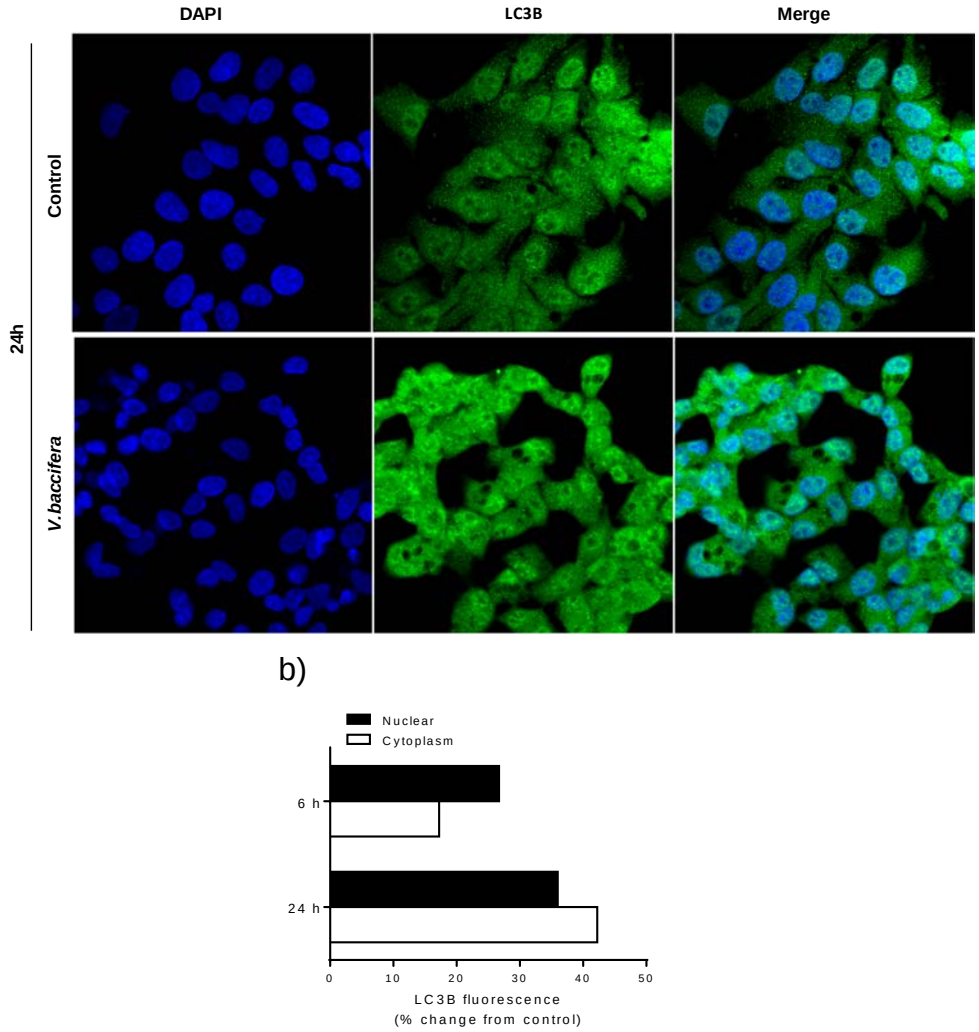

Figure 4.45. Effect of *V. baccifera* on LC3B localization in HepG2. (a) Cells were incubated without (control) and with *V. baccifera* (75 µg/ml) at the indicated times and the protein was detected by immunocytochemistry. (b) Representation of the subcellular fluorescence distribution in the micrography analyzed using the ImageJ software.

According to these data V. baccifera *induces the activation of proteins involved in the autophagy process.*

4.6. Influence of pO_2 on tumor liver cell growth

The oxygen partial pressure (pO_2) at ambient atmosphere is 150 mmHg, which is equivalent to 21% oxygen. However, the level of inhaled O_2 progressively decreases as it reaches various internal organs and tissues. The level of O_2 and its distribution among the various tissues depends on the rate of capillary blood flow and the tissue metabolic activity. For instance, in humans, under physiological conditions, the pO_2 in well-irrigated organs such as lungs, liver and kidneys, ranges from 4 to 14% (Brooks et al., 2004). To determine whether pO_2 has influence on hepatocarcinoma growth and ROS accumulation, the previously referred hepatoma cell lines (HepG2, Huh7 and Hep3B), were studied under 21% (atmospheric) and 8% (low) pO_2.

4.6.1. Cell growth

Cell growth rate, in terms of the time required for doubling the number of cells, was determined in HepG2, Huh7 and Hep3B cell lines under 21% and 8% pO_2.

	Doubling time (h)	
Cell type	**21% pO_2**	**8% pO_2**
HepG2	31.8 ± 0.9 [a]	29.1 ± 1.1 [a]
Huh7	32.1 ± 0.7 [a]	33.9 ± 0.5 [b]
Hep3B	26.4 ± 1.1 [b]	23.6 ± 0.9 [c]

Table 4.2. Effect of pO_2 on hepatoma cell lines growth. Cells were incubated under 21 and 8% pO_2. Doubling times were derived from semilogarithm representations of the crystal violet absorbance versus the culture time. Results are expressed as the mean ± SE of 3-15 experiments. Data in the same column with different superscript are statistically significant different, $^{a,b,c}p < 0.05$.

Hep3B showed the highest proliferation rate independently on the pO_2 (Table 4.2). Huh7 had the highest doubling time at 8% pO_2. Cells did not exhibit any statistically significant change in the proliferation rate depending on the pO_2, although Huh7 tended to behave differently to the other two cell types.

The proliferation rate of HepG2, Huh7 and Hep3B is not influenced by the decrease of pO_2 from 21% to 8%.

4.6.2. Intracellular ROS

Intracellular ROS levels were measured by flow cytometry in the different cancer cell lines under both 21% and 8% pO_2.

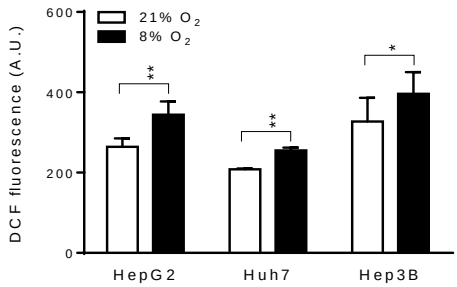

Figure 4.46. Effect of pO_2 on intracellular ROS levels in hepatoma cell lines. Cells were incubated under 21 and 8% pO_2. Arbitrary units of DCF fluorescence under both pO_2 are represented. Results are the mean + SE of 4-16 experiments. *P < 0.05, **P < 0.01.

Huh7 showed the lowest intracellular ROS levels under both pO_2 assay conditions ($p<0.001$). Reduction of pO_2 from 21% to 8% significantly increased intracellular ROS in all three cell lines (Fig. 4.46).

Reduction in the oxygen partial pressure induced an increased in intracellular ROS independently of the characteristics of the cell lines.

4.6.3. Mitochondrial O_2^-

Mitochondrial O_2^- levels under 21% and 8% pO_2 were studied by flow cytometry.

O_2^- production was observed in all the hepatoma cell types, the highest levels being in Hep3B ($p<0.05$). Fluorescence signals were unaffected by pO_2 culture conditions (Fig. 4.47).

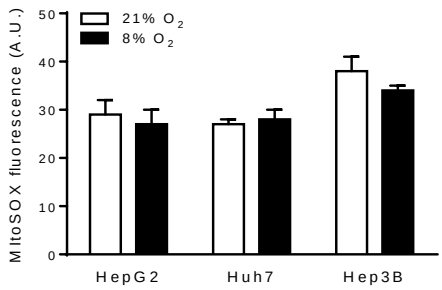

Figure 4.47. Effect of pO_2 on mitochondrial $O_2^{\cdot-}$ levels in hepatoma cell lines. Cells were incubated under 21 and 8% pO_2. Arbitrary units of MitoSOX fluorescence under both pO_2 are represented. Results are the mean + SE of 3-5 experiments.

Steady-state levels of $O_2^{\cdot-}$ are independent of the pO_2 in the studied range.

4.6.4. Cell migration

The role of ROS in triggering signaling pathways for cell migration has been well established. Through a series of cellular events, including cytoskeletal remodeling, cells are able to detach from the primary tumor and metastasize to distant sites (Tochhawng et al., 2013). To study the influence of oxygen on cell migration, transwell assay was performed.

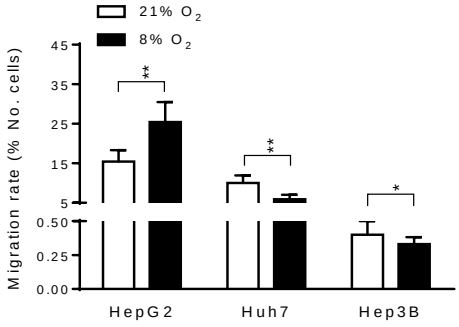

Figure 4.48. Effect of pO_2 on migration rate in hepatoma cell lines. Cells were incubated under 21 and 8% pO_2. Migration rate (number of migrated cells respecting seeded cells) under both pO_2 are represented. Results are the mean + SE of 8-13 experiments. *P < 0.05, **P < 0.01.

Independently of the pO_2 conditions, the highest migration rate was found in HepG2, and the lowest in Hep3B ($p<0.001$). The reduction of pO_2 from 21% to 8% affected differently the migration capacity of the studied cells. Thus, the migration rate decreased in Huh7 and Hep3B, while HepG2 showed a higher migration capacity (Fig. 4.48).

4.6.5. Cell adhesion

The effect of pO_2 on cell adhesion capacity was evaluated as early as one hour after incubation by the crystal violet stain method.

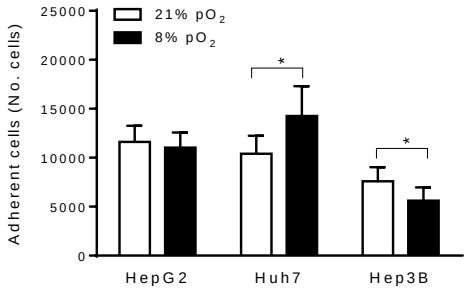

Figure 4.49. Effect of pO_2 on adhesion in hepatoma cell lines. Cells were incubated under 21 and 8% pO_2 at 20,000 cells per well and the number of adherent cells is represented. Results are the mean + SE of 4-8 experiments. *P < 0.05.

Under 8% pO_2, Huh7 showed the highest adhesion capacity, while Hep3B showed the lowest one (Fig. 4.49). Cell adhesion was differently affected by pO_2 in every of the studied hepatoma cell lines. Thus, a low pO_2 favoured Huh7 adhesiveness, contrary to the effect in Hep3B. The HepG2 adhesion capacity did not depend on pO_2.

4.7. Effect of pO_2 on *V. baccifera*-induced toxicity in HepG2

4.7.1. Cell toxicity

The cell growth in HepG2 incubated with *V. baccifera* under both pO_2 was studied by crystal violet stain method.

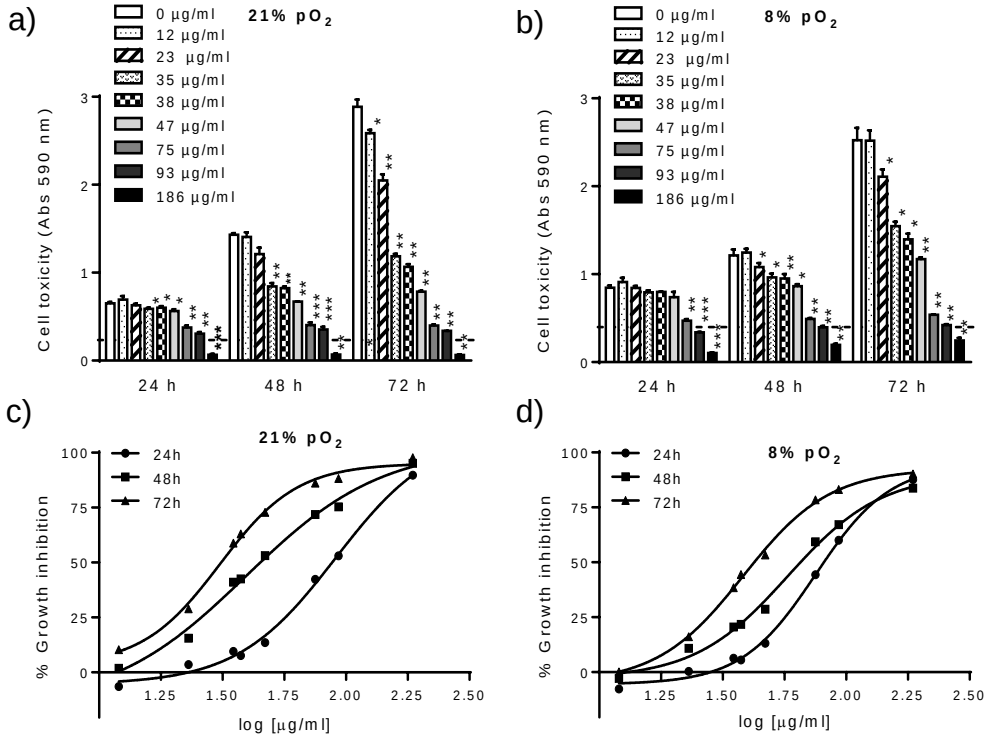

e)

	IC_{50} (µg/ml)		
HepG2	**24h**	**48h**	**72h**
21% pO_2	87.6 ± 3.4	44.9 ± 0.8	31.2 ± 0.3
8% pO_2	81.1 ± 1.5	65.5 ± 2.4 *	42.3 ± 2.1 *

Figure 4.50. Effect of pO_2 on *V. baccifera*-induced toxicity in HepG2. HepG2 were exposed at different concentrations of *V. baccifera* and incubated under (a) 21% and (b) 8% pO_2 for the indicated times. Results are the mean + SE from 3 experiments. The value of the control at time zero was 0.3 and 0.39 absorbance units for 21 and 8% pO_2 respectively at 590 nm, and is represented as a dashed line in the figure. (c, d) Dose-response curve to pO_2 of HepG2 exposed to *V. baccifera* and (e) calculation of the concentration that inhibits 50% of cell growth (IC_{50}). The data were fit to a dose-response curve (sigmoid) by nonlinear regression (R_2 = 0.99). *P < 0.05, **P < 0.01, ***P < 0.001 compared with control (without *V. baccifera*).

The IC_{50} derived values showed higher sensitivity (around 40%) of HepG2 to *V. baccifera* under 21% pO_2 at 48 and 72 h (Fig. 4.50). There was no oxygen influence at 24 h.

4.7.2. Intracellular ROS

Taking into account the effect of pO_2 on the intracellular ROS accumulation in HepG2, we studied the *V. baccifera*- induced DCF fluorescence dependence on pO_2.

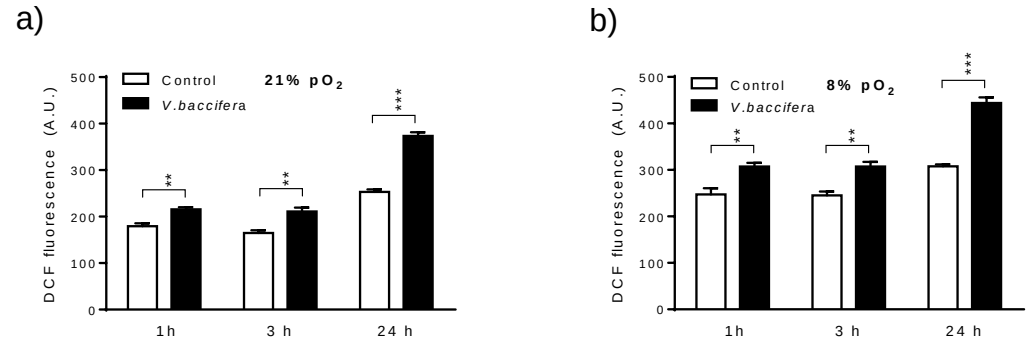

Figure 4.51. Effect of pO_2 on *V. baccifera*-induced intracellular ROS levels in HepG2. Cells were incubated without (control) and with *V. baccifera* (75 mg/ml) under (a) 21 and (b) 8% O_2 at the indicated times. Arbitrary units of DCF fluorescence are represented and results are the mean + SE of 6 experiments. **P < 0.01, ***P < 0.001.

Changes in ROS accumulation induced by the plant extract were similar under both pO_2 conditions along the time studied (Fig. 4.51).

4.7.3. Mitochondrial O_2^-

Mitochondrial O_2^- levels were studied by MitoSOX fluorescence in HepG2 treated with *V. baccifera* under different pO_2.

The plant extract induced similar changes in mitochondrial O_2^- steady-state levels independently on pO_2 (Fig. 4.52).

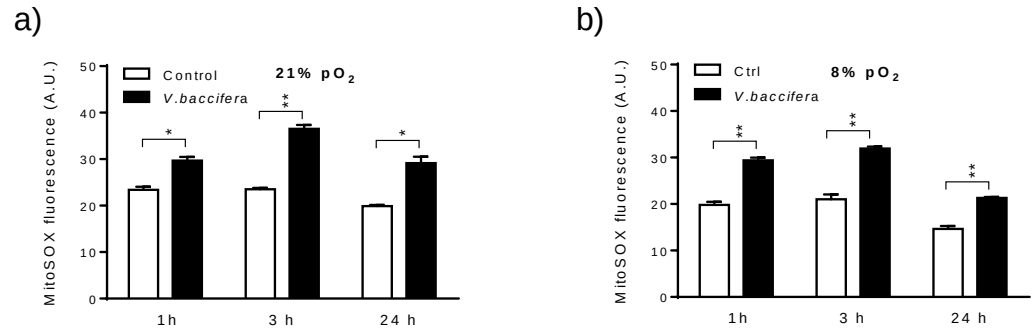

Figure 4.52. Effect of pO_2 on *V. baccifera*-induced mitochondrial O_2^- levels in HepG2. Cells were incubated without (control) and with *V. baccifera* (75 mg/ml) under (a) 21 and (b) 8% O_2 at the indicated times. Arbitrary units of MitoSOX fluorescence are represented and results are the mean + SE of 3 experiments. *P < 0.05, **P < 0.01.

These results indicate that the stress superimposed conditions in culturing do not modify the ROS response of HepG2 to the plant extract.

5. DISCUSSION

5. DISCUSSION

In this work we have studied the antitumoral actions of the Amazonian *Vismia baccifera* plant against human hepatocarcinoma cell lines. This system, easy to manipulate, serves as a model for human cancer to study the activities of novel anticancer drugs, the sensitivity patterns, and their mechanisms of action that could lead to the development of new therapeutic targets. The results of the research in cancer cell lines are usually extrapolated to *in vivo* human tumors (van Staveren et al., 2009) and have been recognized by pharmaceutical companies as models for the screening and characterization of anticancer therapeutics (Gazdar et al., 2010). The use of cell lines has, however, some limitations; for example, the cell culture environment is different from that of the original tumor, and tumor cell lines have lost the natural heterogeneity of the tumor. Nevertheless, cancer cell lines are adequate models for the research of cancer, and data have demonstrated that the tumor cell lines have a similar response to anticancer drugs when compared to the original tumor (Finlay and Baguley, 1984).

The assayed plant leaves were prepared as aqueous infusions, according to the common method used in the traditional medicine in Amazonian communities. The procedure implies the contact between the plant and the solvent (water in this case) to achieve greater extraction of active ingredients. This procedure is in line with the guidelines of the World Health Organization (WHO), an organization for which medicinal plant extracts are products obtained by various techniques (mashing, baking, brewing, distillation) and/or solvent (water, ethanol, methanol, chloroform) whereby substances or molecules are obtained as part of the valid preparations in traditional medicine, trying to keep the active ingredients of the plant (WHO, 2000). However, the exact distribution of the compounds from plants is influenced by the extraction method due to the solubility properties of the plant components; the use of solvents with different polarity determines the type of compound finally extracted. Thus, an aqueous extract will be rich in polar compounds, such as flavonoids, while an oily extract will be enriched in nonpolar molecules. Alcohol is somewhere in between these two extremes. Although the effectiveness of other extraction methods (extraction with supercritical fluids, assisted microwave extraction and removal of pressurized liquid) has been proved, the aqueous extracts have shown equal or greater effectiveness (Huie, 2002; Eguale et al., 2011).

We have seen that at concentrations at or below 75 µg/ml the extract inhibited cell proliferation of human hepatocellular carcinoma HepG2, and higher concentrations of the extract induced cell viability loss (Fig. 4.1). On the contrary, similar or even higher concentrations of the extract (up to 150 µg/ml) were innocuous in nontransformed HH4 hepatocytes (the human fetal hepatocyte-derived cell line). Moreover, we have previously determined in our group that *V. baccifera* did not induced cell viability loss in non-malignant rat hepatocytes while it was toxic in the rat Mc-ARh7777 tumor cell line (Lizcano et al., 2014). To our knowledge, this is the first work describing the cytotoxic actions of *V. baccifera* targeted to human hepatoma cells.

Vismia baccifera species are commonly used in folk medicine in indigenous populations with different curative purposes such as purgative, protective against snake bites, treatment of skin diseases, antirheumatic, antipyretic and against uterine haemorrhage (Peres, 1978). In the literature, a work described that an aqueous extract of *V. baccifera L. var. dealbata* leaf produced *in vivo* a moderate analgesic activity in experimental animals, similar to that found for acetylsalicylic acid (Salas et al., 2007). One of the *V. baccifera* constituents, sesamin, was shown to inhibit the production of prostaglandins and the tumor necrosis factor α, a molecule involved in inflammation (Utsunomiya et al., 2000). Cancer and inflammation are closely related, since the proinflammatory prostaglandins generated from arachidonic acid play an important role in metastasis and proliferation in various cancer types, and in tumoral progression (Balkwill and Coussens, 2004; Fulton et al., 2006). In this sense, the plant could block *in vivo* the inflammatory process associated to cancer, due to the actions of its constituents.

In a work reported by Hussein et al. (Hussein et al., 2003), methanolic extracts of *V. baccifera* leaves exhibited cytotoxic effects on three human breast, lung and central nervous system cancer cell lines. Three bioactive compounds fractionated from the methanolic leaf extracts of *V. baccifera* (vismione B, deacetylvismione A, and deacetylvismione H) showed antitumoral activity on these cell types, therefore they could be responsible for the actions of the *V. baccifera* extract. The efficiency of methanolic extracts of plants is, however, different from that shown in aqueous extracts. In general, the phenolic, flavonoid and saponin contents

of methanol and ethanol extracts are higher than in aqueous extracts (Wintola and Afolayan, 2011).

In a previous work of our group, the polyphenolic composition of aqueous infusions of *V. baccifera* leaves was detected by reverse-phase HPLC coupled to diode-array detector and MS/MS analysis (Lizcano et al., 2012). The extract contained high levels of flavanols, particularly epicatechin monomers, dimers and trimers, and to a lesser extent flavonols (glucosides of kampferol and quercetin), and hydroxycinnamic acids (caffeoylquinic acids).

In the literature flavanols from green tea (epicatechin derivatives among them) have been reported to exert antitumor activities *in vitro* and have also been associated with antitumor properties *in vivo* (Afzal et al., 2015; Shi et al., 2015). In order to asses whether the cytotoxic effects of *V. baccifera* could be ascribed to its epicatechin constituent, experiments were performed using commercial (-)-epicatechin monomer, isolated from green tea. The flavanol was unable to stop cell proliferation or induce toxicity to HepG2 cells, even at concentrations as high as 200 µg/ml during periods up to 72 h (Fig. 4.5), thus excluding this constituent as responsible of the antitumoral action of *V. baccifera*.

Some studies suggest that the oligomer chain length of polymerized oligomers of (-)-epicatechin may be a critical factor determining the pro-apoptotic effects of procyanidins (Chia-Chi et al., 2009). Thus, only flavanol oligomers and polymers, but not monomers or dimers, increased apoptosis of oesophageal adenocarcinoma cells (Pierini et al., 2008). In our system, we do not know whether (-)-epicatechin dimers or trimers (the major flavanol oligomers) are responsible of the observed effects in hepatoma cell lines, since these components alone were not assayed.

Procyanidins (dimers through tetramers) are absorbable *in vivo* (Stoupi et al., 2010), whereas larger procyanidins are not absorbable by human intestinal epithelial cells (Zumdick et al., 2010). On the other hand, while monomers and dimers can be transported inside the cells to modulate signaling, larger and non-absorbable procyanidins can regulate signaling by interacting with proteins of the cell membrane or the lipid bilayer (Fraga and Oteiza, 2011).

Previous studies using the (-)-epigallocatechin-3-gallate tea polyphenol showed that the flavanol had anticarcinogenic effects via modulation in protein expression of p53 (Huang et al.,

2009). Moreover, the apigenin flavonoid induced p53-dependent apoptosis in human breast cancer cells (Eun Jeong and Gun-Hee, 2009). In order to elucidate whether p53 was involved in the *V. baccifera*-induced toxicity, we used several models of hepatoma cell lines with differential p53 status: Hep3B, and Huh7, in addition to HepG2. HepG2 has a normal wild-type p53 expression, while in Hep3B cells a major portion of the p53 gene is deleted. Although Huh7 presents an increased p53 expression, this cell line contains a mutation, the cells being p53-transcriptionally dysfunctional (Hsu et al., 1993). Results showed that HepG2 was the most sensitive cell line to the plant extract, while the p53-null Hep3B were the most resistant (Fig. 4.4). These results suggest that p53 could be implicated in *V. baccifera*-induced toxicity, but also show that other mechanisms independent on p53 are operating.

Several natural polyphenols have been proposed to induce oxidative stress by affecting the mitochondrial respiratory chain, thereby generating a downstream flux of ROS (Noonan et al., 2007). With the intention of elucidating whether oxidative stress was regulating the cytotoxic effect of *V. baccifera*, changes in MitoSOX and DCF dyes fluorescence were measured by flow cytometry. *V. baccifera* markedly increased both the mitochondrial O_2^- and the intracellular ROS levels as early as 1 h. This effect was time- and dose- dependent, with sustained levels at 24 h (Fig. 4.6). Oxidative stress regulates numerous cellular functions, including proliferation, cell cycle, and cell death (Chiu and Dawes, 2012). Cell cycle phases were studied by flow cytometry. The results showed that the plant extract markedly increased the number of cells in subG_0, which is evidence of apoptotic cell death. Moreover, *V. baccifera* also reduced the number of cells undergoing DNA replication and increased the number of cells in G_2/M, indicating that the plant extract blocked cell cycle selectively at G_2/M phase. Thiol oxidation of proteins such as glutathionylation, disulfide bonds and sulfenic acid formation -which are reversible-, can be an indicator of redox stress in cells. Cell-cycle regulators with reactive cysteine residues are responsible to permit cells to enter in the next cell cycle phase (Janssen-Heininger et al., 2008). Many cancer cells have a defective G_1 checkpoint, resulting in a higher dependence on the G_2 checkpoint to protect against DNA damage during cell replication; as a consequence, the G_2 checkpoint is therefore considered as a specific target for anticancer therapy (Kawabe, 2004). The plant extract could affect the expression of proteins that regulate G_2/M transition, as has been reported for the isoflavone genistein in human ovarian and colon cancer cells (Ouyang et al., 2009; Zhang et al., 2013) and

theaflavins, the major components of black tea in human prostate carcinoma cells (Prasad et al., 2007). It has been reported in the bibliography that the cell cycle progression disruption is closely related with apoptotic cell death. Thus, quercetin, the most representative flavonol, which is also present in the *V. baccifera* aqueous extract we have used, may induce cell cycle arrest and apoptosis by direct activation of the caspase cascade in human breast cancer cells (Choi et al., 2001; Chou et al., 2010). We have seen that *V. baccifera*-induced HepG2 death trough a caspase-dependent mechanism where the initiator caspase-2 and the executioner caspase-3 were implicated (Fig. 4.10). Caspase-2 is a nuclear initiator caspase which does not require cleavage for its initial activation from others caspases (Baliga et al., 2004). Furthermore, caspase-2 is activated under oxidative stress conditions upstream of mitochondrial outer membrane permeabilization and also is implicated in cell cycle regulation (Puccini et al., 2013; Vakifahmetoglu-Norberg and Zhivotovsky, 2010). In addition, it has been reported that caspase-2 and -8 can activate caspase-3 under stress conditions in human dopaminergic neurons (Chaudhry and Ahmed, 2013).

In our scenario we also observed an increase in the mitochondrial membrane potential in HepG2 cells exposed to *V. baccifera* (Fig.4.8). In HeLa cells exposed to the plant pigment violacein, mitochondrial membrane hyperpolarization has been detected as the main cause of HeLa cell death (Leal et al., 2015). Indeed, early hyperpolarization of mitochondrial membrane has been reported that occurs in other cell death pathways (Banki et al., 1999). In addition to that, loss of the mitochondrial Ca^{2+} induced by HIV-1 Tat in cortical neurons resulted in hyperpolarization of mitochondrial membrane potential leading to cell death (Norman et al., 2008). All these results suggest that mitochondrial membrane hyperpolarization induced by *V. baccifera* could trigger apoptosis through a caspase-dependent pathway.

We have tried to elucidate the source/nature of ROS implicated in *V. baccifera*-induced toxicity, and several possibilities have been explored. NADPH oxidase (NOX) can be involved as a main intracellular free radical generator. NADPH oxidases (NOX 1-5; Duox 1,2) are a family of transmembrane proteins that carry across electrons, catalyzing the partial reduction of oxygen to superoxide anion or hydrogen peroxide. NOX is formed by cytosolic regulators (p22phox, p47phox, p40phox, p67phox and Rac), which are assembled constituting the oxidase complex (Brandes et al. 2014). These enzymes are expressed in several tissues and have different

subcellular localizations. The NOX-generated free radicals are involved in cellular functions, such as intracellular signaling of cell proliferation and differentiation (Bonner and Arbiser, 2012; Brandes et al., 2014). A cancer-specific NOX protein, called tNOX, has also identified in the surface of cancer cells, a protein that is absent in normal cells and has also been considered as target for cancer therapies due to its correlation with tumor growth (Davies and Bozzo, 2006). There are controversies in the literature regarding the role of polyphenols in NOX regulation. By one hand, various polyphenols inhibit NOX activity in several tissues (Maraldi, 2013), and naturally occurring polyphenols, such as catechin (-)-epigallocatechin gallate and vanilloid capsaicin, have also been shown to inhibit tNOX, producing cell death (Morré et al., 2006). On the other hand, several polyphenolic compounds, particularly phenolic acids and capsaicin, induced apoptosis in HepG2, and the ROS generated through the activation of NOX were responsible of the apoptotic response (Lee et al., 2004; Lee et al., 2005). Interestingly, regarding the possible inhibition of NOX by (-)-epicatechin metabolites, one of them the (-)-epicatechin O-methylated metabolite has structural similarities with apocynin (Fraga and Oteiza, 2011). Apocynin acts as a NADPH-oxidase inhibitor, rendering a radical which forms adducts with p47phox, inhibiting its assembly at the membrane (Ximenes et al., 2007). To asses the possible role of NOX in our system, pharmacological inhibition of the enzymes with apocynin was challenged in the presence of the extract. Our results do not support a role for NOX in the cytotoxicity triggered by *V. baccifera* in HepG2 (Fig. 4.17.a).

The xanthine oxidase enzyme is another source of ROS that could be involved in cell death, and the specific enzyme inhibitor allopurinol was used to analyze its implication. Allopurinol had a null effect on preventing *V. baccifera*-induced toxicity (Fig. 4.17.b); therefore, xanthine oxidase did not appear to mediate *V. baccifera* toxicity to HepG2. Recently, it has been reported that xanthine oxidase-generated H_2O_2 is a consequence, but not a mediator of cell death in various cancer cell types (Czupryna and Tsourkas, 2012). However, in our system intracellular ROS levels increased as early as 1 h, suggesting that *V. baccifera* H_2O_2 induction is an early response, not a consequence of *V. baccifera*-induced cell death. Trolox, the water-soluble analogue of vitamin E, is a lipoperoxyl radical scavenger that was unable to prevent cell growth inhibition (Fig. 4.15). Thus, these polyunsaturated fatty acid-derived radicals were discarded in the toxic mechanism of action. The mechanism of the free radical scavenging reaction by Tiron (sodium 4,5-dihydroxybenzene-1,3-disulfonate) is

thought to be its direct oxidation by first-formed superoxide radical, thus acting as an O_2^- scavenger. Tiron partially prevented the decrease in the cell number and the accumulation of ROS and O_2^- induced by the plant extract, suggesting that O_2^- could be involved in the *V. baccifera*-induced toxicity. It is noteworthy that Tiron was toxic in a dose- and time-dependent manner, and higher concentrations of the compound could not be used in the assay, thus limiting the study of its protective effect (data not shown).

The possible role of hydrogen peroxide in the toxicity triggered by *V. baccifera* was afforded by incubating the cells in the presence of catalase. Catalase completely prevented ROS formation, cell toxicity, mitochondrial membrane hyperpolarization, cell cycle arrest at G_2/M, and apoptosis. These results indicate how the increase in intracellular ROS is essential to induce apoptosis after exposure of HepG2 cells to *V. baccifera,* and support a role for H_2O_2 in the apoptotic process induced by the plant. Moreover, the rate of H_2O_2 production increased since 3 h of *V. baccifera* treatment, being detected by the non-permeant Amplex probe, specific for H_2O_2 detection. We cannot evaluate with these experiments whether H_2O_2 was initially produced inside the cells and then it spread outside, or whether *V. baccifera* acts as a pro-oxidant in the cell solution, generating H_2O_2. Anyway, the measured H_2O_2 production has a cell origin, since the cells were washed out of the extract after the treatment and before the kinetic analysis.

The glutathione cycle constitutes one of the main defence systems against oxidative stress (Wu et al., 2004). GSH is the major nonprotein thiol source that functions as a sulfhydryl buffer inside the cells; GSH also plays a role in detoxification reactions of xenobiotics, acting as the nucleophilic substrate of glutathione S-transferases, and reacting with peroxides in reactions catalyzed by GSH peroxidases. Therefore, its intracellular levels are tightly controlled, and the ratio of glutathione disulfide (GSSG) to GSH needs to be low for the correct cellular function (Ballatori et al., 2009, review). Depletion of GSH involves increase in ROS and, inversely, a ROS increase often leads to GSH depletion and alterations in the redox balance. The *in vitro* addition of NAC to HepG2 has been shown to prevent toxicity triggered by different prooxidant stimuli (Yedjou et al., 2010). NAC is a thiol-containing compound that acts as a sulfide source, necessary in glutathione synthesis. Inside the cell, it is readily deacetylated to yield L-cysteine, functioning as a GSH precursor (Rushworth and Megson 2014, review). NAC

has also been applied *in vivo* to various diseases associated with oxidative stress (Santana-Santos et al., 2014), against drug-induced hepatotoxicity (Baniasadi et al., 2010), and against cancer, acting as antioxidant adjuvant that reduces the chemotherapy-related toxicity (Lin et al., 2006). In our system, NAC was unable to protect cells against *V. baccifera*-induced toxicity, despite it prevented GSH depletion by the plant. These results suggest that GSH depletion is not the cause of the observed cytotoxicity, but rather the consequence of an initial oxidative stress generated by the extract. Moreover, the thiol containing antioxidant NAC was unable to prevent ROS accumulation inside the cells, contrary to the catalase effect, what could reassert that GSH depletion is not crucial for *V. baccifera*-induced cell death.

In this work, we have analyzed the antioxidant enzyme status in HepG2 treated with the plant extract. Our results showed that *V. baccifera* produced significant long-term changes in the activities of antioxidant enzymes, which were reflected by an overall increase in superoxide dismutase activity and a reduction of GPx activity at 24 h, suggesting the accumulation of hydrogen peroxide inside the cells. However, we found no changes in the antioxidant activities at short times, in which an increase in ROS was detected. The early oxidative stress induced by the extract could be responsible for the subsequent changes in the antioxidant activities, which could contribute to the long-term toxic response. According to these results, it has been recently described that resveratrol, a phenolic phytochemical present in vegetables and red wine, regulates the expression of proteins involved in the redox balance in different tumor cell lines, suggesting that it causes the deregulation of antioxidant proteins, and consequently increases oxidative damage and apoptosis (Khan et al., 2013). Oxidative stress also decreases the expression of selenoproteins (Papp et al., 2006), and the administration of the pro-oxidant paraquat to mice decreases tissue GPx1 protein and activity (Cheng et al., 1999). Moreover, it has been described that certain kinases that phosphorylate specific tyrosine residues of GPx1 regulate its activity and proteolytic degradation; when the intracellular ROS levels are low, the GPx activity is stimulated by phosphorylation, and in response to high oxidant levels GPx1 activity is diminished by targeting the phosphorylated protein towards its degradation (Cao et al., 2003).

According to our results from the experiments in the presence of catalase, it seems that H_2O_2 has a different role in the regulation of GPx and SOD activities. Thus, H_2O_2 scavenging by

catalase prevented the GPx activity reduction, but not the SOD activity increase, suggesting that the early H_2O_2 generation modulates GPx activity, but not SOD activity at 24 h.

There are two intracellular SOD enzymes with different subcellular localizations, namely Cu,Zn-SOD and Mn-SOD, which are located in the cytosol and mitochondria, respectively. We found that the Cu,Zn-SOD amount in control cells (without treatment) was 1.85-fold higher than Mn-SOD in HepG2 cells. Moreover, *V. baccifera*-induced H_2O_2 increased Mn-SOD expression, although the plant extract did not modify Cu,Zn-SOD expression. Thus, it is reasonable attributing a higher contribution of Mn-SOD to the total SOD activity increase, and this remarkable up-regulation of Mn-SOD and the reduction of GPx would result in the elevation of H_2O_2 concentration in the cells. Indeed, our results are in accordance to the study of Khan et al. (2013), where resveratrol up-regulated Mn-SOD, not affecting Cu,Zn-SOD, and increased SOD activity, inducing H_2O_2 accumulation in prostate, hepatic and breast tumor cell lines. The induction of *SOD2* in response to oxidative stress has been well established in organisms, tissues and cells growing under various stress conditions. Stimuli such as ionizing radiation (Eastgate et al., 1993; Akashi et al., 1995), 12-O-tetradecanoylphorbol-13-acetate (Fujii and Taniguchi, 1991), interferon-γ (Harris et al., 1991) and proinflammatory cytokines (tumor necrosis factor α, interleukin-1β, interleukin-4 and interleukin-6), rapidly modulate *SOD2* gene transcription (Visner et al., 1990; St Clair et al., 2002). It can be noticed that all these mentioned regulators are mediators of ROS generation.

In an attempt to characterize the main signaling pathways implicated in the cytotoxic mechanism of *V. baccifera* in hepatocarcinoma HepG2 cells, several key proteins involved in cell death and proliferation were assayed by immunoblotting and immmunofluorescence. First of all, we studied some of the Ser/Thr kinases, such as Akt, ERK, JNK and p38 in response to *V. baccifera*. The direct downstream targets of Akt are implicated in cell survival, proliferation and cell growth, among others (*reviewed in section 1.4.1*). The plant extract significantly inhibited Akt phosphorylation at 24 h, this decrease being prevented by catalase. This result suggests that the *V. baccifera*-induced H_2O_2 generation inhibited the cell survival Akt pathway, which is mediated by PI3K. On the other hand, the MAPKs activation can be triggered by ROS (McCubrey et al., 2006). Regarding ERK, its early activation (of both ERK1/2) reverted to control levels with the incubation time, and even an inhibition of ERK2 was observed at 24 h.

The fact that catalase modified the effect of the plant extract only at 24 h suggests that hydrogen peroxide has no role in the early ERK1/2 phosphorylation, but perhaps is involved in ERK inactivation. In the literature, some authors argue that ERK1 and ERK2 may have different and not redundant functions (Lloyd, 2006). ERK2 seems to be the mediator of proliferation and Ras induction, whereas ERK1 has an opposed function, blocking Ras transformation. This idea is supported by some studies in mouse embryo fibroblasts and NIH 3T3 cells where ERK2 had a positive role in Ras-dependent proliferation, while ERK1 probably antagonized this action (Vantaggiato et al., 2006). Due to the fact that ERK can contribute to the tumor cell growth (McCubrey et al., 2007), our results of ERK2 inhibition by *V. baccifera*-induced hydrogen peroxide at 24 h are in accordance with the fact that *V. baccifera* induces cell death. In addition, ERK pathway is related with the induction of cell migration. Indeed, it has been demonstrated that breast cancer cell migration is regulated through the ERK pathway (Chen et al., 2009). Our results connected the ERK2 down-regulation at 24 h with the reduction in HepG2 migration (Fig. 4.12). Regarding JNK, which is activated by oxidative stress and is implicated in controlling apoptosis, *V. baccifera* promoted sharply JNK phosphorylation from the first time assayed, and this activation was sustained along the time studied (Fig. 4.30). Taking into account the effect of catalase, these results would indicate that *V. baccifera*-induced hydrogen peroxide promotes JNK activation.

At the G_2/M boundary CDC25B has been reported to be the starting phosphatase that initially activates CDK1/cyclin B, which activates CDC25C, creating an autoactivation loop (Donzelli and Draetta, 2003). CDC25B-1/2 and CDC25C are functionally inactivated upon phosphorylation on Ser309/323 and Ser216, respectively, leading to 14-3-3 binding and nuclear exclusion (Zeng and Piwnica-Worms, 1999). The p38/MAPK-K2 (MK2) signaling complex is considered to be a general stress response pathway, which is activated in response to a variety of extrinsic and intrinsic stimuli including osmotic stress, heat shock, various toxins, UV and ionizing radiation, ROS, cytokines, loss of centrosome integrity, and DNA damage (Kyriakis and Avruch, 2001). The p38α protein exists in a stable complex with its downstream substrate, the kinase MK2. Many upstream MAPKKKs participate in the activation of the p38 cascade, including MEKK1/4, ASK1, and TAO kinases, depending on the particular type of initiating stimulus to which the cell is responding. Besides UV, p38α and p38β are activated by other DNA damage-specific agents. Treatment of cells with etoposide revealed

that p38 is activated following the induction of DNA DSBs after topoisomerase II inhibition and a G_2/M arrest was induced (Kurosu et al., 2005). This arrest is the result of the CDC25B and CDC25C phosphorylations by the complex p38/MK2, generating crucial 14-3-3-binding sites (Manke et al., 2005). In our system, p38 was markedly activated since 1 h of treatment and the activation was sustained along the time studied. Moreover, we could verify that catalase was unable to prevent p38 phosphorylation, suggesting that H_2O_2 does not regulate p38 activity. In an effort to elucidate whether p38 was mediating *V. baccifera*-induced cell death, the selective p38α inhibitor doramapimod and SB203580, which inhibits both p38α and β catalytic activities, were used. These results showed that p38 inhibitors were unable to prevent *V. baccifera*-induced toxicity, and even increased cell death. Thus, p38 is not implicated in the cell death induced by the extract. On the contrary, p38 MAPK could be promoting a protective or reparative effect in response to the pro-oxidant actions of *V. baccifera*. The co-incubation with catalase induced a p38 phosphorylation higher than the plant extract alone, preventing cytotoxicity. Moreover, studies with human cervix and lung cancer cell lines indicated that p38 is rapidly activated by DNA damage, although this protein was not required for the G_2 DNA damage checkpoint; thus, p38 played an important prosurvival role during the G_2 checkpoint (Phong et al., 2010).

On the other hand, another cell signaling pathway which can be modulated by ROS is NFκB (Morgan et al., 2011). Under basal conditions, the inactive NFκB heterodimer is found in the cytosol forming a complex with its inhibitory IκBα protein. However, when NFκB pathway is activated, the IκBα protein is phosphorylated, polyubiquitinated and proteosomally degraded, releasing the p65-p50 complex that translocates into the nucleus. In our system *V. baccifera* induced the degradation of both p65 and IκBα since 3 h of treatment. However, the decrease in IκBα content was lower than the p65 decrease, suggesting a net inhibition of the p65 translocation into the nucleus, these effects not being prevented by catalase. The results suggest that the NFκB pathway was inhibited by *V. baccifera*. These data are in accordance with the fact that, depending on the context, ROS can interact with the NFκB pathway elements either upstream or downstream, promoting a stimulatory or inhibitory effect on the NFκB pathway (Morgan et al., 2011).

In light of the cell cycle arrest at G_2/M phase induced by *V. baccifera* in HepG2, a deep analysis of the molecular pathways regulating cell cycle was performed. DNA damage is one of the main reasons for arresting at G_2 phase (*reviewed in section Introduction 1.5.5.*). Taking this into account, proteins implicated in the DNA damage response were studied. First of all, the γH2AX histone, which is rapidly expressed minutes after DNA damage, was studied (Savic et al., 2009). We observed that the plant extract activated γH2AX at 24 h of treatment, but not at early times (data not shown). Moreover, γH2AX activation was clearly prevented by catalase, suggesting that the elevated levels of hydrogen peroxide generated by *V. baccifera* regulated γH2AX expression. ATM protein is activated after DNA damage (Kurz et al., 2004), and in turn phosphorylates γH2AX for being spread over large chromatin domains flanking the DNA breaks (Savic et al., 2009). In our study, the ATM phosphorylation increased at 24 h of treatment (Fig. 4.36). Moreover, this ATM activation was even higher in the presence of catalase. Thus, the completely prevention of γH2AX phosphorylation by catalase suggests that γH2AX activation is not promoted by ATM pathway. Indeed, it has been described in the literature that γH2AX can also be activated by ATR pathway (Ward and Chen, 2001). Taking into account these data, we suggest that the pathway elicited by *V. baccifera* for the DNA damage repairing during cell cycle arrest at G_2/M is the ATR/γH2AX pathway. Furthermore, the significant higher ATM activation with the co-incubation with catalase would indicate that catalase is promoting a defence response against *V. baccifera* genotoxic effect through ATM. This genotoxic effect is specific of tumor cells, since no change was detected with normal HH4 hepatocytes (data not shown).

ATM is involved in p53 induction, and p53 in turn activates 14-3-3σ and GADD45 proteins implicated in blocking the transition from G_2 to M phase after DNA damage (Peng et al., 1997). The immunoblotting results did not reveal p53 Ser15 phosphorylation. However, by confocal microscopy we observed an enrichment of this phosphoprotein in the nucleus along the time studied (Fig. 4.37). In addition, it was previously suggested that p53 may have a certain role in *V. baccifera*-induced toxicity, since HepG2, Huh7 and Hep3B cell lines demonstrated differentiated sensitivity to the plant extract (Fig. 4.4). Taking into account these results, p53 could be implicated in the G_2 arrest to repair DNA damage induced by *V. baccifera*.

It has been described that upon DNA damage, the CDK inhibitor p21 can be activated during the G_2 cell cycle arrest. Oxidative stress-induced p21 expression is generally mediated via a p53-dependent mechanism (Giono and Manfredi, 2006). Nevertheless, there is also a p53-independent pathway that involves p38 (O'Reilly, 2005; Kim et al., 2002). We found that *V. baccifera* promoted p21 accumulation that was not prevented by p38 inhibition (data not shown). Interestingly, it has been reported that oxidants induce p21 expression in a p53-independent manner (Esposito et al., 2001). In our system, catalase delayed the accumulation of p21, reinforcing the role of ROS in cell cycle arrest (data not shown).

It is generally accepted that during cellular stress, cells activate the *unfolded protein response* (UPR) (*reviewed in section Introduction 1.6.*). In this context, we analyzed the GRP78 expression, a chaperone that binds to unfolded proteins during ER stress. As a result of the UPR, there is also induction of *de novo* GRP78 synthesis through the ATF6 pathway to help proteins to be folded. Our results revealed that *V. baccifera* induced the GRP78 expression at early times (3-6 h), and catalase was able to prevent GRP78 accumulation at 6 h. This point suggests that high levels of hydrogen peroxide can be implicated in the ER stress response. Moreover, it has been suggested that GRP78 has an anti-apoptotic role during ER stress in breast cancer cells (Zhou et al., 2011). The *unfolded protein response* induced by IRE1 pathway was studied, due to the fact that GRP78 activation is related with the splicing of X-box-binding protein 1 (XBP1) mRNA (Masahiro et al., 2003). The RNase activity of IRE1 initiates the cleavage of XBP1 mRNA to produce the active XBP1-spliced. The spliced XBP1 acts as a transcription factor for genes involved in ER protein maturation and ER-associated degradation. XBP1-deficient cells are more sensitive to oxidative stress induced by H_2O_2, due to the repressed expression of antioxidant enzymes (Liu et al., 2009). *V. baccifera* activated the IRE1 pathway, inducing the XBP1 splicing in the presence of catalase; however, the plant extract alone did not induce significantly the XBP1 splicing, although *V. baccifera* activated GRP78 expression. These results may indicate that catalase activated a defence mechanism against *V. baccifera*-induced ER stress trough XBP1 splicing for higher expression of antioxidant enzymes. Indeed, in our system we observed that the SOD activity in cells co-incubated with catalase was even higher than with the plant extract alone. On the other hand, one study revealed that IRE1 degrades through a post-transcriptional modification specific microRNAs that target the mRNA encoding casapase-2 to induce expression of pro-caspase-2

(Upton et al., 2012). It has been determined that caspase-2 induces apoptosis through Bid cleavage to truncated Bid (t-Bid), inducing Bax/Bak complex and cytochrome c release from mitochondria (Bonzon et al., 2006; Wei et al., 2001). Once the key executioner caspase-3 is activated, it is also able to process pro-caspase-2, which potentially provides an amplification loop for the caspase-2 activation (Puccini et al., 2013). Taking into account that both the caspase-2 and -3 activities increased by the plant extract, and that caspase-2 can proteolyze Bid protein for inducing apoptosis, we decided to study the Bcl2 protein family. We observed an increase in the pro-apoptotic protein Bax, and a decrease in the anti-apoptotic protein Bcl-x_L at 24 h. We also observed an increase of the Bax/Bcl-2 ratio at 24 h, which is an index to evaluate the mitochondrial membrane permeability due to the formation of pores by the Bax family (Tian et al., 2012). In our study, we also evaluated the caspase-8 and -9 activities, and tried to study the expression of these caspases by immunoblotting. We could attribute neither enzymatically nor by immunodetection any role of these caspases in *V. baccifera*-induced toxicity. The increase of caspase-2 and -3 activities was correlated with the PARP cleavage observed in the presence of *V. baccifera,* which was inhibited by catalase (Fig. 4.27). Bid protein migrates to the mitochondrial membrane where it induces cytochrome c release (Haupt et al., 2003). t-Bid interacts with the Bcl-x_L anti-apoptotic protein (Garcia-Saez et al., 2009), this ratio being a possible apoptotic marker. Our results revealed that the ratio of Bid to Bcl-x_L was increased near 6-fold in the presence of *V. baccifera*. Catalase prevented these alterations by modulating the pro-apoptotic and anti-apototic proteins, suggesting that hydrogen peroxide induced by *V. baccifera* promotes HepG2 death through a caspase-dependent mechanism. In this regard, in our system caspase-2 could be activated through several mechanisms: a) IRE1-mediaed caspase-2 up-regulation, which is XBP1-independent, b) through caspase-3, and c) directly by ROS or by DNA damage (Puccini et al., 2013). Moreover, *V. baccifera*-induced caspase-2 activity could trigger the mitochondrial cytochrome c release and subsequent apoptosis through Bid proteolysis and the formation of the Bax/Bak complex.

Natural polyphenols can trigger a non-apoptotic form of programmed cell death independent of caspases, i.e., autophagy (Hasima and Ozpolat, 2014). It has been determined that the signal for selection of apoptosis or autophagy under ER stress depends on ATF4 expression in HepG2 (Matsumoto et al., 2013). Autophagy is a catabolic process which manages the recycling of cellular components under cellular stress. Autophagy is an adaptive

and essential process required for cellular homeostasis, which can function as a cell survival or death mechanism. During autophagosome formation, the pro-autophagic LC3-II isoform is accumulated, which is lipidated through the conjugation to phosphatidylethanolamine through Atg4 protein. In our scenario, LC3-II accumulated in the presence of *V. baccifera*, this process being prevented by catalase (Fig. 4.43). This suggests that *V. baccifera*-induced H_2O_2 activated autophagy in HepG2. In addition, ROS can modulate autophagy under oxidative stress, allowing the translocation of Nrf2 to the nucleus, where it binds to the antioxidant response elements, activating the transcription of genes encoding several antioxidant enzymes and p62/SQSTM1. The p62 protein participates in the degradation of unfolded and ubiquitinated proteins by delivering them to the autophagosomes. Several works reveal the autophagic properties of polyphenolic compounds in different tumor cell lines (Hasima and Ozpolat, 2014). Indeed, resveratrol promotes Beclin-1-dependent autophagy through JNK-mediated p62/SQSTM1 expression (Puissant and Auberger, 2010). In our study, *V. baccifera* induced p62 accumulation at 24 h, and this accumulation was higher in the presence of the H_2O_2 scavenger catalase (Fig. 4.43). Moreover, in fetal hepatocyte HH4 cells the extract was unable to induce p62 accumulation (data not shown), stressing again the specific effect of the extract on tumor cells. These results suggest that *V. baccifera*-induced hydrogen peroxide promotes autophagy, and that catalase induces a pro-survival pathway against *V. baccifera* toxicity through p62.

According to our results and the bibliography we propose the *V. baccifera*-induced signaling mechanism depicted in Fig. 5.1:

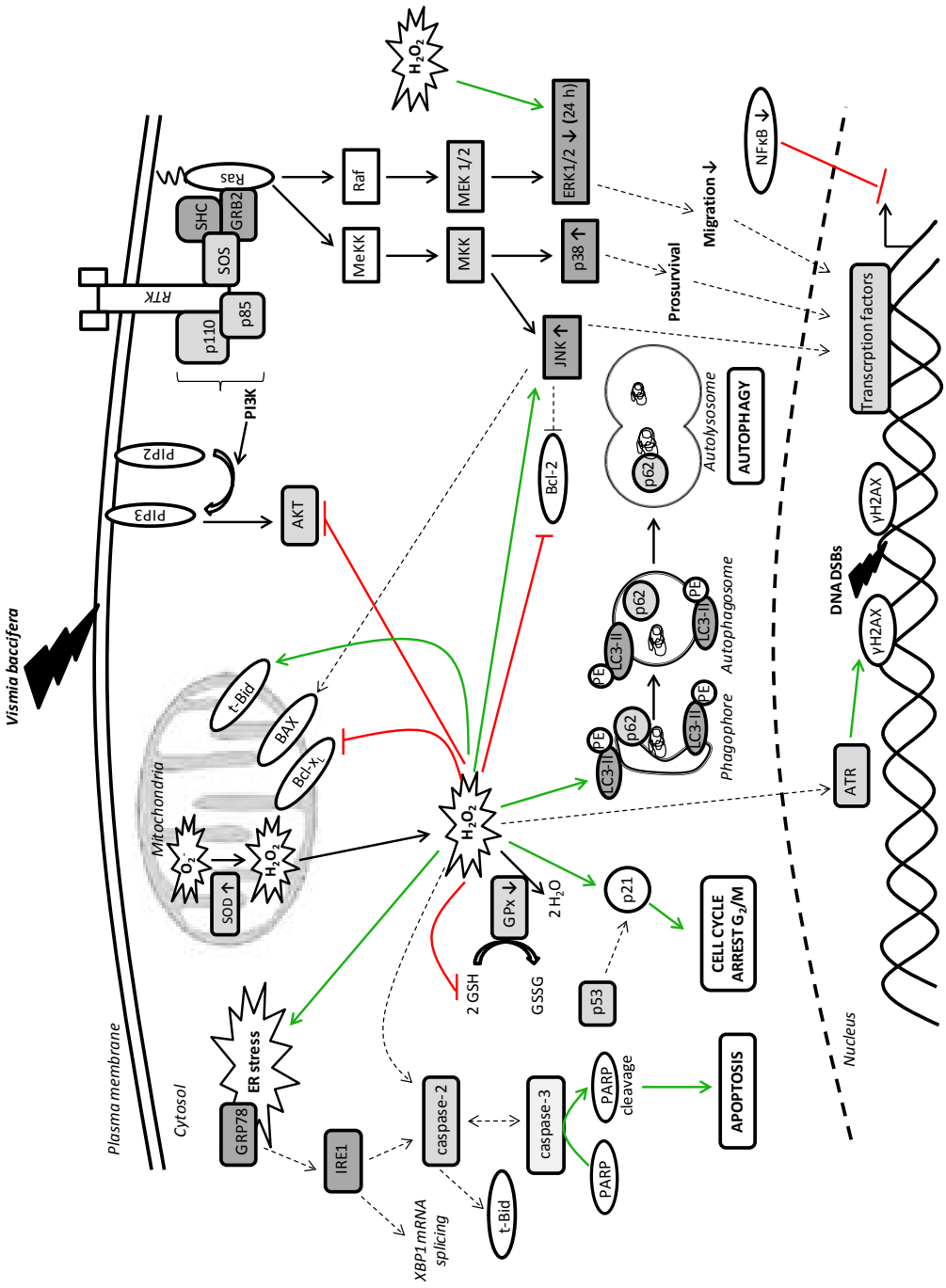

Figure 5.1. Scheme of intracellular signaling induced by *V. baccifera* based on our experimental results and in the literature. *(→) activation by H_2O_2 ; (⊣) inhibition by H_2O_2; (---->) possible activation, described in the bibliography.*

The oxygen partial pressure (pO_2) is a key component of the physiological state of an organ, which results from the balance between oxygen delivery and its consumption. Oxygen delivery is dependent on the metabolic requirements and functional status of each organ. Tissue oxygenation is severely disturbed during pathological conditions such as cancer, diabetes, coronary heart disease or stroke, which are associated with decreased pO_2, also known as hypoxia. Hypoxia can be caused by several factors, such as 1) low O_2 partial pressure in arterial blood, 2) reduced ability of blood to carry O_2, 3) reduced or deterioration of tissue perfusion, or 4) inability of cells to use O_2. This condition can induce changes on the proteome and the genome of the genetically unstable neoplastic cells (Hockel and Vaupel, 2001). *In vitro* cultures are mostly performed in a 95% air atmosphere (79% N_2/21% O_2), supplemented with 5% carbon dioxide. These conditions do not represent the endogenous oxygen pressure either of the majority of normal organs or tumor cells. Indeed, during tumor development pO_2 is becoming lower, producing important consequences for oxygenation and chemotherapy efficiency (Carreau et al., 2011). Knowing the drastic consequences of oxidative stress on the cell physiology, we thought essential to study some of the cellular behaviours, such as cell proliferation, ROS levels, migration and cell adhesion, under low (8%) oxygen partial pressure. To carry out this study, we used three different hepatoma cell lines with different p53 status: HepG2, Huh7 and Hep3B cell lines. Huh7 and HepG2 had similar growth rates, while Hep3B showed the lowest doubling time. However, the growth rate of these three cell lines was unaffected by the pO_2. In contrast, the oxygen partial pressure in the culture modified the intracellular steady-state ROS levels; thus, a lower pO_2 resulted in higher ROS levels in all the cell types. Interestingly, although the ROS levels were pO_2-dependent, the steady-state mitochondrial levels of O_2^- were not modified by the oxygen concentration. On the other hand, the migratory and adhesiveness capacities depended on the cell line characteristics. In fact, HepG2 had the highest migration and adhesion rates. Moreover, the pO_2 modified the cell migration depending on the cell p53 status. A low pO_2 increased the migration rate in wild-type p53 HepG2 cells, while p53 deficient cells exhibited a lower migration rate. Interestingly, in our laboratory we have detected by immunoblotting higher p53 stabilization when HepG2 were cultured under 8% pO_2 (data not shown).

The possible influence of pO_2 on the cytotoxicity elicited by *V. baccifera* was addressed. The oxygen tension did not modify the measured cytotoxic parameters, IC_{50}, ROS and

mitochondrial O_2^- induced by the extract at 24 h. Only at longer incubation times the low pO_2 rendered cells more resistant to the extract.

6. CONCLUSIONS

6. CONCLUSIONS

1. The *V. baccifera* aqueous leaf extract elicits a cytotoxic response in human hepatocellular carcinoma HepG2 cells, increasing the levels of mitochondrial O_2^- and intracellular ROS (particularly hydrogen peroxide), inducing depletion of GSH, cell cycle arrest at G_2/M phase, endoplasmic reticulum stress, autophagy and apoptosis.

2. The cytotoxic actions exerted by *V. baccifera* are exclusive of cancer cells, since the human nontransformed HH4 hepatocytes were unaffected by the extract.

3. Hydrogen peroxide, whose intracellular accumulation is early induced by the extract, mediates the cytotoxic response.

4. *V. baccifera* induces deregulation of antioxidant enzymes, this effect being secondary to the accumulation of hydrogen peroxide.

5. The intracellular GSH depletion is not the cause but the consequence of *V. baccifera*-induced toxicity.

6. *V. baccifera* affects HepG2 signaling via activation of JNK and p38 MAPKs, and inhibiting Akt prosurvival- and ERK pathways. The alterations of Akt, JNK and ERK activation states are dependent on hydrogen peroxide, whereas p38 is activated through H_2O_2-independent mechanisms.

7. A similar response in terms of early ROS production was observed at both atmospheric 21% pO_2 and normal tissue 8% pO_2. These results suggest that similar mechanism of signaling and toxicity are taking place, thus validating the experimental approach using 21% pO_2 to study the toxicity response to *V. baccifera*, and ruling out any possible superimposed oxidative stress derived from the culture conditions.

7. BIBLIOGRAPHY

7. BIBLIOGRAPHY

Actis-Goretta, L., Romanczyk, L.J., Rodriguez, C.A., Kwik-Uribe, C., and Keen, C.L. (2008). Cytotoxic effects of digalloyl dimer procyanidins in human cancer cell lines. J. Nutr. Biochem. 12, 797-808.

Aebi, H. (1984). Catalase in vitro. Methods Enzymol. 121-126.

Afzal, M., Safer, A.M., and Menon, M. (2015). Green tea polyphenols and their potential role in health and disease. Inflammopharmacology 4, 151-161.

Akashi, M., Hachiya, M., Paquette, R.L., Osawa, Y., Shimizu, S., and Suzuki, G. (1995). Irradiation increases manganese superoxide dismutase mRNA levels in human fibroblasts. Possible mechanisms for its accumulation. J. Biol. Chem. 26, 15864-15869.

Aleem, E., Kiyokawa, H., and Kaldis, P. (2005). Cdc2-cyclin E complexes regulate the G1/S phase transition. Nat. Cell Biol. 8, 831-836.

Alexander, A., Cai, S.L., Kim, J., Nanez, A., Sahin, M., MacLean, K.H., Inoki, K., Guan, K.L., Shen, J., Person, M.D., Kusewitt, D., Mills, G.B., Kastan, M.B., and Walker,C.L. (2010). ATM signals to TSC2 in the cytoplasm to regulate mTORC1 in response to ROS. Proc. Natl. Acad. Sci. U. S. A. 9, 4153-4158.

Avivar-Valderas, A., Salas, E., Bobrovnikova-Marjon, E., Diehl, J.A., Nagi, C., Debnath, J., and Aguirre-Ghiso, J.A. (2011). PERK integrates autophagy and oxidative stress responses to promote survival during extracellular matrix detachment. Mol. Cell. Biol. 17, 3616-3629.

Aziz, M.H., Kumar, R., and Ahmad, N. (2003). Cancer chemoprevention by resveratrol: in vitro and in vivo studies and the underlying mechanisms (review). Int. J. Oncol. 1, 17-28.

Bae, S.H., Sung, S.H., Oh, S.Y., Lim, J.M., Lee, S.K., Park, Y.N., Lee, H.E., Kang, D., and Rhee, S.G. (2013). Sestrins activate Nrf2 by promoting p62-dependent autophagic degradation of Keap1 and prevent oxidative liver damage. Cell. Metab. 1, 73-84.

Bakkenist, C.J., and Kastan, M.B. (2003). DNA damage activates ATM through intermolecular autophosphorylation and dimer dissociation. Nature 6922, 499-506.

Baliga, B.C., Read, S.H., and Kumar, S. (2004). The biochemical mechanism of caspase-2 activation. Cell Death Differ. 11, 1234-1241.

Balkwill, F., and Coussens, L.M. (2004). Cancer: an inflammatory link. Nature 7007, 405-406.

Ballatori, N., Krance, S.M., Notenboom, S., Shi, S., Tieu, K., and Hammond, C.L. (2009). Glutathione dysregulation and the etiology and progression of human diseases. Biol. Chem. 3, 191-214.

Baniasadi, S., Eftekhari, P., Tabarsi, P., Fahimi, F., Raoufy, M.R., Masjedi, M.R., and Velayati, A.A. (2010). Protective effect of N-acetylcysteine on antituberculosis drug-induced hepatotoxicity. Eur. J. Gastroenterol. Hepatol.10, 1235-1238.

Banki, K., Hutter, E., Gonchoroff, N.J., and Perl, A. (1999). Elevation of mitochondrial transmembrane potential and reactive oxygen intermediate levels are early events and occur independently from activation of caspases in Fas signaling. J. Immunol. 3, 1466-1479.

Baretic, D., and Williams, R.L. (2014). PIKKs--the solenoid nest where partners and kinases meet. Curr. Opin. Struct. Biol. 134-142.

Bartek, J., and Lukas, J. (2003). Chk1 and Chk2 kinases in checkpoint control and cancer. Cancer Cell 5, 421-429.

Beamish, H., Williams, R., Chen, P., and Lavin, M.F. (1996). Defect in multiple cell cycle checkpoints in ataxia-telangiectasia postirradiation. J. Biol. Chem. 34, 20486-20493.

Bedard, K., and Krause, K.H. (2007). The NOX family of ROS-generating NADPH oxidases: physiology and pathophysiology. Physiol. Rev. 1, 245-313.

Bellacosa, A., Chan, T.O., Ahmed, N.N., Datta, K., Malstrom, S., Stokoe, D., McCormick, F., Feng, J., and Tsichlis, P. (1998). Akt activation by growth factors is a multiple-step process: the role of the PH domain. Oncogene 3,313-325.

Bellot, G., Garcia-Medina, R., Gounon, P., Chiche, J., Roux, D., Pouyssegur, J., and Mazure, N.M. (2009). Hypoxia-induced autophagy is mediated through hypoxia-inducible factor induction of BNIP3 and BNIP3L via their BH3 domains. Mol. Cell. Biol. 10, 2570-2581.

Bhandary, B., Marahatta, A., Kim, H.R., and Chae, H.J. (2012). An involvement of oxidative stress in endoplasmic reticulum stress and its associated diseases. Int. J. Mol. Sci. 1, 434-456.

Billen, L.P., Shamas-Din, A., and Andrews, D.W. (2008). Bid: a Bax-like BH3 protein. Oncogene S93-104.

Bonner, M.Y., and Arbiser, J.L. (2012). Targeting NADPH oxidases for the treatment of cancer and inflammation. Cell Mol. Life Sci. 14, 2435-2442.

Bonzon, C., Bouchier-Hayes, L., Pagliari, L.J., Green, D.R., and Newmeyer, D.D. (2006). Caspase-2-induced apoptosis requires bid cleavage: a physiological role for bid in heat shock-induced death. Mol. Biol. Cell 5, 2150-2157.

Bradford, M.M. (1976). A rapid and sensitive method for the quantitation of microgram quantities of protein utilizing the principle of protein-dye binding. Anal. Biochem. 248-254.

Bragado, P., Armesilla, A., Silva, A., and Porras, A. (2007). Apoptosis by cisplatin requires p53 mediated p38alpha MAPK activation through ROS generation. Apoptosis 9, 1733-1742.

Brandes, R.P., Weissmann, N., and Schröder, K. (2014). Nox family NADPH oxidases: Molecular mechanisms of activation. Free Radical Biology and Medicine 208-226.

Bressac, B., Galvin, K.M., Liang, T.J., Isselbacher, K.J., Wands, J.R., and Ozturk, M. (1990). Abnormal structure and expression of p53 gene in human hepatocellular carcinoma. Proc. Natl. Acad. Sci. U. S. A. 5, 1973-1977.

Brooks, A.J., Eastwood, J., Beckingham, I.J., and Girling, K.J. (2004). Liver tissue partial pressure of oxygen and carbon dioxide during partial hepatectomy. Br. J. Anaesth. 5, 735-737.

Brunet, A., Bonni, A., Zigmond, M.J., Lin, M.Z., Juo, P., Hu, L.S., Anderson, M.J., Arden, K.C., Blenis, J., and Greenberg, M.E. (1999). Akt promotes cell survival by phosphorylating and inhibiting a Forkhead transcription factor. Cell 6, 857-868.

Burhans, W.C., and Heintz, N.H. (2009). The cell cycle is a redox cycle: Linking phase-specific targets to cell fate. Free Radical Biology and Medicine 9, 1282-1293.

Cao, C., Leng, Y., Huang, W., Liu, X., and Kufe, D. (2003). Glutathione peroxidase 1 is regulated by the c-Abl and Arg tyrosine kinases. J. Biol. Chem. 41, 39609-39614.

Cao, S.S., and Kaufman, R.J. (2012). Unfolded protein response. Current Biology 16, R622-R626.

Cardaci, S., Filomeni, G., Rotilio, G., and Ciriolo, M.R. (2008). Reactive oxygen species mediate p53 activation and apoptosis induced by sodium nitroprusside in SH-SY5Y cells. Mol. Pharmacol. 5, 1234-1245.

Cardone, M.H., Roy, N., Stennicke, H.R., Salvesen, G.S., Franke, T.F., Stanbridge, E., Frisch, S., and Reed, J.C. (1998). Regulation of cell death protease caspase-9 by phosphorylation. Science 5392, 1318-1321.

Cargnello, M., and Roux, P.P. (2011). Activation and function of the MAPKs and their substrates, the MAPK-activated protein kinases. Microbiol. Mol. Biol. Rev. 1, 50-83.

Carreau, A., El Hafny-Rahbi, B., Matejuk, A., Grillon, C., and Kieda, C. (2011). Why is the partial oxygen pressure of human tissues a crucial parameter? Small molecules and hypoxia. J. Cell. Mol. Med. 6, 1239-1253.

Chaudhry, Z.L., and Ahmed, B.Y. (2013). Caspase-2 and caspase-8 trigger caspase-3 activation following 6-OHDA-induced stress in human dopaminergic neurons differentiated from ReNVM stem cells. Neurol. Res. 4, 435-440.

Chellappan, S.P., Hiebert, S., Mudryj, M., Horowitz, J.M., and Nevins, J.R. (1991). The E2F transcription factor is a cellular target for the RB protein. Cell 6, 1053-1061.

Chen, H., Zhu, G., Li, Y., Padia, R.N., Dong, Z., Pan, Z.K., Liu, K., and Huang, S. (2009). Extracellular signal-regulated kinase signaling pathway regulates breast cancer cell migration by maintaining slug expression. Cancer Res. 24, 9228-9235.

Chen, H., Zhu, G., Li, Y., Padia, R.N., Dong, Z., Pan, Z.K., Liu, K., and Huang, S. (2009). Extracellular signal-regulated kinase signaling pathway regulates breast cancer cell migration by maintaining slug expression. Cancer Res. 24, 9228-9235.

Chen, K., Albano, A., Ho, A., and Keaney, J.F.,Jr. (2003). Activation of p53 by oxidative stress involves platelet-derived growth factor-beta receptor-mediated ataxia telangiectasia mutated (ATM) kinase activation. J. Biol. Chem. 41, 39527-39533.

Chene, P. (2001). The role of tetramerization in p53 function. Oncogene 21, 2611-2617.

Cheng, W., Fu, Y.X., Porres, J.M., Ross, D.A., and Lei, X.G. (1999). Selenium-dependent cellular glutathione peroxidase protects mice against a pro-oxidant-induced oxidation of NADPH, NADH, lipids, and protein. FASEB J. 11,1467-1475.

Chiu, J., and Dawes, I.W. (2012). Redox control of cell proliferation. Trends Cell Biol. 11, 592-601.

Choi, E.J., and Kim, G. (2009). Apigenin causes G2/M arrest associated with the modulation of p21Cip1 and Cdc2 and activates p53-dependent apoptosis pathway in human breast cancer SK-BR-3 cells. J. Nutr. Biochem. 4,285-290.

Choi, J.A., Kim, J.Y., Lee, J.Y., Kang, C.M., Kwon, H.J., Yoo, Y.D., Kim, T.W., Lee, Y.S., and Lee, S.J. (2001). Induction of cell cycle arrest and apoptosis in human breast cancer cells by quercetin. Int. J. Oncol. 4, 837-844.

Chomczynski, P. (1993). A reagent for the single-step simultaneous isolation of RNA, DNA and proteins from cell and tissue samples. BioTechniques 3, 532-4, 536-7.

Chou, C.C., Yang, J.S., Lu, H.F., Ip, S.W., Lo, C., Wu, C.C., Lin, J.P., Tang, N.Y., Chung, J.G., Chou, M.J., Teng, Y.H., and Chen, D.R. (2010). Quercetin-mediated cell cycle arrest and apoptosis involving activation of a caspase cascade through the mitochondrial pathway in human breast cancer MCF-7 cells. Arch. Pharm. Res. 8, 1181-1191.

Chou, C.C., Yang, J.S., Lu, H.F., Ip, S.W., Lo, C., Wu, C.C., Lin, J.P., Tang, N.Y., Chung, J.G., Chou, M.J., Teng, Y.H., and Chen, D.R. (2010). Quercetin-mediated cell cycle arrest and apoptosis involving activation of a caspase cascade through the mitochondrial pathway in human breast cancer MCF-7 cells. Arch. Pharm. Res. 8, 1181-1191.

Cicchillitti, L., Fasanaro, P., Biglioli, P., Capogrossi, M.C., and Martelli, F. (2003). Oxidative stress induces protein phosphatase 2A-dependent dephosphorylation of the pocket proteins pRb, p107, and p130. J. Biol. Chem. 21,19509-19517.

Circu, M.L., and Aw, T.Y. (2008). Glutathione and apoptosis. Free Radic. Res. 8, 689-706.

Cistulli, C.A., and Kaufmann, W.K. (1998). p53-dependent signaling sustains DNA replication and enhances clonogenic survival in 254 nm ultraviolet-irradiated human fibroblasts. Cancer Res. 9, 1993-2002.

Colitti, M. (2012). BCL-2 Family of Proteins and Mammary Cellular Fate. Anat. Histol. Embryol. 4, 237-247.

Czupryna, J., and Tsourkas, A. (2012). Xanthine oxidase-generated hydrogen peroxide is a consequence, not a mediator of cell death. FEBS J. 5, 844-855.

D'Archivio, M., Filesi, C., Di Benedetto, R., Gargiulo, R., Giovannini, C., and Masella, R. (2007). Polyphenols, dietary sources and bioavailability. Ann. Ist. Super. Sanita 4, 348-361.

Davies, S.L., and Bozzo, J. (2006). Spotlight on tNOX: a tumor-selective target for cancer therapies. Drug News. Perspect. 4, 223-225.

Dewaele, M., Maes, H., and Agostinis, P. (2010). ROS-mediated mechanisms of autophagy stimulation and their relevance in cancer therapy. Autophagy 7, 838-854.

Dhouib, I.E., Annabi, A., Jallouli, M., Elfazaa, S., and Lasram, M.M. (2016). A minireview on N-acetylcysteine: An old drug with new approaches. Life Sci.

Dick, F.A. (2007). Structure-function analysis of the retinoblastoma tumor suppressor protein - is the whole a sum of its parts? Cell. Div. 26.

Djavaheri-Mergny, M., Amelotti, M., Mathieu, J., Besancon, F., Bauvy, C., and Codogno, P. (2007). Regulation of autophagy by NFkappaB transcription factor and reactives oxygen species. Autophagy 4, 390-392.

Donzelli, M., and Draetta, G.F. (2003). Regulating mammalian checkpoints through Cdc25 inactivation. EMBO Rep. 7, 671-677.

Downward, J. (2003). Targeting RAS signaling pathways in cancer therapy. Nat. Rev. Cancer. 1, 11-22.

Eastgate, J., Moreb, J., Nick, H.S., Suzuki, K., Taniguchi, N., and Zucali, J.R. (1993). A role for manganese superoxide dismutase in radioprotection of hematopoietic stem cells by interleukin-1. Blood 3, 639-646.

Eguale, T., Tadesse, D., and Giday, M. (2011). In vitro anthelmintic activity of crude extracts of five medicinal plants against egg-hatching and larval development of Haemonchus contortus. J. Ethnopharmacol. 1, 108-113.

Ehrenberg, B., Montana, V., Wei, M.D., Wuskell, J.P., and Loew, L.M. (1988). Membrane potential can be determined in individual cells from the nernstian distribution of cationic dyes. Biophys. J. 5, 785-794.

Elbling, L., Weiss, R.M., Teufelhofer, O., Uhl, M., Knasmueller, S., Schulte-Hermann, R., Berger, W., and Micksche, M. (2005). Green tea extract and (-)-epigallocatechin-3-gallate, the major tea catechin, exert oxidant but lack antioxidant activities. FASEB J. 7, 807-809.

Esposito, F., Russo, L., Chirico, G., Ammendola, R., Russo, T., and Cimino, F. (2001). Regulation of p21waf1/cip1 expression by intracellular redox conditions. IUBMB Life 1-2, 67-70.

Ewan, J. (1962). The South American Species of Vismia (Guttiferae). .Nat. Museum, Contribution from the National Herbarium., (5): 293.

Fang, G., Yu, H., and Kirschner, M.W. (1998). Direct binding of CDC20 protein family members activates the anaphase-promoting complex in mitosis and G1. Mol. Cell 2, 163-171.

Fang, Y., Hu, X.H., Jia, Z.G., Xu, M.H., Guo, Z.Y., and Gao, F.H. (2012). Tiron protects against UVB-induced senescence-like characteristics in human dermal fibroblasts by the inhibition of superoxide anion production and glutathione depletion. Australas. J. Dermatol. 3, 172-180.

Fazi, B., Melino, S., De Rubeis, S., Bagni, C., Paci, M., Piacentini, M., and Di Sano, F. (2009). Acetylation of RTN-1C regulates the induction of ER stress by the inhibition of HDAC activity in neuroectodermal tumors. Oncogene 43, 3814-3824.

Feig, L.A., Urano, T., and Cantor, S. (1996). Evidence for a Ras/Ral signaling cascade. Trends Biochem. Sci. 11, 438-441.

Ferreira, M.F., Santocanale, C., Drury, L.S., and Diffley, J.F. (2000). Dbf4p, an essential S phase-promoting factor, is targeted for degradation by the anaphase-promoting complex. Mol. Cell. Biol. 1, 242-248.

Filomeni, G., De Zio, D., and Cecconi, F. (2015). Oxidative stress and autophagy: the clash between damage and metabolic needs. Cell Death Differ. 3, 377-388.

Filomeni, G., Desideri, E., Cardaci, S., Rotilio, G., and Ciriolo, M.R. (2010). Under the ROS...thiol network is the principal suspect for autophagy commitment. Autophagy 7, 999-1005.

Finlay, G.J., and Baguley, B.C. (1984). The use of human cancer cell lines as a primary screening system for antineoplastic compounds. Eur. J. Cancer Clin. Oncol. 7, 947-954.

Fisher, A.B. (2009). Redox signaling across cell membranes. Antioxid. Redox Signal. 6, 1349-1356.

Flohe, L., and Gunzler, W.A. (1984). Assays of glutathione peroxidase. Methods Enzymol. 114-121.

Fraga, C.G., and Oteiza, P.I. (2011). Dietary flavonoids: Role of (-)-epicatechin and related procyanidins in cell signaling. Free Radic. Biol. Med. 4, 813-823.

Fujii, J., and Taniguchi, N. (1991). Phorbol ester induces manganese-superoxide dismutase in tumor necrosis factor-resistant cells. J. Biol. Chem. 34, 23142-23146.

Fulton, A.M., Ma, X., and Kundu, N. (2006). Targeting prostaglandin E EP receptors to inhibit metastasis. Cancer Res. 20, 9794-9797.

Fuster, J.J., Fernandez, P., Gonzalez-Navarro, H., Silvestre, C., Nabah, Y.N., and Andres, V. (2010). Control of cell proliferation in atherosclerosis: insights from animal models and human studies. Cardiovasc. Res. 2, 254-264.

Gallant, P., and Nigg, E.A. (1992). Cyclin B2 undergoes cell cycle-dependent nuclear translocation and, when expressed as a non-destructible mutant, causes mitotic arrest in HeLa cells. J. Cell Biol. 1, 213-224.

Gallego, A., Torres, F., Robledo, S., Vélez, ID., Carrillo, L., Muñoz, DL., Quiñones, W., Fonnegra, R., Roldán, J., Valencia, L., Triana, O., Echeverri, F. (2006). Actividad leishmanicida y tripanocida de acacia farnesiana, piper arierianum, P. subpedale y Vismia baccifera subsp. Ferruginea.28: 39-49.

Gao, X., and Pan, D. (2001). TSC1 and TSC2 tumor suppressors antagonize insulin signaling in cell growth. Genes Dev. 11, 1383-1392.

Garcia-Saez, A.J., Ries, J., Orzaez, M., Perez-Paya, E., and Schwille, P. (2009). Membrane promotes tBID interaction with BCL(XL). Nat. Struct. Mol. Biol. 11, 1178-1185.

Gautier, J., Solomon, M.J., Booher, R.N., Bazan, J.F., and Kirschner, M.W. (1991). Cdc25 is a Specific Tyrosine Phosphatase that Directly Activates P34cdc2. Cell 1, 197-211.

Gazdar, A.F., Girard, L., Lockwood, W.W., Lam, W.L., and Minna, J.D. (2010). Lung cancer cell lines as tools for biomedical discovery and research. J. Natl. Cancer Inst. 17, 1310-1321.

Ghosh, A.P., Klocke, B.J., Ballestas, M.E., and Roth, K.A. (2012). CHOP potentially co-operates with FOXO3a in neuronal cells to regulate PUMA and BIM expression in response to ER stress. PLoS One 6, e39586.

Gillies, R.J., Didier, N., and Denton, M. (1986). Determination of cell number in monolayer cultures. Anal. Biochem. 1, 109-113.

Giono, L.E., and Manfredi, J.J. (2006). The p53 tumor suppressor participates in multiple cell cycle checkpoints. J. Cell. Physiol. 1, 13-20.

Girard, F., Strausfeld, U., Fernandez, A., and Lamb, N.J. (1991). Cyclin A is required for the onset of DNA replication in mammalian fibroblasts. Cell 6, 1169-1179.

Girling, R., Partridge, J.F., Bandara, L.R., Burden, N., Totty, N.F., Hsuan, J.J., and La Thangue, N.B. (1993). A new component of the transcription factor DRTF1/E2F. Nature 6445, 468.

Glotzer, M., Murray, A.W., and Kirschner, M.W. (1991). Cyclin is degraded by the ubiquitin pathway. Nature 6305, 132-138.

Gomez-Cansino, R., Espitia-Pinzon, C.I., Campos-Lara, M.G., Guzman-Gutierrez, S.L., Segura-Salinas, E., Echeverria-Valencia, G., Torras-Claveria, L., Cuevas-Figueroa, X.M., and Reyes-Chilpa, R. (2015). Antimycobacterial and HIV-1 Reverse Transcriptase Activity of Julianaceae and Clusiaceae Plant Species from Mexico. Evid Based. Complement. Alternat Med. 183036.

Green, D.R., and Llambi, F. (2015). Cell Death Signaling. Cold Spring Harb Perspect. Biol. 12, 10.1101/cshperspect.a006080.

Gross, E., Kastner, D.B., Kaiser, C.A., and Fass, D. (2004). Structure of Ero1p, Source of Disulfide Bonds for Oxidative Protein Folding in the Cell. Cell 5, 601-610.

Guo, Z., Kozlov, S., Lavin, M.F., Person, M.D., and Paull, T.T. (2010). ATM activation by oxidative stress. Science 6003, 517-521.

Gurib-Fakim, A. (2006). Medicinal plants: Traditions of yesterday and drugs of tomorrow. Mol. Aspects Med. 1, 1-93.

Gwinn, D.M., Shackelford, D.B., Egan, D.F., Mihaylova, M.M., Mery, A., Vasquez, D.S., Turk, B.E., and Shaw, R.J. (2008). AMPK phosphorylation of raptor mediates a metabolic checkpoint. Mol. Cell 2, 214-226.

Habig, W.H., and Jakoby, W.B. (1981). Assays for differentiation of glutathione S-transferases. Methods Enzymol. 398-405.

Hailey, D.W., Rambold, A.S., Satpute-Krishnan, P., Mitra, K., Sougrat, R., Kim, P.K., and Lippincott-Schwartz, J. (2010). Mitochondria supply membranes for autophagosome biogenesis during starvation. Cell 4, 656-667.

Hamasaki, M., Furuta, N., Matsuda, A., Nezu, A., Yamamoto, A., Fujita, N., Oomori, H., Noda, T., Haraguchi, T., Hiraoka, Y., Amano, A., and Yoshimori, T. (2013). Autophagosomes form at ER-mitochondria contact sites. Nature 7441, 389-393.

Harding, H.P., Zhang, Y., Bertolotti, A., Zeng, H., and Ron, D. (2000). Perk is essential for translational regulation and cell survival during the unfolded protein response. Mol. Cell 5, 897-904.

Harding, H.P., Zhang, Y., Zeng, H., Novoa, I., Lu, P.D., Calfon, M., Sadri, N., Yun, C., Popko, B., Paules, R., Stojdl, D.F., Bell, J.C., Hettmann, T., Leiden, J.M., and Ron,D. (2003). An integrated stress response regulates amino acid metabolism and resistance to oxidative stress. Mol. Cell 3, 619-633.

Harris, C.A., Derbin, K.S., Hunte-McDonough, B., Krauss, M.R., Chen, K.T., Smith, D.M., and Epstein, L.B. (1991). Manganese superoxide dismutase is induced by IFN-gamma in multiple cell types. Synergistic induction by IFN-gamma and tumor necrosis factor or IL-1. J. Immunol. 1, 149-154.

Hasima, N., and Ozpolat, B. (2014). Regulation of autophagy by polyphenolic compounds as a potential therapeutic strategy for cancer. Cell. Death Dis. e1509.

Haupt, S., Berger, M., Goldberg, Z., and Haupt, Y. (2003). Apoptosis - the p53 network. J. Cell. Sci. Pt 20, 4077-4085.

Haupt, Y., Maya, R., Kazaz, A., and Oren, M. (1997). Mdm2 promotes the rapid degradation of p53. Nature 6630, 296-299.

Havens, C.G., Ho, A., Yoshioka, N., and Dowdy, S.F. (2006). Regulation of late G1/S phase transition and APC Cdh1 by reactive oxygen species. Mol. Cell. Biol. 12, 4701-4711.

He, C., and Klionsky, D.J. (2009). Regulation mechanisms and signaling pathways of autophagy. Annu. Rev. Genet. 67-93.

Herranz-Lopez, M., Fernandez-Arroyo, S., Perez-Sanchez, A., Barrajon-Catalan, E., Beltran-Debon, R., Menendez, J.A., Alonso-Villaverde, C., Segura-Carretero, A., Joven, J., and Micol, V. (2012). Synergism of plant-derived polyphenols in adipogenesis: perspectives and implications. Phytomedicine 3-4, 253-261.

Herzinger, T., Funk, J.O., Hillmer, K., Eick, D., Wolf, D.A., and Kind, P. (1995). Ultraviolet B irradiation-induced G2 cell cycle arrest in human keratinocytes by inhibitory phosphorylation of the cdc2 cell cycle kinase. Oncogene10, 2151-2156.

Hitomi, M., and Stacey, D.W. (1999). Cyclin D1 production in cycling cells depends on ras in a cell-cycle-specific manner. Curr. Biol. 19, 1075-1084.

Hockel, M., and Vaupel, P. (2001). Tumor hypoxia: definitions and current clinical, biologic, and molecular aspects. J. Natl. Cancer Inst. 4, 266-276.

Hsu, I.C., Tokiwa, T., Bennett, W., Metcalf, R.A., Welsh, J.A., Sun, T., and Harris, C.C. (1993). p53 gene mutation and integrated hepatitis B viral DNA sequences in human liver cancer cell lines. Carcinogenesis 5, 987-992.

Hsu, J.Y., Reimann, J.D., Sorensen, C.S., Lukas, J., and Jackson, P.K. (2002). E2F-dependent accumulation of hEmi1 regulates S phase entry by inhibiting APC(Cdh1). Nat. Cell Biol. 5, 358-366.

Hu, C.T., Wu, J.R., Cheng, C.C., Wang, S., Wang, H.T., Lee, M.C., Wang, L.J., Pan, S.M., Chang, T.Y., and Wu, W.S. (2011). Reactive oxygen species-mediated PKC and integrin signaling promotes tumor progression of human hepatoma HepG2. Clin. Exp. Metastasis 8, 851-863.

Huang, C., Tsai, S., Wang, Y., Pan, M., Kao, J., and Way, T. (2009). EGCG inhibits protein synthesis, lipogenesis, and cell cycle progression through activation of AMPK in p53 positive and negative human hepatoma cells. Molecular Nutrition & Food Research 9, 1156-1165.

Huang, D., Ou, B., Hampsch-Woodill, M., Flanagan, J.A., and Prior, R.L. (2002). High-throughput assay of oxygen radical absorbance capacity (ORAC) using a multichannel liquid handling system coupled with a microplate fluorescence reader in 96-well format. J. Agric. Food Chem. 16, 4437-4444.

Huie, C.W. (2002). A review of modern sample-preparation techniques for the extraction and analysis of medicinal plants. Anal. Bioanal Chem. 1-2, 23-30.

Hussein, A.A., Bozzi, B., Correa, M., Capson, T.L., Kursar, T.A., Coley, P.D., Solis, P.N., and Gupta, M.P. (2003). Bioactive constituents from three Vismia species. J. Nat. Prod. 6, 858-860.

Ip, Y.T., and Davis, R.J. (1998). Signal transduction by the c-Jun N-terminal kinase (JNK) — from inflammation to development. Curr. Opin. Cell Biol. 2, 205-219.

Itoh, K., Chiba, T., Takahashi, S., Ishii, T., Igarashi, K., Katoh, Y., Oyake, T., Hayashi, N., Satoh, K., Hatayama, I., Yamamoto, M., and Nabeshima, Y. (1997). An Nrf2/small Maf heterodimer mediates the induction of phase II detoxifying enzyme genes through antioxidant response elements. Biochem. Biophys. Res. Commun. 2, 313-322.

Ivanov, A.V., Bartosch, B., Smirnova, O.A., Isaguliants, M.G., and Kochetkov, S.N. (2013). HCV and oxidative stress in the liver. Viruses 2, 439-469.

Jain, A., Lamark, T., Sjottem, E., Larsen, K.B., Awuh, J.A., Overvatn, A., McMahon, M., Hayes, J.D., and Johansen, T. (2010). p62/SQSTM1 is a target gene for transcription factor NRF2 and creates a positive feedback loop by inducing antioxidant response element-driven gene transcription. J. Biol. Chem. 29, 22576-22591.

Janssen-Heininger, Y.M., Mossman, B.T., Heintz, N.H., Forman, H.J., Kalyanaraman, B., Finkel, T., Stamler, J.S., Rhee, S.G., and van der Vliet, A. (2008). Redox-based regulation of signal transduction: principles, pitfalls, and promises. Free Radic. Biol. Med. 1, 1-17.

Jiang, D., Niwa, M., and Koong, A.C. (2015). Targeting the IRE1α–XBP1 branch of the unfolded protein response in human diseases. Semin. Cancer Biol. 48-56.

Jin, P., Hardy, S., and Morgan, D.O. (1998). Nuclear localization of cyclin B1 controls mitotic entry after DNA damage. J. Cell Biol. 4, 875-885.

Johnson, G.L., and Lapadat, R. (2002). Mitogen-activated protein kinase pathways mediated by ERK, JNK, and p38 protein kinases. Science 5600, 1911-1912.

Johnson, T.M., Yu, Z.X., Ferrans, V.J., Lowenstein, R.A., and Finkel, T. (1996). Reactive oxygen species are downstream mediators of p53-dependent apoptosis. Proc. Natl. Acad. Sci. U. S. A. 21, 11848-11852.

Joza, N., Pospisilik, J.A., Hangen, E., Hanada, T., Modjtahedi, N., Penninger, J.M., and Kroemer, G. (2009). AIF: not just an apoptosis-inducing factor. Ann. N. Y. Acad. Sci. 2-11.

Jung, C.H., Jun, C.B., Ro, S.H., Kim, Y.M., Otto, N.M., Cao, J., Kundu, M., and Kim, D.H. (2009). ULK-Atg13-FIP200 complexes mediate mTOR signaling to the autophagy machinery. Mol. Biol. Cell 7, 1992-2003.

Kamata, H., Honda, S., Maeda, S., Chang, L., Hirata, H., and Karin, M. (2005). Reactive Oxygen Species Promote TNFα-Induced Death and Sustained JNK Activation by Inhibiting MAP Kinase Phosphatases. Cell 5, 649-661.

Kastan, M.B., Onyekwere, O., Sidransky, D., Vogelstein, B., and Craig, R.W. (1991). Participation of p53 protein in the cellular response to DNA damage. Cancer Res. 23 Pt 1, 6304-6311.

Kawabe, T. (2004). G2 checkpoint abrogators as anticancer drugs. Mol. Cancer. Ther. 4, 513-519.

Khan, H.Y., Zubair, H., Ullah, M.F., Ahmad, A., and Hadi, S.M. (2012). A prooxidant mechanism for the anticancer and chemopreventive properties of plant polyphenols. Curr. Drug Targets 14, 1738-1749.

Khan, M.A., Chen, H.C., Wan, X.X., Tania, M., Xu, A.H., Chen, F.Z., and Zhang, D.Z. (2013). Regulatory effects of resveratrol on antioxidant enzymes: a mechanism of growth inhibition and apoptosis induction in cancer cells. Mol. Cells 3, 219-225.

Kim, E.M., Yang, H.S., Kang, S.W., Ho, J.N., Lee, S.B., and Um, H.D. (2008). Amplification of the gamma-irradiation-induced cell death pathway by reactive oxygen species in human U937 cells. Cell. Signal. 5, 916-924.

Kim, G.Y., Mercer, S.E., Ewton, D.Z., Yan, Z., Jin, K., and Friedman, E. (2002). The stress-activated protein kinases p38 alpha and JNK1 stabilize p21(Cip1) by phosphorylation. J. Biol. Chem. 33, 29792-29802.

Kim, J., Kundu, M., Viollet, B., and Guan, K.L. (2011). AMPK and mTOR regulate autophagy through direct phosphorylation of Ulk1. Nat. Cell Biol. 2, 132-141.

Kobayashi, A., Kang, M.I., Okawa, H., Ohtsuji, M., Zenke, Y., Chiba, T., Igarashi, K., and Yamamoto, M. (2004). Oxidative stress sensor Keap1 functions as an adaptor for Cul3-based E3 ligase to regulate proteasomal degradation of Nrf2. Mol. Cell. Biol. 16, 7130-7139.

Komatsu, M., Kurokawa, H., Waguri, S., Taguchi, K., Kobayashi, A., Ichimura, Y., Sou, Y.S., Ueno, I., Sakamoto, A., Tong, K.I., Kim, M., Nishito, Y., Iemura, S., Natsume, T., Ueno, T., Kominami, E., Motohashi, H., Tanaka, K., Yamamoto, M. (2010). The selective autophagy substrate p62 activates the stress responsive transcription factor Nrf2 through inactivation of Keap1. Nat. Cell Biol. 3, 213-223.

Kornblau, S.M. (1998). The Role of Apoptosis in the Pathogenesis, Prognosis, and Therapy of Hematologic Malignancies. Leukemia (08876924) S41-S46.

Kroemer, G., Dallaporta, B., and Resche-Rigon, M. (1998). The mitochondrial death/life regulator in apoptosis and necrosis. Annu. Rev. Physiol. 619-642.

Kroemer, G., Marino, G., and Levine, B. (2010). Autophagy and the integrated stress response. Mol. Cell 2, 280-293.

Kuo, P.L., Chen, C.Y., and Hsu, Y.L. (2007). Isoobtusilactone A induces cell cycle arrest and apoptosis through reactive oxygen species/apoptosis signal-regulating kinase 1 signaling pathway in human breast cancer cells. Cancer Res. 15, 7406-7420.

Kurosu, T., Takahashi, Y., Fukuda, T., Koyama, T., Miki, T., and Miura, O. (2005). p38 MAP kinase plays a role in G2 checkpoint activation and inhibits apoptosis of human B cell lymphoma cells treated with etoposide. Apoptosis 5, 1111-1120.

Kurz, E.U., and Lees-Miller, S.P. (2004). DNA damage-induced activation of ATM and ATM-dependent signaling pathways. DNA Repair 8–9, 889-900.

Kwee, J.K. (2015). Yin and yang of polyphenols in cancer prevention. A short review. Anticancer Agents Med. Chem.

Kwon, J., Lee, S., Yang, K., Ahn, Y., Kim, Y.J., Stadtman, E.R., and Rhee, S.G. (2004). Reversible oxidation and inactivation of the tumor suppressor PTEN in cells stimulated with peptide growth factors. Proceedings of the National Academy of Sciences of the United States of America 47, 16419-16424.

Kyriakis, J.M., and Avruch, J. (2001). Mammalian mitogen-activated protein kinase signal transduction pathways activated by stress and inflammation. Physiol. Rev. 2, 807-869.

Laemmli, U.K. (1970). Cleavage of structural proteins during the assembly of the head of bacteriophage T4. Nature 5259, 680-685.

Lavin, M.F., and Gueven, N. (2006). The complexity of p53 stabilization and activation. Cell Death Differ. 6, 941-950.

Leal, A.M., de Queiroz, J.D., de Medeiros, S.R., Lima, T.K., and Agnez-Lima, L.F. (2015). Violacein induces cell death by triggering mitochondrial membrane hyperpolarization in vitro. BMC Microbiol. 115-015-0452-2.

Lecci, R.M., Logrieco, A., and Leone, A. (2014). Pro-oxidative action of polyphenols as action mechanism for their pro-apoptotic activity. Anticancer Agents Med. Chem. 10, 1363-1375.

Lee, J.H., Goodarzi, A.A., Jeggo, P.A., and Paull, T.T. (2010). 53BP1 promotes ATM activity through direct interactions with the MRN complex. EMBO J. 3, 574-585.

Lee, K., Tirasophon, W., Shen, X., Michalak, M., Prywes, R., Okada, T., Yoshida, H., Mori, K., and Kaufman, R.J. (2002). IRE1-mediated unconventional mRNA splicing and S2P-mediated ATF6 cleavage merge to regulate XBP1 in signaling the unfolded protein response. Genes Dev. 4, 452-466.

Lee, M.H., Reynisdottir, I., and Massague, J. (1995). Cloning of p57KIP2, a cyclin-dependent kinase inhibitor with unique domain structure and tissue distribution. Genes Dev. 6, 639-649.

Lee, S.R., Yang, K.S., Kwon, J., Lee, C., Jeong, W., and Rhee, S.G. (2002). Reversible inactivation of the tumor suppressor PTEN by H2O2. J. Biol. Chem. 23, 20336-20342.

Lee, Y.S. (2005). Role of NADPH oxidase-mediated generation of reactive oxygen species in the mechanism of apoptosis induced by phenolic acids in HepG2 human hepatoma cells. Arch. Pharm. Res. 10, 1183-1189.

Lee, Y.S., Kang, Y.S., Lee, J.S., Nicolova, S., and Kim, J.A. (2004). Involvement of NADPH oxidase-mediated generation of reactive oxygen species in the apototic cell death by capsaicin in HepG2 human hepatoma cells. Free Radic. Res. 4, 405-412.

Lee, Y., Hwang, J., Kwon, D.Y., Surh, Y., and Park, O.J. (2010). Induction of apoptosis by quercetin is mediated through AMPKα1/ASK1/p38 pathway. Cancer Lett. 2, 228-236.

Lees, J.A., Buchkovich, K.J., Marshak, D.R., Anderson, C.W., and Harlow, E. (1991). The retinoblastoma protein is phosphorylated on multiple sites by human cdc2. EMBO J. 13, 4279-4290.

Li, Y., Duan, S., Jia, H., Bai, C., Zhang, L., and Wang, Z. (2014). Flavonoids from tartary buckwheat induce G2/M cell cycle arrest and apoptosis in human hepatoma HepG2 cells. Acta Biochim. Biophys. Sin. (Shanghai) 6,460-470.

Liang, J., Zubovitz, J., Petrocelli, T., Kotchetkov, R., Connor, M.K., Han, K., Lee, J.H., Ciarallo, S., Catzavelos, C., Beniston, R., Franssen, E., and Slingerland, J.M. (2002). PKB/Akt phosphorylates p27, impairs nuclear import of p27 and opposes p27-mediated G1 arrest. Nat. Med. 10, 1153-1160.

Lin, P.C., Lee, M.Y., Wang, W.S., Yen, C.C., Chao, T.C., Hsiao, L.T., Yang, M.H., Chen, P.M., Lin, K.P., and Chiou, T.J. (2006). N-acetylcysteine has neuroprotective effects against oxaliplatin-based adjuvant chemotherapy in colon cancer patients: preliminary data. Support. Care Cancer 5, 484-487.

Lin, Y., Shi, C.Y., Li, B., Soo, B.H., Mohammed-Ali, S., Wee, A., Oon, C.J., Mack, P.O., and Chan, S.H. (1996). Tumor suppressor p53 and Rb genes in human hepatocellular carcinoma. Ann. Acad. Med. Singapore 1, 22-30.

Liu, ,Dongping, and Xu, ,Yang. (2011). p53, Oxidative Stress, and Aging. Antioxid Redox Signal. 6, 1669.

Liu, S., Shiotani, B., Lahiri, M., Maréchal, A., Tse, A., Leung, C., Glover, J.N. ., Yang, X., and Zou, L. (2011). ATR Autophosphorylation as a Molecular Switch for Checkpoint Activation. Mol. Cell 2, 192-202.

Liu, Y., Adachi, M., Zhao, S., Hareyama, M., Koong, A.C., Luo, D., Rando, T.A., Imai, K., and Shinomura, Y. (2009). Preventing oxidative stress: a new role for XBP1. Cell Death Differ. 6, 847-857.

Lizcano, L.J., Siles, M., Trepiana, J., Hernandez, M.L., Navarro, R., Ruiz-Larrea, M.B., and Ruiz-Sanz, J.I. (2014). Piper and Vismia species from Colombian Amazonia differentially affect cell proliferation of hepatocarcinoma cells. Nutrients 1, 179-195.

Lizcano, L.J., Viloria-Bernal, M., Vicente, F., Berrueta, L.A., Gallo, B., Martinez-Canamero, M., Ruiz-Larrea, M.B., and Ruiz-Sanz, J.I. (2012). Lipid oxidation inhibitory effects and phenolic composition of aqueous extracts from medicinal plants of Colombian Amazonia. Int. J. Mol. Sci. 5, 5454-5467.

Lizcano, L.J., Bakkali, F., Begoña Ruiz-Larrea, M., and Ignacio Ruiz-Sanz, J. (2010). Antioxidant activity and polyphenol content of aqueous extracts from Colombian Amazonian plants with medicinal use. Food Chem. 4,1566-1570.

Lloyd, A.C. (2006). Distinct functions for ERKs? J. Biol. 5, 13.

Lorin, S., Hamaï, A., Mehrpour, M., and Codogno, P. (2013). Autophagy regulation and its role in cancer. Semin. Cancer Biol. 5, 361-379.

Magenta, A., Fasanaro, P., Romani, S., Di Stefano, V., Capogrossi, M.C., and Martelli, F. (2008). Protein phosphatase 2A subunit PR70 interacts with prB and mediates its dephosphorylation. Mol. Cell. Biol. 2, 873-882.

Magnaghi-Jaulin, L., Groisman, R., Naguibneva, I., Robin, P., Lorain, S., Le Villain, J.P., Troalen, F., Trouche, D., and Harel-Bellan, A. (1998). Retinoblastoma protein represses transcription by recruiting a histone deacetylase. Nature 6667, 601-605.

Malhotra, J.D., and Kaufman, R.J. (2007). Endoplasmic reticulum stress and oxidative stress: a vicious cycle or a double-edged sword? Antioxid. Redox Signal. 12, 2277-2293.

Maly, D.J., and Papa, F.R. (2014). Druggable sensors of the unfolded protein response. Nat. Chem. Biol. 11, 892-901.

Manke, I.A., Nguyen, A., Lim, D., Stewart, M.Q., Elia, A.E., and Yaffe, M.B. (2005). MAPKAP kinase-2 is a cell cycle checkpoint kinase that regulates the G2/M transition and S phase progression in response to UV irradiation. Mol. Cell 1, 37-48.

Manning, B.D., and Cantley, L.C. (2007). AKT/PKB Signaling: Navigating Downstream. Cell 7, 1261-1274.

Maraldi, T. (2013). Natural compounds as modulators of NADPH oxidases. Oxid Med. Cell. Longev 271602.

Marechal, A., and Zou, L. (2013). DNA damage sensing by the ATM and ATR kinases. Cold Spring Harb Perspect. Biol. 9, 10.1101/cshperspect.a012716.

Martín, M.A., Ramos, S., Mateos, R., Izquierdo-Pulido, M., Bravo, L., and Goya, L. (2010). Protection of human HepG2 cells against oxidative stress by the flavonoid epicatechin. Phytotherapy Research 4, 503-509.

Matsumoto, H., Miyazaki, S., Matsuyama, S., Takeda, M., Kawano, M., Nakagawa, H., Nishimura, K., and Matsuo, S. (2013). Selection of autophagy or apoptosis in cells exposed to ER-stress depends on ATF4 expression pattern with or without CHOP expression. Biol. Open 10, 1084-1090.

Matsuoka, S., Ballif, B.A., Smogorzewska, A., McDonald, E.R.,3rd, Hurov, K.E., Luo, J., Bakalarski, C.E., Zhao, Z., Solimini, N., Lerenthal, Y., Shiloh, Y., Gygi, S.P., and Elledge, S.J. (2007). ATM and ATR substrate analysis reveals extensive protein networks responsive to DNA damage. Science 5828, 1160-1166.

Matsuoka, S., Huang, M., and Elledge, S.J. (1998). Linkage of ATM to cell cycle regulation by the Chk2 protein kinase. Science 5395, 1893-1897.

Mayo, L.D., and Donner, D.B. (2001). A phosphatidylinositol 3-kinase/Akt pathway promotes translocation of Mdm2 from the cytoplasm to the nucleus. Proc. Natl. Acad. Sci. U. S. A. 20, 11598-11603.

McClung, J.M., Judge, A.R., Powers, S.K., and Yan, Z. (2010). p38 MAPK links oxidative stress to autophagy-related gene expression in cachectic muscle wasting. Am. J. Physiol. Cell. Physiol. 3, C542-9.

McCord, J.M., and Fridovich, I. (1969). Superoxide dismutase. An enzymic function for erythrocuprein (hemocuprein). J. Biol. Chem. 22, 6049-6055.

McCubrey, J.A., Lahair, M.M., and Franklin, R.A. (2006). Reactive oxygen species-induced activation of the MAP kinase signaling pathways. Antioxid. Redox Signal. 9-10, 1775-1789.

McCubrey, J.A., Steelman, L.S., Chappell, W.H., Abrams, S.L., Wong, E.W.T., Chang, F., Lehmann, B., Terrian, D.M., Milella, M., Tafuri, A., Chiarini, F., Evangelisti, C., Cocco, L., and Martelli, A.M. (2007). Roles of the Raf/MEK/ERK pathway in cell growth, malignant transformation and drug resistance. Biochimica et Biophysica Acta (BBA) - Molecular Cell Research 8, 1263-1284.

Menon, S.G., Sarsour, E.H., Spitz, D.R., Higashikubo, R., Sturm, M., Zhang, H., and Goswami, P.C. (2003). Redox regulation of the G1 to S phase transition in the mouse embryo fibroblast cell cycle1. Cancer Res. 9, 2109-2117.

Michieli, P., Chedid, M., Lin, D., Pierce, J.H., Mercer, W.E., and Givol, D. (1994). Induction of WAF1/CIP1 by a p53-independent pathway. Cancer Res. 13, 3391-3395.

Mizushima, N., and Komatsu, M. (2011). Autophagy: renovation of cells and tissues. Cell 4, 728-741.

Mizushima, N., and Komatsu, M. (2011). Autophagy: Renovation of Cells and Tissues. Cell 4, 728-741.

Mordes, D.A., and Cortez, D. (2008). Activation of ATR and related PIKKs. Cell. Cycle 18, 2809-2812.

Morgan, M.J., and Liu, Z.G. (2011). Crosstalk of reactive oxygen species and NF-kappaB signaling. Cell Res. 1, 103-115.

Morre, D.M., and Morre, D.J. (2006). Catechin-vanilloid synergies with potential clinical applications in cancer. Rejuvenation Res. 1, 45-55.

Morre, D.M., and Morre, D.J. (2006). Catechin-vanilloid synergies with potential clinical applications in cancer. Rejuvenation Res. 1, 45-55.

Na, H., and Surh, Y. (2008). Modulation of Nrf2-mediated antioxidant and detoxifying enzyme induction by the green tea polyphenol EGCG. Food and Chemical Toxicology 4, 1271-1278.

Nelson, W.G., and Kastan, M.B. (1994). DNA strand breaks: the DNA template alterations that trigger p53-dependent DNA damage response pathways. Mol. Cell. Biol. 3, 1815-1823.

Noonan, D.M., Benelli, R., and Albini, A. (2007). Angiogenesis and cancer prevention: a vision. Recent Results Cancer Res. 219-224.

Norman, J.P., Perry, S.W., Reynolds, H.M., Kiebala, M., De Mesy Bentley, K.L., Trejo, M., Volsky, D.J., Maggirwar, S.B., Dewhurst, S., Masliah, E., and Gelbard, H.A. (2008). HIV-1 Tat activates neuronal ryanodine receptors with rapid induction of the unfolded protein response and mitochondrial hyperpolarization. PLoS One 11, e3731.

Nurse, P., Masui, Y., and Hartwell, L. (1998). Understanding the cell cycle. Nat. Med. 10, 1103-1106.

O'Connor, P.M., Ferris, D.K., Hoffmann, I., Jackman, J., Draetta, G., and Kohn, K.W. (1994). Role of the cdc25C phosphatase in G2 arrest induced by nitrogen mustard. Proc. Natl. Acad. Sci. U. S. A. 20, 9480-9484.

Okuda, M., Li, K., Beard, M.R., Showalter, L.A., Scholle, F., Lemon, S.M., and Weinman, S.A. (2002). Mitochondrial injury, oxidative stress, and antioxidant gene expression are induced by hepatitis C virus core protein. Gastroenterology 2, 366-375.

Olsson, A., Manzl, C., Strasser, A., and Villunger, A. (2007). How important are post-translational modifications in p53 for selectivity in target-gene transcription and tumor suppression? Cell Death Differ. 9, 1561-1575.

O'Neill, E., and Kolch, W. (2004). Conferring specificity on the ubiquitous Raf/MEK signaling pathway. Br. J. Cancer 2, 283-288.

O'Reilly, M.A. (2005). Redox activation of p21Cip1/WAF1/Sdi1: a multifunctional regulator of cell survival and death. Antioxid. Redox Signal. 1-2, 108-118.

Ortega, S., Malumbres, M., and Barbacid, M. (2002). Cyclin D-dependent kinases, INK4 inhibitors and cancer. Biochimica et Biophysica Acta (BBA) - Reviews on Cancer 1, 73-87.

Ou, B., Hampsch-Woodill, M., and Prior, R.L. (2001). Development and validation of an improved oxygen radical absorbance capacity assay using fluorescein as the fluorescent probe. J. Agric. Food Chem. 10, 4619-4626.

Ouyang, G., Yao, L., Ruan, K., Song, G., Mao, Y., and Bao, S. (2009). Genistein induces G2/M cell cycle arrest and apoptosis of human ovarian cancer cells via activation of DNA damage checkpoint pathways. Cell Biol. Int. 12,1237-1244.

Ozes, O.N., Mayo, L.D., Gustin, J.A., Pfeffer, S.R., Pfeffer, L.M., and Donner, D.B. (1999). NF-kappaB activation by tumor necrosis factor requires the Akt serine-threonine kinase. Nature 6748, 82-85.

Pan, J.S., Hong, M.Z., and Ren, J.L. (2009). Reactive oxygen species: a double-edged sword in oncogenesis. World J. Gastroenterol. 14, 1702-1707.

Papp, L.V., Lu, J., Striebel, F., Kennedy, D., Holmgren, A., and Khanna, K.K. (2006). The redox state of SECIS binding protein 2 controls its localization and selenocysteine incorporation function. Mol. Cell. Biol. 13, 4895-4910.

Peng, C.Y., Graves, P.R., Thoma, R.S., Wu, Z., Shaw, A.S., and Piwnica-Worms, H. (1997). Mitotic and G2 checkpoint control: regulation of 14-3-3 protein binding by phosphorylation of Cdc25C on serine-216. Science 5331,1501-1505.

Peres A. (1978). Plantas útiles de Colombia 4 th ed. Litografía Arco. Bogotá. 4a Edición. 131, 752.

Peres V, Nagin T. (1997). Trioxygenated naturally occurring xanthones. Phytochemistry 44: 191 - 214.

Phong, M.S., Van Horn, R.D., Li, S., Tucker-Kellogg, G., Surana, U., and Ye, X.S. (2010). p38 mitogen-activated protein kinase promotes cell survival in response to DNA damage but is not required for the G(2) DNA damage checkpoint in human cancer cells. Mol. Cell. Biol. 15, 3816-3826.

Pierini, R., Kroon, P.A., Guyot, S., Ivory, K., Johnson, I.T., and Belshaw, N.J. (2008). Procyanidin effects on oesophageal adenocarcinoma cells strongly depend on flavan-3-ol degree of polymerization. Molecular Nutrition & Food Research 12, 1399-1407.

Pisoschi, A.M., and Pop, A. (2015). The role of antioxidants in the chemistry of oxidative stress: A review. Eur. J. Med. Chem. 55-74.

Prasad, S., Kaur, J., Roy, P., Kalra, N., and Shukla, Y. (2007). Theaflavins induce G2/M arrest by modulating expression of p21waf1/cip1, cdc25C and cyclin B in human prostate carcinoma PC-3 cells. Life Sci. 17–18, 1323-1331.

Puccini, J., Dorstyn, L., and Kumar, S. (2013). Caspase-2 as a tumor suppressor. Cell Death Differ. 9, 1133-1139.

Puissant, A., and Auberger, P. (2010). AMPK- and p62/SQSTM1-dependent autophagy mediate resveratrol-induced cell death in chronic myelogenous leukemia. Autophagy 5, 655-657.

Rahman, I., Kode, A., and Biswas, S.K. (2006). Assay for quantitative determination of glutathione and glutathione disulfide levels using enzymatic recycling method. Nat. Protoc. 6, 3159-3165.

Rajalingam, K., Schreck, R., Rapp, U.R., and Albert, Š. (2007). Ras oncogenes and their downstream targets. Biochimica et Biophysica Acta (BBA) - Molecular Cell Research 8, 1177-1195.

Raudsepp-Hearne, C., Aiello, A., Hussein, A.A., Heller, M.V., Johns, T., and Capson, T.L. (2015). Differential Sequestration of a Cytotoxic Vismione from the Host Plant Vismia baccifera by Periphoba arcaei and Pyrrhopyge thericles. J. Chem. Ecol. 9, 816-821.

Ray, P.D., Huang, B., and Tsuji, Y. (2012). Reactive oxygen species (ROS) homeostasis and redox regulation in cellular signaling. Cell. Signal. 5, 981-990.

Re, R., Pellegrini, N., Proteggente, A., Pannala, A., Yang, M., and Rice-Evans, C. (1999). Antioxidant activity applying an improved ABTS radical cation decolorization assay. Free Radical Biology and Medicine 9–10, 1231-1237.

Reimann, J.D., Gardner, B.E., Margottin-Goguet, F., and Jackson, P.K. (2001). Emi1 regulates the anaphase-promoting complex by a different mechanism than Mad2 proteins. Genes Dev. 24, 3278-3285.

Robinson, K.A., Stewart, C.A., Pye, Q.N., Nguyen, X., Kenney, L., Salzman, S., Floyd, R.A., and Hensley, K. (1999). Redox-sensitive protein phosphatase activity regulates the phosphorylation state of p38 protein kinase in primary astrocyte culture. J. Neurosci. Res. 6, 724-732.

Roos, G., and Messens, J. (2011). Protein sulfenic acid formation: From cellular damage to redox regulation. Free Radical Biology and Medicine 2, 314-326.

Ruiz, P.A., Braune, A., Holzlwimmer, G., Quintanilla-Fend, L., and Haller, D. (2007). Quercetin inhibits TNF-induced NF-kappaB transcription factor recruitment to proinflammatory gene promoters in murine intestinal epithelial cells. J. Nutr. 5, 1208-1215.

Rushworth, G.F., and Megson, I.L. (2014). Existing and potential therapeutic uses for N-acetylcysteine: The need for conversion to intracellular glutathione for antioxidant benefits. Pharmacol. Ther. 2, 150-159.

Ryves, W.J., and Harwood, A.J. (2003). The interaction of glycogen synthase kinase-3 (GSK-3) with the cell cycle. Prog. Cell Cycle Res. 489-495.

Salas F, Ciangherotti C, Salazar-Bookaman M, Rojas J, Morales A. (2007). Toxicidad aguda y actividad analgésica del extracto acuoso de hojas de Vismia baccifera L. var. dealbata (Guttiferae) en animales de experimentación.49: 5-9,

Sancar, A., Lindsey-Boltz, L.A., Unsal-Kacmaz, K., and Linn, S. (2004). Molecular mechanisms of mammalian DNA repair and the DNA damage checkpoints. Annu. Rev. Biochem. 39-85.

Sánchez, I., and Dynlacht, B.D. (2005). New insights into cyclins, CDKs, and cell cycle control. Semin. Cell Dev. Biol. 3, 311-321.

Santana-Santos, E., Gowdak, L.H., Gaiotto, F.A., Puig, L.B., Hajjar, L.A., Zeferino, S.P., Drager, L.F., Shimizu, M.H., Bortolotto, L.A., and De Lima, J.J. (2014). High dose of N-acetylcystein prevents acute kidney injury in chronic kidney disease patients undergoing myocardial revascularization. Ann. Thorac. Surg. 5, 1617-1623.

Santos, C.X., Tanaka, L.Y., Wosniak, J., and Laurindo, F.R. (2009). Mechanisms and implications of reactive oxygen species generation during the unfolded protein response: roles of endoplasmic reticulum oxidoreductases, mitochondrial electron transport, and NADPH oxidase. Antioxid. Redox Signal. 10, 2409-2427.

Sarbassov, D.D., Guertin, D.A., Ali, S.M., and Sabatini, D.M. (2005). Phosphorylation and regulation of Akt/PKB by the rictor-mTOR complex. Science 5712, 1098-1101.

Savic, V., Yin, B., Maas, N.L., Bredemeyer, A.L., Carpenter, A.C., Helmink, B.A., Yang-Iott, K.S., Sleckman, B.P., and Bassing, C.H. (2009). Formation of Dynamic γ-H2AX Domains along Broken DNA Strands Is Distinctly Regulated by ATM and MDC1 and Dependent upon H2AX Densities in Chromatin. Mol. Cell 3, 298-310.

Scherz-Shouval, R., Shvets, E., Fass, E., Shorer, H., Gil, L., and Elazar, Z. (2007). Reactive oxygen species are essential for autophagy and specifically regulate the activity of Atg4. EMBO J. 7, 1749-1760.

Sengupta, A., Molkentin, J.D., Paik, J.H., DePinho, R.A., and Yutzey, K.E. (2011). FoxO transcription factors promote cardiomyocyte survival upon induction of oxidative stress. J. Biol. Chem. 9, 7468-7478.

Shi, J., Liu, F., Zhang, W., Liu, X., Lin, B., and Tang, X. (2015). Epigallocatechin-3-gallate inhibits nicotine-induced migration and invasion by the suppression of angiogenesis and epithelial-mesenchymal transition in non-small cell lung cancer cells. Oncol. Rep. 6, 2972-2980.

Shields, J.M., Pruitt, K., McFall, A., Shaub, A., and Der, C.J. (2000). Understanding Ras: 'it ain't over 'til it's over'. Trends Cell Biol. 4, 147-154.

Shimamura, H., Terada, Y., Okado, T., Tanaka, H., Inoshita, S., and Sasaki, S. (2003). The PI3-kinase-Akt pathway promotes mesangial cell survival and inhibits apoptosis in vitro via NF-kappa B and Bad. J. Am. Soc. Nephrol. 6, 1427-1434.

Shiotani, B., and Zou, L. (2009). Single-Stranded DNA Orchestrates an ATM-to-ATR Switch at DNA Breaks. Mol. Cell 5, 547-558.

Sionov, R.V., and Haupt, Y. (1999). The cellular response to p53: the decision between life and death. Oncogene 45, 6145-6157.

Smith, J., Tho, L.M., Xu, N., and Gillespie, D.A. (2010). The ATM-Chk2 and ATR-Chk1 pathways in DNA damage signaling and cancer. Adv. Cancer Res. 73-112.

Smith, M.H., Ploegh, H.L., and Weissman, J.S. (2011). Road to ruin: targeting proteins for degradation in the endoplasmic reticulum. Science 6059, 1086-1090.

St Clair, D.K., Porntadavity, S., Xu, Y., and Kiningham, K. (2002). Transcription regulation of human manganese superoxide dismutase gene. Methods Enzymol. 306-312.

Stepanic, V., Gasparovic, A.C., Troselj, K.G., Amic, D., and Zarkovic, N. (2015). Selected attributes of polyphenols in targeting oxidative stress in cancer. Curr. Top. Med. Chem. 5, 496-509.

Stiff, T., Walker, S.A., Cerosaletti, K., Goodarzi, A.A., Petermann, E., Concannon, P., O'Driscoll, M., and Jeggo, P.A. (2006). ATR-dependent phosphorylation and activation of ATM in response to UV treatment or replication fork stalling. EMBO J. 24, 5775-5782.

Stoupi, S., Williamson, G., Viton, F., Barron, D., King, L.J., Brown, J.E., and Clifford, M.N. (2010). In vivo bioavailability, absorption, excretion, and pharmacokinetics of [14C]procyanidin B2 in male rats. Drug Metab. Dispos. 2,287-291.

Stucki, M., Clapperton, J.A., Mohammad, D., Yaffe, M.B., Smerdon, S.J., and Jackson, S.P. (2005). MDC1 Directly Binds Phosphorylated Histone H2AX to Regulate Cellular Responses to DNA Double-Strand Breaks. Cell 7,1213-1226.

Sur, S., and Agrawal, D.K. (2016). Phosphatases and kinases regulating CDC25 activity in the cell cycle: clinical implications of CDC25 overexpression and potential treatment strategies. Mol. Cell. Biochem. 1-2, 33-46.

Tabas, I., and Ron, D. (2011). Integrating the mechanisms of apoptosis induced by endoplasmic reticulum stress. Nat. Cell Biol. 3, 184-190.

Tang, D., Kang, R., Livesey, K.M., Cheh, C.W., Farkas, A., Loughran, P., Hoppe, G., Bianchi, M.E., Tracey, K.J., Zeh, H.J.,3rd, and Lotze, M.T. (2010). Endogenous HMGB1 regulates autophagy. J. Cell Biol. 5, 881-892.

Teske, B.F., Wek, S.A., Bunpo, P., Cundiff, J.K., McClintick, J.N., Anthony, T.G., and Wek, R.C. (2011). The eIF2 kinase PERK and the integrated stress response facilitate activation of ATF6 during endoplasmic reticulum stress. Mol. Biol. Cell 22, 4390-4405.

Thoppil, R.J., Bhatia, D., Barnes, K.F., Haznagy-Radnai, E., Hohmann, J., Darvesh, A.S., and Bishayee, A. (2012). Black currant anthocyanins abrogate oxidative stress through Nrf2-mediated antioxidant mechanisms in a rat model of hepatocellular carcinoma. Curr. Cancer. Drug Targets 9, 1244-1257.

Tian, H., Zhang, B., Di, J., Jiang, G., Chen, F., Li, H., Li, L., Pei, D., and Zheng, J. (2012). Keap1: One stone kills three birds Nrf2, IKKβ and Bcl-2/Bcl-xL. Cancer Lett. 1, 26-34.

Tobiume, K., Matsuzawa, A., Takahashi, T., Nishitoh, H., Morita, K., Takeda, K., Minowa, O., Miyazono, K., Noda, T., and Ichijo, H. (2001). ASK1 is required for sustained activations of JNK/p38 MAP kinases and apoptosis. EMBO Rep. 3, 222-228.

Tochhawng, L., Deng, S., Pervaiz, S., and Yap, C.T. (2013). Redox regulation of cancer cell migration and invasion. Mitochondrion 3, 246-253.

Toledo, F., and Wahl, G.M. (2006). Regulating the p53 pathway: in vitro hypotheses, in vivo veritas. Nat. Rev. Cancer. 12, 909-923.

Trujillo-C W, C.M. (2010). Plantas usadas por una comunidad indígena Coreguaje en la Amazonía colombiana. .

Tu, B.P., and Weissman, J.S. (2002). The FAD- and O(2)-dependent reaction cycle of Ero1-mediated oxidative protein folding in the endoplasmic reticulum. Mol. Cell 5, 983-994.

Upton, J.P., Wang, L., Han, D., Wang, E.S., Huskey, N.E., Lim, L., Truitt, M., McManus, M.T., Ruggero, D., Goga, A., Papa, F.R., and Oakes, S.A. (2012). IRE1alpha cleaves select microRNAs during ER stress to derepress translation of proapoptotic Caspase-2. Science 6108, 818-822.

Urano, F., Wang, X., Bertolotti, A., Zhang, Y., Chung, P., Harding, H.P., and Ron, D. (2000). Coupling of stress in the ER to activation of JNK protein kinases by transmembrane protein kinase IRE1. Science 5453, 664-666.

Utsunomiya, T., Chavali, S., Zhong, W., Forse, R. (2000). Effects of sesamin-supplemented dietary fat emulsions on the ex vivo production of lipopolysaccharide-induced prostanoids and tumor necrosis factor alpha in rats. .

Utsunomiya, T., Chavali, S.R., Zhong, W.W., and Forse, R.A. (2000). Effects of sesamin-supplemented dietary fat emulsions on the ex vivo production of lipopolysaccharide-induced prostanoids and tumor necrosis factor alpha in rats. Am. J. Clin. Nutr. 3, 804-808.

Vakifahmetoglu-Norberg, H., and Zhivotovsky, B. (2010). The unpredictable caspase-2: what can it do? Trends Cell Biol. 3, 150-159.

Valavanidis, A., Vlachogianni, T., and Fiotakis, C. (2009). 8-hydroxy-2' -deoxyguanosine (8-OHdG): A critical biomarker of oxidative stress and carcinogenesis. J. Environ. Sci. Health. C. Environ. Carcinog. Ecotoxicol. Rev. 2,120-139.

van der Vlies, D., Makkinje, M., Jansens, A., Braakman, I., Verkleij, A.J., Wirtz, K.W., and Post, J.A. (2003). Oxidation of ER resident proteins upon oxidative stress: effects of altering cellular redox/antioxidant status and implications for protein maturation. Antioxid. Redox Signal. 4, 381-387.

van Staveren, W.C., Solis, D.Y., Hebrant, A., Detours, V., Dumont, J.E., and Maenhaut, C. (2009). Human cancer cell lines: Experimental models for cancer cells in situ? For cancer stem cells? Biochim. Biophys. Acta 2, 92-103.

Vantaggiato, C., Formentini, I., Bondanza, A., Bonini, C., Naldini, L., and Brambilla, R. (2006). ERK1 and ERK2 mitogen-activated protein kinases affect Ras-dependent cell signaling differentially. J. Biol. 5, 14.

Vara, J.Á.F., Casado, E., de Castro, J., Cejas, P., Belda-Iniesta, C., and González-Barón, M. (2004). PI3K/Akt signaling pathway and cancer. Cancer Treat. Rev. 2, 193-204.

Vermeulen, K., Van Bockstaele, D.R., and Berneman, Z.N. (2003). The cell cycle: a review of regulation, deregulation and therapeutic targets in cancer. Cell Prolif. 3, 131-149.

Visner, G.A., Dougall, W.C., Wilson, J.M., Burr, I.A., and Nick, H.S. (1990). Regulation of manganese superoxide dismutase by lipopolysaccharide, interleukin-1, and tumor necrosis factor. Role in the acute inflammatory response. J. Biol. Chem. 5, 2856-2864.

Vizcaya M, Morales A, Rojas J, Nuñez R. (2012). Revisión bibliográfica sobre la composición química y actividades farmacológicas del género Vismia (Guttiferae).

Vurusaner, B., Poli, G., and Basaga, H. (2012). Tumor suppressor genes and ROS: complex networks of interactions. Free Radical Biology and Medicine 1, 7-18.

Wang, C., Huang, P., Liu, T., and Jan, T. (2009). Highly oligomeric procyanidins from areca nut induce lymphocyte apoptosis via the depletion of intracellular thiols. Toxicology in Vitro 7, 1234-1241.

Wang, K. (2015). Autophagy and apoptosis in liver injury. Cell. Cycle 11, 1631-1642.

Wang, W., Sun, Q., Wu, Z., Zhou, D., Wei, J., Xie, H., Zhou, L., and Zheng, S. (2013). Mitochondrial dysfunction-related genes in hepatocellular carcinoma. Front. Biosci. (Landmark Ed) 1141-1149.

Wang, X.W., Zhan, Q., Coursen, J.D., Khan, M.A., Kontny, H.U., Yu, L., Hollander, M.C., O'Connor, P.M., Fornace, A.J.,Jr, and Harris, C.C. (1999). GADD45 induction of a G2/M cell cycle checkpoint. Proc. Natl. Acad. Sci. U. S. A. 7, 3706-3711.

Wang, X.Z., Harding, H.P., Zhang, Y., Jolicoeur, E.M., Kuroda, M., and Ron, D. (1998). Cloning of mammalian Ire1 reveals diversity in the ER stress responses. EMBO J. 19, 5708-5717.

Ward, I.M., and Chen, J. (2001). Histone H2AX is phosphorylated in an ATR-dependent manner in response to replicational stress. J. Biol. Chem. 51, 47759-47762.

Wei, M.C., Zong, W.X., Cheng, E.H., Lindsten, T., Panoutsakopoulou, V., Ross, A.J., Roth, K.A., MacGregor, G.R., Thompson, C.B., and Korsmeyer, S.J. (2001). Proapoptotic BAX and BAK: a requisite gateway to mitochondrial dysfunction and death. Science 5517, 727-730.

Welihinda, A.A., and Kaufman, R.J. (1996). The unfolded protein response pathway in Saccharomyces cerevisiae. Oligomerization and trans-phosphorylation of Ire1p (Ern1p) are required for kinase activation. J. Biol. Chem.30, 18181-18187.

Wintola, O.A., and Afolayan, A.J. (2011). Phytochemical constituents and antioxidant activities of the whole leaf extract of Aloe ferox Mill. Pharmacogn Mag. 28, 325-333.

Wong, C.H., Iskandar, K.B., Yadav, S.K., Hirpara, J.L., Loh, T., and Pervaiz, S. (2010). Simultaneous induction of non-canonical autophagy and apoptosis in cancer cells by ROS-dependent ERK and JNK activation. PLoS One 4,e9996.

Woodgett, J.R. (2005). Recent advances in the protein kinase B signaling pathway. Curr. Opin. Cell Biol. 2, 150-157.

Wu, G., Fang, Y.Z., Yang, S., Lupton, J.R., and Turner, N.D. (2004). Glutathione metabolism and its implications for health. J. Nutr. 3, 489-492.

Wu, W.S., Wu, J.R., and Hu, C.T. (2008). Signal cross talks for sustained MAPK activation and cell migration: the potential role of reactive oxygen species. Cancer Metastasis Rev. 2, 303-314.

Ximenes, V.F., Kanegae, M.P., Rissato, S.R., and Galhiane, M.S. (2007). The oxidation of apocynin catalyzed by myeloperoxidase: proposal for NADPH oxidase inhibition. Arch. Biochem. Biophys. 2, 134-141.

Yacoub, D., Theoret, J.F., Villeneuve, L., Abou-Saleh, H., Mourad, W., Allen, B.G., and Merhi, Y. (2006). Essential role of protein kinase C delta in platelet signaling, alpha IIb beta 3 activation, and thromboxane A2 release. J. Biol. Chem. 40, 30024-30035.

Ye, J., Rawson, R.B., Komuro, R., Chen, X., Dave, U.P., Prywes, R., Brown, M.S., and Goldstein, J.L. (2000). ER stress induces cleavage of membrane-bound ATF6 by the same proteases that process SREBPs. Mol. Cell 6,1355-1364.

Yedjou, C.G., Tchounwou, C.K., Haile, S., Edwards, F., and Tchounwou, P.B. (2010). N-acetyl-cysteine protects against DNA damage associated with lead toxicity in HepG2 cells. Ethn. Dis. 1 Suppl 1, S1-101-3.

Yoon, S., and Seger, R. (2006). The extracellular signal-regulated kinase: multiple substrates regulate diverse cellular functions. Growth Factors 1, 21-44.

Yoshida, H. (2007). ER stress and diseases. FEBS J. 3, 630-658.

Yoshida, H., Matsui, T., Hosokawa, N., Kaufman, R.J., Nagata, K., and Mori, K. (2003). A time-dependent phase shift in the mammalian unfolded protein response. Dev. Cell. 2, 265-271.

Yoshida, H., Matsui, T., Yamamoto, A., Okada, T., and Mori, K. (2001). XBP1 mRNA is induced by ATF6 and spliced by IRE1 in response to ER stress to produce a highly active transcription factor. Cell 7, 881-891.

Yoshida, H., Okada, T., Haze, K., Yanagi, H., Yura, T., Negishi, M., and Mori, K. (2001). Endoplasmic reticulum stress-induced formation of transcription factor complex ERSF including NF-Y (CBF) and activating transcription factors 6alpha and 6beta that activates the mammalian unfolded protein response. Mol. Cell. Biol. 4, 1239-1248.

Zeng, Y., and Piwnica-Worms, H. (1999). DNA damage and replication checkpoints in fission yeast require nuclear exclusion of the Cdc25 phosphatase via 14-3-3 binding. Mol. Cell. Biol. 11, 7410-7419.

Zhang, Z., Wang, C.Z., Du, G.J., Qi, L.W., Calway, T., He, T.C., Du, W., and Yuan, C.S. (2013). Genistein induces G2/M cell cycle arrest and apoptosis via ATM/p53-dependent pathway in human colon cancer cells. Int. J. Oncol. 1, 289-296.

Zhou, B.P., Liao, Y., Xia, W., Spohn, B., Lee, M.H., and Hung, M.C. (2001). Cytoplasmic localization of p21Cip1/WAF1 by Akt-induced phosphorylation in HER-2/neu-overexpressing cells. Nat. Cell Biol. 3, 245-252.

Zhou, H., Zhang, Y., Fu, Y., Chan, L., and Lee, A.S. (2011). Novel mechanism of anti-apoptotic function of 78-kDa glucose-regulated protein (GRP78): endocrine resistance factor in breast cancer, through release of B-cell lymphoma 2 (BCL-2) from BCL-2-interacting killer (BIK). J. Biol. Chem. 29, 25687-25696.

Zhou, J.Y., and Prognon, P. (2006). Raw material enzymatic activity determination: a specific case for validation and comparison of analytical methods--the example of superoxide dismutase (SOD). J. Pharm. Biomed. Anal. 5,1143-1148.

Zou, L., and Elledge, S.J. (2003). Sensing DNA damage through ATRIP recognition of RPA-ssDNA complexes. Science 5625, 1542-1548.

Zumdick, S., Deters, A., and Hensel, A. (2012). In vitro intestinal transport of oligomeric procyanidins (DP 2 to 4) across monolayers of Caco-2 cells. Fitoterapia 7, 1210-1217.

8. ANNEX

Nutrients **2015**, *7*, 179-195; doi:10.3390/nu7010179

OPEN ACCESS

nutrients

ISSN 2072-6643

www.mdpi.com/journal/nutrients

Article

Piper and *Vismia* Species from Colombian Amazonia Differentially Affect Cell Proliferation of Hepatocarcinoma Cells

Leandro J. Lizcano, Maite Siles, Jenifer Trepiana, M. Luisa Hernández, Rosaura Navarro, M. Begoña Ruiz-Larrea * and José Ignacio Ruiz-Sanz

Department of Physiology, Medicine and Dentistry School, University of the Basque Country UPV/EHU, Leioa 48940, Spain; E-Mails: lizcanomvz@gmail.com (L.J.L.); msg_@hotmail.com (M.S.); jtrepiana001@ikasle.ehu.es (J.T.); luisa.hernandez@ehu.es (M.L.H.); rosaura.navarro@ehu.es (R.N.); joseignacio.ruizs@ehu.es (J.I.R.S.)

* Author to whom correspondence should be addressed; E-Mail: mbego.ruizlarrea@ehu.es; Tel.: +34-946012829; Fax: +34-946015662.

Received: 10 November 2014 / Accepted: 18 December 2014 / Published: 30 December 2014

Abstract: There is an increasing interest to identify plant-derived natural products with antitumor activities. In this work, we have studied the effects of aqueous leaf extracts from Amazonian *Vismia* and *Piper* species on human hepatocarcinoma cell toxicity. Results showed that, depending on the cell type, the plants displayed differential effects; thus, *Vismia baccifera* induced the selective killing of HepG2, while increasing cell growth of PLC-PRF and SK-HEP-1. In contrast, these two last cell lines were sensitive to the toxicity by *Piper krukoffii* and *Piper putumayoense*, while the *Piperaceae* did not affect HepG2 growth. All the extracts induced cytotoxicity to rat hepatoma McA-RH7777, but were innocuous (*V. baccifera* at concentrations < 75 μg/mL) or even protected cells from basal death (*P. putumayoense*) in primary cultures of rat hepatocytes. In every case, cytotoxicity was accompanied by an intracellular accumulation of reactive oxygen species (ROS). These results provide evidence for the anticancer activities of the studied plants on specific cell lines and suggest that cell killing could be mediated by ROS, thus involving mechanisms independent of the plants free radical scavenging activities. Results also support the use of these extracts of the *Vismia* and *Piper* genera with opposite effects as a model system to study the mechanisms of the antitumoral activity against different types of hepatocarcinoma.

Keywords: antioxidant activity; free radical; polyphenol; hepatoma cell line; cell cycle arrest; flow cytometry; superoxide dismutase; catalase

1. Introduction

Cancer is a major cause of death worldwide and the liver cancer the third most common cause of cancer death [1]. Among the different tumors the incidence of primary liver malignancy has increased dramatically over the past 20 years, with hepatocellular carcinoma being the most common primary liver tumor [2]. Therefore, the development of chemotherapeutic agents is important to reduce the incidence of mortality, and thus requiring better knowledge of the biology of cancer cells, *i.e.*, their differential signaling systems, protein expression, and specific metabolism. Cancer cells have a different genotype and phenotype from noncancerous cells. Thus, they show a high glycolysis rate, this pathway supporting the increase in energy demand to allow cellular function, proliferation, and tumor growth [3–7].

There are also differences in the activity of drug metabolizing enzymes; hepatoma cells have negligible levels on various P450 cytochromes [8,9]. This lack of phase I enzymes makes tumor cells more tolerant to certain concentrations of drugs that generate toxicity in normal hepatocytes after they have been metabolized. These differential characteristics between cancer and normal cells could have clinical applications.

There is an increasing interest in identifying chemotherapeutic agents that can prevent tumor initiation, delay or stop tumor growth and metastasis or reduce mortality. Natural products derived from plants have recently received considerable attention because of their properties, including antioxidant, anti-inflammatory and antitumor activities. Plants play a key role as sources of effective anticancer agents. It is significant that about 60% of the anticancer drugs currently used are derived from natural sources, including plants, marine organisms and microorganisms. Medicine based on plants and their active components has found a role in cancer treatment. Phenolic compounds extracted from medicinal herbs have shown interesting biochemical properties and pharmacological activities, mainly due to their antioxidant potential and the inhibition exerted on key enzymes in the inflammatory response, such as cyclooxygenase [10,11].

Colombia has a great diversity of plant species that are a source of natural products that can be used in treating diseases. Many of these species are used in folk medicine, and have been found to exert antimicrobial [12], antiplasmodial [13], antiprotozoal, anti-inflammatory [14], anti-HIV [15], and anticancer [16] activities. In previous reports we described the content of total phenols and flavonoids, and the *in vitro* antioxidant activities of aqueous extracts from Colombian Amazonian plants prepared as infusions as are commonly used in traditional medicine [17,18]. From the analyzed extracts we have selected, due to their high antioxidant potential, *Vismia baccifera*, *Piper krukoffii* and *Piper putumayoense* species. Aqueous extracts from leaves of these plants from *Hypericaceae* and *Piperaceae* families were tested for their effect on toxicity of hepatocarcinoma cells. An initial approach to the possible mechanism of action involved was also studied.

2. Experimental Section

2.1. Materials

The human hepatoma cell lines HepG2, PLC/PRF/5 and SK-HEP-1 and the rat hepatoma cell line McA-RH7777 were purchased from American Type Culture Collection (ATCC) (Manassas, VA, USA). Eagle's Minimum Essential Medium (EMEM), fetal bovine serum (FBS) and horse serum were obtained also from ATCC. L-glutamine, streptomycin-penicillin solution, propidium iodide, Tween-20, glutahione reductase (GR) (EC 1.6.4.2), NaN_3, trypsin, EDTA-Na_2, 30% H_2O_2 solution, and 3-(4,5-dimethylthiazo-2-yl)-2,5-diphenyl-tetrazolium bromide (MTT) were all obtained from Sigma-Aldrich (St Louis, MO, USA). 2′,7′-dichlorodihydrofluorescein diacetate (H_2DCF-DA) was obtained from Molecular Probes (Eugene, OR, USA). NADPH was purchased from Calbiochem (Darmstadt, Germany). GSH was from Boehringer Mannheim GmbH (Ingelheim am Rheim, Germany). RNase A was obtained from Roche Biochemicals (Indianapolis, IN, USA). Superoxide dismutase determination kit was purchased from Fluka (Basel, Switzerland).

2.2. Preparation and Characterization of the Plant Extracts

The plants were collected from the Macagual Research Centre forest in Florencia, Caquetá (Colombia), and taxonomically identified by botanical experts and deposited at the Herbarium of the Botanical Garden of Amazonia University—HUAZ (Florencia, Colombia). The samples were processed in the laboratory within a maximum of 24 h after harvesting. Otherwise, the material was stored under refrigeration at 4 °C. The plant extracts were prepared as aqueous infusions, as generally used in folk medicine. For this purpose, the leaves of the fresh plants were rinsed in water, cut into tiny pieces and boiled in 500 mL of water with constant shaking for 15 min. The mixture was allowed to settle for 10 min and stored at −20 °C. The samples were carried to the Department of Physiology of the University of the Basque Country (Spain). Once defrosted, samples were centrifuged at 1200 g for 5 min at 4 °C, and the supernatant was sterilized by filtration (0.22 μm pore size). Aliquots were stored at −80 °C until use. Several aliquots of the extracts were dried in a Savant SpeedVac concentrator (Thermo Fisher Scientific, Waltham, MA, USA) to estimate the dry weight. The extracts were characterized in terms of the content of total phenols and flavonoids (by colorimetric assays), and the total antioxidant activity, measured as the Trolox equivalent antioxidant capacity (TEAC) and the oxygen radical absorbance capacity (ORAC), as is described in [17].

The leaf extracts that we have used in this work contained per gram of dry weight: a) 43.2 ± 0.3 mg gallic acid (total phenols) and 23.4 ± 0.2 mg catechin (total flavonoids) for *V. baccifera*; b) 16.8 ± 0.1 mg gallic acid (total phenols) and 8.7 ± 0.1 mg catechin (total flavonoids) in the case of *Piper krukoffii* [17]; and c) 22.2 ± 0.1 mg gallic acid (total phenols), and 10.2 ± 0.1 mg catechin (total flavonoids) for *Piper putumayoense* [17]. The total antioxidant activity of the extracts were: a) 355.3 ± 5.2 μmol Trolox/g (TEAC) and 922.3 ± 19.5 μmol Trolox/g (ORAC) for *V. baccifera*; b) 92.0 ± 3.8 μmol Trolox/g (TEAC) and 247.1 ± 18.5 μmol Trolox/g (ORAC) in the case of *Piper krukoffii* [17]; and c) 91.0 ± 12.3 μmol Trolox/g (TEAC) and 359.1 ± 44.4 μmol Trolox/g (ORAC) for *Piper putumayoense* [17].

2.3. Rat Liver Hepatocyte Isolation and Maintenance in Primary Cultures

Hepatocytes were isolated from male Sprague-Dawley rats (180–200 g) by collagenase perfusion, as previously described [19]. The cellular suspension obtained was filtered through a nylon mesh and incubated for 3 min in a syliconized Erlenmeyer for 3 min at 37 °C under a 95% O_2/5% CO_2 atmosphere and constant shaking. Cells were centrifuged at 50× *g* for 3 min at room temperature to remove death cells and cellular debris. The hepatocyte viability, determined by the trypan blue exclusion test, was typically greater than 90%. Hepatocyte primary cultures were prepared as previously reported [20].

The experimental use of animals followed the European Directives and Recommendation (2003/65/CE and 2007/526/CE) regarding the welfare of animals used in scientific procedures and the protocol was approved by the Ethical Committee of Animal Welfare of the University of the Basque Country UPV/EHU (ref. CEBA/24-P02/2009).

2.4. Culture and Maintenance of Hepatocarcinoma Cell Lines

Human liver cancer HepG2, PLC/PRF/5 and SK-HEP-1 cell lines were maintained in EMEM supplemented with 10% heat inactivated FBS, 2 mM L-glutamine, 0.1 mg/mL streptomycin and 100 U/mL penicillin. The rat hepatoma McA-RH7777 cell line was maintained in EMEM supplemented with 20% heat inactivated horse serum, 5% heat inactivated FBS, 2 mM L-glutamine, 0.1 mg/mL streptomycin and 100 U/mL penicillin. Cells were grown in 75 cm^2 flasks at 37 °C in humidified atmosphere with 5% CO_2. Medium was replaced every 2 to 3 days. When the cell monolayer reached 70% of confluence, cells were detached with a solution of 0.1% trypsin-0.04% EDTA and then harvested to perform subsequent experiments.

The cell line culture procedures used in this work were approved by the Ethical Committee of Research involving Biological Agents and Genetically Modified Organisms (CEIAB/ABIEB) of the University of the Basque Country UPV/EHU (refs. CEIAB/121/2012 and CEIAB/122/2012).

2.5. Cellular Toxicity

Cell toxicity was assessed by MTT assay based on the enzymatic reduction of the yellow tetrazolium salt into purple formazan by metabolically active cells [21]. Briefly, liver cell lines and primary rat hepatocytes were seeded onto Petri dishes and treated without (control) or with the aqueous plant extracts at different concentrations for 24 and 48 h. After treatments cells were washed and incubated with MTT for 3 h, and the resultant formazan crystals were solubilized with a dimethyl sulfoxide (DMSO):NaOH 10 N solution for 30 min in the dark. Aliquots were taken up and moved into 96-well plates and the absorbance registered at 550 nm in a microplate reader.

The toxic effectiveness of the extracts was measured in terms of LC50, the extract concentration leading to 50% reduction of the formazan absorbance. It was calculated by non-linear regression analysis, fitting the data to polynomial equations, using GraphPad Prism version 4.01 (GraphPad, San Diego, CA, USA).

2.6. Cell Cycle Analysis

Cells were seeded at a density of 300,000 cells onto Petri dishes and incubated for 24 h without (control) or with the plant leaf extracts. After treatments, cells were washed with phosphate buffered saline (PBS), trypsinized, harvested and fixed in 70% ice-cold ethanol overnight at 4 °C. The following day, the cells were washed with ice-cold PBS after discarding the ethanol and stained with 25 μg/mL propidium iodide in the presence of 200 μg/mL RNase A for 45 min at 37 °C in the dark. The cell cycle distribution of cells was determined by flow cytometry (Beckman Coulter Gallios) in the General Research Services SGIker of the UPV/EHU (http://www.ikerkuntza.ehu.es/p273-sgikerhm/en/) with a total acquisition of 10,000 events. The percentage of cells in different phases of the cell cycle was analyzed by Summit 4.3 software (Dako, Glostrup, Hovedstaden, Denmark).

2.7. Intracellular ROS Detection

Intracellular ROS generation was estimated by using the cell-permeant reagent 2′,7′-dichlorodihydrofluorescein diacetate (H_2DCF-DA), which is deacetylated and oxidized inside the cell forming the fluorescent compound, 2′,7′-dichlorofluorescein (DCF). Primary rat hepatocytes were seeded at a density of 10,000 cells per well onto 96-well plates 24 h prior the addition of treatments. HepG2, SK-HEP-1 and McA-RH7777 were seeded at a density of 2000 cells per well 48 h before starting the corresponding treatments. The media were renewed and cells were incubated for 24 h in their corresponding medium without (control) and with the plant leaf extracts. The cells were washed and incubated with 10 μM H_2DCF-DA for 30 min at 37 °C in the dark. Then the probe solution was removed and, after washing twice with PBS, the cells were lysed by the addition of 200 μL of 1% Tween-20 solution. The DCF fluorescence was measured using a 96-well plate reader at an excitation wavelenght of 485 nm and an emission wavelength of 528 nm. Cell fluorescence without the addition of H_2DCF-DA was used to correct for autofluorescence. Results were expressed as the percentage fluorescence in control cells.

2.8. Cell Protein Assay

Cells were harvested and lysed in PBS by two freeze-thaw cycles in liquid nitrogen. Protein was quantified spectrophotometrically at 595 nm by Coomassie Blue dying [22], using bovine serum albumin as standard.

2.9. Enzymatic Assays

Superoxide dismutase (SOD), catalase and glutathione peroxidase activities were measured in HepG2, SK-HEP-1 and McA-RH7777 cell lines. Glutathione peroxidase and catalase specific activities were derived from regression lines obtained by plotting the rate of absorbance change *versus* assayed protein amounts. At least four different protein amounts were assayed for each independent experiment.

2.9.1. Superoxide Dismutase

SOD activity was measured using a SOD assay kit, according to manufacturer's instructions. The assay is based on inhibition of WST-1 (a water soluble tetrazolium salt) reduction with xanthine-xanthine oxidase system used as a superoxide generator. The reaction took place in a final volume of 275 µL and started with the addition of WST-1, which is transformed to chromogenic WST-1 formazan. The increase in absorbance was monitored at 450 nm every 60 s for 15 min in a 96-well plate reader at 37 °C. A calibration curve was obtained assaying known quantities of a SOD commercial source (Sigma-Aldrich, St Louis, MO, USA). The results were expressed as SOD units/mg of protein.

2.9.2. Glutathione Peroxidase

Glutathione peroxidase activity was assayed by the indirect method of Flohé and Güntzler [23], based on a coupled enzyme system where NADPH is consumed by glutahione reductase to convert the generated glutathione disulfide (GSSG) to its reduced form. The reaction mixture contained 50 mM potassium phosphate buffer (pH 7.0), 1 mM EDTA-Na_2, 0.5 mM NaN_3, 0.45 mM GSH, 0.2 mM NADPH and 0.45 U of glutahione reductase in a total volume of 225 µL. The reaction started by the addition of cumene hydroperoxide (0.72 mM final concentration). The decrease in absorbance was monitored at 340 nm every 60 s for 15 min in a 96-well plate reader at 30 °C. The results were expressed as nmol/min/mg protein using the experimental extinction coefficient of 3.065 mM^{-1}.

2.9.3. Catalase

Catalase activity was measured according to Aebi [24] by spectrophotometric detection of the H_2O_2 disappearance at 240 nm. The reaction took place at 25 °C in a final volume of 1 mL containing 90 mM potassium phosphate buffer (pH 6.8) and started with the addition of H_2O_2 (30 mM final concentration). Decrease in absorbance was continuously measured every 2 s over 1 min. Catalase activity was expressed as µmol/min/mg of protein using the extinction coefficient at 240 nm $\varepsilon = 0.04$ mM/cm.

2.10. Statistical Analysis

Data were expressed as mean ± standard error (SE) from at least three independent experiments. Means of related groups were compared by Paired-Samples Student's *t*-test using SPSS 17.0 statistical package (SPSS Inc., Chicago, IL, USA). Statistical significance was assumed at $p < 0.05$.

3. Results

3.1. Cell Toxicity

The effects of different concentrations of the extracts on MTT in the human hepatoma cell lines HepG2, PLC-PRF, and SK-HEP-1, the rat hepatoma McA-RH7777 cell line and rat hepatocytes are depicted in Figure 1. The *V. baccifera* extract markedly decreased the MTT formazan absorbance in human HepG2 cells in a dose- and time-dependent manner (significant effects were observed at 19 µg/mL, and up to a 95% loss of viability was noted with 150 µg/mL). In the rat hepatoma McA-RH7777 cell line only the highest concentrations produced a significant toxicity (higher than 80%) (Figure 1a).

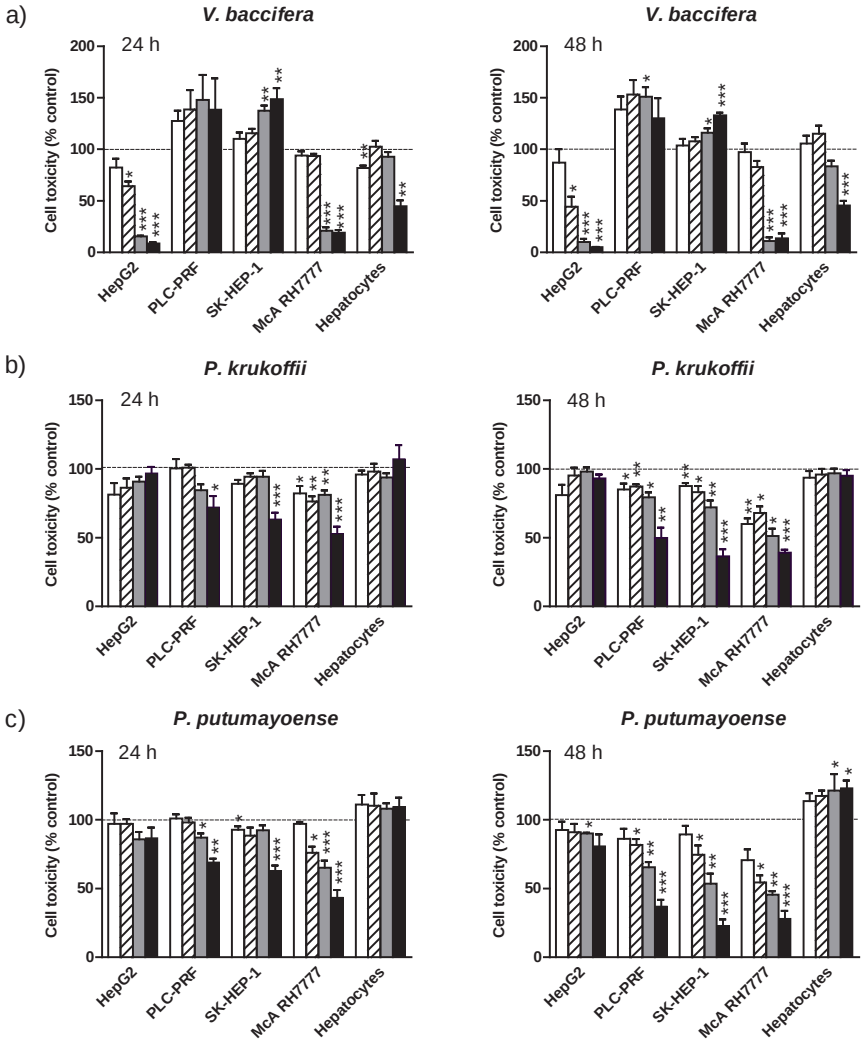

Figure 1. Effects of (**a**) *V. baccifera*; (**b**) *P. krukoffii*; and (**c**) *P. putumayoense* leaf extracts on the cytotoxicity to tumor cell lines and primary hepatocyte cultures. The extracts were assayed at the concentrations: ☐ 19 µg/mL; ▨ 38 µg/mL; ▭ 75 µg/mL; ■ 150 µg/mL for 24 h and 48 h. Cell toxicity was determined by the MTT cholorimetric assay, as described in Mat and Met. Results are the means + standard error (SE) of the mean of $n = 3–6$ experiments. * $p < 0.05$; ** $p < 0.01$; *** $p < 0.005$.

At 150 µg/mL, the extract strongly decreased cell viability in non-malignant rat hepatocytes (55% reduction at 24 h and 48 h). SK-HEP-1 and PLC-PRF tumor cell lines behaved differently. Thus, the extract increased cellular proliferation, the differences being statistically significant in SK-HEP-1 with the highest doses (up to 37% increase was observed with 75 µg/mL and up to 49% increase with 150 µg/mL by 24 h) and in PLC-PRF with intermediate concentrations (50% increase at 38 µg/mL by 48 h).

P. krukoffii displayed cytotoxic activities in PLC-PRF and SK-HEP-1 human cell lines, and the rat hepatoma McA-RH7777 (Figure 1b). The toxicity was dose- and time-dependent. The extract did not modify cell growth of HepG2 or the viability of non-transformed hepatocytes.

The *P. putumayoense* leaf (19 μg/mL–150 μg/mL) was clearly cytotoxic to McA-RH7777, SK-HEP-1, and PLC-PRF hepatoma cell lines, HepG2 being less susceptible to the extract toxicity (Figure 1c). By contrast, the aqueous extract increased the viability of non-transformed rat liver cells by at least 10%.

The LC50 value (concentration that is toxic to 50% of the cells) at 48 h was used as a parameter for cytotoxicity. From the experiments it can be summarized that the rat hepatoma McA-RH7777 cell line is the most susceptible to toxicity, since the two-day exposure to any of the aqueous extracts (at concentrations lower than 80 μg/mL) resulted in cell toxicity by 50% (Table 1). Also, *V. baccifera*, depending on the cell type, displayed differential effects; so, it was highly cytotoxic to human tumor HepG2 (LC50 lower than 40 μg/mL), while increasing human malignant liver PLC-PRF and SK-HEP-1 cell growth. *P. krukoffii* induced toxicity to human PLC-PRF and SK-HEP-1 hepatic cancer cells, but at the highest concentration used it did not affect the viability of HepG2 or nontumoral hepatocytes. Finally, *P. putumayoense* was cytotoxic to human PLC-PRF and SK-HEP-1 hepatoma cells, did not affect HepG2 growth, and even protected non-transformed hepatocytes from basal death.

Table 1. Concentration (μg/mL) that causes 50% of cell toxicity (LC50) at 48 h.

Cell type	LC50 (μg/mL)		
	V. baccifera	***P. krukoffii***	***P. putumayoense***
HepG2	35	n.d.	n.d.
PLC-PRF	Proliferative	149	106
SK-HEP-1	Proliferative	126	83
McA RH7777	57	76	47
Primary cultured hepatocytes	100	n.d.	Protective against basal cell death

n.d., not detected (assayed at the maximal concentration of 150 μg/mL). Results are the means of $n = 4$. LC50 values were derived by non-linear regression analysis, fitting the data to polynomial equations.

3.2. Mechanism of Toxicity

As indicated above, *P. krukoffii* and *P. putumayoense* extracts were particularly interesting, since they induced selective killing in human (*i.e.*, SK-HEP-1) and rat (McA-RH7777) tumor cells, but were innocuous (*P. krukoffii*) or even increased cell viability (*P. putumayoense*) in normal rat hepatocytes. *V. baccifera* leaf in a concentration lower than 100 μg/mL behaved similarly, as it was cytotoxic in human (HepG2) and rat (McA-RH7777) hepatoma cells, but did not affect nontransformed hepatocyte viability. Deregulation of cell cycle progression, an excessive production of ROS or a reduced protective defense in cancer cells are processes often involved in cell death. We then assessed specific parameters that could provide some information on the mechanism involved in cytotoxicity. Thus, we analyzed cell cycle arrest by flow cytometry and ROS generation by the 2′,7′-dichlorofluorescein fluorescent probe. For comparative purposes, ROS generation was also determined in normal rat hepatocytes exposed to the extracts.

3.2.1. Cell Cycle Arrest

Cell cycle was studied in McA-RH7777 cells, which were sensitive to all the extracts. As can be seen in Table 2, *V. baccifera* assayed at the concentration inducing cytotoxicity increased significantly the number of cells in subG0 phase, blocking cell cycle at G2/M. The population of cells in G2/M increased by 55% ($p < 0.05$); this increase in the number of cells in G2/M was accompanied by a 10% reduction in the *S*-phase.

P. krukoffii did not alter cell cycle in the rat hepatoma McA-RH7777 cell line. By contrast, *P. putumayoense* dramatically increased the number of cells in subG0 ($p < 0.005$) and induced cell cycle arrest at the G2/M phase.

Table 2. Flow cytometry analysis of the effects of plant leaf extracts on rat hepatoma McA-RH7777 cells. Cells in subG$_0$ were expressed as the percentage of the total cells (SubG0 + G0/G1 + S + G2/M).

Treatment	SubG0 (%)	Cell cycle		
		G0/G1(%)	S (%)	G2/M (%)
No additions	8.9 ± 3.1	59.8 ± 1.0	27.8 ± 1.9	12.8 ± 1.3
V. baccifera (75 µg/mL)	66.1 ± 14.5 *	39.6 ± 7.5 *	27.1 ± 2.0 *	33.3 ± 4.9 *
P. krukoffii (150 µg/mL)	9.5 ± 2.3	57.2 ± 2.2	29.0 ± 0.4	13.8 ± 0.7
P. putumayoense (150 µg/mL)	16.3 ± 1.4 ***	45.9 ± 1.4 ***	36.2 ± 1.5 *	17.9 ± 1.8 *

Results are the mean ± standard error of the mean of $n = 3$–6 experiments. * $p < 0.05$; ** $p < 0.01$; *** $p < 0.005$, significantly different from control (no additions).

3.2.2. ROS Production

Next, we examined the effects of the plant extracts on the intracellular ROS production. SK-HEP-1 was chosen as the representative cell line of those sensitive to the *Piperaceae* toxicity. Figure 2 shows ROS levels in hepatoma cell lines and normal hepatocytes exposed to the extracts. *V. baccifera* increased ROS formation in the *Hypericaceae*-sensitive cell line HepG2. In McA-RH7777, *V. baccifera* dose-dependently induced the generation of ROS at 1 h and to a lesser extent at 3 h. Similarly to *Vismia*, both *Piperaceae* induced the formation of ROS in McA-RH7777 in a dose- and time-dependent manner. In SK-HEP-1 the *Piper* extracts increased ROS levels. In contrast to tumor cell lines, *Vismia* and *Piper* extracts either maintained constant the basal levels of ROS or even reduced them in normal rat hepatocytes (Figure 2).

3.3. Antioxidant Activities

Table 3 shows the antioxidant activities detected in the cell lines after 24 h and 48 h of exposure with the extracts. Under control conditions (no additions) the activity of catalase in HepG2 was about 8-fold higher than in SK-HEP-1, while basal SOD and glutathione peroxidase activities were similar in both human cell lines. The rat hepatoma cell line exhibited higher glutathione peroxidase and catalase basal activities than in the human cell lines.

The *V. baccifera* leaf extract significantly reduced catalase activity in McA-RH7777 cells (19% decrease at 24 h, $p < 0.05$; 33% decrease at 48 h, $p < 0.01$). SOD activity was also decreased at 48 h. The *P. krukoffii* and *P. putumayoense* extracts markedly reduced catalase activity in this rat hepatoma cell line (40% and 23% reduction at 24 h, respectively; 45% reduction at 48 h by both *Piper* species). The *Piper* extracts increased glutathione peroxidase activity by 25% at 24 h. Hydrogen peroxide can be neutralized by the enzymatic scavengers, catalase and glutahione peroxidase. Although both enzymes play similar roles in transforming hydrogen peroxide into water, glutathione peroxidase *per se* is not an efficient decomposer, and high levels of hydrogen peroxide have been detected in glutahtione peroxidase-sufficient but catalase-depleted cells [25]. Catalase exhibits one of the highest turnover rates among all known biological enzymes, and in the studied cells it showed an activity against hydrogen peroxide decomposition three orders of magnitude higher than glutathione peroxidase (Table 3).

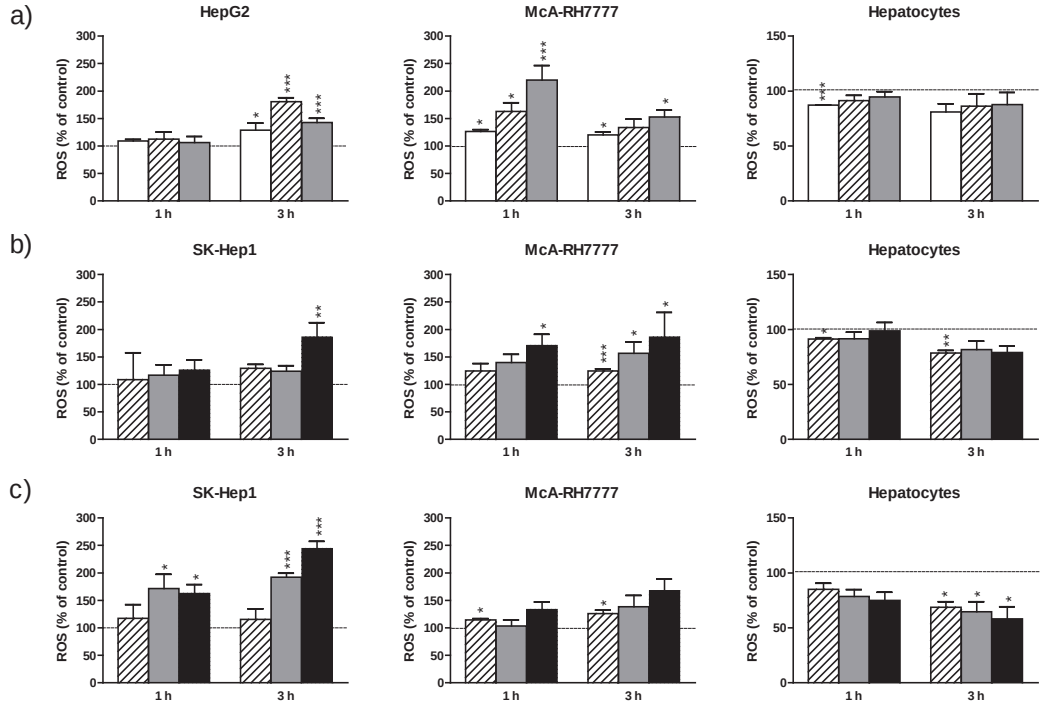

Figure 2. Effects of (**a**) *Vismia*; (**b**) *P. krukoffii*; and (**c**) *P. putumayoense* leaf extracts on ROS formation in hepatoma lines, and primary cultures of rat hepatocytes. The cells were incubated without (control) or with the plant extracts at the concentrations: ☐ 19 µg/mL; ▨ 38 µg/mL; ▭ 75 µg/mL; ■ 150 µg/mL for 1 and 3 h. After incubation, cells were loaded with the fluorescent probe as described in Mat. and Meth. Results are expressed as the percentage of the control values and are the mean + standard error (SE) of the mean of $n = 3$ experiments. * $p < 0.05$; ** $p < 0.01$; *** $p < 0.005$.

Table 3. Antioxidant enzyme activities in hepatoma cell lines exposed to *V. baccifera* (75 µg/mL), *P. krukoffii* (150 µg/mL), and *P. putumayoense* (150 µg/mL) leaf extracts for 24 and 48 h. Results are the mean ± SE of $n = 3–9$. * $p < 0.05$; ** $p < 0.01$; *** $p < 0.005$, significantly different from control.

Treatment		24 h			48 h		
		SOD	GPx	Catalase	SOD	GPx	Catalase
		U/mg	nmol/min/mg	µmol/min/mg	U/mg	nmol/min/mg	µmol/min/mg
McA-RH7777	Control	22.0 ± 0.9	38.0 ± 4.2	134.0 ± 8.6	23.4 ± 5.2	40.6 ± 3.6	143.7 ± 5.2
	V. baccifera	19.3 ± 3.4	44.6 ± 7.4	108.2 ± 8.1 *	14.8 ± 3.2 *	54.6 ± 9.3	95.8 ± 15.8 **
	P. krukoffii	22.1 ± 2.3	47.0 ± 1.7 **	80.4 ± 3.6 ***	23.3 ± 1.8	45.8 ± 3.1	77.3 ± 6.6 **
	P. putumayoense	21.0 ± 1.7	47.9 ± 3.5 **	103.2 ± 5.9 ***	23.4 ± 1.9	49.5 ± 2.3 *	81.0 ± 7.3 **
HepG2	Control	15.5 ± 1.5	1.86 ± 0.50	104.6 ± 10.1	18.9 ± 1.7	1.84 ± 0.16	101.2 ± 8.0
	V. baccifera	21.4 ± 1.8 *	1.57 ± 0.27	65.2 ± 15.5*	20.8 ± 2.8	1.76 ± 0.51	73.0 ± 17.5
SK-HEP-1	Control	16.0 ± 1.0	2.18 ± 0.46	11.6 ± 2.3	17.4 ± 0.7	3.72 ± 0.63	13.6 ± 3.3
	P. krukoffii	19.0 ± 1.0 *	2.62 ± 0.69	3.9 ± 3.0	22.9 ± 1.1 ***	2.57 ± 1.33	7.8 ± 1.9
	P. putumayoense	19.4 ± 0.4 ***	1.30 ± 0.80	7.6 ± 3.4	25.3 ± 1.1 ***	2.10 ± 0.26*	9.6 ± 5.3

SOD, superoxide dismutase; GPx, glutathione peroxidase.

V. baccifera increased SOD activity in HepG2, while reducing catalase activity at 24 h. *P. krukoffii* and *P. putumayoense* significantly increased SOD activity in SK-HEP-1, the hepatoma cell line target of the cytotoxic actions of these *Piperaceae*. In the case of *P. putumayoense*, a decrease was also found in the activity of glutathione peroxidase.

These results on the effects of the plant extracts on antioxidant activities, *i.e.*, a general increase in SOD activity and a reduced catalase activity, suggest that the extracts increase the intracellular hydrogen peroxide levels at long periods.

4. Discussion

In this work we have used several human hepatoma cell lines as model system to study the cytotoxic and antiproliferative activities of various plant species from Colombian Amazonia. This system, easy to manipulate, serves as a model for human cancer to study the activities of novel anticancer drugs, the sensitivity patterns, and their mechanisms of action that could lead to the development of new therapeutic targets. The results of the research in cancer cell lines are usually extrapolated to *in vivo* human tumors [26] and have been recognized by pharmaceutical companies as models for the screening and characterization of anticancer therapeutics [27]. The use of cell lines has, however, some limitations; for example, the cell culture environment is different from that of the original tumor, and tumor cell lines have lost the natural heterogeneity of the tumor. Nevertheless, cancer cell lines are adequate models for the research of cancer, and data have demonstrated that the tumor cell lines have a similar response to anticancer drugs when compared to the original tumor [28].

The different human hepatoma cell lines used herein represent various types of tumors with different phenotypes, histhopatologies, protein profiles and clinical outcomes [29–31]. These differences limit the search of a unique drug with effective actions on all liver tumors, and encourage the understanding of the distinctive mechanism of action, specific for each tumor. We have found that the aqueous extracts

of the *Vismia* and *Piper* genera differentially affected the cell lines. We have found that HepG2 was very sensitive to *V. baccifera*, but not to the *Piper* species; in contrast, the *Piperaceae* induced toxicity to PLC-PRF and SK-HEP-1, but *V. baccifera* did not exert toxic effects. We have seen, therefore, differences in the actions of the extracts depending on the cell type, and this observation is particularly relevant if we consider that not all the patients with liver cancer respond similarly under the same anticancer therapy.

The differential response to the extract may be attributed to differences in genotype and the gene expression profiles in the hepatoma cells, thus leading to the final response. Hepatoma cells secrete high levels of specific proteins, many of which are involved in cell growth and its regulation, and are poorly or not secreted by nontransformed liver cells [32–34]. The same proteins have also been detected in clinical specimens from patients' hepatocarcinomas, thus validating the use of hepatoma cell lines as biological model [34]. One of these markers is alpha-fetoprotein, a protein that is present in 60%–70% of patients with hepatocarcinoma, and represents the only clinical available marker of this liver neoplasm [29]. HepG2 represents a liver cancer cell line with positive alpha-fetoprotein expression, while PLC-PRF and SK-HEP-1 are typical cell lines negative for this protein [28]. As indicated above, these two last cell lines were insensitive to *V. baccifera* toxicity, while the alpha-fetoprotein positive HepG2 cells were highly sensitive to *Vismia*-induced toxicity. In contrast to *V. baccifera*, the *Piperaceae* extracts did not affect the viability of HepG2, but induced toxicity in the two alpha-fetoprotein negative PLC-PRF and SK-HEP-1 lines. Other differences between these two cell types have also been described; PLC-PRF and SK-HEP-1 cells are able to form tumors when injected in nude mice or rats, while no tumors were observed for HepG2 cells [31]. In the present work we describe for the first time a toxic treatment based on aqueous plant extracts that discriminates between these two types of hepatocarcinoma cells that do not share a common protein expression profile.

The anticarcinogenic activity of a potential drug implies the combination of its innocuousness or cytoprotective effect on normal cells and its cytotoxic action on neoplasic cells. The actions of the extracts in normal cells were assayed using primary cultures of rat hepatocytes and the results were compared with those of the rat neoplasic McA-RH7777 cells. This cell line was very sensitive to the extracts-induced toxicity, while the normal counterpart cells were highly resistant, and *P. putumayoense* even protected hepatocytes from cell death. Although data obtained with rat hepatocytes cannot be extrapolated to human normal liver cells, results obtained *in vitro* for several natural compounds point out similar mechanisms of action for the compounds in cells of different origin [35,36]. Nevertheless, the hormetic effects of many compounds should also be considered, as several studies demonstrate opposite effects for the same compound when applied at high or low doses; commonly, there is a stimulatory or beneficial effect at low doses and a toxic effect at high doses [37,38]. Thus, how the plant extracts do regulate and induce the therapeutical effects in cancer needs to be elucidated.

In McA-RH7777 *V. baccifera* and *P. putumayoense* altered cell cycle progression inducing arrest at G2/M phase. These results indicate that these plant extracts probably affected the expression of proteins that regulate transition through the G2 checkpoint, such as cyclin B. Similar effects on cell cycle arrest at G2/M have been reported for theaflavins in human prostate carcinoma and leukemia cells [39,40]. In contrast to *P. putumayoense*, *P. krukoffii* showed no effects on cell cycle progression, suggesting differences in the toxicity mechanism between the two *Piper* species.

We also found that cytotoxicity to human and rat hepatoma cell lines was accompanied by a marked increase of the intracellular ROS production. By contrast, in non-tumor hepatocytes the extracts did not generate ROS and even prevented their basal formation, promoting cell survival. These results suggest that the plant-derived extracts could cause cytotoxicity in malignant human and rat liver cell lines by induction of oxidative stress, and, therefore, by mechanisms independent of their antioxidant actions. Growing evidence suggests that food-derived antioxidants act as chemopreventive agents independent of their free radical scavenging activity. Moreover, antioxidants can become pro-oxidants under specific conditions, such as in the presence of high levels of transition metals. This is the case of naturally occurring compounds, including ascorbic acid and several known anticancer drugs, which act as pro-oxidants in the presence of transition metal ions [41–43]. It has been recently described that resveratrol, a phenolic phytochemical present in vegetables and red wine, regulates the expression of proteins involved in the redox balance and apoptosis in SK-HEP-1, suggesting that it causes hepatic cancer cell death by suppressing the expression of antioxidant proteins, and consequently increasing oxidative damage to cells [44]. Our results also showed that the extracts produced significant long-term changes in the activities of antioxidant enzymes, which were reflected by an overall increase in superoxide dismutase activity and a reduction of catalase activity, suggesting the accumulation of hydrogen peroxide. However, we detected no changes in the antioxidant activities at short times (shown in Figure S1); the early oxidative stress induced by the extracts could be responsible for subsequent changes in antioxidant activities, which could contribute to the long-term toxic response.

The early toxic response to the extracts could also be initiated by oxidative stress-independent mechanisms, the intracellular increase of ROS levels being a consequence rather than the cause of cell death. The potential mechanisms involved in the antitumor activities include a) interactions of the components of the extracts with the DNA helix and inhibition of topoisomerases, thus blocking DNA replication and inducing apoptosis; b) inhibition of cytoskeletal proteins which play a key role in cell division; c) perturbations of cell cycle specific proteins, such as cyclins, p27 and p53, blocking proliferation; and d) deregulation (activation/inhibition) of key proteins involved in diverse signaling transduction pathways, such as regulation of cell proliferation and apoptosis (members of the bcl-2 family, phosphatidylinositol-3-kinase, Akt, mitogen activated protein kinases, nuclear factor kappa B or caspases), as has been proposed for natural polyphenols [35]. The role of these signaling pathways in our system are under investigation.

The *in vitro* antitumor activity of plant extracts and infusions, such as tea beverages, has been attributed to their polyphenol components, among them, catechins and epicatechins flavanols being the most abundant [45]. Flavonoids have been extensively reported to exert antitumor actions [46–48]. In a preliminary phytochemical screening we found the presence of high levels of flavanols, particularly epicatechin (monomers, dimers and trimers), in *V. baccifera* aqueous infusions [18]. These polyphenols could be responsible for the toxicity induced by the *Hypericaceae* to tumoral cells. Nevertheless, flavanols and other polyphenols of the families flavanones, flavonols, hydroxycinnamic acids, hydroxybenzoic acids, flavones, and coumarins were not detected in *P. krukoffii* and *P. putumayoense* aqueous infusions [18], and here we have shown that the *Piper* species also induced toxicity to tumor cell lines. Other bioactive components of the plant extracts could exert cytotoxicity. In addition, different polyphenolic compounds can also interact synergistically in mediate toxicity and contribute to the final toxic response.

5. Conclusions

The present study indicates that aqueous infusions of *V. baccifera*, *P. krukoffii* and *P. putumayoense* induce selective killing of hepatocarcinoma cells, and suggests that ROS could mediate the induced cell toxicities. This system based on the selective responses to plants represents an *in vitro* model to study the mechanisms of action and signaling of cancer cells, and therefore, to better understand cancer biology. In addition, the results described here suggest a need for further research into these plants as promising sources of antitumoral drugs against different types of hepatocarcinoma.

Acknowledgments

This work was supported by Research grants from the Basque Country Government, Deptartment of Education, Universities and Research [code IT687-13], University of the Basque Country UPV/EHU (CLUMBER UFI11/20, and predoctoral grant to J.T.) and Research Institute of Free Radicals and Metabolism (ERRASMIK/IRALMET) (grant to L.J.L). We would like to thank Marco A. Correa-Múnera, of Herbario Enrique Forero (HUAZ) from the University of Amazonia (Florencia, Colombia) and Ricardo Callejas-Posada, from the Biology Institute of the University of Antioquia (Colombia) for the identification and classification of the plants. Technical and human support provided by SGIKer (UPV/EHU, MICINN, GV/EJ, ESF) is gratefully acknowledged.

Author Contributions

Conceived and designed the experiments: J.I. Ruiz-Sanz, M.B. Ruiz-Larrea, L.J. Lizcano; Performed the experiments: L.J. Lizcano, M. Siles, J. Trepiana; Analyzed the data: J.I. Ruiz-Sanz, M.B. Ruiz-Larrea, L.J. Lizcano, M. Siles, J. Trepiana; Contributed reagents/materials/analysis tools: M.L. Hernández, R. Navarro; Wrote the paper: M.B. Ruiz-Larrea.

Conflicts of Interest

The authors declare no conflict of interest.

References

1. Ferlay, J.; Shin, H.R.; Bray, F.; Forman, D.; Mathers, C.; Parkin, D.M. Estimates of worldwide burden of cancer in 2008, GLOBOCAN 2008. *Int. J. Cancer* **2010**, *127*, 2893–2917.
2. Parkin, D.M.; Bray, F.; Ferlay, J.; Pisani, P. Global cancer statistics, 2002. *C.A. Cancer J. Clin.* **2005**, *55*, 74–108.
3. Acebo, P.; Giner, D.; Calvo, P.; Blanco-Rivero, A.; Ortega, A.D.; Fernández, P.L.; Roncador, G.; Fernández-Malavé, E.; Chamorro, M.; Cuezva, J.M. Cancer abolishes the tissue type-specific differences in the phenotype of energetic metabolism. *Transl. Oncol.* **2009**, *2*, 138–145.
4. Bensinger, S.J.; Christofk, H.R. New aspects of the Warburg effect in cancer cell biology. *Semin. Cell. Dev. Biol.* **2012**, *23*, 352–361.
5. Dang, C.V. Links between metabolism and cancer. *Genes Dev.* **2012**, *26*, 877–890.

6. Granchi, C.; Minutolo, F. Anticancer agents that counteract tumor glycolysis. *Chem. Med. Chem.* **2012**, *7*, 1318–1350.
7. Mucaj, V.; Shay, J.E.; Simon, M.C. Effects of hypoxia and HIFs on cancer metabolism. *Int. J. Hematol.* **2012**, *95*, 464–470.
8. Aninat, C.; Piton, A.; Glaise, D.; Le Charpentier, T.; Langouët, S.; Morel, F.; Guguen-Guillouzo, C.; Guillouzo, A. Expression of cytochromes P450, conjugating enzymes and nuclear receptors in human hepatoma HepaRG cells. *Drug Metab. Dispos.* **2006**, *34*, 75–83.
9. Donato, M.T.; Lahoz, A.; Castell, J.V.; Gómez-Lechón, M.J. Cell lines: A tool for *in vitro* drug metabolism studies. *Curr. Drug Metab.* **2008**, *9*, 1–11.
10. Vane, J.R.; Botting, R.M. Anti-inflammatory drugs and their mechanism of action. *Inflamm. Res.* **1998**, *47*, S78–S87.
11. Surh, Y.J.; Chun, K.S.; Cha, H.H.; Han, S.S.; Keum, Y.S.; Park, K.K.; Lee, S.S. Molecular mechanisms underlying chemopreventive activities of anti-inflammatory phytochemicals: Down-regulation of $CO_{x\text{-}2}$ and iNOS through suppression of NF-kappa B activation. *Mutat. Res.* **2001**, *480–481*, 243–268.
12. Kuete, V.; Nguemeving, J.R.; Beng, V.P.; Azebaze, A.G.B.; Etoa, F.X.; Meyer, M.; Bodo, B.; Nkengfack, A.E. Antimicrobial activity of the methanolic extracts and compounds from *Vismia laurentii* De Wild (Guttiferae). *J. Ethnopharmacol.* **2007**, *109*, 372–379.
13. Osorio, E.; Arango, G.J.; Jiménez, N.; Alzate, F.; Ruiz, G.; Gutiérrez, D.; Paco, M.A.; Giménez, A.; Robledo, S. Antiprotozoal and cytotoxic activities *in vitro* of Colombian Annonaceae. *J. Ethnopharmacol.* **2007**, *111*, 630–635.
14. Carvalho, M.V.; Penido, C.; Siani, A.C.; Valente, L.M.; Henriques, M.G. Investigations on the anti-inflammatory and anti-allergic activities of the leaves of *Uncaria guianensis* (Aublet) J. F. Gmelin. *Inflammopharmacology* **2006**, *14*, 48–56.
15. Fuller, R.W.; Westergaard, C.K.; Collins, J.W.; Cardellina, J.H.; Boyd, M.R. Vismiaphenones D-G, new prenylated benzophenones from *Vismia cayennensis*. *J. Nat. Prod.* **1999**, *62*, 67–69.
16. Hussein, A.A.; Bozzi, B.; Correa, M.; Capson, T.L.; Kursar, T.A.; Coley, P.D.; Solis, P.N.; Gupta, M.P. Bioactive constituents from three Vismia species. *J. Nat. Prod.* **2003**, *66*, 858–860.
17. Lizcano, L.J.; Bakkali, F.; Ruiz-Larrea, M.B.; Ruiz-Sanz, J.I. Antioxidant activity and polyphenol content of Colombian Amazonian plants with medicinal use. *Food Chem.* **2010**, *119*, 1566–1570.
18. Lizcano, L.J.; Viloria-Bernal, M.; Vicente, F.; Berrueta, L.A.; Gallo, B.; Martínez-Cañamero, M.; Ruiz-Larrea, M.B.; Ruiz-Sanz, J.I. Lipid oxidation inhibitory effects and phenolic composition of aqueous extracts from medicinal plants of Colombian Amazonia. *Int. J. Mol. Sci.* **2012**, *13*, 5454–5467.
19. Ruiz-Larrea, M.B.; Garrido, M.J.; Lacort, M. Estradiol-induced effects on glutathione metabolism in rat hepatocytes. *J. Biochem.* **1993**, *113*, 563–567.
20. Navarro, R.; Martínez, R.; Busnadiego, I.; Ruiz-Larrea, M.B.; Ruiz-Sanz, J.I. Doxorubicin-induced MAPK activation in hepatocyte cultures is independent of oxidant damage. *Ann. N. Y. Acad. Sci.* **2006**, *1090*, 408–418.
21. Mosmann, T. Rapid colorimetric assay for cellular growth and survival: Application to proliferation and cytotoxicity assays. *J. Immunol. Methods* **1983**, *65*, 55–63.
22. Bradford, M.M. A rapid and sensitive method for the quantification of microgram quantities of protein utilizing the principle of protein-dye binding. *Anal. Biochem.* **1976**, *72*, 248–254.

23. Flohé, L.; Günzler, W.A. Assay of glutathione peroxidase. *Methods Enzymol.* **1984**, *105*, 114–121.
24. Aebi, H. Catalase *in Vitro*. In *Methods in Enzymology, Oxygen Radicals in Biological Systems*; Packer, L. Ed.; Academic Press: San Diego, CA, USA, 1984; Volume 105, pp. 121–126.
25. López-Torres, M.; Pérez-Campo, R.; Rojas, C.; Cadenas, S.; Barja, G. Simultaneous induction of sod, glutathione reductase, GSH, and ascorbate in liver and kidney correlates with survival during aging. *Free Radic. Biol. Med.* **1993**, *15*, 133–142.
26. Van Staveren, W.C.; Solis, D.Y.; Hebrant, A.; Detours, V.; Dumont, J.E.; Maenhaut, C. Human cancer cell lines: Experimental models for cancer cells *in situ*? For cancer stem cells? *Biochim. Biophys. Acta* **2009**, *1795*, 92–103.
27. Gazdar, A.F.; Girard, L.; Lockwood, W.W.; Lam, W.L.; Minna, J.D. Lung cancer cell lines as tools for biomedical discovery and research. *JNCI-J. Natl. Cancer Inst.* **2010**, *102*, 1310–1321.
28. Finlay, G.J.; Baguley, B.C. The use of human cancer cell lines as a primary screening system for antineoplastic compounds. *Eur. J. Cancer Clin. Oncol.* **1984**, *20*, 947–954.
29. Fujiyama, S.; Tanaka, M.; Maeda, S.; Ashihara, H.; Hirata, R.; Tomita, K. Tumor markers in early diagnosis, follow-up and management of patients with hepatocellular carcinoma. *Oncology* **2002**, *62*, 57–63.
30. Knowles, B.B.; Howe, C.C.; Aden, D.P. Human hepatocellular carcinoma cell lines secrete the major plasma proteins and hepatitis B surface antigen. *Science* **2001**, *209*, 497–499.
31. Shouval, D.; Schuger, L.; Levij, I.S.; Reid, L.M.; Neeman, Z.; Shafritz, D.A. Comparative morphology and tumourigenicity of human hepatocellular carcinoma cell lines in athymic rats and mice. *Virchows Arch. A.* **1988**, *412*, 595–606.
32. Chen, C.H.; Su, K.Y.; Tao, M.H.; Lin, S.W.; Su, Y.H.; Tsai, Y.C.; Cheng, K.C.; Jeng, Y.M.; Sheu, J.C. Decreased expressions of hepsin in human hepatocellular carcinomas. *Liver Int.* **2006**, *26*, 774–780.
33. Seow, T.K.; Liang, R.C.; Leow, C.K.; Chung, M.C. Hepatocellular carcinoma: From bedside to proteomics. *Proteomics* **2001**, *1*, 1469.
34. Sun, Y.; Mi, W.; Cai, J.; Ying, W.; Liu, F.; Lu, H.; Qiao, Y.; Jia, W.; Bi, X.; Lu, N.; *et al*. Quantitative proteomic signature of liver cancer cells: Tissue transglutaminase 2 could be a novel protein candidate of human hepatocellular carcinoma. *J. Proteome Res.* **2008**, *7*, 3847–3859.
35. Ramos, S. Cancer chemoprevention and chemotherapy: Dietary polyphenols and signalling pathways. *Mol. Nutr. Food Res.* **2008**, *52*, 507–526.
36. Keum, Y.S.; Han, Y.H.; Liew, C.; Kim, J.H.; Xu, C.; Yuan, X.; Shakarjian, M.P.; Chong, S.; Kong, A.N. Induction of heme oxygenase-1 (HO-1) and NAD[P]H: Quinone oxidoreductase 1 (NQO1) by a phenolic antioxidant, butylated hydroxyanisole (BHA) and its metabolite, tert-butylhydroquinone (tBHQ) in primary-cultured human and rat hepatocytes. *Pharm. Res.* **2006**, *23*, 2586–2594.
37. Zanichelli, F.; Capasso, S.; Di Bernardo, G.; Cipollaro, M.; Pagnotta, E.; Cartenì, M.; Casale, F.; Iori, R.; Giordano, A.; Galderisi, U. Low concentrations of isothiocyanates protect mesenchymal stem cells from oxidative injuries, while high concentrations exacerbate DNA damage. *Apoptosis* **2012**, *17*, 964–974.
38. Zanichelli, F.; Capasso, S.; Cipollaro, M.; Pagnotta, E.; Cartenì, M.; Casale, F.; Iori, R.; Galderisi, U. Dose-dependent effects of R-sulforaphane isothiocyanate on the biology of human mesenchymal stem cells, at dietary amounts, it promotes cell proliferation and reduces senescence and apoptosis, while at anti-cancer drug doses, it has a cytotoxic effect. *Age* **2012**, *34*, 281–293.

39. Prasad, S.; Kaur, J.; Roy, P.; Kalra, N.; Shukla, Y. Theaflavins induce G2/M arrest by modulating expression of p21waf1/cip1, cdc25c and cyclin B in human prostate carcinoma PC-3 cells. *Life Sci.* **2007**, *81*, 1323–1331.
40. Ohata, M.; Koyama, Y.; Suzuki, T.; Hayakawa, S.; Saeki, K.; Nakamura, Y.; Isemura, M. Effects of tea constituents on cell cycle progression of human leukemia U937 cells. *Biomed. Res.* **2005**, *26*, 1–7.
41. Ehrenfeld, G.M.; Shipley, J.B.; Heimbrook, D.C.; Sugiyama, H.; Long, E.C.; van Boom, J.H.; van der Marel, G.A.; Oppenheimer, N.J.; Hecht, S.M. Copper-dependent cleavage of DNA by bleomycin. *Biochemistry* **1987**, *26*, 931–942.
42. Hadi, S.M.; Ullah, M.F.; Shamim, U.; Bhatt, S.H.; Azmi, A.S. Catalytic therapy of cancer by ascorbic acid involves redox cycling of exogenous/endogenous copper ions and generation of reactive oxygen species. *Chemotherapy* **2010**, *56*, 280–284.
43. Rahman, A.; Shahabuddin; Hadi, S.M.; Parish, J.H. Complexes involving quercetin, DNA and Cu(II). *Carcinogenesis* **1990**, *11*, 2001–2003.
44. Choi, H.Y.; Chong, S.A.; Nam, M.J. Resveratrol induces apoptosis in human SK-HEP-1 hepatic cancer cells. *Cancer Genomics Proteomics* **2009**, *6*, 263–268.
45. Babich H.; Krupka M.E.; Nissim H.A.; Zuckerbraun H.L. Differential *in vitro* cytotoxicity of (−)-epicatechin gallate (ECG) to cancer and normal cells from the human oral cavity. *Toxicol In Vitro.* **2005**, *19*, 231–242.
46. Clere, N.; Faure, S.; Martinez, M.C.; Andriantsitohaina, R. Anticancer properties of flavonoids: Roles in various stages of carcinogenesis. *Cardiovasc. Hematol. Agents Med. Chem.* **2011**, *9*, 62–77.
47. Shimizu, M.; Adachi, S.; Masuda, M.; Kozawa, O.; Moriwaki, H. Cancer chemoprevention with green tea catechins by targeting receptor tyrosine kinases. *Mol. Nutr. Food Res.* **2011**, *55*, 832–843
48. Yang, C.S.; Lambert, J.D.; Sang, S. Antioxidative and anti-carcinogenic activities of tea polyphenols. *Arch. Toxicol.* **2009**, *83*, 11–21.